Numerical Simulation of Acoustic Streaming on SAW-driven Biochips

Dissertation zur Erlangung des Doktorgrades der
Mathematisch-Naturwissenschaftlichen Fakultät der
Universität Augsburg

vorgelegt von Daniel Köster
Juni 2006

Erster Gutachter:	Prof. Dr. K. G. Siebert, Augsburg, Deutschland
Zweiter Gutachter:	Prof. Dr. R. H. W. Hoppe, Augsburg, Deutschland
Dritter Gutachter:	Prof. Dr. A. Wixforth, Augsburg, Deutschland
Vierter Gutachter:	Prof. Dr. P. Morin, Santa Fe, Argentinien

Mündliche Prüfung: 18. Oktober, 2006

Ich möchte an dieser Stelle einigen Menschen meinen Dank aussprechen, die zum erfolgreichen Gelingen dieser Arbeit beigetragen haben.

An erster Stelle möchte ich meinem Doktorvater Kunibert G. Siebert danken, der mich auf dieses spannende und aktuelle Thema gebracht hat und mir stets hervorragende Betreuung geboten hat. Weiterhin danke ich allen Kollegen, vor allem Oliver Kriessl und Christian Kreuzer, welche immer für Fragen und verrückte Einfälle die berühmten fünf Minuten Zeit hatten.

Contents

1 Introduction **1**
- 1.1 Outline of the thesis . . . 2
- 1.2 Notation and function spaces . . . 3
  - 1.2.1 Spaces on bounded domains . . . 3
  - 1.2.2 Lipschitz domains . . . 5
  - 1.2.3 Further spaces . . . 8

2 Physical background and modeling **9**
- 2.1 Fluid manipulation using SAWs . . . 9
- 2.2 Overview of the fluidics problem . . . 10
- 2.3 Acoustic streaming . . . 11
  - 2.3.1 Physical origin of acoustic streaming . . . 11
  - 2.3.2 Acoustic subproblem . . . 12
  - 2.3.3 Acoustic streaming subproblem . . . 13
  - 2.3.4 Free capillary boundaries . . . 15
- 2.4 Dimensionless formulation . . . 16
  - 2.4.1 Acoustic subproblem . . . 16
  - 2.4.2 Acoustic streaming subproblem . . . 17
  - 2.4.3 Free capillary boundaries . . . 18

3 Analysis of the subproblems **19**
- 3.1 Problems on fixed domains . . . 19
  - 3.1.1 Solution spaces and variational formulation . . . 21
- 3.2 Solvability results . . . 25
  - 3.2.1 Existence and uniqueness of the stationary problem . . . 25
  - 3.2.2 Existence and uniqueness of time dependent solutions . . . 25
  - 3.2.3 Existence and uniqueness of periodic solutions . . . 26
  - 3.2.4 Oscillating equilibrium states . . . 35
- 3.3 Quasi-stationary approach . . . 38
- 3.4 Some generalizations . . . 41
  - 3.4.1 Inhomogeneous velocity boundary conditions . . . 42
  - 3.4.2 Pressure with arbitrary mean . . . 47

4 Numerical discretization **57**
- 4.1 Finite elements . . . 57
  - 4.1.1 Triangulations and finite element spaces . . . 57

4.1.2 Lagrange and Taylor-Hood elements . . . 59
4.1.3 Properties of the Taylor-Hood element . . . 61
4.2 Discretized problems on fixed domains . . . 63
4.2.1 Stationary problem . . . 63
4.2.2 Quasi-stationary approach . . . 65
4.2.3 Instationary problem . . . 66
4.2.4 Periodic problem . . . 73

5 Free boundary problems 75
5.1 Free capillary boundaries . . . 75
5.1.1 Free boundaries and acoustic streaming . . . 75
5.1.2 Variational formulation including curvature . . . 76
5.2 Discretization of free boundary problem . . . 78
5.2.1 Concepts of moving finite elements . . . 78
5.2.2 Algorithm . . . 80

6 Details of the implementation 87
6.1 Efficient solution of linear systems . . . 87
6.1.1 Sample derivation of a linear system . . . 87
6.1.2 Krylov space methods . . . 89
6.1.3 Preconditioning . . . 94
6.2 Saddle point solvers . . . 95
6.3 Overview of algorithms . . . 99
6.3.1 Fixed meshes . . . 99
6.3.2 Free capillary boundaries . . . 101
6.4 Software . . . 102

7 Numerical Results 105
7.1 Test problems . . . 105
7.1.1 Fixed domains . . . 105
7.1.2 Free boundaries . . . 117
7.2 Realistic problems . . . 124
7.2.1 Fixed domains . . . 125
7.2.2 Free boundaries . . . 130
7.3 Physical experiments . . . 133
7.3.1 Experimental layout . . . 134
7.3.2 Particle tracking . . . 135
7.3.3 Streaming velocity versus SAW amplitude . . . 136
7.3.4 Results . . . 138
7.4 Conclusions and outlook . . . 140

A Bibliography 141

B Reference of notation and symbols 147

Chapter 1

Introduction

The last decades have seen unprecedented advances in the production of miniaturized electronic circuits, from the leviathan computers filling entire rooms in the humble beginnings to the powerful and omnipresent microchips of today. A similar revolution under the motto "smaller is better" is currently taking place in the life sciences regarding the manipulation of fluids, with the transition from test tubes and beakers to micropipettes and microtitre plates.

In contrast to the field of microelectronics where the aim is still to reduce the size of transistors, in microfluidics the main concern nowadays is to manufacture increasingly complex systems of channels with sophisticated pumps, valves, mixers, separators, and filters, all on a scale of micrometers. A popular concept today is known as *lab-on-a-chip*. The goal of a lab-on-a-chip is the integration of a complete analysis and reaction system on a small surface ($\approx 1\text{cm}^2$ or less). A sample device is shown in Figure 1.1 below.

There are many reasons for desiring small scale. Less energy and lesser amounts of expensive reagents are needed, reducing costs. Devices can be used in parallel and with automatic control, useful in applications such as gene sequencing. From the physical point of view we have more efficient heat and material transport, leading to better yields and faster analysis.

Despite all of these promising aspects there are certain technical difficulties arising in the production of microfluidic components. Specifically, the task of performing controlled pumping or mixing of nano- or picoliter quantities of fluids becomes difficult. For instance, the low Reynolds number of typical flows on this scale signifies that flows in this regime are laminar and not turbulent. This is an obstacle in designing a component to mix reagents.

A novel type of microfluidic biochip employs surface waves as a driving force. The key of this technology is a pump able to position reagents on the surface of chips or in microfluidic channels without mechanical contact. This is achieved using surface acoustic waves induced using radio frequency electric signals. The waves arise through the use of piezoelectric substrate materials in the chip, e.g. lithium niobate. The electromagnetic signal is efficiently converted into an elastic wave confined to the surface layer of the substrate, hence Surface Acoustic Wave (SAW).

The interaction of these waves with the fluid leads to streaming patterns

in the fluid, or of the motion of the fluid as a whole. It is thus possible to mix minute amounts of fluid or conduct chemical reactions through precisely controlled transport of reagents. See e. g. [73, 38] for further details.

The mathematical modeling and numerical simulation of this fluid-structure interaction is a mostly unexplored field. This is mainly due to the novelty of the applied technology. The few known approaches are mostly based on dimension reduced models solved using widespread numerical methods, see [41]. It is the aim of this thesis to develop specialized and efficient techniques to promote the understanding of microfluidic phenomena with the methods of scientific computing.

Figure 1.1: Example of a biochip.

In this work we will use the compressible Navier-Stokes equations as a starting point to describe fluid flow. This is justified since the typical value of the Knudsen number, defined as the ratio of the characteristic physical length scale to the molecular mean free path length, is much less than 1. Due to the presence of widely different time scales in the physical problem we will derive further model equations to describe the fluid behavior.

The resulting two subproblems describe fluid flow at a microscopic time scale where acoustic effects are dominant, and at a macroscopic time scale where the streaming effects are observable. The solution of the microscopic model is necessary to calculate the effective force terms in the macroscopic model.

Furthermore, we will consider the case of free capillary fluid boundaries which raises the complexity of the problem tremendously. This problem is of interest because some biochip models do not employ closed fluid channels. Instead these chips are constructed with a virtual channel geometry defined by planar regions with different wetting properties on the chip surface. Fluids adhere to the hydrophilic regions by surface tension and are thus contained, see [77]. A second use of free capillary boundaries is passive filling of small cavities by surface tension, see [16].

1.1 Outline of the thesis

This work starts from the physical fundamentals in Chapter 2 in which we describe how the classical Navier-Stokes equations of hydrodynamics serve as a basis to develop the numerical model. The model consists of two separate

systems of partial differential equations to describe the flow variables at pressure p and velocity $\boldsymbol{v}$ on two different time scales.

The following Chapter 3 presents an analysis of the central mathematical problem arising in the model. The problem may be characterized as a generalized instationary, compressible Stokes problem, supplied with initial and boundary conditions. We define suitable function spaces as well as the used concept of weak solutions within these spaces. The main theoretical result of this work is a theorem proving the convergence of solutions with time-periodic data towards oscillating equilibrium states.

Chapter 4 introduces the methods for gaining approximate solutions through discretization in space and time. We present some easily accessible results on the convergence of discrete solutions to the continuous solutions of Chapter 3.

Chapter 5 is entirely devoted to the extension of the prior problems to problems incorporating free capillary boundaries. Due to the complexity of the problem we restrict ourselves to the study of appropriate numerical algorithms.

More details of the numerical discretization, especially the important issue of solving the resulting large linear systems, are presented in Chapter 6. This chapter also serves as a recapitulation of how all the smaller tools and methods are put together to simulate the behavior of a SAW-driven fluidic device.

The final chapter presents results of numerical experiments. Academic test problems are formulated which serve to validate the software implementation. Problems with realistic physical parameters are also defined which demonstrate the applicability to real-life situations. These are compared to the results of physical experiments. Finally, we give an outlook on unsolved issues and possible future improvements.

1.2 Notation and function spaces

In this work we choose $\mathbb{R}$ to signify the set of real numbers, $\mathbb{N}$ as the set of natural numbers, as well as $\mathbb{N}_0 := \mathbb{N} \cup \{0\}$. For any set $A \subset \mathbb{R}^d$, $d \in \mathbb{N}$ we denote $\overline{A}$ as the (topological) closure of A and ∂A as the boundary of A. If A is Lebesgue-measurable we denote the Lebesgue measure of A as $\lambda^d(A)$.

We will generally use **bold type** for symbols to suggest that these are functions assuming values in $\mathbb{R}^d$. A typical usage is $\boldsymbol{v}$ as a velocity field over $\Omega \subset \mathbb{R}^d$. We employ "non-italic" symbols such as x, A to denote vectors or matrices in $\mathbb{R}^n$ for some (typically large) $n \in \mathbb{N}$. We will use the symbol C to denote constant terms in the variables of interest which may or may not be the same at different occurrences. For convenience we have provided a table of symbols and notations at the end of the work on page 147.

1.2.1 Spaces on bounded domains

In the sequel we will denote by Ω a bounded domain in $\mathbb{R}^d$. We will now introduce some notation and review a few basic results.

Definition 1.2.1 (Spaces of polynomials)
For a multi-index $\alpha = (\alpha_i)_{i=1,\dots,d} \in \mathbb{N}_0^d$ we define $|\alpha| := \sum_{i=1}^d \alpha_i$ and $x^\alpha :=$

$\prod_{i=1}^{d} x_i^{\alpha_i}$ for all $x \in \mathbb{R}^d$. For $k \in \mathbb{N}_0$ we define

$$\mathbb{P}_k(\Omega) := \left\{ p : \Omega \to \mathbb{R} \mid p(x) = \sum_{|\alpha|=0}^{k} c_\alpha x^\alpha, \quad c_\alpha \in \mathbb{R} \right\}.$$

Definition 1.2.2 (Spaces of smooth functions)
Let $\alpha \in \mathbb{N}_0^d$. If $f : \Omega \to \mathbb{R}$ is an $|\alpha|$ times continuously differentiable function, let

$$D^\alpha f := \frac{\partial^{|\alpha|} f}{\partial x_1^{\alpha_1} \cdots \partial x_d^{\alpha_d}},$$
$$D^{(0,\ldots,0)} f := f.$$

For any $m \in \mathbb{N}_0$ we define the following spaces of continuous and differentiable functions

$$\begin{aligned} C^m(\Omega) &:= \{ f : \Omega \to \mathbb{R} \mid f \text{ is continuous and} \\ &\qquad\qquad m \text{ times cont. differentiable} \} \\ C^m(\overline{\Omega}) &:= \{ f \in C^m(\Omega) \mid \text{all derivatives } D^\alpha f, |\alpha| \le m \\ &\qquad\qquad \text{may be continuously extended to } \overline{\Omega} \} \end{aligned}$$

as well as

$$\begin{aligned} C^\infty(\Omega) &:= \bigcap_{m \in \mathbb{N}_0} C^m(\Omega) \\ C_0^m(\Omega) &:= \{ f \in C^m(\Omega) \mid \operatorname{supp} f \subset\subset \Omega \} \qquad \text{for } m \in \mathbb{N}_0 \cup \{\infty\}. \end{aligned}$$

The notation $A \subset\subset \Omega$ implies that the set A is compactly contained in Ω.

Definition 1.2.3 (Lebesgue spaces)
Let $p \in [1, \infty]$. We define the standard Lebesgue spaces

$$\begin{aligned} L^p(\Omega) &:= \{ f : \Omega \to \mathbb{R} \mid f \text{ is Lebesgue-measurable and } \|f\|_{L^p(\Omega)} < \infty \}, \\ \text{where } \|f\|_{L^p(\Omega)} &:= \begin{cases} \left(\int_\Omega |f(x)|^p \, dx \right)^{\frac{1}{p}} & \text{for } p < \infty, \\ \operatorname{ess\,sup}_{x \in \Omega} |f(x)| & \text{for } p = \infty, \end{cases} \\ L_0^p(\Omega) &:= \{ f \in L^p(\Omega) \mid \int_\Omega f(x) dx = 0 \}. \end{aligned}$$

As usual, the Lebesgue spaces are actually defined as classes of functions whose values coincide almost everywhere. With this identification the Lebesgue spaces $L^p(\Omega)$ together with $\|\cdot\|_{L^p(\Omega)}$ are Banach spaces. In the case $p = 2$ we may define a scalar product

$$(f, g)_{L^2(\Omega)} := \int_\Omega f(x) g(x) dx \qquad \text{for all } f, g \in L^2(\Omega)$$

giving $L^2(\Omega)$ the additional structure of a Hilbert space.

Definition 1.2.4 (Sobolev spaces)
Let $p \in [1, \infty]$. We define the Sobolev spaces

a) Let $m \in \mathbb{N}$. Then

$$W^{m,p}(\Omega) := \{f \in L^p(\Omega) \mid \text{There exist weak derivatives } D^\alpha f \in L^p(\Omega) \text{ for all } |\alpha| \leq m\}$$

with the norm

$$\|f\|_{m,p} := \begin{cases} \left(\sum_{|\alpha|\leq m} \|D^\alpha f\|^p_{L^p(\Omega)}\right)^{\frac{1}{p}} & \text{for } p < \infty, \\ \max_{|\alpha|\leq m} \|D^\alpha f\|_{L^\infty(\Omega)} & \text{for } p = \infty, \end{cases}$$

as well as the seminorm

$$|f|_{m,p} := \begin{cases} \left(\sum_{|\alpha|=m} \|D^\alpha f\|^p_{L^p(\Omega)}\right)^{\frac{1}{p}} & \text{for } p < \infty, \\ \max_{|\alpha|=m} \|D^\alpha f\|_{L^\infty(\Omega)} & \text{for } p = \infty. \end{cases}$$

b) For $m > 0$ we define $W_0^{m,p}(\Omega)$ as the closure of $C_0^\infty(\Omega)$ in $W^{m,p}(\Omega)$.

c) For $m < 0$ we define $W^{m,p}(\Omega)$ as the dual space of $W_0^{-m,q}(\Omega)$, with the dual exponent $\frac{1}{q} + \frac{1}{p} = 1$.

The Sobolev spaces $W^{m,p}(\Omega)$ with corresponding norms are Banach spaces. In the case $p = 2$ we will write $H^s(\Omega)$, $\|\cdot\|_s$ instead of $W^{s,2}(\Omega)$, $\|\cdot\|_{s,2}$ and $H_0^s(\Omega)$ instead of $W_0^{s,2}(\Omega)$. $H^s(\Omega)$ and $H_0^s(\Omega)$ are Hilbert spaces.

1.2.2 Lipschitz domains

For prescribing boundary values we will need the concepts of Lebesgue spaces defined on the boundary Γ of Ω as well as trace and extension operators.

The following definitions follow [1].

Definition 1.2.5 (Lipschitz domain)
Given are $j \in \{1, \ldots, l\}$, $l \in \mathbb{N}$, a Euclidean coordinate system $e_1^j, \ldots, e_d^j$ of $\mathbb{R}^d$, a reference point $y^j \in \mathbb{R}^{d-1}$, parameters $r^j, h^j > 0$ as well as a Lipschitz-continuous function $g^j : \mathbb{R}^{d-1} \to \mathbb{R}$. Define

$$\tilde{x}^j := (x_1^j, \ldots, x_{d-1}^j) \qquad \text{for } x = \sum_{i=1}^d x_i^j e_i^j,$$

$$U^j := \{x \in \mathbb{R}^d \mid \left|\tilde{x}^j - y^j\right| < r^j \text{ and } \left|x_d^j - g^j(\tilde{x}^j)\right| < h^j\}.$$

Ω is called a *Lipschitz domain*, iff for all $x \in U^j$

$$\begin{aligned} 0 < x_d^j - g^j(\tilde{x}^j) < h^j &\Rightarrow x \in \Omega, \\ x_d^j = g^j(\tilde{x}^j) &\Rightarrow x \in \partial\Omega, \\ 0 > x_d^j - g^j(\tilde{x}^j) > -h^j &\Rightarrow x \notin \Omega, \end{aligned}$$

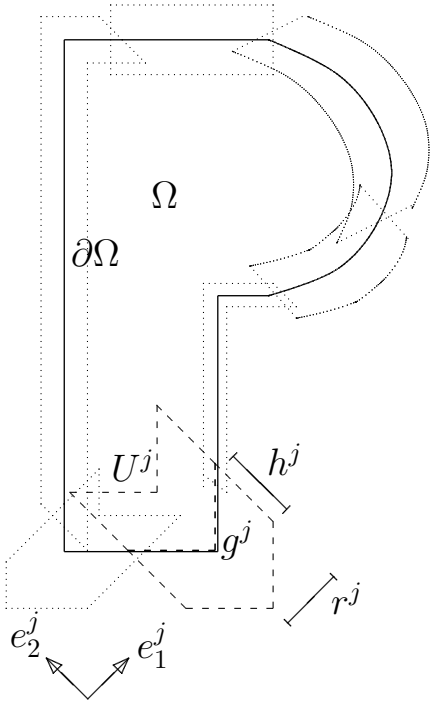

Figure 1.2: Partitioning of a domain Ω.

as well as

$$\partial\Omega \subset \bigcup_{j=1}^{l} U^j.$$

Assume $U^0 \subset \Omega$ as a suitable further open set, so that $U^0, \ldots, U^l$ cover $\overline{\Omega}$.

We will need a partition of unity on $\overline{\Omega}$ corresponding to the covering U^j, e. g.

$$\begin{aligned} \eta^j \in C_0^\infty(U^j), \quad 0 \le \eta^j \le 1 \qquad & \text{for } j = 0, \ldots, l, \\ \sum_{j=0}^{l} \eta^j = 1 \qquad & \text{on } \overline{\Omega}. \end{aligned}$$

We now define a boundary integral as well as Lebesgue spaces on the boundary $\Gamma = \partial\Omega$.

Definition 1.2.6 (Boundary integral and Lebesgue spaces)
Let Ω be an open bounded Lipschitz domain with boundary $\Gamma = \partial\Omega$.

a) A function $f : \Gamma \to \mathbb{R}$ is measurable/integrable, iff (using the notation of 1.2.5) for $j = 1, \ldots, l$ the functions

$$y \mapsto (\eta^j f)\left(\sum_{i=1}^{d-1} y_i e_i^j + g^j(y) e_d^j\right) \qquad \text{for } y \in \mathbb{R}^{d-1} \text{ with } \left|y - y^j\right| < r^j$$

are measurable/integrable with respect to the $(d-1)$-dimensional Lebesgue measure. For integrable f with support in U^j define

$$\int_\Gamma f \, d\mathcal{H}^{d-1} := \int_{\mathbb{R}^{d-1}} f\left(\sum_{i=1}^{d-1} y_i e_i^j + g^j(y) e_d^j\right) \sqrt{1 + |\nabla g^j(y)|^2} dy.$$

For a general integrable $f : \Gamma \to \mathbb{R}$ set

$$\int_\Gamma f \, d\mathcal{H}^{d-1} := \sum_{j=1}^{l} \int_\Gamma \eta^j f \, d\mathcal{H}^{d-1}.$$

b) For $1 \le p \le \infty$ we define the Lebesgue spaces

$$L^p(\Gamma) := \{f : \Gamma \to \mathbb{R} \mid f \text{ is measurable and } \|f\|_{L^p(\Gamma)} < \infty\}.$$

Here we define $\|\cdot\|_{L^p(\Gamma)}$ analogously to the above L^p norms.

c) The *outer unit normal* to Γ may be defined almost everywhere on Γ as

$$\boldsymbol{n}(x) := \left(1 + \left|\nabla g^j(\tilde{x})\right|^2\right)^{-\frac{1}{2}} \left(\sum_{i=1}^{d-1} \frac{\partial g^j}{\partial x_i}(\tilde{x}) e_i^j - e_d^j\right)$$

for

$$x = \sum_{i=1}^{d-1} x_i e_i^j + g^j(\tilde{x}) e_d^j \in U^j \cap \Gamma.$$

$\boldsymbol{n}$ is measurable on Γ with $|\boldsymbol{n}| = 1$. With this sign the vector $\boldsymbol{n}$ will point outward, meaning $x + \varepsilon \boldsymbol{n}(x) \notin \Omega$ if $\boldsymbol{n}$ is defined in x and $\varepsilon > 0$ small enough.

These definitions are independent of the used partitioning of the boundary. With the help of the boundary integral we are able to prove the following important trace theorem, stated e. g. in [30].

Theorem 1.2.7 (Trace theorem)
Let $\Omega \subset \mathbb{R}^d$ be an open bounded Lipschitz set and $1 < p < \infty$. There exists a unique linear continuous mapping

$$T : W^{1,p}(\Omega) \to L^p(\Gamma),$$

with

$$Tf = f|_\Gamma \qquad \text{for } f \in W^{1,p}(\Omega) \cap C^0(\overline{\Omega}).$$

Using this mapping we obtain

$$W_0^{1,p}(\Omega) = \{f \in W^{1,p}(\Omega) \mid Tf = 0\}$$

as the kernel and

$$W^{1-1/p,p}(\Gamma) = \{g \in L^p(\Gamma) \mid g = Tf, f \in W^{1,p}\} \tag{1.1}$$

as the image[1] *of T. We will equip $W^{1-1/p,p}(\Gamma)$ with the image norm*

$$\|g\|_{1-1/p,p} := \inf\{\|f\|_{1,p} \mid g = Tf\}.$$

Finally, there exists a continuous right inverse $E : W^{1-1/p,p}(\Gamma) \to W^{1,p}(\Omega)$ to T. This extension operator E is not unique with this property.

[1] For our purposes it will be sufficient to regard (1.1) as a definition of $W^{1-1/p,p}(\Gamma)$. For the general theory behind fractional order Sobolev spaces refer to the literature.

1.2.3 Further spaces

In this work we will often be dealing with vector valued functions, e. g. velocity fields. For a normed space X of functions $f : \Omega \to \mathbb{R}$ we define the corresponding vector valued space X^d, $d \in \mathbb{N}$, as the standard Cartesian product with norm:

$$X^d := \{\boldsymbol{f} : \Omega \to \mathbb{R}^d \mid f_i \in X \text{ for } i = 1, \dots, d\}$$
$$\|f\|_{X^d} := \left(\sum_{i=1}^{d} \|f_i\|_X^2 \right)^{\frac{1}{2}}.$$

In the case of a scalar product defined on X, we extend it to X^d by

$$(f, g)_{X^d} := \sum_{i=1}^{d} (f_i, g_i)_X$$

In the cases $X = C^m(\Omega)$, $L^p(\Omega)$, $H^m(\Omega)$ we simply denote $\boldsymbol{C}^m(\Omega)$ instead of $(C^m(\Omega))^d$, etc.

For evolution PDEs such as parabolic equations we require functions with values in a real Banach space. Let $(X, \|\cdot\|_X)$ be a Banach space, $a < b \in \mathbb{R}$ and $p \in [1, \infty]$.

$$C^0([a,b]; X) := \{f : [a,b] \to X \mid f \text{ is continuous}\},$$
$$\|f\|_{C^0([a,b];X)} := \max_{x \in [a,b]} \|f(x)\|_X,$$
$$L^p(a,b;X) := \{f : (a,b) \to X \mid f \text{ is Lebesgue-measurable and } \|f\|_{L^p(a,b;X)} < \infty\},$$
$$\text{where } \|f\|_{L^p(a,b;X)} := \begin{cases} \left(\int_a^b \|f(x)\|_X^p \, dx \right)^{\frac{1}{p}} & \text{for } p < \infty, \\ \operatorname{ess\,sup}_{x \in [a,b]} \|f(x)\|_X & \text{for } p = \infty, \end{cases}$$
$$H^k(a,b;X) := \{f \in L^2(a,b;X) \mid \text{There exist weak derivatives } D^\alpha f \in L^2(a,b;X) \text{ for all } |\alpha| \le k\}.$$

Chapter 2

Physical background and modeling

2.1 Fluid manipulation using SAWs

The biochips treated in this work contain a substrate layer consisting of a piezoelectric material, e. g. lithium niobate. Embedded on the substrate surface are fine electrodes known as *Interdigital Transducers* (IDTs) due to their comb-like structure. When a radio frequency signal (typical frequencies are 100 MHz) is applied to the IDTs the inverse piezoelectric effect causes a distortion of the substrate layer. Using special crystal cuts one is able to obtain coupled elastic-electromagnetic waves in the substrate.

The chips used for manipulating fluid are designed to favor a special type of wave known as *Surface Acoustic Wave* (SAW), also called *Rayleigh waves*. These waves spread out along the surface of the substrate in the fashion of a miniature earthquake. The wavelength is defined by the IDT geometry, typical amplitudes of displacement are in the nanometer regime. Rayleigh waves are restricted to a thin layer of several wavelengths on the surface of the chip.

If the surface of the substrate is in contact with fluid and if the normal component of displacement is nonzero, part of the energy will be radiated into the fluid. The thus damped SAW is known as a *leaky SAW*, (LSAW). The interaction between the LSAW and the fluid causes an internal streaming effect as explained below, see Figure 2.1 for an illustration. This streaming can be used to mix the fluid or as a contact free pump. It is even possible [77] to define a virtual fluidic network on the chip surface using hydrophobic and/or hydrophilic materials etched onto the substrate using photolithographic techniques. Here we will also be interested in the effect of the streaming on free capillary boundaries.

The full physical process is a coupled system involving elastic, electromagnetic, and hydrodynamic effects. The numerical simulation of the full system is a very complex problem. In [7] a simulation of a biosensor is presented using a fully coupled model. The physical setup is similar to the one used in this work, with solid piezoelectric layers radiating acoustic waves into a liquid layer. However, only the microscopic time scale is relevant in that work. This means

that a simpler single scale model can be used.

Our approach is based on a splitting into two subproblems, with coupling being either neglected or treated empirically. The analysis and numerical simulation of the elastic/electromagnetic subproblem describing the creation of SAWs was the subject of [28]. In this thesis we will focus on the coupling of LSAWs with the fluid. This interaction will be modeled in only one direction. To be precise, we use an empiric LSAW displacement as input parameter for the streaming effect and neglect the backward coupling of the fluid on the elastic substrate.

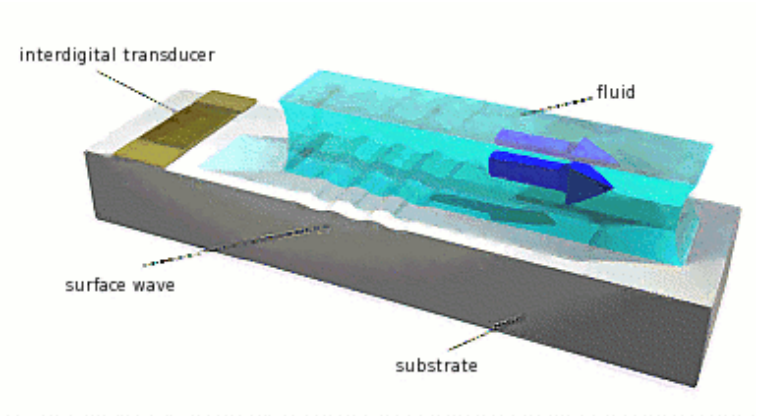

Figure 2.1: Working principles of a SAW-driven fluidic device.

2.2 Overview of the fluidics problem

For the modeling of the fluid flow we use the compressible Navier-Stokes equations, see [44,8]. Assume a bounded fluid domain $\Omega(t)$ with part of the boundary $\Gamma_d(t) \subseteq \partial\Omega(t)$ in contact with elastic walls traversed by SAWs.

$$\begin{aligned}
\rho\left(\frac{\partial \boldsymbol{v}}{\partial t} + (\nabla \boldsymbol{v})\boldsymbol{v}\right) &= \nabla \cdot \Sigma && \text{in } \Omega(t),\ t > 0,\\
\frac{\partial \rho}{\partial t} + \nabla \cdot (\rho \boldsymbol{v}) &= 0 && \text{in } \Omega(t),\ t > 0,\\
\boldsymbol{v}(t, \boldsymbol{x} + \boldsymbol{u}(t, \boldsymbol{x})) &= \frac{\partial \boldsymbol{u}}{\partial t}(t, \boldsymbol{x}) && \text{on } \Gamma_d(t),\ t > 0\\
\boldsymbol{v} \cdot \boldsymbol{n} &= 0 && \text{on } \Gamma_s,\\
\Sigma \boldsymbol{n} &= 0 && \text{on } \Gamma_n,\\
\boldsymbol{v} = 0, \quad p = p_0, \quad \Omega(0) &= \Omega_0 && \text{for } t = 0.
\end{aligned} \tag{2.1}$$

with the Newtonian stress tensor $\Sigma = \Sigma(\boldsymbol{v}, p)$ defined as

$$\Sigma_{ij}(\boldsymbol{v}, p) = -p\delta_{ij} + \eta\left(\frac{\partial v_i}{\partial x_j} + \frac{\partial v_j}{\partial x_i}\right) + (\zeta - \frac{2}{3}\eta)(\nabla \cdot \boldsymbol{v})\delta_{ij}.$$

The quantities that appear are

$\boldsymbol{v}$	fluid velocity,
p	fluid pressure,
ρ	fluid density,
η, ζ	standard and bulk viscosity coefficients[1],
$\boldsymbol{u}$	SAW displacement from equilibrium position, typically a harmonic function of time,
$\boldsymbol{n}$	outer unit normal vector on $\partial\Omega$.

The boundary segments $\Gamma \subset \partial\Omega$ have the following physical interpretation:

Γ_d	Dirichlet boundary conditions for velocity,
Γ_s	tangential slip boundary conditions for velocity,
Γ_n	do-nothing boundary conditions, meaning absence of stress on this boundary.

See Figure 2.2 for an illustration. The divergence of the stress tensor yields

$$\nabla \cdot \Sigma = -\nabla p + \eta \Delta \boldsymbol{v} + \left(\zeta + \frac{\eta}{3}\right) \nabla(\nabla \cdot \boldsymbol{v}).$$

We will need a supplementary equation to close this system. We use an equation of state arising from the assumption of constant entropy in time and space (see [20]). This leads to a simple relation of the form

$$p - p_0 = a(\rho - \rho_0)^\gamma, \tag{2.2}$$

where p_0, ρ_0 are equilibrium states and $a, \gamma > 0$. We assume a linear dependence for liquids such as water, thus $\gamma = 1$.

2.3 Acoustic streaming

2.3.1 Physical origin of acoustic streaming

As discussed above we assume that flow in the fluid region arises exclusively from the harmonic oscillation of the solid boundary. When using standard acoustics theory, where nonlinear effects are neglected and low frequencies and amplitudes are assumed, we expect the propagation of acoustic waves in the fluid. An additional effect observed in real life, however, is that of a *stationary* average flow field, not accounted for by standard acoustic theory.

This effect, known as *acoustic streaming*, was first studied by Lord Rayleigh [55]. Further contributions to the study of this phenomenon were made by Lighthill, Eckart, Nyborg, Riley, and others [56, 57, 49, 50, 46, 58, 25]. Two types of acoustic streaming are generally distinguished today:

[1] Physically reasonable values fulfill $\eta > 0$, $\zeta - \frac{2}{3}\eta > 0$.

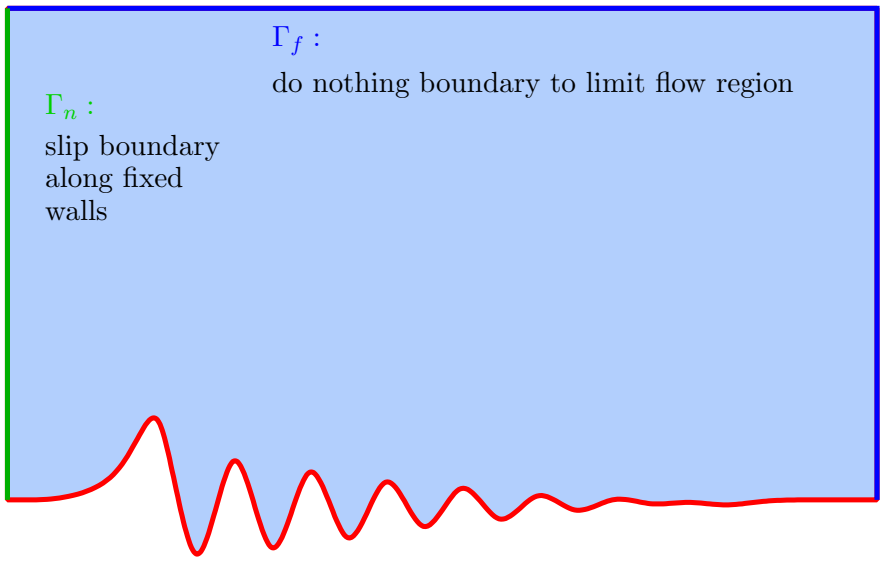

Figure 2.2: Sample computational domain $\Omega(t)$ demonstrating the three types of boundary conditions. The Dirichlet boundary is time dependent because of the motion of the surface acoustic waves.

- *Rayleigh streaming* is associated with the boundary layers of a fluid near solid surfaces.
- *Quartz wind* is associated with the dissipation of acoustic energy in the main body of the fluid.

Acoustic streaming effects are a result of the nonlinearity of the Navier-Stokes equations (2.1) in combination with the viscosity. For the derivation of the model we follow a recent paper by Bradley [8] which provides a rigorous treatment of boundary conditions often neglected in other works.

The main problem for the numerical treatment of acoustic streaming is that extremely different time scales are involved. Typical frequencies of the harmonic oscillation are 100 MHz, requiring a time discretization on the order of 10^{-8} s. The acoustic streaming relaxation times are of the order 10^{-3}–10^{-1} s.

2.3.2 Acoustic subproblem

We assume an expansion of the unknowns $\boldsymbol{v}$, p, and ρ of the form

$$\begin{aligned} p &= p^{(0)} + \epsilon p' + \epsilon^2 p'' + \mathcal{O}(\epsilon^3)\,, \\ \rho &= \rho^{(0)} + \epsilon \rho' + \epsilon^2 \rho'' + \mathcal{O}(\epsilon^3)\,, \\ \boldsymbol{v} &= 0 + \epsilon \boldsymbol{v}' + \epsilon^2 \boldsymbol{v}'' + \mathcal{O}(\epsilon^3)\,. \end{aligned} \tag{2.3}$$

The small parameter $0 < \epsilon \ll 1$ is later fixed as the ratio $\boldsymbol{u}_0/L$, with $\boldsymbol{u}_0$

being the maximal SAW displacement of the domain boundary and L being the typical length scale used for a dimensionless formulation.

Set $p^{(1)} := \epsilon p'$, $p^{(2)} := \epsilon^2 p''$, and analogously ρ, $\boldsymbol{v}$, Σ. All terms with index 0 are constant in time and space and represent the known equilibrium state without SAW driving. By gathering all terms of order $\mathcal{O}(\epsilon)$ we arrive at

$$\rho^{(0)} \frac{\partial \boldsymbol{v}^{(1)}}{\partial t} - \nabla \cdot \Sigma^{(1)} = 0 \qquad \text{in } \Omega(t),\ t > 0, \tag{2.4a}$$

$$\frac{\partial \rho^{(1)}}{\partial t} + \rho^{(0)} \nabla \cdot \boldsymbol{v}^{(1)} = 0 \qquad \text{in } \Omega(t)\ t > 0, \tag{2.4b}$$

$$p^{(1)} = c_0^2 \rho^{(1)}, \tag{2.4c}$$

$$\boldsymbol{v}^{(1)}(t, \boldsymbol{x}) = \frac{\partial \boldsymbol{u}}{\partial t}(t, \boldsymbol{x}), \qquad \text{on } \Gamma_d(t),\ t > 0, \tag{2.4d}$$

$$\boldsymbol{v}^{(1)} \cdot \boldsymbol{n} = 0 \qquad \text{on } \Gamma_s, \tag{2.4e}$$

$$\Sigma^{(1)} \boldsymbol{n} = 0 \qquad \text{on } \Gamma_n, \tag{2.4f}$$

$$\boldsymbol{v}^{(1)} = 0, \quad p^{(1)} = 0 \qquad \Omega(0) = \Omega_0 \qquad \text{for } t = 0. \tag{2.4g}$$

where c_0 is the small signal sound velocity in the fluid. The boundary condition is derived by observing that $\boldsymbol{u} = \mathcal{O}(\epsilon)$ and performing a Taylor expansion:

$$\boldsymbol{v}(t, \boldsymbol{x} + \boldsymbol{u}) = \boldsymbol{v}(t, \boldsymbol{x}) + (\nabla \boldsymbol{v})\boldsymbol{u} + \mathcal{O}(\|\boldsymbol{u}\|^2) = \frac{\partial \boldsymbol{u}}{\partial t}(t, \boldsymbol{x}).$$

In the future we will neglect the time dependence of Ω arising through the SAW oscillation. This is possible since the SAW displacement $\boldsymbol{u}$ is much smaller than the typical length L, equivalent to the fact that $\epsilon \ll 1$.

This linear system describes the *damped* propagation of acoustic waves. These arise solely as a reaction to the time harmonic boundary values (2.4d) since the right hand sides are zero. Due to the parabolic character of the system and the boundedness of Ω we expect the solution to converge into a time harmonic quasi-equilibrium state for large t. A formal proof of this property is presented in Chapter 3. Since the goal is the solution of the system (2.1) on the large time scale the startup effects are of less interest than this equilibrium state.

2.3.3 Acoustic streaming subproblem

Assuming that the above first order system (2.4) is solved we may proceed to gather terms of second order in ϵ while treating the solution of (2.4) as given data. The result is

$$\rho^{(0)}\frac{\partial \boldsymbol{v}^{(2)}}{\partial t} - \nabla\cdot\Sigma^{(2)} = -\rho^{(1)}\frac{\partial \boldsymbol{v}^{(1)}}{\partial t} - \rho^{(0)}(\nabla \boldsymbol{v}^{(1)})\boldsymbol{v}^{(1)} \quad \text{in } \Omega(t),\ t>0, \tag{2.5a}$$

$$\frac{\partial \rho^{(2)}}{\partial t} + \rho^{(0)}\nabla\cdot\boldsymbol{v}^{(2)} = -\nabla\cdot(\rho^{(1)}\boldsymbol{v}^{(1)}) \quad \text{in } \Omega(t),\ t>0, \tag{2.5b}$$

$$p^{(2)} = c_0^2\rho_2, \tag{2.5c}$$

$$\boldsymbol{v}^{(2)} = -(\nabla \boldsymbol{v}^{(1)})\boldsymbol{u} \quad \text{on } \Gamma_d(t),\ t>0, \tag{2.5d}$$

$$\boldsymbol{v}^{(2)}\cdot\boldsymbol{n} = 0 \quad \text{on } \Gamma_s, \tag{2.5e}$$

$$\Sigma^{(2)}\boldsymbol{n} = 0 \quad \text{on } \Gamma_n, \tag{2.5f}$$

$$\boldsymbol{v}^{(2)} = 0, \quad p^{(2)} = 0, \quad \Omega(0) = \Omega_0 \quad \text{for } t = 0. \tag{2.5g}$$

This system may be interpreted as an instationary Stokes problem describing creeping flow and containing mass sources and body forces.

Define $T := 2\pi\omega$ as the period of the harmonic SAW oscillation. Since we are interested in the acoustic streaming effects observable on the larger time scale we take a temporal average of the right hand sides. More precisely, we apply the operation

$$\langle a\rangle := \frac{1}{T}\int_{t_0}^{t_0+T} a(t)\,dt.$$

We thereby obtain the system

$$\rho^{(0)}\frac{\partial \bar{\boldsymbol{v}}^{(2)}}{\partial t} - \nabla\cdot\bar{\Sigma}^{(2)} = \left\langle -\rho^{(1)}\frac{\partial \boldsymbol{v}^{(1)}}{\partial t} - \rho^{(0)}(\nabla \boldsymbol{v}^{(1)})\boldsymbol{v}^{(1)}\right\rangle \quad \text{in } \Omega(t),\ t>0,$$

$$\frac{\partial \bar{\rho}^{(2)}}{\partial t} + \rho^{(0)}\nabla\cdot\bar{\boldsymbol{v}}^{(2)} = \left\langle -\nabla\cdot(\rho^{(1)}\boldsymbol{v}^{(1)})\right\rangle \quad \text{in } \Omega(t),\ t>0,$$

$$\bar{p}^{(2)} = c_0^2\bar{\rho}_2,$$

$$\bar{\boldsymbol{v}}^{(2)} = -\left\langle(\nabla \boldsymbol{v}_1)\boldsymbol{u}\right\rangle \quad \text{on } \Gamma_d(t),\ t>0,$$

$$\bar{\boldsymbol{v}}^{(2)}\cdot\boldsymbol{n} = 0 \quad \text{on } \Gamma_s,$$

$$\bar{\Sigma}^{(2)}\boldsymbol{n} = 0 \quad \text{on } \Gamma_n,$$

$$\bar{\boldsymbol{v}}^{(2)} = 0, \quad p^{(2)} = 0, \quad \Omega(0) = \Omega_0 \quad \text{for } t = 0.$$

In the following we will deal only with the average terms $\bar{\boldsymbol{v}}^{(2)}$, $\bar{p}^{(2)}$, $\bar{\rho}^{(2)}$ and therefore denote these without the bars for simplicity. The corresponding stationary problem is also of interest when performing simulations without free capillary boundaries. For the remainder of this chapter we will restrict ourselves to the stationary system when solving problems without free capillary boundaries.

$$
\begin{aligned}
-\nabla \cdot \Sigma^{(2)} &= \left\langle -\rho^{(1)} \frac{\partial \boldsymbol{v}^{(1)}}{\partial t} - \rho^{(0)} (\nabla \boldsymbol{v}^{(1)}) \boldsymbol{v}^{(1)} \right\rangle && \text{in } \Omega, && (2.6a)\\
\rho^{(0)} \nabla \cdot \boldsymbol{v}^{(2)} &= \left\langle -\nabla \cdot (\rho^{(1)} \boldsymbol{v}^{(1)}) \right\rangle, && \text{in } \Omega, && (2.6b)\\
p^{(2)} &= c_0^2 \rho_2, && && (2.6c)\\
\boldsymbol{v}^{(2)} &= -\left\langle (\nabla \boldsymbol{v}_1) \boldsymbol{u} \right\rangle && \text{on } \Gamma_d, && (2.6d)\\
\boldsymbol{v}^{(2)} \cdot \boldsymbol{n} &= 0 && \text{on } \Gamma_s, && (2.6e)\\
\Sigma^{(2)} \boldsymbol{n} &= 0 && \text{on } \Gamma_n. && (2.6f)
\end{aligned}
$$

Remark 2.3.1
If we assume that $\Gamma_d = \partial\Omega$ and $\Omega \subset \mathbb{R}^3$ then we may verify that the boundary values $\boldsymbol{h} = -\left\langle (\nabla \boldsymbol{v}^{(1)}) \boldsymbol{u} \right\rangle$ and the right hand side $f_p = \left\langle -\nabla \cdot (\rho^{(1)} \boldsymbol{v}^{(1)}) \right\rangle$ of (2.6) are compatible in the sense that Gauß's theorem is satisfied:

$$
\begin{aligned}
\int_{\Gamma_d} \boldsymbol{v}^{(2)} \cdot \boldsymbol{n} \, d\mathcal{H}^2 &= -\int_{\Gamma_d} \left\langle (\nabla \boldsymbol{v}^{(1)}) \boldsymbol{u} \right\rangle \cdot \boldsymbol{n} \, d\mathcal{H}^2 \\
&= \int_{\Gamma_d} \left\langle \frac{-1}{\rho^{(0)}} \rho^{(1)} \boldsymbol{v}^{(1)} + \frac{1}{2} \nabla \times (\boldsymbol{\zeta}^{(1)} \times \boldsymbol{v}^{(1)}) \right\rangle \cdot \boldsymbol{n} \, d\mathcal{H}^2 \\
&= -\int_{\Omega} \frac{1}{\rho^{(0)}} \langle \nabla \cdot (\rho^{(1)} \boldsymbol{v}^{(1)}) \rangle = \int_{\Omega} \nabla \cdot \boldsymbol{v}^{(2)}.
\end{aligned}
$$

Here we have defined $\boldsymbol{\zeta}^{(1)} := \int \boldsymbol{v}^{(1)} dt$ as an extension of $\boldsymbol{u}$ to Ω. We have used (2.4b), the vector property $\nabla \times (\boldsymbol{a} \times \boldsymbol{b}) = (\nabla \boldsymbol{a})\boldsymbol{b} - (\nabla \boldsymbol{b})\boldsymbol{a} + (\nabla \cdot \boldsymbol{b})\boldsymbol{a} - (\nabla \cdot \boldsymbol{a})\boldsymbol{b}$, and the periodicity of $\boldsymbol{v}^{(1)}$. The cross product terms in the second step vanish because the manifold $\partial\Omega$ does not possess a relative boundary (classical Stokes law).

The general idea behind this multiscale modeling is known in physics as *approximation theory*. On the mathematical side, the model we use may also be interpreted in the formal framework of *Heterogeneous Multiscale Methods* as described in [23, 24]. This general approach attempts to formalize the idea of performing microscale simulations to close macroscale models. For the problem of acoustic streaming we have the macroscale variables $\boldsymbol{v}^{(2)}$, $p^{(2)}$ which require macroscale forcing terms. To derive these we have performed temporal averaging using the microscale, quickly oscillating terms $\boldsymbol{v}^{(1)}$, $p^{(1)}$.

There is also a certain connection to the methods of classical *homogenization theory*, as stated in [26, Section 4.5.4]. The problems treated in homogenization theory, however, involve rapidly oscillating coefficients of the differential operator rather than problem data.

2.3.4 Free capillary boundaries

In addition to the problems with fixed channel geometries we will also treat the case of free capillary surfaces along parts of the boundary. To prepare this we first rewrite (2.1) using additional boundary conditions which are valid on a free

capillary boundary $\Gamma_f(t)$ between liquid and air. The new boundary conditions are necessary to determine the normal velocity of the moving interface as well as the stress acting due to capillary forces.

$$\rho\left(\frac{\partial \boldsymbol{v}}{\partial t} + (\nabla \boldsymbol{v})\boldsymbol{v}\right) = \nabla \cdot \Sigma \qquad \text{in } \Omega(t),\ t > 0, \tag{2.7a}$$

$$\frac{\partial \rho}{\partial t} + \nabla \cdot (\rho \boldsymbol{v}) = 0 \qquad \text{in } \Omega(t),\ t > 0, \tag{2.7b}$$

$$\boldsymbol{v}(t, \boldsymbol{x} + \boldsymbol{u}(t, \boldsymbol{x})) = \frac{\partial \boldsymbol{u}}{\partial t}(t, \boldsymbol{x}) \qquad \text{on } \Gamma_d, \tag{2.7c}$$

$$\boldsymbol{v} \cdot \boldsymbol{n} = 0 \qquad \text{on } \Gamma_s, \tag{2.7d}$$

$$\Sigma \boldsymbol{n} = 0 \qquad \text{on } \Gamma_n, \tag{2.7e}$$

$$\Sigma \boldsymbol{n} = \sigma(d-1)\boldsymbol{\kappa} \qquad \text{on } \Gamma_f(t),\ t > 0, \tag{2.7f}$$

$$\boldsymbol{v} \cdot \boldsymbol{n} = V \qquad \text{on } \Gamma_f(t),\ t > 0, \tag{2.7g}$$

$$\boldsymbol{v} = 0, \quad p = p_0, \quad \Omega(0) = \Omega_0 \qquad \text{for } t = 0. \tag{2.7h}$$

Here we have σ as the constant of surface tension between water and vacuum, the difference to the conditions of water/air-interfaces being negligible, (cf. [44]), $\Gamma_f \subset \partial\Omega(t)$ as the free boundary, and V as the normal velocity component of the free boundary. Furthermore we have $\boldsymbol{\kappa}$ as the vector of curvature. By definition this vector has magnitude H (mean curvature of $\partial\Omega(t)$) and points in the direction of $\boldsymbol{n}$ (outer unit normal vector of $\partial\Omega(t)$).

The location of $\Gamma_f(t)$ will change significantly in time and now represents one of the unknowns of the problem. To adapt the two scale model for the inclusion of capillary boundary effects, we include the capillary stress condition (2.7f) in both subproblems.

For the sake of consistency we will continue to neglect the motion of the domain when solving the first order acoustics problem (2.4). However, we will need to take it into account when solving the large time scale acoustic streaming subproblem (2.6).

2.4 Dimensionless formulation

2.4.1 Acoustic subproblem

From the physical formulation of the acoustic equations (2.4) we will need to derive a corresponding dimensionless system with proper scaling for numerical computations. The first step is to divide the momentum equation by the density $\rho^{(0)}$ and to eliminate $\rho^{(1)}$:

$$\frac{\partial \boldsymbol{v}^{(1)}}{\partial t} - \widetilde{\nu}_1 \Delta \boldsymbol{v}^{(1)} - \widetilde{\nu}_2 \nabla(\nabla \cdot \boldsymbol{v}^{(1)}) + \nabla \widetilde{p}^{(1)} = 0, \tag{2.8a}$$

$$\frac{1}{c_0^2}\frac{\partial \widetilde{p}^{(1)}}{\partial t} + \nabla \cdot \boldsymbol{v}^{(1)} = 0 \qquad \text{in } \Omega. \tag{2.8b}$$

Here we have $\widetilde{p} = p/\rho^{(0)}$ as the so-called relative pressure, $\widetilde{\nu}_1 = \eta/\rho^{(0)}$ and $\widetilde{\nu}_2 = (\eta + \zeta/3)/\rho^{(0)}$ as constants of kinematic viscosity. As a next step we choose scales for length L, time T, and velocity V. Symbols with hat denote the dimensionless physical terms and operators:

$$\begin{aligned} x &= L\widehat{x} && \text{position,} \\ t &= T\widehat{t} && \text{time,} \\ v &= V\widehat{v} && \text{velocity,} \\ \widetilde{p} &= \frac{L^2}{T^2}\widehat{p} && \text{relative pressure,} \\ \frac{\partial}{\partial t} &= \frac{1}{T}\frac{\partial}{\partial \widehat{t}} && \text{time derivative,} \\ \nabla &= \frac{1}{L}\widehat{\nabla} && \text{gradient,} \\ \Delta &= \frac{1}{L^2}\widehat{\Delta} && \text{Laplacian.} \end{aligned} \tag{2.9}$$

A dimensionless formulation of the stress tensor Σ may be obtained by defining

$$\widehat{\Sigma}^{(1)}(\widehat{p}^{(1)}, \widehat{\boldsymbol{v}}^{(1)})_{ij} = -\widehat{p}^{(1)}\delta_{ij} + \frac{VT^2}{L^3\rho_0}\eta\left(\frac{\partial \widehat{v}_i^{(1)}}{\partial \widehat{x}_j} + \frac{\partial \widehat{v}_j^{(1)}}{\partial \widehat{x}_i}\right) + \frac{VT^2}{L^3\rho_0}(\zeta - \frac{2}{3}\eta)(\widehat{\nabla}\cdot\widehat{\boldsymbol{v}}^{(1)})\delta_{ij}.$$

We may now formulate a dimensionless version of the acoustic problem:

$$\begin{aligned} \frac{VT}{L}\frac{\partial \widehat{\boldsymbol{v}}^{(1)}}{\partial \widehat{t}} - \frac{VT^2}{L^3}\left(\widetilde{\nu}_1\widehat{\Delta}\widehat{\boldsymbol{v}}^{(1)} + \widetilde{\nu}_2\widehat{\nabla}(\widehat{\nabla}\cdot\widehat{\boldsymbol{v}}^{(1)})\right) + \widehat{\nabla}\widehat{p}^{(1)} &= 0 && \text{in } \Omega, \\ \frac{L^3}{c_0^2 VT^3}\frac{\partial \widehat{p}^{(1)}}{\partial \widehat{t}} + \widehat{\nabla}\cdot\widehat{\boldsymbol{v}}^{(1)} &= 0 && \text{in } \Omega, \\ \frac{VT}{L}\widehat{\boldsymbol{v}}^{(1)} &= \frac{\partial \widehat{u}}{\partial \widehat{t}} && \text{on } \Gamma_d, \\ \widehat{\boldsymbol{v}}^{(1)}\cdot\boldsymbol{n} &= 0 && \text{on } \Gamma_s, \\ \widehat{\Sigma}^{(1)}\boldsymbol{n} &= 0 && \text{on } \Gamma_n, \\ \widehat{\boldsymbol{v}}^{(1)} = 0, \quad \widehat{p}^{(1)} &= 0 && \text{for } \widehat{t} = 0. \end{aligned} \tag{2.10}$$

2.4.2 Acoustic streaming subproblem

As for the acoustic subproblem, we now derive a dimensionless version of (2.6). We will begin by stating an alternative form of the forcing terms in (2.6a):

$$\langle -\rho^{(1)}\frac{\partial \boldsymbol{v}^{(1)}}{\partial t}\rangle = \langle +\frac{\partial \rho^{(1)}}{\partial t}\boldsymbol{v}^{(1)}\rangle = \langle -\rho^{(0)}(\nabla\cdot\boldsymbol{v}^{(1)})\boldsymbol{v}^{(1)}\rangle$$

Here we have used the periodicity of $\boldsymbol{v}^{(1)}$ and $\rho^{(1)}$ as well as the equation of mass conservation (2.6b). We divide again by $\rho^{(0)}$ and obtain

$$\begin{aligned} -\widetilde{\nu}_1\Delta\boldsymbol{v}^{(2)} - \widetilde{\nu}_2\nabla(\nabla\cdot\boldsymbol{v}^{(2)}) + \nabla\widetilde{p}^{(2)} &= -\Big\langle(\nabla\cdot\boldsymbol{v}^{(1)})\boldsymbol{v}^{(1)} + (\nabla\boldsymbol{v}^{(1)})\boldsymbol{v}^{(1)}\Big\rangle && \text{in } \Omega,\\ \nabla\cdot\boldsymbol{v}^{(2)} &= -\frac{1}{c_0^2}\big\langle\nabla\cdot(\widetilde{p}^{(1)}\boldsymbol{v}^{(1)})\big\rangle && \text{in } \Omega,\\ \boldsymbol{v}^{(2)} &= -\Big\langle(\nabla\boldsymbol{v}^{(1)})\boldsymbol{u}\Big\rangle && \text{on } \Gamma_d. \end{aligned}$$

Using the same scales L,T, and V as before yields

$$\begin{aligned} -\frac{VT^2}{L^3}\Big(\widetilde{\nu}_1\widehat{\Delta}\widehat{\boldsymbol{v}}^{(2)} + \widetilde{\nu}_2\widehat{\nabla}(\widehat{\nabla}\cdot\widehat{\boldsymbol{v}}^{(2)})\Big) + \widehat{\nabla}\widehat{p}^{(2)}&\\ = -\frac{V^2T^2}{L^2}\Big\langle(\widehat{\nabla}\cdot\widehat{\boldsymbol{v}}^{(1)})\widehat{\boldsymbol{v}}^{(1)} + (\widehat{\nabla}\widehat{\boldsymbol{v}}^{(1)})\widehat{\boldsymbol{v}}^{(1)}\Big\rangle && \text{in } \Omega,\\ \widehat{\nabla}\cdot\widehat{\boldsymbol{v}}^{(2)} = -\frac{L^2}{T^2c_0^2}\big\langle\widehat{\nabla}\cdot(\widehat{p}^{(1)}\widehat{\boldsymbol{v}}^{(1)})\big\rangle && \text{in } \Omega,\\ \widehat{\boldsymbol{v}}^{(2)} = -\Big\langle(\widehat{\nabla}\widehat{\boldsymbol{v}}^{(1)})\widehat{\boldsymbol{u}}\Big\rangle && \text{on } \Gamma_d,\\ \widehat{\boldsymbol{v}}^{(2)}\cdot\boldsymbol{n} = 0 && \text{on } \Gamma_s,\\ \widehat{\Sigma}^{(2)}\boldsymbol{n} = 0 && \text{on } \Gamma_n. \end{aligned} \tag{2.11}$$

2.4.3 Free capillary boundaries

The corresponding dimensionless free capillary boundary conditions are

$$\widehat{\Sigma}\boldsymbol{n} = \widehat{\sigma}(d-1)\widehat{\boldsymbol{\kappa}}, \tag{2.12}$$

$$\widehat{\boldsymbol{v}}\cdot\boldsymbol{n} = \widehat{V} \qquad \text{on } \Gamma_f(t), \tag{2.13}$$

Here we define $\widehat{\sigma} = \frac{T^2\sigma}{L^3\rho_0}$ as the dimensionless coefficient of surface tension, $\widehat{\kappa} = L\kappa$ is the dimensionless curvature vector of the interface, and $\widehat{V}$ as the dimensionless speed of the capillary free boundary in normal direction.

Chapter 3

Analysis of the subproblems

In this chapter we will introduce and analyze a mathematical model of the acoustics and acoustic streaming subproblems introduced in Chapter 2 for a fixed domain without free boundaries. For simplicity we will limit the discussion to the case of Dirichlet boundary conditions for the velocity specified on the entire boundary $\partial\Omega$ of the domain. Both subproblems (2.10) and (2.11) then have the following general form: Given right hand sides $\boldsymbol{f}_v$, f_p, boundary values $\boldsymbol{g}$, and initial values $\boldsymbol{v}_0, p_0$, find $\boldsymbol{v}$ and p satisfying

$$\mu_v \frac{\partial \boldsymbol{v}}{\partial t} - \nu_1 \Delta \boldsymbol{v} - \nu_2 \nabla(\nabla \cdot \boldsymbol{v}) + \nabla p = \boldsymbol{f}_v \qquad \text{in } \Omega,\ t > 0 \tag{3.1a}$$

$$\mu_p \frac{\partial p}{\partial t} + \nabla \cdot \boldsymbol{v} = f_p \qquad \text{in } \Omega,\ t > 0 \tag{3.1b}$$

$$\boldsymbol{v} = \boldsymbol{g} \qquad \text{on } \partial\Omega,\ t > 0, \tag{3.1c}$$

$$\boldsymbol{v} = \boldsymbol{v}_0, \quad p = p_0 \qquad \text{in } \Omega,\ t = 0, \tag{3.1d}$$

with positive constant parameters μ_v, μ_p, ν_1, ν_2. We will consider both the time dependent and the stationary case $\mu_v = \mu_p = 0$ which requires different methods.

3.1 Problems on fixed domains

As before, we assume Ω to be a bounded Lipschitz domain. We will first proceed to derive a variational formulation of (3.1). This is done in the standard way of multiplying with test functions, integrating over the domain Ω, and then making use of integration by parts at fixed time $t > 0$:

$$\begin{aligned}
\mu_v \int_\Omega \frac{\partial \boldsymbol{v}}{\partial t} \cdot \boldsymbol{w} + \nu_1 \int_\Omega \nabla \boldsymbol{v} : \nabla \boldsymbol{w} + \nu_2 \int_\Omega (\nabla \cdot \boldsymbol{v})(\nabla \cdot \boldsymbol{w}) & \\
- \int_\Omega p \nabla \cdot \boldsymbol{w} = \int_\Omega \boldsymbol{f}_v \cdot \boldsymbol{w} & \qquad \text{for all } \boldsymbol{w} \in \boldsymbol{C}_0^\infty(\Omega), \\
\mu_p \int_\Omega \frac{\partial p}{\partial t} q + \int_\Omega q \nabla \cdot \boldsymbol{v} = \int_\Omega f_p q & \qquad \text{for all } q \in C_0^\infty(\Omega).
\end{aligned}$$

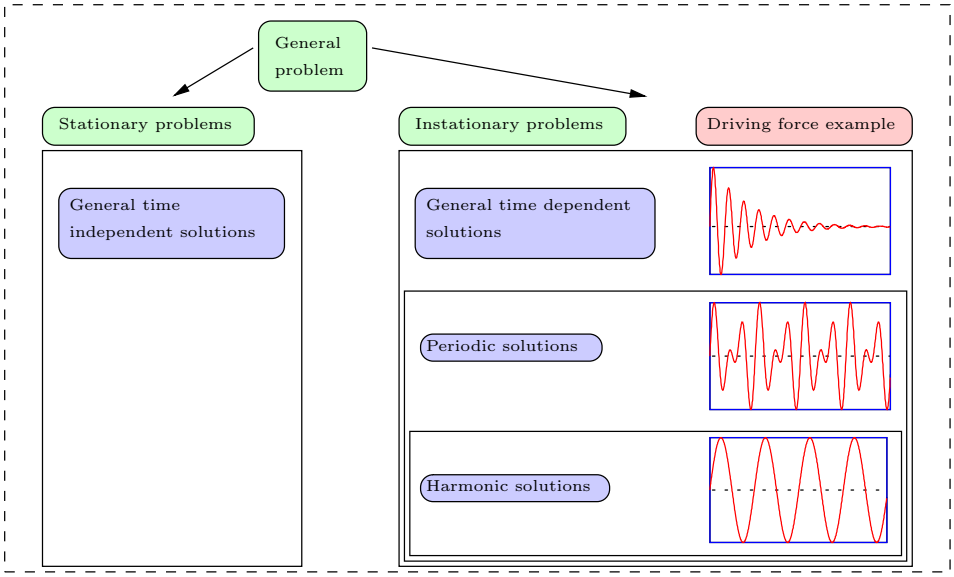

Figure 3.1: Different solution concepts.

Remark 3.1.1
In our analysis we will assume $\mu_v = \mu_p$. This can be achieved by setting the characteristic velocity V in (2.9) on page 17 to $V = L^2/(c_0 T^2)$. This is actually done in the numerical calculations. It is also sufficient to assume $\mu_v = \mu_p = 1$ – otherwise execute a rescaling of the time variable $t \mapsto t/\mu_v$.

Furthermore, we will assume homogeneous boundary conditions ($\boldsymbol{g} = 0$) for now and treat the more general situation later in the chapter.

To deal with the instationary problem we will introduce three different solution concepts each requiring a separate theoretical treatment and numerical implementation. The validity of each approach is determined by the form of the problem data (right hand sides $\boldsymbol{f}_v$, f_p and boundary conditions $\boldsymbol{g}$):

- General time dependent solutions, requiring no assumptions on the form of the problem data
- Time periodic solutions, requiring periodic problem data
- Time harmonic solutions, requiring problem data given as a superposition of sine and cosine terms

Periodic solutions are of interest since the application to SAW driven acoustic streaming often involves time periodic data $\boldsymbol{f}_v$, f_p, $\boldsymbol{g}$. In the case of time harmonic problem data it is possible to eliminate the time dependence altogether and reduce the problem to an equivalent stationary system. This so-called *quasi-stationary approach* is treated later in this chapter. Figure 3.1 presents an overview of the different approaches.

3.1.1 Solution spaces and variational formulation

For the variational formulation we define the following spaces

$$\begin{aligned} \boldsymbol{V} &= \boldsymbol{H}_0^1(\Omega), \\ Q &= L_0^2(\Omega), \\ U &= \boldsymbol{H}_0^1(\Omega) \times L_0^2(\Omega), \\ H &= \boldsymbol{L}^2(\Omega) \times L_0^2(\Omega), \\ U' &= \boldsymbol{H}^{-1}(\Omega) \times L_0^2(\Omega) \qquad \text{as the dual space of } U. \end{aligned}$$

We may define embeddings

$$\begin{aligned} i_1 &: U \to H, \qquad & i_1(f) &= f, \\ i_2 &: H \to U', \qquad & \langle i_2(f), g\rangle_{U'\times U} &= (f, i_1(g))_H. \end{aligned} \tag{3.2}$$

This yields a Gelfand triple

$$U \hookrightarrow_{i_1} H \hookrightarrow_{i_2} U' \tag{3.3}$$

with each space continuously embedded and dense in the subsequent space, see e. g. [78]. Observe that this implies a different concept of $f \in U$ interpreted as a functional in U' than the embedding defined by the Riesz Representation Theorem. In particular, we will not identify U with U'.

For a given bounded time interval $[0,T] \subset \mathbb{R}$ we define

$$\begin{aligned} W(0,T) = \{f \in H^1(0,T;U') \mid &\text{ There exists } g \in L^2(0,T;U) \\ &\text{with } i_2(i_1(g(t))) = f(t) \text{ f. a. a. } t \in (0,T)\}. \end{aligned}$$

The function g is unique with this property. We define the following scalar product on $W(0,T)$:

$$(f_1, f_2)_{W(0,T)} = \int_0^T (g_1(t), g_2(t))_U dt + \int_0^T \left(f_1'(t), f_2'(t)\right)_{U'} dt$$

for all $f_1, f_2 \in W(0,T)$ with corresponding $g_1, g_2 \in L^2(0,T;U)$. Since the distinction between f and g is cumbersome we will use the notation

$$f \in L^2(0,T;U), \qquad f' \in L^2(0,T;U')$$

for functions $f \in W(0,T)$ in the following.

From [78] we cite the following theorem:

Theorem 3.1.2
The space $W(0,T)$ is a Hilbert space. The functions of $W(0,T)$ are continuous with values in H, or to be precise, there exists a continuous embedding

$$W(0,T) \hookrightarrow C([0,T];H). \tag{3.4}$$

Thanks to the continuity property we will be able to justify the specification of initial values in H. We now define the following bilinear forms:

$$a : \boldsymbol{V} \times \boldsymbol{V} \to \mathbb{R}, \tag{3.5a}$$
$$a(\boldsymbol{v}, \boldsymbol{w}) = \nu_1 \int_\Omega \nabla \boldsymbol{v} : \nabla \boldsymbol{w} + \nu_2 \int_\Omega (\nabla \cdot \boldsymbol{v})(\nabla \cdot \boldsymbol{w}), \tag{3.5b}$$
$$b : Q \times \boldsymbol{V} \to \mathbb{R}, \tag{3.5c}$$
$$b(p, v) = -\int_\Omega p \nabla \cdot \boldsymbol{v}, \tag{3.5d}$$
$$s : U \times U \to \mathbb{R}, \tag{3.5e}$$
$$s((\boldsymbol{v}, p), (\boldsymbol{w}, q)) = a(\boldsymbol{v}, \boldsymbol{w}) + b(q, \boldsymbol{v}) - b(p, \boldsymbol{w}). \tag{3.5f}$$

We will need an important analytical result concerning the solvability of the divergence equation.

Theorem 3.1.3 (Solution of the divergence equation)
There exists a constant $\beta > 0$ such that for all $p \in Q$ there is a $\boldsymbol{v} \in \boldsymbol{V}$ with

$$p = \nabla \cdot \boldsymbol{v}, \qquad \|\boldsymbol{v}\|_1 \leq \beta^{-1} \|p\|_0 .$$

Proof. See [15] or [32, Theorem 12.2.14]. □

Lemma 3.1.4
The following properties hold for the bilinear forms defined in (3.5):

*a) The form a is $\boldsymbol{V}$-*elliptic*, meaning that there exist constants $c_a, C_a > 0$ so that for all $\boldsymbol{v}, \boldsymbol{w} \in \boldsymbol{V}$*

$$|a(\boldsymbol{v}, \boldsymbol{w})| \leq C_a \|\boldsymbol{v}\|_1 \|\boldsymbol{w}\|_1 ,$$
$$a(\boldsymbol{v}, \boldsymbol{v}) \geq c_a \|\boldsymbol{v}\|_1^2 .$$

b) There exist constants $c_b, C_b > 0$ so that for all $\boldsymbol{v} \in \boldsymbol{V}$ and $p \in Q$

$$|b(p, \boldsymbol{v})| \leq C_b \|p\|_0 \|v\|_1 , \tag{3.6}$$
$$\inf_{p \in Q \setminus \{0\}} \sup_{\boldsymbol{v} \in \boldsymbol{V} \setminus \{0\}} \frac{b(p, \boldsymbol{v})}{\|p\|_0 \|\boldsymbol{v}\|_1} \geq c_b. \tag{LBB}$$

The inequality (LBB) is the well-known Ladyzhenskaya-Babuška-Brezzi condition.

*c) The form s is U-*coercive *(see e. g. [47]), in other words there are constants $c_s, C_s > 0$, $k_s \in \mathbb{R}$ so that for all $f, g \in U$*

$$|s(f, g)| \leq C_s \|f\|_U \|g\|_U , \tag{3.7}$$
$$s(f, f) + k_s \|f\|_H^2 \geq c_s \|f\|_U^2 . \tag{3.8}$$

We may choose $c_s = k_s = c_a$.

Proof. a) The first inequality is a simple application of the Hölder inequality. Let $\boldsymbol{v} \in \boldsymbol{V}$. Using the Poincaré inequality (e. g. [78], Theorem 7.6) we get

$$\|\boldsymbol{v}\|_1^2 \leq C_p \, |\boldsymbol{v}|_1^2 = C_p \int_\Omega \nabla \boldsymbol{v} : \nabla \boldsymbol{v} \leq \frac{C_p}{\nu_1} a(\boldsymbol{v}, \boldsymbol{v}),$$

where C_p denotes the constant of the Poincaré inequality.

b) Again, the first inequality is obvious. For any $p \in Q$ choose $\boldsymbol{v}_p \in \boldsymbol{V}$ with $\nabla \cdot \boldsymbol{v}_p = -p$ according to Theorem 3.1.3. We calculate

$$\begin{aligned}
\inf_{p \in Q \setminus \{0\}} \sup_{\boldsymbol{v} \in \boldsymbol{V} \setminus \{0\}} \frac{b(p, \boldsymbol{v})}{\|p\|_0 \, \|\boldsymbol{v}\|_1} &= \inf_{p \in Q \setminus \{0\}} \sup_{\boldsymbol{v} \in \boldsymbol{V} \setminus \{0\}} \frac{-\int_\Omega p \nabla \cdot \boldsymbol{v}}{\|p\|_0 \, \|\boldsymbol{v}\|_1} \\
&\geq \inf_{p \in Q \setminus \{0\}} \frac{-\int_\Omega p \nabla \cdot \boldsymbol{v}_p}{\|p\|_0 \, \|\boldsymbol{v}_p\|_1} \\
&\geq \inf_{p \in Q \setminus \{0\}} \frac{\|p\|_0^2}{\beta^{-1} \, \|p\|_0^2} \\
&= \beta.
\end{aligned}$$

c) For the first inequality let $\boldsymbol{v}, \boldsymbol{w} \in \boldsymbol{V}$ and $p, q \in Q$. Then

$$\begin{aligned}
|s((\boldsymbol{v}, p), (\boldsymbol{w}, q))| &= |a(\boldsymbol{v}, \boldsymbol{w}) + b(q, \boldsymbol{v}) - b(p, \boldsymbol{w})| \\
&\leq C_a \, \|\boldsymbol{v}\|_1 \, \|\boldsymbol{w}\|_1 + C_b \left(\|q\|_0 \, \|\boldsymbol{v}\|_1 + \|p\|_0 \, \|\boldsymbol{w}\|_1 \right) \\
&\leq \max(C_a, C_b) \left(\|\boldsymbol{v}\|_1 + \|p\|_0 \right) \left(\|\boldsymbol{w}\|_1 + \|q\|_0 \right) \\
&\leq C_s \left(\|\boldsymbol{v}\|_1^2 + \|p\|_0^2 \right)^{\frac{1}{2}} \left(\|\boldsymbol{w}\|_1^2 + \|q\|_0^2 \right)^{\frac{1}{2}} \\
&= C_s \, \|(\boldsymbol{v}, p)\|_U \, \|(\boldsymbol{w}, q)\|_U \, .
\end{aligned}$$

The second equality follows thus:

$$\begin{aligned}
s((\boldsymbol{v}, p), (\boldsymbol{v}, p)) &= a(\boldsymbol{v}, \boldsymbol{v}) \geq c_a \, \|\boldsymbol{v}\|_1^2 \\
&= c_a \left(\|\boldsymbol{v}\|_1^2 + \|p\|_0^2 \right) - c_a \, \|p\|^2 \\
&\geq c_a \, \|(\boldsymbol{v}, p)\|_U^2 - c_a \, \|(\boldsymbol{v}, p)\|_H^2 \, .
\end{aligned}$$

□

Definition 3.1.5 (Operators for the bilinear forms)
Using Lemma 3.1.4 we may define the following bounded linear operators. Let $\boldsymbol{v}, \boldsymbol{w} \in \boldsymbol{V}$, $p, q \in Q$, $f, g \in U$.

$$\begin{aligned}
A \in L(\boldsymbol{V}, \boldsymbol{V}') : &\qquad \langle A\boldsymbol{v}, \boldsymbol{w} \rangle_{\boldsymbol{V}' \times \boldsymbol{V}} = a(\boldsymbol{v}, \boldsymbol{w}), \\
B \in L(Q, \boldsymbol{V}') : &\qquad \langle Bp, \boldsymbol{v} \rangle_{\boldsymbol{V}' \times \boldsymbol{V}} = b(p, \boldsymbol{v}), \\
B^* \in L(\boldsymbol{V}, Q) : &\qquad \langle B^* \boldsymbol{v}, p \rangle_{Q \times Q} = b(p, \boldsymbol{v}), \\
S \in L(U, U') : &\qquad \langle Sf, g \rangle_{U' \times U} = s(f, g), \\
K \in L(Q, Q) : &\qquad K = B^* A^{-1} B.
\end{aligned} \tag{3.9}$$

Also useful will be the bilinear form corresponding to the Schur complement operator K:

$$k : Q \times Q \to \mathbb{R},$$
$$k(p, q) = (Kp, q)_0.$$

We can now formulate the variational formulation of (3.1).

Problem 3.1.6 (Weak formulation of the instationary problem)
Let $u_0 = (\boldsymbol{v}_0, p_0) \in H$ and $f = (\boldsymbol{f}_v, f_p) \in L^2(0, T; U')$. Find $u = (\boldsymbol{v}, p) \in W(0, T)$ so that

$$\begin{aligned} \langle w, u'(t)\rangle_{U\times U'} + s(w, u(t)) &= \langle w, f(t)\rangle_{U\times U'} && \text{for all } w \in U, \text{ f. a. a. } t \in (0, T), \\ u(0) &= u_0 && \text{in } H. \end{aligned} \tag{P}$$

We remark that Problem 3.1.6 is well posed due to the properties of the solution space $W(0, T)$. In particular, the specification of initial values in H makes sense due to Theorem 3.1.2.

Lemma 3.1.7
The Problem (P) may be equivalently formulated as
Find $(\boldsymbol{v}, p) \in W(0, T)$ so that

$$\begin{aligned} \langle \boldsymbol{w}, \boldsymbol{v}'(t)\rangle_{\boldsymbol{V}\times\boldsymbol{V}'} + a(\boldsymbol{w}, \boldsymbol{v}(t)) + b(p(t), \boldsymbol{w}) &= \langle \boldsymbol{w}, \boldsymbol{f}_v(t)\rangle_{\boldsymbol{V}\times\boldsymbol{V}'} && \text{for all } \boldsymbol{w} \in \boldsymbol{V}, \\ (q, p'(t))_0 - b(q, \boldsymbol{v}(t)) &= (q, f_p(t))_0 && \text{for all } q \in Q, \\ & && \text{f. a. a. } t \in (0, T), \\ \boldsymbol{v}(0) &= \boldsymbol{v}_0 && \text{in } \boldsymbol{L}^2(\Omega), \\ p(0) &= p_0 && \text{in } Q. \end{aligned} \tag{P$'$}$$

Proof. Assume (P$'$) holds. Set $w = (\boldsymbol{w}, q)$, $u_0 = (\boldsymbol{v}_0, p_0)$ and sum the first two equations to get (P). Now assume (P) holds. Select first $\psi = (\boldsymbol{w}, 0)$ to obtain the first variational equality in (P$'$) and then $\psi = (0, q)$ for the second one. The initial condition is clear. □

The stationary problem corresponding to (3.1) is the well-known Stokes system, except for the definition of the bilinear form a and possibly nonzero divergence of $\boldsymbol{v}$.

Problem 3.1.8 (Weak formulation of the stationary problem)
Let $f = (\boldsymbol{f}_v, f_p) \in U'$. Find $u = (\boldsymbol{v}, p) \in U$ so that

$$\begin{aligned} a(\boldsymbol{w}, \boldsymbol{v}) + b(p, \boldsymbol{w}) &= \langle \boldsymbol{w}, \boldsymbol{f}_v\rangle_{\boldsymbol{V}\times\boldsymbol{V}'} && \text{for all } \boldsymbol{w} \in \boldsymbol{V}, \\ -b(q, \boldsymbol{v}) &= (q, f_p)_0 && \text{for all } q \in Q. \end{aligned} \tag{P$_{stat}$}$$

We remark that an equivalent reformulation of (P$_{stat}$) using the form s is possible using the same methods as in Lemma 3.1.7.

Remark 3.1.9
Concerning the choice of spaces a few remarks seem justified.

a) The choice of $\boldsymbol{V} = \boldsymbol{H}_0^1(\Omega)$ implies homogeneous Dirichlet boundary conditions for velocity in a weak sense as stated by Theorem 1.2.7.

b) The choice of Q as pressure space is also a real restriction as the following example shows:

Given $\Omega = (0,1)^2$, solve the problem

$$\begin{aligned} \frac{\partial \boldsymbol{v}}{\partial t}(t) - \Delta \boldsymbol{v} - \nabla(\nabla \cdot \boldsymbol{v}) + \nabla p = 0 \qquad & \text{in } \Omega, \\ \frac{\partial p}{\partial t}(t) + \nabla \cdot \boldsymbol{v} = 1 \qquad & \text{in } \Omega, \\ \boldsymbol{v}(x,t) = 0 \qquad & \text{on } \partial\Omega, \\ \boldsymbol{v}_0(x) = 0, \quad p_0(x) = 0. & \end{aligned} \tag{3.10}$$

We immediately verify that a solution is given by $\boldsymbol{v}(x,t) = 0$, $p(x,t) = t$. Solutions with a mean value of pressure that is not constant in time may be physically meaningful when studying compressible flows.

We will extend the existence and uniqueness theory of the following two sections to the case of generalized solutions $(\boldsymbol{v}, p)$ sought in the larger space $\boldsymbol{H}^1(\Omega) \times L^2(\Omega)$. This is presented in the final section of the chapter.

3.2 Solvability results

3.2.1 Existence and uniqueness of the stationary problem

Since the Ladyzhenskaya-Babuška-Brezzi condition (LBB) is fulfilled we may deduce existence and uniqueness of solutions of Problem 3.1.8.

Lemma 3.2.1
Problem (P_{stat}) *has a unique solution* $(\boldsymbol{v}, p) \in U$. *The following a-priori estimate holds:*

$$\|\boldsymbol{v}\|_1 + \|p\|_0 \leq C(\|\boldsymbol{f}_v\|_{\boldsymbol{V}'} + \|f_p\|_0),$$

with a constant $C > 0$.

Proof. Given the properties of the bilinear forms in Lemma 3.1.4, we may use the saddle point theory specified in [53]. Additional references are [32, 43, 12]. □

3.2.2 Existence and uniqueness of time dependent solutions

We observe that (P) defines a parabolic problem due to the properties of $s(\cdot,\cdot)$ explained in Lemma 3.1.4. We cite the following theorem.

Theorem 3.2.2 (Existence and Uniqueness of (P))
For $0 < T < \infty$ *the problem* (P) *possesses a unique solution* $(\boldsymbol{v}, p) \in W(0,T)$. *Furthermore, we have the following stability estimate*

$$\|(\boldsymbol{v}, p)\|_{W(0,T)} \leq C \left(\|(\boldsymbol{v}_0, p_0)\|_H + \|(\boldsymbol{f}_v, f_p)\|_{L^2(0,T;U')} \right).$$

The constant C *will generally depend on* T.

Proof. [78, Theorem 26.1]. □

We also state the following result for time regularity of the solution.

Theorem 3.2.3 (Time regularity of the solution of (P))
Assume $u = (\boldsymbol{v}, p)$ as the solution of the parabolic problem (P) stated in the following form

$$\begin{aligned} u'(t) + Su(t) &= f(t) && \text{a. e. in } (0,T), \\ u(0) &= u_0 && \text{for } t = 0. \end{aligned}$$

Let $0 < k \in \mathbb{N}$. We assume $f \in H^k(0,T;U')$ and u_0 fulfilling the following compatibility conditions:

$$\begin{aligned} w_0 &:= u_0 \in U, \\ w_j &:= \frac{d^{j-1}f}{dt^{j-1}}(0) - Sw_{j-1} \in U, \ j = 1, \dots, k-1, \\ w_k &:= \frac{d^{k-1}f}{dt^{k-1}}(0) - Sw_{k-1} \in H. \end{aligned}$$

We then have

$$u \in H^k(0,T;U) \qquad \text{and} \qquad \frac{d^{k+1}u}{dt^{k+1}} \in L^2(0,T;U').$$

Proof. [78, Theorem 27.2]. □

3.2.3 Existence and uniqueness of periodic solutions

For the acoustics subproblem (2.10) on page 17 we generally have a periodic driving force. It is therefore of interest to reformulate Problem 3.1.6 for right hand sides f which have period T and search for periodic solutions. This changes the character of the problem from an initial value problem to a periodic problem, where $u(0)$ and $u(T)$ are unknown a-priori.

Later in this section we will compare the solution u of the initial value problem (P) supplied with a periodic forcing f to the solution u_{per} of the corresponding periodic problem. We expect the solution of the initial value problem to converge in some sense towards a periodic equilibrium state, that is u_{per}, for large times. This phenomenon is known as *forced oscillation* in physics. We will present a theorem confirming this convergent behavior.

We first specify what is meant by a periodic solution. The definition may be surprising at first since periodicity is not mentioned explicitly. The characterization given in Proposition 3.2.5 will justify the terminology.

Problem 3.2.4 (Periodic solutions)
Let $0 < T < \infty$ and $f = (\boldsymbol{f}_v, f_p) \in L^2(0,T;H)$. Find $u = (\boldsymbol{v}, p) \in W(0,T)$ so that

$$\begin{aligned} \langle w, u'(t)\rangle_{U\times U'} + s(w, u(t)) &= (w, f(t))_H && \text{for all } w \in U, \text{ f. a. a. } t \in (0,T), \\ u(0) &= u(T) && \text{in } H. \end{aligned} \tag{P$_{per}$}$$

Note that $u(0)$ and $u(T)$ are unknowns, not data of the problem. We demand more regularity in space, i. e. $f(t) \in H$. This will enable us to use elementary results of Fourier analysis (see [1]) for the derivation of a-priori estimates.

Proposition 3.2.5 (Characterization of periodic solutions)
Assume that the right hand side f is extended to a periodic function $\widetilde{f}$ by

$$\widetilde{f}(t+kT) = f(t) \qquad \text{for } t \in [0,T),\ k \in \mathbb{Z}.$$

A solution u of (P_{per}) may be then be uniquely extended to a periodic solution $\widetilde{u}$ fulfilling

$$\langle w, \widetilde{u}'(t)\rangle_{U\times U'} + s(w, \widetilde{u}(t)) = (w, \widetilde{f}(t))_H \qquad \text{for all } w \in U,\ \text{f. a. a. } t \in \mathbb{R}.$$

Proof. The existence and uniqueness theorem 3.2.2 implies that the solution u with initial values $u(0)$ is well defined for an arbitrarily large interval $[0,\tau]$. Define $z(t) := u(T+t) - u(t)$. The function z is a solution of the following initial value problem:

$$\begin{aligned} z'(t) + Sz(t) &= 0, \\ z(0) &= 0. \end{aligned}$$

The a-priori estimate of Theorem 3.2.2 then implies $z = 0$, therefore $u(t) = u(T+t)$. A similar argument shows that the solution may be uniquely extended backwards in time. □

We now state an existence and uniqueness result for periodic solutions.

Theorem 3.2.6 (Existence and Uniqueness of (P_{per}))
The problem (P_{per}) has a unique solution $(\boldsymbol{v}, p) \in W(0,T)$. We have the stability estimate

$$\|(\boldsymbol{v}, p)\|_{W(0,T)} \le C \,\|(\boldsymbol{f}_v, f_p)\|_{L^2(0,T;H)}\,.$$

The constant C will generally depend on the period T.

The theorem will be proven using the standard Galerkin method. The idea is to establish stability properties of corresponding finite dimensional problems and to use a compactness argument to extend these to the infinite dimensional case. Before proving the theorem we therefore first consider the corresponding finite dimensional problem.

Lemma 3.2.7
Let $\boldsymbol{V}_k \subset \boldsymbol{V}$, $Q_k \subset Q$, $k \in \mathbb{N}$ be finite dimensional subspaces which are stable with respect to $b(\cdot,\cdot)$. By this we mean that the following inf-sup condition holds with $\widetilde{c}_{b,k}$:

$$\inf_{p\in Q_k\setminus\{0\}} \sup_{\boldsymbol{v}\in \boldsymbol{V}_k\setminus\{0\}} \frac{b(p,\boldsymbol{v})}{\|p\|_0 \,\|\boldsymbol{v}\|_1} \ge \widetilde{c}_{b,k} > 0. \tag{LBB$_k$}$$

Assume $f \in L^2(0,T;H)$. Then there exists a unique solution of the finite dimensional problem:

Find $u_k = (\boldsymbol{v}_k, p_k) \in H^1(0,T;\boldsymbol{V}_k \times Q_k)$ so that

$$\begin{aligned} \big(w_k, u_k'(t)\big)_H + s(w_k, u_k(t)) &= (w_k, f(t))_H \quad \text{for all } w_k \in U_k,\ \text{f. a. a. } t \in (0,T), \\ u_k(0) &= u_k(T). \end{aligned} \tag{3.11}$$

Proof. We assume $\{\psi_l\}_{l=1,\dots,n}$ to be an H-orthonormal system spanning $\boldsymbol{V}_k \times Q_k$, $n = n_v + n_p = \dim \boldsymbol{V}_k + \dim Q_k < \infty$. Without restriction we may suppose that $\psi_l = (\boldsymbol{\psi}_{v,l}, 0) \in \boldsymbol{V}_k \times \{0\}$ for $l = 1, \dots, n_v$ and $\psi_l = (0, \psi_{p,l-n_v}) \in \{0\} \times Q_k$ for $l = n_v + 1, \dots, n$.

As stated in the introduction we reserve "non-italic" symbols U, S, etc. for vectors or matrices over $\mathbb{R}$ or $\mathbb{C}$ in contrast to elements in "abstract" vector spaces. Set

$$\begin{aligned} u_k(t) &= \sum_{m=1}^{n} \mathrm{U}_m(t)\psi_m, & \mathrm{U}_m(t) &\in \mathbb{R}, \\ \mathrm{F}_l(t) &= (\psi_l, f(t))_H, & l &= 1, \dots, n, \\ \mathrm{S}_{lm} &= s(\psi_l, \psi_m), & l, m &= 1, \dots, n. \end{aligned}$$

We see that (3.11) is equivalent to the following periodic boundary value problem in $\mathbb{R}^n$:

Find $\mathrm{U} \in H^1(0, T; \mathbb{R}^n)$ fulfilling

$$\begin{aligned} \mathrm{U}'(t) + \mathrm{S}\mathrm{U}(t) &= \mathrm{F}(t) && \text{for almost all } t \in (0, T), \\ \mathrm{U}(0) &= \mathrm{U}(T). \end{aligned}$$

The method of "variation of constants" yields the following solution formula

$$\mathrm{U}(t) = \exp(-\mathrm{S}t)\mathrm{U}(0) + \int_0^t \exp(-\mathrm{S}(t-\tau))\mathrm{F}(\tau)d\tau$$

Thus, we may reformulate the finite dimensional problem (3.11) as

Find $\mathrm{U} \in H^1(0, T; \mathbb{R}^n)$ with

$$\mathrm{U}(T) = \exp(-\mathrm{S}T)\mathrm{U}(0) + \int_0^T \exp(-\mathrm{S}(T-\tau))\mathrm{F}(\tau)d\tau = \mathrm{U}(0).$$

The problem is thus reduced to finding $\mathrm{U}_0 = \mathrm{U}(0)$ satisfying the following linear equation in $\mathbb{R}^n$:

$$(\exp(\mathrm{S}T) - \mathrm{I})\,\mathrm{U}_0 = \int_0^T \exp(\mathrm{S}\tau)\mathrm{F}(\tau)d\tau. \tag{3.12}$$

It is sufficient to prove that the matrix $\exp(\mathrm{S}T) - \mathrm{I}$ is regular. The matrix is singular iff 1 is an eigenvalue of $\exp(\mathrm{S}T)$. According to [27, Corollary A1.8], this happens iff $2N\pi i/T$ is an eigenvalue of S for some $N \in \mathbb{Z}$, where $i \in \mathbb{C}$ is the imaginary unit. The remaining proof serves to show that S does not have eigenvalues of this form.

The Stokes operator $S \in L(\boldsymbol{V}_k \times Q_k)$ corresponding to S is regular thanks to the stability of the couple $\boldsymbol{V}_k \times Q_k$, ($\mathrm{LBB}_k$). This may be seen e. g. using [32, Theorem 12.2.7]. We may therefore exclude 0 as an eigenvalue of S.

Decompose S as follows:

$$\mathrm{S}\begin{bmatrix} \mathrm{v} \\ \mathrm{p} \end{bmatrix} = \begin{bmatrix} \mathrm{A} & \mathrm{B} \\ -\mathrm{B}^T & 0 \end{bmatrix} \begin{bmatrix} \mathrm{v} \\ \mathrm{p} \end{bmatrix},$$

with $\mathrm{v} \in \mathbb{R}^{n_v}$, $\mathrm{p} \in \mathbb{R}^{n_p}$.

Let $l, m \in \{1, \dots, n_v\}$. We have

$$\mathrm{A}_{lm} = \mathrm{S}_{lm} = s(\psi_l, \psi_m) = a(\boldsymbol{\psi}_{v,l}, \boldsymbol{\psi}_{v,m}),$$

which implies that $\mathrm{A} \in \mathbb{R}^{n_v \times n_v}$ is symmetric and positive definite.

We will denote by $(\cdot,\cdot)_{\mathbb{C}^j}$, $|\cdot|_{\mathbb{C}^j}$ the Euclidean scalar product and norm on $\mathbb{C}^j$, analogously $(\cdot,\cdot)_{\mathbb{R}^j}$ and $|\cdot|_{\mathbb{R}^j}$ on $\mathbb{R}^j$, $j \in \mathbb{N}$. Assume $\lambda \in \mathbb{C} \setminus 0$ is an arbitrary eigenvalue of S with corresponding eigenvector $\Phi \in \mathbb{C}^n$, $|\Phi|_{\mathbb{C}^n} = 1$. Let $\Phi_v \in \mathbb{C}^{n_v}$, $\Phi_p \in \mathbb{C}^{n_p}$ be the components of Φ. We calculate

$$\begin{aligned}
\Re\,\lambda = \Re(\lambda\Phi, \Phi)_{\mathbb{C}^n} &= \Re(\mathrm{S}\Phi, \Phi)_{\mathbb{C}^n}, \\
&= \Re[(\mathrm{A}\Phi_v, \Phi_v)_{\mathbb{C}^{n_v}} + \underbrace{(B\Phi_p, \Phi_v)_{\mathbb{C}^{n_v}} - (B^T\Phi_v, \Phi_p)_{\mathbb{C}^{n_p}}}_{\in i\mathbb{R}}] \\
&= \Re(\mathrm{A}\Phi_v, \Phi_v)_{\mathbb{C}^{n_v}} \\
&= \Re\left(\mathrm{A}(\Re\,\Phi_v + i\,\Im\,\Phi_v), (\Re\,\Phi_v + i\,\Im\,\Phi_v)\right)_{\mathbb{C}^{n_v}} \\
&= (\mathrm{A}\,\Re\,\Phi_v, \Re\,\Phi_v)_{\mathbb{R}^{n_v}} + (\mathrm{A}\,\Im\,\Phi_v, \Im\,\Phi_v)_{\mathbb{R}^{n_v}} \geq 0,
\end{aligned}$$

since A is symmetric positive definite. Please note the transition from the complex scalar product to the real scalar product in the final step. This already shows $\Re\,\lambda \geq 0$. We will make use of more detailed eigenvalue estimates specified in [6, Proposition 2.11]. In the case $\Im\,\lambda \neq 0$ we have

$$0 < \frac{1}{2}\lambda_{\mathrm{A,min}} \leq \Re\,\lambda,$$

with $\lambda_{\mathrm{A,min}}$ as the minimal eigenvalue of the matrix A. If $\Im\,\lambda = 0$ we immediately arrive at $\Re\,\lambda \neq 0$, since $\lambda \neq 0$. We therefore do not have purely imaginary eigenvalues of S. This completes the proof. □

The next lemma proves the stability of finite dimensional solutions.

Lemma 3.2.8

Let the spaces $\boldsymbol{V}_k$, Q_k be defined with the same properties as in Lemma 3.2.7. The solution of (3.11) fulfills the following a-priori estimate:

$$\|u_k\|_{W(0,T)} \leq C\,\|f\|_{L^2(0,T;H)}\,. \tag{3.13}$$

The constant C will generally depend on T, k_s, c_s, C_b (see Lemma 3.1.4 for definitions) but not on $\tilde{c}_{b,k}$.

Proof. We will use the same notation as in the proof of Lemma 3.2.7. For any $\mathrm{X} \in \mathbb{C}^n$ we define $|\mathrm{X}|_U$ on $\mathbb{C}^n$ as follows:

$$|\mathrm{X}|_U^2 := \left\|\sum_{l=1}^{n} \Re(\mathrm{X}_l)\psi_l\right\|_U^2 + \left\|\sum_{l=1}^{n} \Im(\mathrm{X}_l)\psi_l\right\|_U^2.$$

$|\cdot|_U$ is a norm on $\mathbb{C}^n$. We restrict ourselves to proving definiteness. Assume $\mathrm{X} \in \mathbb{C}^n$ with $|\mathrm{X}|_U = 0$. Then

$$0 = \sum_{l=1}^{n} \Re(\mathrm{X}_l)\psi_l = \sum_{l=1}^{n} \Im(\mathrm{X}_l)\psi_l.$$

Since the ψ_l form a basis of $\boldsymbol{V}_k \times Q_k$ this implies

$$\Re \mathrm{X}_l = \Im \mathrm{X}_l = 0, \qquad \text{for all } l = 1, \dots, n,$$

and thus $\mathrm{X} = 0$. Before we start the proof itself it is worth noting a few useful properties that will ease the calculations. Let $\mathrm{U} \in \mathbb{R}^n$, $u = \sum_{l=1}^n \mathrm{U}_l \psi_l \in \boldsymbol{V}_k \times Q_k$, and $\mathrm{V} \in \mathbb{C}^n$. Then

$$\begin{aligned}
|\mathrm{V}|_U^2 = |\Re \mathrm{V} + i\, \Im \mathrm{V}|_U^2 &= |\Re \mathrm{V}|_U^2 + |\Im \mathrm{V}|_U^2 \,, \\
|\mathrm{V}|_{\mathbb{C}^n}^2 &= |\Re \mathrm{V}|_{\mathbb{R}^n}^2 + |\Im \mathrm{V}|_{\mathbb{R}^n}^2 \,, \\
\|u\|_H^2 = \sum_{l,m=1}^n \mathrm{U}_l \mathrm{U}_m (\psi_l, \psi_m)_H &= |\mathrm{U}|_{\mathbb{R}^n}^2 \,, \\
\|u\|_U^2 = \left\| \sum_{l=1}^n \mathrm{U}_l \psi_l \right\|_U^2 &= |\mathrm{U}|_U^2 \,.
\end{aligned}$$

We will use Fourier analysis to derive the estimate (3.13). Define the following terms:

$$\begin{aligned}
e_j(t) = \frac{1}{\sqrt{T}} \exp(2\pi i j t / T) \in \mathbb{C}, &\qquad j \in \mathbb{Z}, \\
\mathrm{U}_l(t) \in \mathbb{R} \text{ with } u_k(t) = \sum_{l=1}^n \mathrm{U}_l(t) \psi_l, & \\
\mathrm{F}_l(t) = (\psi_l, f(t))_H, & \\
\widehat{\mathrm{U}}_l^j = \int_0^T \mathrm{U}_l(t) \bar{e}_j(t) dt, & \\
\widehat{\mathrm{F}}_l^j = \int_0^T \mathrm{F}_l(t) \bar{e}_j(t) dt. &
\end{aligned}$$

Here we denote $\bar{e}_j(t) \in \mathbb{C}$ as the complex conjugate of $e_j(t) \in \mathbb{C}$. Elementary results of Fourier analysis (see e. g. [1, Example 7.9]) yield

$$\mathrm{U}_l = \sum_{j \in \mathbb{Z}} \widehat{\mathrm{U}}_l^j e_j, \qquad \mathrm{U}_l' = \sum_{j \in \mathbb{Z}} \frac{2\pi i j}{T^{3/2}} \widehat{\mathrm{U}}_l^j e_j, \qquad \mathrm{F}_l = \sum_{j \in \mathbb{Z}} \widehat{\mathrm{F}}_l^j e_j,$$

with convergence of the sums in $L^2(0, T; \mathbb{C})$, as well as the Parseval identities

$$\int_0^T |\mathrm{U}_l(t)|^2 \, dt = \sum_{j \in \mathbb{Z}} \left| \widehat{\mathrm{U}}_l^j \right|^2, \qquad \int_0^T |\mathrm{F}_l(t)|^2 \, dt = \sum_{j \in \mathbb{Z}} \left| \widehat{\mathrm{F}}_l^j \right|^2.$$

Now fix $j \in \mathbb{Z}$ and $l \in \{1, \dots, n\}$. Choose $w_k := \psi_l$ in (3.11). Then multiply by $\bar{e}_j(t)$ and integrate from 0 to T. This yields

$$-\int_0^T (\psi_l, u_k(t))_H \bar{e}_j'(t) dt + \int_0^T s(\psi_l, u_k(t)) \bar{e}_j(t) dt = \int_0^T (\psi_l, f(t))_H \bar{e}_j(t) dt,$$

after integrating by parts in the first term. Substituting the basis representation of $u_k(t)$ leads to

$$\sum_{m=1}^{n}\int_0^T \frac{2\pi ij}{T^{3/2}}(\psi_l,\psi_m)_H \mathrm{U}_m(t)\bar{e}_j(t)dt + \sum_{m=1}^{n}\int_0^T s(\psi_l,\psi_m)\mathrm{U}_m(t)\bar{e}_j(t)dt = \int_0^T \mathrm{F}_l(t)\bar{e}_j(t)dt.$$

The last equation is equivalent to the stationary Stokes system in $\mathbb{C}^n$

$$\frac{2\pi ij}{T^{3/2}}\widehat{\mathrm{U}}^j + \mathrm{S}\widehat{\mathrm{U}}^j = \widehat{\mathrm{F}}^j.$$

We test this equation with $\widehat{\mathrm{U}}^j$ which gives

$$\frac{2\pi ij}{T^{3/2}}(\widehat{\mathrm{U}}^j,\widehat{\mathrm{U}}^j)_{\mathbb{C}^n} + (\mathrm{S}\widehat{\mathrm{U}}^j,\widehat{\mathrm{U}}^j)_{\mathbb{C}^n} = (\widehat{\mathrm{F}}^j,\widehat{\mathrm{U}}^j)_{\mathbb{C}^n}. \tag{3.14}$$

Let $u_R := (\boldsymbol{v}_R, p_R) := \sum_{l=1}^n \Re\,\widehat{\mathrm{U}}_l^j\psi_l$, $u_I := (\boldsymbol{v}_I, p_I) := \sum_{l=1}^n \Im\,\widehat{\mathrm{U}}_l^j\psi_l$. We estimate

$$\begin{aligned}
\Re(\mathrm{S}\widehat{\mathrm{U}}^j,\widehat{\mathrm{U}}^j)_{\mathbb{C}^n} &= (\mathrm{S}(\Re\,\widehat{\mathrm{U}}^j),\Re\,\widehat{\mathrm{U}}^j)_{\mathbb{R}^n} + (\mathrm{S}(\Im\,\widehat{\mathrm{U}}^j),\Im\,\widehat{\mathrm{U}}^j)_{\mathbb{R}^n}\\
&= s(u_R,u_R) + s(u_I,u_I)\\
&\geq c_s\left(\|u_R\|_U^2 + \|u_I\|_U^2\right) - k_s\left(\|u_R\|_H^2 + \|u_I\|_H^2\right)\\
&= c_s\left(\left|\Re\,\widehat{\mathrm{U}}^j\right|_U^2 + \left|\Im\,\widehat{\mathrm{U}}^j\right|_U^2\right) - k_s\left(\left|\Re\,\widehat{\mathrm{U}}^j\right|_{\mathbb{R}^n}^2 + \left|\Im\,\widehat{\mathrm{U}}^j\right|_{\mathbb{R}^n}^2\right)\\
&= c_s\left|\widehat{\mathrm{U}}^j\right|_U^2 - k_s\left|\widehat{\mathrm{U}}^j\right|_{\mathbb{C}^n}^2,
\end{aligned}$$

as well as

$$\begin{aligned}
\left|\Im(\mathrm{S}\widehat{\mathrm{U}}^j,\widehat{\mathrm{U}}^j)_{\mathbb{C}^n}\right| &= \left|(\mathrm{S}(\Im\,\widehat{\mathrm{U}}^j),\Re\,\widehat{\mathrm{U}}^j)_{\mathbb{R}^n} - (S(\Re\,\widehat{\mathrm{U}}^j),\Im\,\widehat{\mathrm{U}}^j)_{\mathbb{R}^n}\right|\\
&= |s(u_I,u_R) - s(u_R,u_I)|\\
&= 2\,|b(p_R,\boldsymbol{v}_I) - b(p_I,\boldsymbol{v}_R)|\\
&\leq 2C_b\left(\|p_R\|_0\,\|\boldsymbol{v}_I\|_1 + \|p_I\|_0\,\|\boldsymbol{v}_R\|_1\right)\\
&\leq 2C_b\left(\|u_R\|_H\,\|u_I\|_U + \|u_I\|_H\,\|u_R\|_U\right)\\
&\leq 2C_b\left(\|u_R\|_H^2 + \|u_I\|_H^2\right)^{\frac{1}{2}}\left(\|u_I\|_U^2 + \|u_R\|_U^2\right)^{\frac{1}{2}}\\
&= 2C_b\left|\widehat{\mathrm{U}}^j\right|_{\mathbb{C}^n}\left|\widehat{\mathrm{U}}^j\right|_U,
\end{aligned}$$

with the constants of Lemma 3.1.4. From (3.14) we therefore get

$$\begin{aligned}
c_s\left|\widehat{\mathrm{U}}^j\right|_U^2 &\leq k_s\left|\widehat{\mathrm{U}}^j\right|_{\mathbb{C}^n}^2 + \Re(\mathrm{S}\widehat{\mathrm{U}}^j,\widehat{\mathrm{U}}^j)_{\mathbb{C}^n}\\
&= k_s\left|\widehat{\mathrm{U}}^j\right|_{\mathbb{C}^n}^2 + \Re(\widehat{\mathrm{F}}^j,\widehat{\mathrm{U}}^j)_{\mathbb{C}^n}\\
&\leq k_s\left|\widehat{\mathrm{U}}^j\right|_{\mathbb{C}^n}^2 + \left|(\widehat{\mathrm{F}}^j,\widehat{\mathrm{U}}^j)_{\mathbb{C}^n}\right|,
\end{aligned}$$

and (using Young's inequality)

$$\begin{aligned}\frac{2\pi j}{T^{3/2}}\left|\widehat{\mathrm{U}}^j\right|_{\mathbb{C}^n}^2 &= \Im(\widehat{\mathrm{F}}^j,\widehat{\mathrm{U}}^j)_{\mathbb{C}^n} - \Im(\mathrm{S}\widehat{\mathrm{U}}^j,\widehat{\mathrm{U}}^j)_{\mathbb{C}^n}\\ &\le \left|(\widehat{\mathrm{F}}^j,\widehat{\mathrm{U}}^j)_{\mathbb{C}^n}\right| + 2C_b\left|\widehat{\mathrm{U}}^j\right|_{\mathbb{C}^n}\left|\widehat{\mathrm{U}}^j\right|_U\\ &\le \left|(\widehat{\mathrm{F}}^j,\widehat{\mathrm{U}}^j)_{\mathbb{C}^n}\right| + c_s\left|\widehat{\mathrm{U}}^j\right|_U^2 + C(c_s,C_b)\left|\widehat{\mathrm{U}}^j\right|_{\mathbb{C}^n}^2.\end{aligned}$$

Combining these last two inequalities we have

$$\frac{2\pi j}{T^{3/2}}\left|\widehat{\mathrm{U}}^j\right|_{\mathbb{C}^n}^2 \le 2\left|\widehat{\mathrm{F}}^j\right|_{\mathbb{C}^n}\left|\widehat{\mathrm{U}}^j\right|_{\mathbb{C}^n} + C(k_s,c_s,C_b)\left|\widehat{\mathrm{U}}^j\right|_{\mathbb{C}^n}^2$$

and thus for large j the relation

$$\left|\widehat{\mathrm{U}}^j\right|_{\mathbb{C}^n} \le \frac{C(T,k_s,c_s,C_b)}{j}\left|\widehat{\mathrm{F}}^j\right|_{\mathbb{C}^n}. \tag{3.15}$$

For the periodic solution u_k we may translate this to

$$\begin{aligned}\int_0^T \|u_k(t)\|_H^2\,dt = \int_0^T |\mathrm{U}(t)|_{\mathbb{R}^n}^2\,dt &= \sum_{j\in\mathbb{Z}}\left|\widehat{\mathrm{U}}^j\right|_{\mathbb{C}^n}^2\\ &\le \sum_{j\in\mathbb{Z}}\frac{C(T,k_s,c_s,C_b)}{j^2}\left|\widehat{\mathrm{F}}^j\right|_{\mathbb{C}^n}^2, \qquad \text{by virtue of (3.15)}\\ &\le C\sum_{j\in\mathbb{Z}}\left|\widehat{\mathrm{F}}^j\right|_{\mathbb{C}^n}^2 = C\int_0^T |\mathrm{F}(t)|_{\mathbb{R}^n}^2\,dt = C\int_0^T \|f(t)\|_H^2\,dt.\end{aligned} \tag{3.16}$$

Note that we have been rather brutal in estimating $1/j^2 \le 1$. For the derivative u_k' we need to be more careful. A similar calculation shows:

$$\begin{aligned}\int_0^T \left\|u_k'(t)\right\|_{U'}^2\,dt \le C\int_0^T \left\|u_k'(t)\right\|_H^2\,dt &= C\int_0^T \left|\mathrm{U}'(t)\right|_{\mathbb{C}^n}^2\,dt\\ &= C\sum_{j\in\mathbb{Z}}\frac{4\pi^2 j^2}{T^3}\left|\widehat{\mathrm{U}}^j\right|_{\mathbb{C}^n}^2\\ &\le C\sum_{j\in\mathbb{Z}}\frac{j^2}{j^2}\left|\widehat{\mathrm{F}}^j\right|_{\mathbb{C}^n}^2 = C\int_0^T \|f(t)\|_H^2\,dt.\end{aligned}$$

We now have estimates for $u_k \in L^2(0,T;H)$ and for $u_k' \in L^2(0,T;U')$. What remains to be done is to estimate $u_k \in L^2(0,T;U)$. For this we return to the original equation (3.11) and now choose $w_k := u_k(t)$. Integration yields

$$\begin{aligned}0 = \frac{1}{2}\left(\|u_k(T)\|_H^2 - \|u_k(0)\|_H^2\right) &= \int_0^T (u_k(t),u_k'(t))_H dt\\ &= \int_0^T (u_k(t),f(t))_H dt - \int_0^T s(u_k(t),u_k)dt.\end{aligned}$$

Using (3.8) then gives us

$$\begin{aligned} c_s \int_0^T \|u_k(t)\|_U^2 \, dt &\leq \int_0^T s(u_k(t), u_k(t)) dt + k_s \int_0^T \|u_k(t)\|_H^2 \, dt \\ &= \int_0^T (u_k(t), f(t))_H dt + k_s \int_0^T \|u_k(t)\|_H^2 \, dt \\ &\leq \left(\frac{1}{2} + k_s \right) \int_0^T \|u_k(t)\|_H^2 \, dt + \frac{1}{2} \int_0^T \|f(t)\|_H^2 \, dt \\ &\leq C \int_0^T \|f(t)\|_H^2 \, dt. \end{aligned}$$

Combining estimates finally proves

$$\|u_k\|_{W(0,T)} \leq C(T, k_s, c_s, C_b) \, \|f\|_{L^2(0,T;H)} \, .$$

□

We now turn to the

Proof of 3.2.6. For the proof we will use a constructive Galerkin approach. Since the proof is rather similar to the case of initial value problems we will concentrate on the essential details.

We first construct a sequence of finite dimensional subspaces $\{U_k\}_{k \in \mathbb{N}} \subset U$ with the following properties:

i) $U_k = \boldsymbol{V}_k \times Q_k$, with subspaces $\boldsymbol{V}_k \subset \boldsymbol{V}$, $Q_k \subset Q$.

ii) $\bigcup_{k \in \mathbb{N}} U_k$ is dense in U (and therefore in H).

iii) An inf-sup condition for $b(\cdot, \cdot)$ is fulfilled for each pair $\boldsymbol{V}_k$, Q_k:

$$\inf_{p \in Q_k \setminus \{0\}} \sup_{\boldsymbol{v} \in \boldsymbol{V}_k \setminus \{0\}} \frac{b(p, \boldsymbol{v})}{\|p\|_0 \, \|\boldsymbol{v}\|_1} \geq \widetilde{c}_{b,k} > 0. \tag{$\widetilde{\text{LBB}}$}$$

This may be done as follows: Take a sequence $\{q_m\}_{m \in \mathbb{N}} \subset Q$ which is linearly independent and with $\operatorname{span}\{q_m\}_m$ dense in Q. Define $\boldsymbol{w}_k = \operatorname{div}^{-1} q_k$ according to 3.1.3 and select another linearly independent sequence $\{\widetilde{\boldsymbol{w}}_l\}_{l \in \mathbb{N}}$ whose span is dense in $\boldsymbol{V}$. Define $Q_k = \operatorname{span}\{q_1, \ldots, q_k\}$ and set

$$\boldsymbol{V}_k = \operatorname{span}\left(\{\boldsymbol{w}_1, \ldots, \boldsymbol{w}_k\} \cup \{\widetilde{\boldsymbol{w}}_1, \ldots, \widetilde{\boldsymbol{w}}_k\} \right).$$

We verify that iii) is fulfilled. Let

$$p = \sum_{l=1}^{k} \lambda_k q_k \in Q_k \setminus \{0\}, \qquad \lambda_k \in \mathbb{R}.$$

Define $\boldsymbol{w} := -\operatorname{div}^{-1} p$. Because of the linearity of div^{-1} we get

$$\boldsymbol{w} \in \operatorname{span}\{\boldsymbol{w}_1, \ldots, \boldsymbol{w}_k\} \subset \boldsymbol{V}_k.$$

Then

$$\frac{b(p,\boldsymbol{w})}{\|p\|_0\,\|\boldsymbol{w}\|_1} = \frac{-\int_\Omega p\,\mathrm{div}\,\boldsymbol{w}}{\|p\|_0\,\|\boldsymbol{w}\|_1} = \frac{\int_\Omega p^2}{\|p\|_0\,\|\boldsymbol{w}\|_1} = \frac{\|p\|_0}{\|\boldsymbol{w}\|_1} \geq c_b > 0.$$

The rest follows by taking first a supremum over all $\boldsymbol{w}$ followed by an infimum over all p.

We may therefore use Lemma 3.2.7 to determine a unique solution $u_k = (\boldsymbol{v}_k, p_k) \in H^1(0,T;U_k)$ of the finite dimensional problem

$$\begin{aligned} \big(\psi_k, u_k'(t)\big)_H + s(\psi_k, u_k(t)) = (\psi_k, f(t))_H \quad &\text{for all } \psi_k \in U_k, \text{ f. a. a. } t \in (0,T), \\ u_k(0) = u_k(T). \end{aligned} \tag{3.17}$$

Using Lemma 3.2.8 we gain the estimate

$$\|u_k\|_{W(0,T)} \leq C\,\|f\|_{L^2(0,T;H)},$$

with a constant C independent of k. This uniform stability property is vitally important for the proof.

Since the space $W(0,T)$ is a Hilbert space and thus reflexive there exists a weakly convergent subsequence $\{u_{k_l}\}_{l\in\mathbb{N}}$, $u_{k_l} \rightharpoonup u \in W(0,T)$, $\|u\|_{W(0,T)} \leq C\,\|f\|_{L^2(0,T;H}$ (see e. g. [1]). We may assume without loss of generality that the original sequence $\{u_k\}$ converges weakly to u. It remains to be proven that $u = (\boldsymbol{v}, p)$ is a solution of (P_{per}).

Let $k \in \mathbb{N}$. By using the continuity of the bilinear forms involved we may pass to the limit for the u_k:

$$\big\langle \psi_k, u'(t)\big\rangle_{U\times U'} + s(\psi_k, u(t)) = (\psi_k, f(t))_H \qquad \text{for all } \psi_k \in U_k, \text{ f. a. a. } t \in (0,T).$$

Since the union of spaces U_k is dense in U we verify that this equation still holds when tested with any element of U:

$$\big\langle w, u'(t)\big\rangle_{U\times U'} + s(w, u(t)) = (w, f(t))_H \qquad \text{for all } w \in U, \text{ f. a. a. } t \in (0,T).$$

It remains to be checked that this solution is periodic. Theorem 3.1.2 states that $W(0,T)$ is continuously embedded in $C([0,T];H)$, thus pointwise evaluation of $u(t)$ is meaningful. Let $\varphi \in C^1([0,T])$ with $\varphi(0) = \varphi(T) = 1$. Define $v(t) := \varphi(t)u(t)$. It follows that $v \in W(0,T)$ and

$$v'(t) = \varphi'(t)u(t) + \varphi(t)u'(t).$$

For almost all $s,t \in [0,T]$ the following equation in U' holds:

$$v(t) - v(s) = \int_s^t v'(\tau)d\tau = \int_s^t \varphi'(\tau)u(\tau) + \varphi(\tau)u'(\tau)d\tau.$$

Let $l \in \mathbb{N}$. Then

$$\begin{aligned} \varphi(t)(\psi_l, u(t))_H - \varphi(s)(\psi_l, u(s))_H &= (\psi_l, v(t) - v(s))_H \\ &= \langle \psi_l, v(t) - v(s)\rangle_{U\times U'} \\ &= \langle \psi_l, \int_s^t \varphi'(\tau)u(\tau) + \varphi(\tau)u'(\tau)d\tau\rangle_{U\times U'} \\ &= \int_s^t \varphi'(\tau)(\psi_l, u(\tau))_H + \varphi(\tau)\langle \psi_l, u'(\tau)\rangle_{U\times U'}d\tau. \end{aligned}$$

Since u is continuous with values in H this equations actually holds for all $s, t \in [0, T]$. We choose $s = 0$, $t = T$. It follows that

$$(\psi_l, u(T) - u(0))_H = \int_0^T \varphi'(\tau)(\psi_l, u(\tau))_H + \varphi(\tau)\langle \psi_l, u'(\tau)\rangle_{U\times U'} d\tau$$

for all $l \in \mathbb{N}$. For the finite dimensional solutions u_k we analogously get

$$0 = (\psi_l, u_k(T) - u_k(0))_H = \int_0^T \varphi'(\tau)(\psi_l, u_k(\tau))_H + \varphi(\tau)\langle \psi_l, u_k'(\tau)\rangle_{U\times U'} d\tau$$

for all $k \geq l$. The right hand side of the last two equations may be interpreted as the action of a functional defined on $W(0, T)$. The weak convergence of u_k to u implies that

$$0 = (\psi_l, u(T) - u(0))_H.$$

Since $\operatorname{span}\{\psi_l\}_{l\in\mathbb{N}}$ is dense in H we get $u(T) = u(0)$ which concludes the proof. □

3.2.4 Oscillating equilibrium states

As a final result of this section we now examine the convergence of time dependent solutions to oscillating equilibrium states, under the assumption of periodic forcing. Similar problems in the setting of periodic solutions defined on $\mathbb{R}^n$ were treated e. g. in [4], [45]. The periodic nonlinear compressible Navier-Stokes problem was treated in [74]. We will introduce a few useful definitions first.

We define the following orthogonal decomposition of $\boldsymbol{V} = \boldsymbol{H}_0^1(\Omega)$:

$$\boldsymbol{V} = \boldsymbol{V}_0 \oplus \boldsymbol{V}_\perp,$$

where $\boldsymbol{V}_0 := \ker B^*$, the kernel of the divergence operator, and $\boldsymbol{V}_\perp := (\boldsymbol{V}_0)^\perp$, its orthogonal complement, are closed subspaces of $\boldsymbol{V}$ (confer [32, Lemma 6.1.17]). These definitions give rise to an orthogonal decomposition of $\boldsymbol{V}'$:

$$\begin{aligned}
\boldsymbol{V}_0' &:= \{\boldsymbol{v}' \in \boldsymbol{V}' \mid \langle \boldsymbol{v}', \boldsymbol{v}\rangle = 0 \text{ for all } \boldsymbol{v} \in \boldsymbol{V}_\perp\},\\
\boldsymbol{V}_\perp' &:= \{\boldsymbol{v}' \in \boldsymbol{V}' \mid \langle \boldsymbol{v}', \boldsymbol{v}\rangle = 0 \text{ for all } \boldsymbol{v} \in \boldsymbol{V}_0\},\\
\boldsymbol{V}' &= \boldsymbol{V}_0' \oplus \boldsymbol{V}_\perp', \qquad \boldsymbol{V}_0' \perp \boldsymbol{V}_\perp'.
\end{aligned}$$

$\boldsymbol{V}_0'$, $\boldsymbol{V}_\perp'$ are therefore the *annihilators* of $\boldsymbol{V}_\perp$, $\boldsymbol{V}_0$ respectively.

Lemma 3.2.9
We have the following property for the operators B and K:

1) *The operator B maps Q onto $\boldsymbol{V}_\perp'$. Furthermore we have $B^{-1} \in L(\boldsymbol{V}_\perp', Q)$ with $\|B^{-1}\| \leq \frac{1}{c_b}$.*

2) *The Schur complement operator K is continuously invertible and satisfies*

$$\begin{aligned}
K \in L(Q, Q), &\qquad \|K\| \leq \frac{C_b^2}{c_a},\\
K^{-1} \in L(Q, Q), &\qquad \|K^{-1}\| \leq \frac{C_a^2}{c_a c_b^2}.
\end{aligned}$$

Proof. 1) Because of (3.6) and the Babuška-Brezzi condition (LBB) we may apply [32, Lemma 12.2.9], yielding the result.

2) The first inequality is clear, since $\left\|A^{-1}\right\| \leq \frac{1}{c_a}$, see [32, Theorem 6.5.8]. Let $p \in Q$. Using part i), we may calculate

$$\begin{aligned}\|p\|_0^2 &\leq \frac{1}{c_b^2}\|Bp\|_{-1}^2 = \frac{1}{c_b^2}\left\|A(A^{-1}Bp)\right\|_{-1}^2 \\ &\leq \frac{C_a^2}{c_b^2}\left\|A^{-1}Bp\right\|_1^2 \leq \frac{C_a^2}{c_a c_b^2}\langle A(A^{-1}Bp), A^{-1}Bp\rangle_{\boldsymbol{V}'\times\boldsymbol{V}} \\ &= \frac{C_a^2}{c_a c_b^2}(p, Kp)_0 = \frac{C_a^2}{c_a c_b^2}k(p,p).\end{aligned}$$

The form k is therefore Q-elliptic. Another application of [32, Theorem 6.5.8] provides the invertibility of K and the bound on the norm of K^{-1}. □

Theorem 3.2.10 (Convergence to periodic states)
Assume f is T-periodic, $f|_{(0,T)} \in L^2(0,T;H)$. The solution $u = (\boldsymbol{v}, p)$ of the initial value problem

$$\begin{aligned}\langle\psi, u'(t)\rangle_{U\times U'} + s(\psi, u(t)) &= (\psi, f(t))_H \quad \text{for all } \psi \in U, \text{ f. a. a } t \in (0,T), \\ u(0) &= u_0 \qquad\qquad \text{in } H.\end{aligned} \tag{P_{dp}}$$

may be extended to arbitrarily large times. Let $u_{per} = (\boldsymbol{v}_{per}, p_{per})$ be the periodic solution, extended to the time interval $[0,\infty)$, corresponding to f. Assume $u, u_{per} \in W^1(0,\tau;U)$, $u', u'_{per} \in L^2(0,\tau;H)$ for arbitrary $\tau > 0$. We then have

$$\|u(t) - u_{per}(t)\|_H \leq \frac{C}{\sqrt{t}},$$

with $C > 0$ independent of t.

Proof. Choose $\tau > 0$. Theorem 3.2.2 yields the existence of a solution u on the interval $[0,\tau)$. Using Proposition 3.2.5 we may also extend the periodic solution u_{per} to the interval $[0,\tau)$. Defining $w = (\boldsymbol{v}, p) = u - u_{per}$ we see that w satisfies the following initial value problem:

$$\begin{aligned}(\psi, w'(t))_H + s(\psi, w(t)) &= 0 \qquad\qquad \text{for all } \psi \in U, \text{ f. a. a. } t \in (0,\tau), \\ w(0) = w_0 &= u(0) - u_{per}(0) \quad \text{in } H.\end{aligned} \tag{3.18}$$

This equation immediately leads to the following estimate:

$$\begin{aligned}c\int_0^\tau \|\boldsymbol{v}(t)\|_0^2\,dt \leq \int_0^\tau s(w(t),w(t))\,dt &= -\int_0^\tau \big(w(t), w'(t)\big)_H\,dt \\ &= \frac{1}{2}\left(\|w(0)\|_H^2 - \|w(\tau)\|_H^2\right) \\ &\leq \frac{1}{2}\|w_0\|_H^2 < \infty.\end{aligned} \tag{3.19}$$

Differentiating (3.18) with respect to time, we may repeat the argument to gain

$$\begin{aligned} c\int_0^\tau \left\|\boldsymbol{v}'(t)\right\|_0^2 \,dt \le \int_0^\tau s(w'(t),w'(t))\,dt &= -\int_0^\tau \left(w'(t),w''(t)\right)_H \,dt \\ &= \frac{1}{2}\left(\left\|w'(0)\right\|_H^2 - \left\|w'(\tau)\right\|_H^2\right) \\ &\le \frac{1}{2}\left\|w'(0)\right\|_H^2 < \infty. \end{aligned} \tag{3.20}$$

For the corresponding property of the pressure we first note that the first equation of the system (3.18) is equivalent to

$$\begin{aligned} \boldsymbol{v}'(t) + A\boldsymbol{v}(t) + Bp(t) &= 0 && \text{in } \boldsymbol{V}', \\ p'(t) - B^*\boldsymbol{v}(t) &= 0 && \text{in } Q, \end{aligned}$$

for almost all $t \in [0,\tau)$. This yields

$$v(t) = A^{-1}\left(-Bp(t) - \boldsymbol{v}'(t)\right)$$

as an equation in $\boldsymbol{V}$ and thus

$$p'(t) + Kp(t) = B^*A^{-1}\boldsymbol{v}'(t)$$

as an equation in Q, where $K = B^*A^{-1}B$ is the Schur complement operator defined above. Testing this equation with $p(t)$ and integrating over time as before yields

$$\begin{aligned} \left\|p(\tau)\right\|_0^2 &= \left\|p_0\right\|_0^2 + 2\int_0^\tau (p(t), B^*A^{-1}\boldsymbol{v}'(t))_0\,dt - 2\int_0^\tau (p(t),Kp(t))_0\,dt \\ &\le \left\|p_0\right\|_0^2 + c_k\int_0^\tau \left\|p(t)\right\|_0^2\,dt + C\int_0^\tau \left\|\boldsymbol{v}'(t)\right\|_{-1}^2\,dt - 2c_k\int_0^\tau \left\|p(t)\right\|_0\,dt \\ &\le \left\|p_0\right\|_0^2 - c_k\int_0^\tau \left\|p(t)\right\|_0^2\,dt + C\int_0^\tau \left\|\boldsymbol{v}'(t)\right\|_0^2\,dt. \end{aligned} \tag{3.21}$$

This, together with (3.20), implies

$$\left\|p(\tau)\right\|_0^2 + c_k\int_0^\tau \left\|p(t)\right\|_0^2\,dt \le C < \infty. \tag{3.22}$$

Combining (3.19) and (3.22) gives

$$\int_0^\tau \left\|w(t)\right\|_H^2\,dt \le C < \infty. \tag{3.23}$$

Now choose $\psi = 2tw(t)$ in (3.18) and integrate over time. Since

$$\begin{aligned} \frac{d}{dt}\left(t\left\|w(t)\right\|_H^2\right) &= \left\|w(t)\right\|_H^2 + 2t\left(w(t),w'(t)\right)_H \\ &= \left\|w(t)\right\|_H^2 - 2ts(w(t),w(t)), \end{aligned}$$

we arrive at

$$\begin{aligned}\tau \|w(\tau)\|_H^2 &= \int_0^\tau \|w(t)\|_H^2 \, dt - 2\int_0^\tau ts(w(t), w(t)) \, dt \\ &= \int_0^\tau \|w(t)\|_H^2 \, dt - 2\int_0^\tau ta(\boldsymbol{v}(t), \boldsymbol{v}(t)) \, dt \\ &\leq \int_0^\tau \|w(t)\|_H^2 \, dt \leq C < \infty,\end{aligned}$$

where we have used (3.23) in the last line. This proves the theorem. □

3.3 Quasi-stationary approach

In the physical applications the forcing terms are typically given by a harmonic signal:

$$\begin{aligned}\boldsymbol{f}_v(t, \boldsymbol{x}) &= \widehat{\boldsymbol{f}}_{vc}(\boldsymbol{x}) \cos(\omega t) + \widehat{\boldsymbol{f}}_{vs}(\boldsymbol{x}) \sin(\omega t), \\ f_p(t, \boldsymbol{x}) &= \widehat{f}_{pc}(\boldsymbol{x}) \cos(\omega t) + \widehat{f}_{ps}(\boldsymbol{x}) \sin(\omega t), \\ \boldsymbol{g}(t, \boldsymbol{x}) &= \widehat{\boldsymbol{g}}_c(\boldsymbol{x}) \cos(\omega t) + \widehat{\boldsymbol{g}}_s(\boldsymbol{x}) \sin(\omega t),\end{aligned} \tag{3.24}$$

with a frequency $\omega = 2\pi/T > 0$. As proven above the solution of the acoustic system will converge against a periodic equilibrium state for $t \to \infty$. As will become clear later this periodic equilibrium state must also be time harmonic. Since the equilibrium state is what we are interested in when solving the full problem we may attempt to split the spatial and temporal dependence of the acoustic field solution. This eliminates the need for a time discretization. To be precise, we consider the following *ansatz*:

$$\begin{aligned}\boldsymbol{v}(t, \boldsymbol{x}) &= \widehat{\boldsymbol{v}}_c(\boldsymbol{x}) \cos(\omega t) + \widehat{\boldsymbol{v}}_s(\boldsymbol{x}) \sin(\omega t), \\ p(t, \boldsymbol{x}) &= \widehat{p}_c(\boldsymbol{x}) \cos(\omega t) + \widehat{p}_s(\boldsymbol{x}) \sin(\omega t),\end{aligned} \tag{3.25}$$

with a frequency ω equal to the driving frequency of the boundary conditions and right hand sides in (3.24). This idea is standard for solving time harmonic problems, although a decomposition using the complex terms $\exp(i\omega t)$, $\exp(-i\omega t)$ is usually used instead.

After substituting these formulae for $\boldsymbol{v}$ and p in system (3.1) and using the linear independence of sine and cosine functions we arrive at four new field equations in the unknowns $\widehat{\boldsymbol{v}}_i$, $\widehat{p}_i$, $i = 1, 2$:

$$\begin{aligned}\omega\mu_v \widehat{\boldsymbol{v}}_s - \nu_1 \Delta \widehat{\boldsymbol{v}}_c - \nu_2 \nabla(\nabla \cdot \widehat{\boldsymbol{v}}_c) + \nabla \widehat{p}_c &= \widehat{\boldsymbol{f}}_{vc}, \\ -\omega\mu_v \widehat{\boldsymbol{v}}_c - \nu_1 \Delta \widehat{\boldsymbol{v}}_s - \nu_2 \nabla(\nabla \cdot \widehat{\boldsymbol{v}}_s) + \nabla \widehat{p}_s &= \widehat{\boldsymbol{f}}_{vp}, \\ \omega\mu_p \widehat{p}_s + \nabla \cdot \widehat{\boldsymbol{v}}_c &= \widehat{f}_{pc}, \\ -\omega\mu_p \widehat{p}_c + \nabla \cdot \widehat{\boldsymbol{v}}_s &= \widehat{f}_{ps} \quad \text{in } \Omega, \\ \widehat{\boldsymbol{v}}_c &= \widehat{\boldsymbol{g}}_c, \\ \widehat{\boldsymbol{v}}_s &= \widehat{\boldsymbol{g}}_s \quad \text{on } \partial\Omega.\end{aligned} \tag{3.26}$$

We are now faced with solving only one stationary system at the price of twice as many unknowns as before.

For the analysis of this system we will again introduce function spaces and bilinear forms.

$$\begin{aligned} X &= \boldsymbol{V} \times \boldsymbol{V}, \\ Y &= Q \times Q, \\ X' &= \boldsymbol{V}' \times \boldsymbol{V}' \quad \text{as the dual space of } X, \\ Y' &= Q \times Q \quad\ \ \text{as the dual space of } Y. \end{aligned} \tag{3.27}$$

We will equip X and Y with the natural scalar products and norms. We define $(f,g)_0 = (\boldsymbol{f}_c, \boldsymbol{g}_c)_0 + (\boldsymbol{f}_s, \boldsymbol{g}_s)_0$ for $f = (\boldsymbol{f}_c, \boldsymbol{f}_s)$, $g = (\boldsymbol{g}_c, \boldsymbol{g}_s) \in X$.

Let $u, v \in X$, $p, q \in Y$ and decompose $u = (\boldsymbol{u}_c, \boldsymbol{u}_s)$, etc. We define the following bilinear forms:

$$\begin{aligned} \mathfrak{a} &: X \times X \to \mathbb{R}, \\ \mathfrak{a}(u,v) &= \nu_1 \int_\Omega (\nabla \boldsymbol{u}_c : \nabla \boldsymbol{v}_c + \nabla \boldsymbol{u}_s : \nabla \boldsymbol{v}_s) \\ &\quad + \nu_2 \int_\Omega ((\nabla \cdot \boldsymbol{u}_c)(\nabla \cdot \boldsymbol{v}_c) + (\nabla \cdot \boldsymbol{u}_s)(\nabla \cdot \boldsymbol{v}_s)) \\ &\quad + \omega \mu_v \int_\Omega (\boldsymbol{u}_c \cdot \boldsymbol{v}_s - \boldsymbol{u}_s \cdot \boldsymbol{v}_c), \\ \mathfrak{b} &: Y \times X \to \mathbb{R}, \\ \mathfrak{b}(p,u) &= b(p_c, \boldsymbol{u}_c) + b(p_s, \boldsymbol{u}_s), \\ \mathfrak{c} &: Y \times Y \to \mathbb{R}, \\ \mathfrak{c}(p,q) &= \omega \mu_p \int_\Omega (p_c q_s - p_s q_c). \end{aligned} \tag{3.28}$$

These properties of $\mathfrak{a}$, $\mathfrak{b}$, $\mathfrak{c}$ are easily verified:

Lemma 3.3.1
The bilinear forms defined in (3.28) fulfill

a) $\mathfrak{a}$ is X-elliptic, meaning there exist $c_\mathfrak{a}, C_\mathfrak{a} > 0$ so that for all $u, v \in X$

$$\begin{aligned} |\mathfrak{a}(u,v)| &\le C_\mathfrak{a} \|u\|_X \|v\|_X, \\ \mathfrak{a}(u,u) &\ge c_\mathfrak{a} \|u\|_X^2. \end{aligned}$$

b) There exist $c_\mathfrak{b}, C_\mathfrak{b} > 0$ so that for all $u \in X$, $p \in Y$

$$|\mathfrak{b}(p,u)| \le C_\mathfrak{b} \|p\|_Y \|u\|_X, \tag{3.29}$$

$$\inf_{q \in Y \setminus \{0\}} \sup_{v \in X \setminus \{0\}} \frac{\mathfrak{b}(p,v)}{\|q\|_Y \|v\|_X} \ge c_\mathfrak{b}. \tag{3.30}$$

c) The form $\mathfrak{c}$ is weakly coercive, *in other words there is $C_\mathfrak{c} > 0$ so that for all $p, q \in Y$*

$$|\mathfrak{c}(p,q)| \le C_\mathfrak{c} \|p\|_Y \|q\|_Y, \tag{3.31}$$

$$\mathfrak{c}(p,p) \ge 0. \tag{3.32}$$

Proof. We restrict ourselves proving to the inf-sup condition (3.30) for $\mathfrak{b}$. Let $p \in Y \setminus \{0\}$. Use Lemma 3.1.4, b) to get $v = (\boldsymbol{v}_c, \boldsymbol{v}_s) \in X$, $\|\boldsymbol{v}_c\|_1 = \|\boldsymbol{v}_s\|_1 = 1$ with

$$\begin{aligned} b(p_c, \boldsymbol{v}_c) &\geq c_b \|p_c\|_0 , \\ b(p_s, \boldsymbol{v}_s) &\geq c_b \|p_s\|_0 . \end{aligned}$$

This implies

$$\begin{aligned} \frac{\mathfrak{b}(p,v)}{\|v\|_X} &= \frac{1}{\sqrt{2}} \left(b(p_c, \boldsymbol{v}_c) + b(p_s, \boldsymbol{v}_s) \right) \\ &\geq \frac{c_b}{\sqrt{2}} \left(\|p_c\|_0 + \|p_s\|_0 \right) \geq C(c_b) \|p\|_Y \end{aligned}$$

and thus

$$\sup_{v \in X \setminus \{0\}} \frac{\mathfrak{b}(p,v)}{\|v\|_X \|p\|_Y} \geq \sup_{v \in X, \|\boldsymbol{v}_c\| = \|\boldsymbol{v}_s\| = 1} \frac{\mathfrak{b}(p,v)}{\|v\|_X \|p\|_Y} \geq C(c_b).$$

□

We may now define a variational formulation of (3.26) in the same way as before.

Problem 3.3.2 (Weak formulation, quasi-stationary problem)
Given $f_X \in X'$, $f_Y \in Y'$ find $v = (\boldsymbol{v}_c, \boldsymbol{v}_s) \in X$ and $p = (p_c, p_s) \in Y$ so that

$$\begin{aligned} \mathfrak{a}(w,v) + \mathfrak{b}(p,w) &= \langle w, f_X \rangle_{X \times X'} \quad \text{for all } w \in X, \\ -\mathfrak{b}(q,v) + \mathfrak{c}(q,p) &= \langle q, f_Y \rangle_{Y \times Y'} \quad \text{for all } q \in Y. \end{aligned} \tag{P_{qs}}$$

Existence and uniqueness for a generalized saddle point system with the given properties are well known.

Theorem 3.3.3
Problem (P_{qs}) possesses a unique solution (v,p). The following a-priori estimate holds:

$$\|v\|_X + \|p\|_Y \leq C(\|f_X\|_{X'} + \|f_Y\|_{Y'}).$$

Proof. The properties stated in Lemma 3.3.1 imply that we are in the saddle point problem framework specified in [53, Theorem 2.2]. See also [43] and [12]. □

Remark 3.3.4 (Convergence to harmonic states)
Let $T = 2\pi/\omega$ and forcing terms $f = (\boldsymbol{f}_v, f_p) \in L^2(0,T;H)$ of the form (3.24) be given. The periodic solution u_{per} of the problem

$$\begin{aligned} \langle w, u'_{per}(t) \rangle_{U \times U'} + s(w, u_{per}(t)) &= (w, f(t))_H \qquad \text{for all } w \in U, \text{ f. a. a. } t \in (0,T), \\ u_{per}(0) &= u_{per}(T), \end{aligned}$$

is obviously given by

$$\begin{aligned}
\boldsymbol{v}_{per} &: [0,T] \to \boldsymbol{V},\\
&\boldsymbol{v}_{per}(t) = \widehat{\boldsymbol{v}}_c \cos(\omega t) + \widehat{\boldsymbol{v}}_s \sin(\omega t),\\
p_{per} &: [0,T] \to Q,\\
&p_{per}(t) = \widehat{p}_c \cos(\omega t) + \widehat{p}_s \sin(\omega t),\\
&u_{per}(t) = (\boldsymbol{v}(t), p(t)),
\end{aligned}$$

which is smooth in time. We extend u_{per} to arbitrary times as in Proposition 3.2.5 yielding $\widetilde{u}_{per} \in C^\infty([0,\tau], U)$, $\tau > 0$. Assuming any sufficiently regular starting value u_0, we may apply Theorem 3.2.10 to guarantee the convergence of the solution u of the corresponding initial value Problem (P_{dp}) against $\widetilde{u}_{per}$ for $t \to \infty$.

3.4 Some generalizations

The theory for the problems presented in Sections 3.2 and 3.3 used the pair of spaces $U = \boldsymbol{V} \times Q = \boldsymbol{H}^1_0(\Omega) \times L^2_0(\Omega)$ which is standard in the treatment of Navier-Stokes equations. We will now present possibilities to extend the prior results to problems with solutions in $\boldsymbol{H}^1(\Omega) \times L^2(\Omega)$ – this implies the possibility of 1) inhomogeneous boundary conditions for velocity and 2) nonzero mean value for pressure.

The methods for both cases are similar in that we attempt to reduce problems back to the setting of the prior sections. Alternatively, the theory of the prior sections could have been formulated in this generalized setting from the beginning. This approach, however, was rejected in favor of a simpler presentation with fewer technical details and different cases to consider.

We first extend the bilinear forms a, b, s of (3.5) to larger spaces:

$$\begin{aligned}
\tilde{\boldsymbol{V}} &:= \boldsymbol{H}^1(\Omega),\\
\tilde{Q} &:= L^2(\Omega),\\
\tilde{H} &:= \boldsymbol{L}^2(\Omega) \times L^2(\Omega),\\
a : \tilde{\boldsymbol{V}} \times \tilde{\boldsymbol{V}} &\to \mathbb{R},\\
a(\boldsymbol{v}, \boldsymbol{w}) &= \nu_1 \int_\Omega \nabla \boldsymbol{v} : \nabla \boldsymbol{w} + \nu_2 \int_\Omega (\nabla \cdot \boldsymbol{v})(\nabla \cdot \boldsymbol{w}),\\
b : \tilde{Q} \times \tilde{\boldsymbol{V}} &\to \mathbb{R},\\
b(p, v) &= -\int_\Omega p \nabla \cdot \boldsymbol{v},\\
s : (\tilde{\boldsymbol{V}} \times \tilde{Q})^2 &\to \mathbb{R},\\
s((\boldsymbol{v}, p), (\boldsymbol{w}, q)) &= a(\boldsymbol{v}, \boldsymbol{w}) + b(q, \boldsymbol{v}) - b(p, \boldsymbol{w}).
\end{aligned} \tag{3.33}$$

In the same way we now extend the bilinear forms $\mathfrak{a}$, $\mathfrak{b}$, $\mathfrak{c}$ defined in (3.28) to

larger spaces.

$$\begin{aligned} \tilde{X} &= \tilde{\boldsymbol{V}} \times \tilde{\boldsymbol{V}}, \\ \tilde{Y} &= \tilde{Q} \times \tilde{Q}, \\ \tilde{X}' &= \tilde{\boldsymbol{V}}' \times \tilde{\boldsymbol{V}}' \quad \text{as the dual space of } \tilde{X}, \\ \tilde{Y}' &= \tilde{Q} \times \tilde{Q} \quad \text{as the dual space of } \tilde{Y}. \end{aligned} \tag{3.34}$$

3.4.1 Inhomogeneous velocity boundary conditions

As a first step we will generalize the following problems to the case of inhomogeneous Dirichlet boundary conditions for velocity:

- the stationary problem 3.1.8,
- the initial value problem 3.1.6,
- the time periodic problem 3.2.4,
- the quasi-stationary problem 3.3.2.

Let $\Gamma = \partial\Omega$ be the boundary of the domain. As before we assume that Dirichlet boundary conditions for the velocity are stated on the entire boundary Γ. We first introduce an analog of the classical harmonic extension adapted to the Stokes operator S. For this we define the space of velocity traces

$$\boldsymbol{H}^{\frac{1}{2}}(\Gamma) = \boldsymbol{W}^{\frac{1}{2},2}(\Gamma) = T(\tilde{\boldsymbol{V}}) \subset \boldsymbol{L}^2(\Gamma)$$

with norm $\|\cdot\|_{\frac{1}{2}} = \|\cdot\|_{\frac{1}{2},2}$ in the notation of Theorem 1.2.7. In this subsection we will need to extend the embedding i_1 of (3.2) as follows

$$\begin{aligned} i_1 : \tilde{\boldsymbol{V}} \times Q &\to H, \\ i_1(f) &= f. \end{aligned}$$

Lemma 3.4.1
Let $\boldsymbol{g} \in \boldsymbol{H}^{\frac{1}{2}}(\Gamma)$ and $g = (\boldsymbol{g}_c, \boldsymbol{g}_s) \in \boldsymbol{H}^{\frac{1}{2}}(\Gamma)^2$.

1. *There exists a unique function $u = (\boldsymbol{v}, p) \in \tilde{\boldsymbol{V}} \times Q$ satisfying*

$$\begin{aligned} a(\boldsymbol{w}, \boldsymbol{v}) + b(p, \boldsymbol{w}) &= 0 \quad \text{for all } \boldsymbol{w} \in \boldsymbol{V}, \\ -b(q, \boldsymbol{v}) &= 0 \quad \text{for all } q \in Q, \\ T\boldsymbol{v} &= \boldsymbol{g}, \end{aligned} \tag{3.35}$$

with T as the trace operator of 1.2.7. The thus defined operator

$$\begin{aligned} E_0 : \boldsymbol{H}^{\frac{1}{2}}(\Gamma) &\to \tilde{\boldsymbol{V}} \times Q, \\ E_0(\boldsymbol{g}) &= u, \end{aligned} \tag{3.36}$$

is furthermore linear and continuous.

2. *Recall the notation of* (3.27). *There exist unique functions* $v \in \tilde{X}$, $p \in Y$ *satisfying*

$$\begin{aligned} \mathfrak{a}(w,v) + \mathfrak{b}(p,w) &= 0 \qquad \text{for all } w \in X, \\ -\mathfrak{b}(q,v) + \mathfrak{c}(q,p) &= 0 \qquad \text{for all } q \in Y, \\ T\boldsymbol{v}_c &= \boldsymbol{g}_c, \\ T\boldsymbol{v}_s &= \boldsymbol{g}_s. \end{aligned} \tag{3.37}$$

This again defines a linear and continuous operator

$$\begin{aligned} E_{qs} : \boldsymbol{H}^{\frac{1}{2}}(\Gamma)^2 &\to \tilde{X} \times Y, \\ E_{qs}(g) &= (v,p). \end{aligned} \tag{3.38}$$

Proof. We first turn to the case of the Stokes extension operator E_0. Let $\boldsymbol{g} \in \boldsymbol{H}^{\frac{1}{2}}(\Gamma)$. Choose an extension $E\boldsymbol{g} \in \tilde{\boldsymbol{V}}$ according to Theorem 1.2.7. This extension is naturally not unique, in fact we may add any element of $\boldsymbol{V}$ to get another possible extension of $\boldsymbol{g}$. Define the function $f = (E\boldsymbol{g}, 0) \in \tilde{\boldsymbol{V}} \times Q$ and let $\tilde{u} = (\tilde{\boldsymbol{v}}, \tilde{p}) \in U$ be the unique solution of

$$\begin{aligned} a(\boldsymbol{w}, \tilde{\boldsymbol{v}}) + b(\tilde{p}, \boldsymbol{w}) &= -a(\boldsymbol{w}, E\boldsymbol{g}) \qquad && \text{for all } \boldsymbol{w} \in \boldsymbol{V}, \\ -b(q, \tilde{\boldsymbol{v}}) &= b(q, E\boldsymbol{g}) && \text{for all } q \in Q. \end{aligned}$$

given by Lemma 3.2.1. Now set $u = (\boldsymbol{v}, p) = \tilde{u} + f \in \tilde{\boldsymbol{V}} \times Q$.

It follows that

$$\begin{aligned} a(\boldsymbol{w}, \boldsymbol{v}) + b(p, \boldsymbol{w}) &= a(\boldsymbol{w}, \tilde{\boldsymbol{v}}) + a(\boldsymbol{w}, E\boldsymbol{g}) + b(\tilde{p}, \boldsymbol{w}) = 0, \\ -b(q, \boldsymbol{v}) &= -b(q, \tilde{\boldsymbol{v}}) - b(q, E\boldsymbol{g}) = 0, \end{aligned}$$

for all $\boldsymbol{w} \in \boldsymbol{V}$, $q \in Q$, and $T\boldsymbol{v} = T\tilde{\boldsymbol{v}} + \boldsymbol{g} = \boldsymbol{g}$, meaning that (3.35) is fulfilled. To show that u is independent of the choice of extension $E\boldsymbol{g}$ let u_1, u_2 be two solutions fulfilling (3.35). It follows that $w = u_1 - u_2$ fulfills $Sw = 0$, $w \in U$. Lemma 3.2.1 yields $w = 0$ and thus uniqueness of u.

The operator E_0 is therefore well-defined. The linearity of E_0 follows from the linearity of the operators E and S. As for continuity we obtain

$$\begin{aligned} \|E_0\boldsymbol{g}\|_U = \|u\|_U &\leq \|\tilde{u}\|_U + \|f\|_U \\ &\leq C \|E\boldsymbol{g}\|_1 \leq C \|\boldsymbol{g}\|_{\frac{1}{2}}, \end{aligned}$$

where we have extended $\|\cdot\|_U$ as $\|\cdot\|_{\tilde{\boldsymbol{V}} \times Q}$. The proof of the second part for E_{qs} is similar. □

We may now reformulate the stationary problems (P_{stat}) and (P_{qs}) to include arbitrary boundary values for velocity.

Problem 3.4.2 (Inhomogeneous stationary problem)
Let $f = (\boldsymbol{f}_v, f_p) \in U'$ *and* $\boldsymbol{g} \in \boldsymbol{H}^{\frac{1}{2}}(\Gamma)$. *Find* $u = (\boldsymbol{v}, p) \in E_0\boldsymbol{g} + U \subset \tilde{\boldsymbol{V}} \times Q$ *so that*

$$\begin{aligned} a(\boldsymbol{w}, \boldsymbol{v}) + b(p, \boldsymbol{w}) &= \langle \boldsymbol{w}, \boldsymbol{f}_v \rangle_{\boldsymbol{V} \times \boldsymbol{V}'} \quad \text{for all } \boldsymbol{w} \in \boldsymbol{V}, \\ -b(q, \boldsymbol{v}) &= (q, f_p)_0 \qquad \text{for all } q \in Q. \end{aligned} \tag{$\mathrm{P}_{stat,\boldsymbol{g}}$}$$

Problem 3.4.3 (Inhomogeneous quasi-stationary problem)
Given right hand sides $f_X \in X'$, $f_Y \in Y'$ and boundary values $g = (\boldsymbol{g}_c, \boldsymbol{g}_s) \in \boldsymbol{H}^{\frac{1}{2}}(\Gamma)$, find $(v,p) \in E_{qs}g + X \times Y$ so that

$$\begin{aligned} \mathfrak{a}(w,v) + \mathfrak{b}(p,w) &= \langle w, f_X\rangle_{X\times X'} \quad \text{for all } w \in X, \\ -\mathfrak{b}(q,v) + \mathfrak{c}(q,p) &= \langle q, f_Y\rangle_{Y\times Y'} \quad \text{for all } q \in Y. \end{aligned} \tag{$\mathrm{P}_{qs,\boldsymbol{g}}$}$$

Lemma 3.4.4
Let $f = (\boldsymbol{f}_v, f_p) \in U'$ and $\boldsymbol{g} \in \boldsymbol{H}^{\frac{1}{2}}(\Gamma)$, as well as $f_X \in X'$, $f_Y \in Y'$, and $g = (\boldsymbol{g}_c, \boldsymbol{g}_s) \in \boldsymbol{H}^{\frac{1}{2}}(\Gamma)$.

1. *There exists a unique solution $u = (\boldsymbol{v}, p) \in E_0\boldsymbol{g} + U$ of ($\mathrm{P}_{stat,\boldsymbol{g}}$). We have the stability estimate*

$$\|\boldsymbol{v}\|_1 + \|p\|_0 \le C(\|\boldsymbol{f}_v\|_{\boldsymbol{V}'} + \|f_p\|_0 + \|\boldsymbol{g}\|_{\frac{1}{2}}). \tag{3.39}$$

2. *There exist unique solutions $v = (\boldsymbol{v}_c, \boldsymbol{v}_s) \in E_{qs}g + X$ and $p = (p_c, p_s) \in Y$ of ($\mathrm{P}_{qs,\boldsymbol{g}}$). We have the estimate*

$$\|v\|_X + \|p\|_Y \le C(\|f_X\|_{X'} + \|f_Y\|_{Y'} + \|g\|_{\boldsymbol{H}^{\frac{1}{2}}(\Gamma)^2}).$$

Proof. To solve ($\mathrm{P}_{stat,\boldsymbol{g}}$) we simply solve the corresponding homogeneous problem of finding $\tilde{u} \in U$ with

$$s(w,\tilde{u}) = \langle w, f\rangle_{U\times U'} \qquad \text{for all } w \in U,$$

and then set $u = \tilde{u} + E_0\boldsymbol{g}$, which does the trick. This solution is unique because a difference of two such solutions is a solution of (P_{stat}) with zero right hand sides. The a-priori bound on the solution u follows using the a-priori bound of Lemma 3.2.1 on $\tilde{u}$ together with the continuity of the operator E_0 given by Lemma 3.4.1.

Similar methods apply to the quasi-stationary problem (P_{qs}). □

For the instationary problem (P) and periodic problem (P_{per}) we may proceed in an analogous manner.

Lemma 3.4.5
Let $\boldsymbol{g} \in H^1(0,T;\boldsymbol{H}^{\frac{1}{2}}(\Gamma))$.

1. *There exists a unique function $u = (\boldsymbol{v}, p) \in H^1(0,T;U') \cap L^2(0,T;\tilde{\boldsymbol{V}} \times Q)$ satisfying*

$$\begin{aligned} \langle w, u'(t)\rangle_{U\times U'} + s(w,u(t)) &= 0 \qquad \text{for all } w \in U, \text{f. a. a. } t \in (0,T), \\ u(0) &= 0 \qquad \text{in } H, \\ T(\boldsymbol{v}(t)) &= \boldsymbol{g}(t) \quad \text{f. a. a. } t \in (0,T). \end{aligned} \tag{3.40}$$

The operator

$$\begin{aligned} \mathcal{E}_0 : H^1(0,T;\boldsymbol{H}^{\frac{1}{2}}(\Gamma)) &\to H^1(0,T;U') \cap L^2(0,T;\tilde{\boldsymbol{V}} \times Q), \\ \mathcal{E}_0(\boldsymbol{g}) &= u, \end{aligned} \tag{3.41}$$

is linear and continuous.

2. *Assume in addition that* $\boldsymbol{g}(0) = \boldsymbol{g}(T)$. *Then there exists a unique function* $u_{per} = (\boldsymbol{v}, p) \in H^1(0,T;U') \cap L^2(0,T;\tilde{\boldsymbol{V}} \times Q)$ *satisfying*

$$\begin{aligned} \langle w, u'_{per}(t)\rangle_{U\times U'} + s(w, u_{per}(t)) &= 0 && \text{for all } w \in U, \text{f. a. a. } t \in (0,T), \\ u_{per}(0) &= u_{per}(T) && \text{in } H, \\ T(\boldsymbol{v}(t)) &= \boldsymbol{g}(t) && \text{f. a. a. } t \in (0,T). \end{aligned} \tag{3.42}$$

The operator

$$\begin{aligned} \mathcal{E}_{per} : H^1(0,T;\boldsymbol{H}^{\frac{1}{2}}(\Gamma)) &\to H^1(0,T;U') \cap L^2(0,T;\tilde{\boldsymbol{V}} \times Q), \\ \mathcal{E}_{per}(\boldsymbol{g}) &= u_{per}, \end{aligned} \tag{3.43}$$

is linear and continuous.

Proof. Let $\boldsymbol{g} \in H^1(0,T;\boldsymbol{H}^{\frac{1}{2}}(\Gamma))$. For almost all $t \in (0,T)$ we may choose the extensions $E_0(\boldsymbol{g}(t)), E_0(\boldsymbol{g}'(t)) \in \tilde{\boldsymbol{V}}$ with the extension operator E_0 of Lemma 3.4.1. Define $f(t) = E_0(\boldsymbol{g}(t))$, $\tilde{f}(t) = E_0(\boldsymbol{g}'(t))$, both of which are in $\tilde{\boldsymbol{V}} \times Q$ for almost all t.

Since the operator E_0 is continuous we obtain that f, $\tilde{f}$ are measurable as functions of t. Furthermore

$$\begin{aligned} \int_0^T \|f(t)\|^2_{\tilde{\boldsymbol{V}}\times Q}\, dt &\le C \int_0^T \|\boldsymbol{g}(t)\|^2_{\frac{1}{2}}\, dt \\ &\le \|\boldsymbol{g}\|^2_{H^1(0,T;\boldsymbol{H}^{\frac{1}{2}}(\Gamma))} < \infty, \end{aligned}$$

similarly for $\tilde{f}$. Thus f, $\tilde{f}$ are functions in $L^2(0,T;\tilde{\boldsymbol{V}} \times Q)$. In addition, we have demonstrated that the linear operator

$$\begin{aligned} \mathcal{E} : H^1(0,T;\boldsymbol{H}^{\frac{1}{2}}(\Gamma)) &\to L^2(0,T;\tilde{\boldsymbol{V}} \times Q), \\ (\mathcal{E}\boldsymbol{g})(t) &= E_0(\boldsymbol{g}(t)), \end{aligned}$$

is continuous. We now show that $\tilde{f}$ is the distributional time derivative of f. Let $\varphi \in C_0^\infty(0,T)$ be a scalar test function on the time interval. Then

$$\begin{aligned} \int_0^T E_0(\boldsymbol{g}'(t))\varphi(t)\, dt + \int_0^T E_0(\boldsymbol{g}(t))\varphi'(t)\, dt &= \int_0^T E_0(\varphi(t)\boldsymbol{g}'(t) + \varphi'(t)\boldsymbol{g}(t))\, dt \\ &= E_0\Big(\int_0^T \varphi(t)\boldsymbol{g}'(t) + \varphi'(t)\boldsymbol{g}(t)\, dt\Big) \\ &= 0, \end{aligned}$$

where the second step was possible since E_0 is continuous. This shows that $\mathcal{E}(\boldsymbol{g})$ possesses the weak derivative $\mathcal{E}(\boldsymbol{g})' = \mathcal{E}(\boldsymbol{g}')$, in other words $f' = \tilde{f}$. As in (3.2) we interpret $f'(t)$ as a functional defined on U by

$$\langle f'(t), w\rangle_{U'\times U} = (f'(t), w)_H,$$

for all $w \in U$. This means that the problem of finding $\tilde{u} \in W(0,T)$ satisfying

$$\begin{aligned} \langle w, \tilde{u}'(t)\rangle_{U\times U'} + s(w,\tilde{u}(t)) & \\ = \langle w, -f'(t) + \underbrace{Sf(t)}_{=S(E_0\boldsymbol{g}(t))=0}\rangle_{U\times U'} & \quad \text{for all } w \in U, \text{f. a. a. } t \in (0,T), \\ \tilde{u}(0) = -f(0) & \quad \text{in } H, \end{aligned}$$

is well posed. As above we then set $u = \tilde{u} + f$. As in Lemma 3.4.1 above we verify that u fulfills (3.40) and is unique with this property. We define $\mathcal{E}_0(\boldsymbol{g}) = u$.

To construct the periodic operator $\mathcal{E}_{per}$ we pose the problem: Find a periodic solution $\tilde{u}_{per} \in W(0,T)$ fulfilling

$$\begin{aligned} \langle w, \tilde{u}'_{per}(t)\rangle_{U\times U'} + s(w,\tilde{u}_{per}(t)) = (w, -f'(t))_H, & \quad \text{for all } w \in U, \text{f. a. at} \in (0,T), \\ \tilde{u}_{per}(0) = \tilde{u}_{per}(T) & \quad \text{in } H, \end{aligned}$$

which is also well posed, *since $f'(t)$ is in H f. a. a. t*, see Theorem 3.2.6. Again, we set $u_{per} = \tilde{u}_{per} + f$ and note that u_{per} satisfies (3.42) and is unique. Then set $\mathcal{E}_{per}(\boldsymbol{g}) = u_{per}$.

It remains to prove continuity of $\mathcal{E}_0$ and $\mathcal{E}_{per}$. We restrict ourselves to demonstrating that $\mathcal{E}_0$ is continuous as a mapping into $L^2(0,T;U')$:

$$\begin{aligned} \int_0^T \|\mathcal{E}_0\boldsymbol{g}(t)\|^2_{U'}\, dt &= \int_0^T \|u(t)\|^2_{U'}\, dt \\ &\le C\int_0^T \|u(t)\|^2_{\tilde{\boldsymbol{V}}\times Q}\, dt \\ &\le C\int_0^T \|\tilde{u}(t) + f(t)\|^2_{\tilde{\boldsymbol{V}}\times Q}\, dt \\ &\le C\int_0^T \left\|f'(t) + Sf(t)\right\|^2_{U'} + \|f(t)\|^2_{\tilde{\boldsymbol{V}}\times Q}\, dt \\ &\le C\int_0^T \left\|f'(t)\right\|^2_{\tilde{\boldsymbol{V}}\times Q} + \|f(t)\|^2_{\tilde{\boldsymbol{V}}\times Q}\, dt \\ &\le C\int_0^T \left\|\boldsymbol{g}'(t)\right\|^2_{\frac{1}{2}} + \|\boldsymbol{g}(t)\|^2_{\frac{1}{2}}\, dt \\ &\le C\left\|\boldsymbol{g}\right\|^2_{H^1(0,T;\boldsymbol{H}^{\frac{1}{2}}(\Gamma))}. \end{aligned}$$

□

After these technical preliminaries we may proceed to generalize the instationary Problem (P) as follows.

Problem 3.4.6 (Inhomogeneous instationary problem)
Let $0 < T < \infty$, $u_0 = (\boldsymbol{v}_0, p_0) \in H$, $f = (\boldsymbol{f}_v, f_p) \in L^2(0,T;U')$, and $\boldsymbol{g} \in H^1(0,T;H^{\frac{1}{2}}(\Gamma))$. Find $u = (\boldsymbol{v}, p) \in \mathcal{E}_0\boldsymbol{g} + W(0,T)$ so that

$$\begin{aligned} \langle w, u'(t)\rangle_{U\times U'} + s(w,u(t)) = \langle w, f(t)\rangle_{U\times U'} & \quad \textit{for all } w \in U, \textit{ f. a. a. } t \in (0,T), \\ u(0) = u_0 & \quad \textit{in } H. \end{aligned} \tag{$\mathrm{P}_{\boldsymbol{g}}$}$$

The periodic problem may be restated for inhomogeneous boundary conditions in much the same way.

Problem 3.4.7 (Inhomogeneous periodic solutions)
Let $0 < T < \infty$, $f = (\boldsymbol{f}_v, f_p) \in L^2(0,T;H)$, and $\boldsymbol{g} \in H^1(0,T;H^{\frac{1}{2}}(\Gamma))$ with $\boldsymbol{g}(0) = \boldsymbol{g}(T)$. Find $u = (\boldsymbol{v}, p) \in \mathcal{E}_{per}\boldsymbol{g} + W(0,T)$ so that

$$\begin{aligned} \langle w, u'(t)\rangle_{U\times U'} + s(w, u(t)) &= (w, f(t))_H \quad \text{for all } w \in U, \text{ f. a. a. } t \in (0,T), \\ u(0) &= u(T) \qquad\qquad \text{in } H. \end{aligned} \tag{$\mathrm{P}_{per,\boldsymbol{g}}$}$$

Again, we may verify the well-posedness of both inhomogeneous problems.

Lemma 3.4.8
Let $0 < T < \infty$ and $f = (\boldsymbol{f}_v, f_p) \in L^2(0,T;U')$, and $\boldsymbol{g} \in H^1(0,T;H^{\frac{1}{2}}(\Gamma))$.

1. *Let $u_0 = (\boldsymbol{v}_0, p_0) \in H$. There exists a unique solution $u = (\boldsymbol{v}, p) \in \mathcal{E}_0\boldsymbol{g} + W(0,T)$ satisfying ($\mathrm{P}_{\boldsymbol{g}}$) and*

$$\|(\boldsymbol{v}, p)\|_{W(0,T)} \le C\left(\|(\boldsymbol{v}_0, p_0)\|_H + \|(\boldsymbol{f}_v, f_p)\|_{L^2(0,T;U')} + \|\boldsymbol{g}\|_{H^1(0,T;H^{\frac{1}{2}}(\Gamma))}\right).$$

2. *Assume additionally that $\boldsymbol{g}(0) = \boldsymbol{g}(T)$. There exists a unique solution $u = (\boldsymbol{v}, p) \in \mathcal{E}_{per}\boldsymbol{g} + W(0,T)$ so that*

$$\|(\boldsymbol{v}, p)\|_{W(0,T)} \le C\left(\|(\boldsymbol{f}_v, f_p)\|_{L^2(0,T;H)} + \|\boldsymbol{g}\|_{H^1(0,T;H^{\frac{1}{2}}(\Gamma))}\right).$$

The constant C will generally depend on T in both cases.

3.4.2 Pressure with arbitrary mean

It is a well-known fact that the pressure solution of the classical *incompressible* Navier-Stokes equations is only determined up to a constant. The standard way to deal with this is to prescribe that pressure solutions must have mean zero in space which fixes this degree of freedom. The situation for compressible Navier-Stokes equations is different, however, as the example of (3.10) demonstrates.

The physical interpretation of such solutions is simple. We have modeled the pressure change to be proportional to the density change. A closed cavity into which fluid is forced from outside at a constant rate will fill with mass. If the volume does not change then the density and thus the pressure must rise – naturally not a situation which would remain stable indefinitely in nature.

As in the last subsection we will adhere to our program of treating each of the four main problems individually.

Problem 3.4.9 (Generalized stationary problem)
Let $f = (\boldsymbol{f}_v, f_p) \in \tilde{\boldsymbol{V}}' \times \tilde{Q}$ and $\boldsymbol{g} \in \boldsymbol{H}^{\frac{1}{2}}(\Gamma)$. Find $u = (\boldsymbol{v}, p) \in \tilde{\boldsymbol{V}} \times \tilde{Q}$ so that

$$\begin{aligned} a(\boldsymbol{w}, \boldsymbol{v}) + b(p, \boldsymbol{w}) &= \langle \boldsymbol{w}, \boldsymbol{f}_v\rangle_{\tilde{\boldsymbol{V}}\times\tilde{\boldsymbol{V}}'} \quad \text{for all } \boldsymbol{w} \in \boldsymbol{V}, \\ -b(q, \boldsymbol{v}) &= (q, f_p)_0 \qquad\quad \text{for all } q \in \tilde{Q}, \\ T\boldsymbol{v} &= \boldsymbol{g}. \end{aligned} \tag{$\mathrm{P}_{stat,gen}$}$$

Observe that we still test the first equation only with functions in $\boldsymbol{V}$. The possibility of extending the theory to include solutions with arbitrary mean (and accordingly arbitrary functions $f_p \in \tilde{Q}$ as right hand sides) is somewhat limited in the case of stationary solutions. To guarantee the existence of solutions we will have to pose a compatibility condition balancing the effect of the Dirichlet velocity boundary conditions $\boldsymbol{g}$ and the right hand side f_p. The physical interpretation: For a net inflow or outflow in the domain we must have volume sources or sinks such that the mass of fluid remains constant. Anything else could not be a stationary, hence equilibrium, solution.

Theorem 3.4.10
Let $f = (\boldsymbol{f}_v, f_p) \in \tilde{\boldsymbol{V}}' \times \tilde{Q}$ and $\boldsymbol{g} \in \boldsymbol{H}^{\frac{1}{2}}(\Gamma)$. There exists a solution $u = (\boldsymbol{v}, p) \in \tilde{\boldsymbol{V}} \times \tilde{Q}$ satisfying ($\mathrm{P}_{stat,gen}$) iff the problem data fulfills the compatibility condition

$$\int_\Gamma \boldsymbol{g} \cdot \boldsymbol{n} = (\mathbb{1}, f_p)_0, \tag{3.44}$$

with $\mathbb{1}$ as the constant function with value 1 on Ω. All solutions of (P_{gen}) are of the form $\tilde{u} := (\boldsymbol{v}, p + c\mathbb{1})$, $c \in \mathbb{R}$ where $(\boldsymbol{v}, p)$ is any given solution. By choosing the constant $c \in \mathbb{R}$ so that $p \in Q$, we retain the a-priori estimate

$$\|\boldsymbol{v}\|_1 + \|p\|_0 \leq C(\|\boldsymbol{f}_v\|_{-1} + \|f_p\|_0 + \|\boldsymbol{g}\|_{\frac{1}{2}}). \tag{3.45}$$

Proof. We first show that any solution $u = (\boldsymbol{v}, p)$ of ($\mathrm{P}_{stat,gen}$) fulfills the compatibility condition (3.44). To this end select $q = \mathbb{1}$. The second equation yields

$$(\mathbb{1}, f_p)_0 = -b(\mathbb{1}, \boldsymbol{v}) = \int_\Omega \nabla \cdot \boldsymbol{v} = \int_\Gamma (T\boldsymbol{v}) \cdot \boldsymbol{n} = \int_\Gamma \boldsymbol{g} \cdot \boldsymbol{n},$$

using Gauß's theorem. Now assume (3.44) holds. We define the reduced functional $\boldsymbol{f}_v|_{\boldsymbol{V}}$ for values in $\boldsymbol{V}$. We also define $\tilde{f}_p$ as the Q-projection of $f_p \in \tilde{Q}$. With this we use Lemma 3.4.4 to solve the problem of finding $(\boldsymbol{v}, p) \in E_0\boldsymbol{g} + U$ with

$$\begin{aligned} a(\boldsymbol{w}, \boldsymbol{v}) + b(p, \boldsymbol{w}) &= \langle \boldsymbol{w}, \boldsymbol{f}_v|_{\boldsymbol{V}} \rangle_{\boldsymbol{V} \times \boldsymbol{V}'} && \text{for all } \boldsymbol{w} \in \boldsymbol{V}, \\ -b(q, \boldsymbol{v}) &= (q, \tilde{f}_p)_0 && \text{for all } q \in Q. \end{aligned}$$

We must now verify that the second equation holds for f_p when tested with any $q \in \tilde{Q}$. We may decompose $q = \bar{q} + (q - \bar{q})$ with the mean value $\bar{q} := (⨍_\Omega q)\mathbb{1}$. This implies $q - \bar{q} \in Q$. Therefore

$$\begin{aligned} (q, f_p)_0 &= (\bar{q}, f_p)_0 + (q - \bar{q}, \tilde{f}_p)_0 \\ &= \int_\Gamma \bar{q}\boldsymbol{g} \cdot \boldsymbol{n} - b(q - \bar{q}, \boldsymbol{v}) \\ &= \int_\Omega \bar{q} \nabla \cdot \boldsymbol{v} - b(q - \bar{q}, \boldsymbol{v}) = -b(q, \boldsymbol{v}). \end{aligned}$$

If $u = (\boldsymbol{v}, p)$ is an arbitrary solution, we may take $\boldsymbol{w} \in \boldsymbol{V}$, $c \in \mathbb{R}$ and calculate

$$\begin{aligned} b(p + c\mathbb{1}, \boldsymbol{w}) &= b(p, \boldsymbol{w}) - c \int_\Omega \nabla \cdot \boldsymbol{w} \\ &= b(p, \boldsymbol{w}) - c \int_\Gamma (T\boldsymbol{w}) \cdot \boldsymbol{n} = b(p, \boldsymbol{w}), \end{aligned} \tag{3.46}$$

meaning that the pressure-shifted function $(\boldsymbol{v}, p + c\mathbb{1})$ is also a solution.

Now let $u = (\boldsymbol{v}, p)$ be the difference of two solutions of ($\mathrm{P}_{stat,gen}$). The function u will then solve the homogeneous equations

$$\begin{aligned} a(\boldsymbol{w}, \boldsymbol{v}) + b(p, \boldsymbol{w}) &= 0 && \text{for all } \boldsymbol{w} \in \boldsymbol{V}, \\ -b(q, \boldsymbol{v}) &= 0 && \text{for all } q \in \tilde{Q}, \\ T\boldsymbol{v} &= 0. \end{aligned}$$

The last equation implies $\boldsymbol{v} \in \boldsymbol{V}$. Choosing $\boldsymbol{w} = \boldsymbol{v}$ in the first equation yields

$$0 = a(\boldsymbol{v}, \boldsymbol{v}) + b(p, \boldsymbol{v}) = a(\boldsymbol{v}, \boldsymbol{v}),$$

and therefore $\boldsymbol{v} = 0$ since a is $\boldsymbol{V}$-coercive. Hence

$$b(p, \boldsymbol{w}) = 0 \qquad \text{for all } \boldsymbol{w} \in \boldsymbol{V},$$

and thus $B(p - \bar{p}) = 0$, where $\bar{p} = (⨍_\Omega p)\mathbb{1} \in \tilde{Q}$ is the mean of p. This in turn implies $p - \bar{p} = 0$ using Lemma 3.2.9, 1). In particular this means p is constant, proving the statement on the form of solutions.

The a-priori bound follows from (3.39) using

$$\begin{aligned} \|\boldsymbol{v}\|_1 + \|p\|_0 &\leq C(\|\boldsymbol{f}_v|\boldsymbol{V}\|_{-1} + \left\|\tilde{f}_p\right\|_0 + \|\boldsymbol{g}\|_{\frac{1}{2}}) \\ &\leq C(\|\boldsymbol{f}_v\|_{-1} + \|f_p\|_0 + \|\boldsymbol{g}\|_{\frac{1}{2}}). \end{aligned}$$

□

This concludes the case of the stationary problem. The instationary problem will require a generalization of the previously used Gelfand triple $U \hookrightarrow H \hookrightarrow U'$. We define

$$\begin{aligned} \tilde{U} &:= \boldsymbol{V} \times \tilde{Q} = \boldsymbol{H}_0^1(\Omega) \times L^2(\Omega), \\ \tilde{i}_1 &: \tilde{U} \to \tilde{H}, \\ \tilde{i}_1(f) &= f, \\ \tilde{i}_2 &: \tilde{H} \to \tilde{U}', \\ \langle \tilde{i}_2(f), g \rangle_{\tilde{U}' \times \tilde{U}} &= (f, \tilde{i}_1(g))_{\tilde{H}}. \end{aligned} \tag{3.47}$$

This is again a Gelfand triple

$$\tilde{U} \hookrightarrow_{\tilde{i}_1} \tilde{H} \hookrightarrow_{\tilde{i}_2} \tilde{U}' \tag{3.48}$$

with each space continuously embedded and dense in the subsequent space. This allows us to formulate a more general solution space

$$\tilde{W}(0,T) := \{f \in L^2(0,T;\tilde{U}) \mid f' \in L^2(0,T;\tilde{U}')\},$$

with $0 < T < \infty$ and the corresponding norm

$$\|f\|_{\tilde{W}}^2 := \|f'\|_{L^2(0,T;\tilde{U}')}^2 + \|f\|_{L^2(0,T;\tilde{U})}^2 .$$

Theorem 3.4.11
The space $\tilde{W}(0,T)$ is a Hilbert space and again permits a continuous embedding

$$\tilde{W}(0,T) \hookrightarrow C([0,T];\tilde{H}).$$

Proof. See [78, 25.4 and 25.5]. □

Problem 3.4.12 (Generalized instationary problem)
Let $0 < T < \infty$, $u_0 = (\boldsymbol{v}_0, p_0) \in \tilde{H}$, $f = (\boldsymbol{f}_v, f_p) \in L^2(0,T;\tilde{\boldsymbol{V}}' \times \tilde{Q})$, and $\boldsymbol{g} \in H^1(0,T;H^{\frac{1}{2}}(\Gamma))$. Find $u = (\boldsymbol{v}, p) \in \mathcal{E}_0\boldsymbol{g} + \tilde{W}(0,T)$ so that

$$\begin{aligned}
\langle \boldsymbol{w}, \boldsymbol{v}'(t)\rangle_{\boldsymbol{V}\times\boldsymbol{V}'} + a(\boldsymbol{w}, \boldsymbol{v}(t)) + b(p(t), \boldsymbol{w}) &= \langle \boldsymbol{w}, \boldsymbol{f}_v(t)\rangle_{\tilde{\boldsymbol{V}}\times\tilde{\boldsymbol{V}}'} && \text{for all } \boldsymbol{w} \in \boldsymbol{V},\\
(q, p'(t))_0 - b(q, \boldsymbol{v}(t)) &= (q, f_p(t))_0 && \text{for all } q \in \tilde{Q},\\
& && \text{f. a. a. } t \in (0,T),\\
(\boldsymbol{v}(0), p(0)) &= (\boldsymbol{v}_0, p_0) && \text{in } \tilde{H}.
\end{aligned} \tag{P_{gen}}$$

In contrast to the stationary case it is not necessary to assume compatibility conditions for the initial value problem. An imbalance between net outflow given by $\int_\Gamma \boldsymbol{g}\cdot\boldsymbol{n}$ and mass generation rate $(\mathbb{1}, f_p)_0$ simply causes an increase of the mean pressure with time.

Theorem 3.4.13
Let $0 < T < \infty$, $u_0 = (\boldsymbol{v}_0, p_0) \in \tilde{H}$, $f = (\boldsymbol{f}_v, f_p) \in L^2(0,T;\tilde{\boldsymbol{V}}' \times \tilde{Q})$, and $\boldsymbol{g} \in H^1(0,T;H^{\frac{1}{2}}(\Gamma))$. There exists a unique solution $u = (\boldsymbol{v}, p) \in \mathcal{E}_0\boldsymbol{g} + \tilde{W}(0,T)$ of (P_{gen}). We have the stability estimate

$$\|(\boldsymbol{v}, p)\|_{\tilde{W}} \le C\left(\|(\boldsymbol{v}_0, p_0)\|_{\tilde{H}} + \|(\boldsymbol{f}_v, f_p)\|_{L^2(0,T;\tilde{\boldsymbol{V}}'\times\tilde{Q})} + \|\boldsymbol{g}\|_{H^1(0,T;H^{\frac{1}{2}}(\Gamma))}\right).$$

Proof. We first define a transformed pressure right hand side $\tilde{f}_p$ as the Q-projection of f_p pointwise a. e.:

$$\begin{aligned}
\tilde{f}_p &\in L^2(0,T;Q),\\
\tilde{f}_p(t) &= f_p(t) - \left(\fint_\Omega f_p(t)\right)\mathbb{1}.
\end{aligned}$$

We also define $\tilde{p}_0$ as the Q-projection of p_0. Using these we solve the problem of finding $(\boldsymbol{v}, p_1)$ with

$$\begin{aligned}
\langle \boldsymbol{w}, \boldsymbol{v}'(t)\rangle_{\boldsymbol{V}\times\boldsymbol{V}'} + a(\boldsymbol{w}, \boldsymbol{v}(t)) + b(p_1(t), \boldsymbol{w}) &= \langle \boldsymbol{w}, \boldsymbol{f}_v(t)\rangle_{\tilde{\boldsymbol{V}}\times\tilde{\boldsymbol{V}}'} && \text{for all } \boldsymbol{w} \in \boldsymbol{V},\\
(q, p_1'(t))_0 - b(q, \boldsymbol{v}(t)) &= (q, \tilde{f}_p(t))_0 && \text{for all } q \in Q,\\
& && \text{f. a. a. } t \in (0,T),\\
T(\boldsymbol{v}(t)) &= \boldsymbol{g}(t) && \text{f. a. a. } t \in (0,T),\\
(\boldsymbol{v}(0), p_1(0)) &= (\boldsymbol{v}_0, \tilde{p}_0) && \text{in } H.
\end{aligned}$$

This is possible due to Lemma 3.4.8, 1). We define a function p_2 as follows:

$$\begin{aligned}
p_2 &\in H^1(0,T;\tilde{Q}),\\
p_2(t) &= \left(\fint_\Omega p_0\right)\mathbb{1} + \int_0^t \frac{1}{\lambda^n(\Omega)}\left(\int_\Omega f_p(\tau) - \int_\Gamma \boldsymbol{g}(\tau)\cdot\boldsymbol{n}\right)\mathbb{1}\,d\tau.
\end{aligned}$$

Note that $p_2'(t) \in \tilde{Q}$ is a constant function and

$$(c\mathbb{1}, p_2'(t))_0 = (c\mathbb{1}, f_p(t))_0 + b(c\mathbb{1}, \boldsymbol{v}(t)),$$

for all $c \in \mathbb{R}$. We have the estimates

$$\begin{aligned}
\|p_2\|_{L^2(0,T;\tilde{Q})} &\leq C \left(\|p_0\|_{\tilde{Q}} + \|f_p\|_{L^2(0,T;\tilde{Q})} + \|\boldsymbol{g}\|_{L^2(0,T;\boldsymbol{H}^{\frac{1}{2}}(\Gamma))} \right), \\
\|p_2'\|_{L^2(0,T;\tilde{Q})} &\leq C \left(\|f_p\|_{L^2(0,T;\tilde{Q})} + \|\boldsymbol{g}\|_{L^2(0,T;\boldsymbol{H}^{\frac{1}{2}}(\Gamma))} \right).
\end{aligned}$$

Now set $p := p_1 + p_2$. Because of (3.46) we will still have

$$\langle \boldsymbol{w}, \boldsymbol{v}'(t) \rangle_{\boldsymbol{V} \times \boldsymbol{V}'} + a(\boldsymbol{w}, \boldsymbol{v}(t)) + b(p(t), \boldsymbol{w}) = \langle \boldsymbol{w}, \boldsymbol{f}_v(t) \rangle_{\tilde{\boldsymbol{V}} \times \tilde{\boldsymbol{V}}'} \qquad \text{for all } \boldsymbol{w} \in \boldsymbol{V},$$

thus the first equation of (P_{gen}) is fulfilled. Concerning the second equation we calculate for any $q \in \tilde{Q}$, $q = \bar{q} + (q - \bar{q})$, $\bar{q} := \left(\fint_\Omega q \right) \mathbb{1}$:

$$\begin{aligned}
(q, p'(t))_0 - b(q, \boldsymbol{v}(t)) &= (\bar{q}, p_2'(t))_0 - b(\bar{q}, \boldsymbol{v}(t)) \\
&\quad \underbrace{(\bar{q}, p_1'(t))_0}_{=0} + \underbrace{(q - \bar{q}, p_2'(t))_0}_{=0} + \underbrace{(q - \bar{q}, p_1'(t))_0 - b(q - \bar{q}, \boldsymbol{v}(t))}_{=(q-\bar{q}, \tilde{f}_p(t))_0 = (q-\bar{q}, f_p(t))_0} \\
&= (\bar{q}, f_p(t))_0 + (q - \bar{q}, f_p(t))_0 \\
&= (q, f_p(t))_0.
\end{aligned}$$

The second equation of (P_{gen}) is therefore also fulfilled. The initial value of p in $\tilde{H}$ is

$$p(0) = p_1(0) + p_2(0) = \left(p_0 - \fint_\Omega p_0 \right) + \fint_\Omega p_0 = p_0.$$

The a-priori estimate is easily verified by combining estimates for p_1 and p_2. It remains to confirm uniqueness of the solution. Assume $(\boldsymbol{v}, p)$ is the difference of two solutions of (P_{gen}). Then $(\boldsymbol{v}, p)$ will be a solution of the homogeneous system

$$\begin{aligned}
\langle \boldsymbol{w}, \boldsymbol{v}'(t) \rangle_{\boldsymbol{V} \times \boldsymbol{V}'} + a(\boldsymbol{w}, \boldsymbol{v}(t)) + b(p(t), \boldsymbol{w}) &= 0 && \text{for all } \boldsymbol{w} \in \boldsymbol{V}, \\
(q, p'(t))_0 - b(q, \boldsymbol{v}(t)) &= 0 && \text{for all } q \in \tilde{Q}, \\
& && \text{f. a. a. } t \in (0, T), \\
T(\boldsymbol{v}(t)) &= 0 && \text{f. a. a. } t \in (0, T), \\
(\boldsymbol{v}(0), p(0)) &= 0 && \text{in } \tilde{H}.
\end{aligned}$$

Choose $q = \mathbb{1}$. The second equation yields

$$(\mathbb{1}, p'(t))_0 = b(\mathbb{1}, \boldsymbol{v}(t)) = 0$$

for almost all $t \in (0, T)$ since $\boldsymbol{v}(t) \in \boldsymbol{V}$ due to the third equation. This implies

$$(\mathbb{1}, p(t))_0 = (\mathbb{1}, p(0))_0 + \int_0^t (\mathbb{1}, p'(\tau))_0 d\tau = 0,$$

for almost all $t \in (0, T)$, in other words $p(t) \in Q$. This means that Lemma 3.4.8 is applicable to $(\boldsymbol{v}, p)$, yielding $\boldsymbol{v} = 0$, $p = 0$. This proves uniqueness. □

We now turn to the third problem on our program, namely periodic solutions. The formulation of generalized periodic solutions is straightforward.

Problem 3.4.14 (Generalized periodic solutions)
Let $0 < T < \infty$, $f = (\boldsymbol{f}_v, f_p) \in L^2(0,T;\tilde{H})$, and $\boldsymbol{g} \in H^1(0,T;H^{\frac{1}{2}}(\Gamma))$ with $\boldsymbol{g}(0) = \boldsymbol{g}(T)$. Find $u = (\boldsymbol{v}, p) \in \mathcal{E}_{per}\boldsymbol{g} + \tilde{W}(0,T)$ so that

$$\begin{aligned}
\langle \boldsymbol{w}, \boldsymbol{v}'(t)\rangle_{\boldsymbol{V}\times\boldsymbol{V}'} + a(\boldsymbol{w}, \boldsymbol{v}(t)) + b(p(t), \boldsymbol{w}) &= \langle \boldsymbol{w}, \boldsymbol{f}_v(t)\rangle_{\tilde{\boldsymbol{V}}\times\tilde{\boldsymbol{V}}'} && \text{for all } \boldsymbol{w} \in \boldsymbol{V},\\
(q, p'(t))_0 - b(q, \boldsymbol{v}(t)) &= (q, f_p(t))_0 && \text{for all } q \in \tilde{Q},\\
& && \text{f. a. a. } t \in (0,T),\\
T(\boldsymbol{v}(t)) &= \boldsymbol{g}(t) && \text{f. a. a. } t \in (0,T),\\
u(0) &= u(T) && \text{in } \tilde{H}.
\end{aligned} \tag{$\mathrm{P}_{per,gen}$}$$

Periodic problems require a compatibility condition similar to the one necessary for the stationary problem. However, it is not necessary to demand a balance between net outflow and mass generation at all points in time. Instead, it is sufficient to demand that the total difference between outflow and mass generation over the time interval $[0,T]$ is zero, as shown by the following theorem.

Theorem 3.4.15
Let $0 < T < \infty$, $f = (\boldsymbol{f}_v, f_p) \in L^2(0,T;\tilde{H})$, and $\boldsymbol{g} \in H^1(0,T;H^{\frac{1}{2}}(\Gamma))$ with $\boldsymbol{g}(0) = \boldsymbol{g}(T)$. There exists a solution $u = (\boldsymbol{v}, p) \in \mathcal{E}_{per}\boldsymbol{g} + \tilde{W}(0,T)$ of ($\mathrm{P}_{per,gen}$) iff the problem data satisfies the compatibility condition

$$\int_0^T \left(\int_\Omega f_p(\tau) - \int_\Gamma \boldsymbol{g}(\tau)\cdot\boldsymbol{n} \right) d\tau = 0. \tag{3.49}$$

All solutions of ($\mathrm{P}_{per,gen}$) are of the form $(\boldsymbol{v}, p + c\mathbb{1})$, $c \in \mathbb{R}$ where $(\boldsymbol{v}, p)$ is any given solution. For the solution with $p(0) = p(T) \in Q$ we have the stability estimate

$$\|(\boldsymbol{v}, p)\|_{\tilde{W}} \le C \left(\|(\boldsymbol{f}_v, f_p)\|_{L^2(0,T;\tilde{H})} + \|\boldsymbol{g}\|_{H^1(0,T;H^{\frac{1}{2}}(\Gamma))} \right).$$

Proof. We first show that the compatibility condition (3.49) is necessary. This may be seen by choosing $q = \mathbb{1}$ in ($\mathrm{P}_{per,gen}$) whence

$$\begin{aligned}
0 = (\mathbb{1}, p(T) - p(0))_0 &= \int_0^T (\mathbb{1}, p'(t))_0 \, dt\\
&= \int_0^T (\mathbb{1}, f_p(t))_0 + b(\mathbb{1}, \boldsymbol{v}(t)) \, dt\\
&= \int_0^T \left(\int_\Omega f_p(t) - \int_\Omega \nabla\cdot\boldsymbol{v}(t) \right) dt\\
&= \int_0^T \left(\int_\Omega f_p(t) - \int_\Gamma \boldsymbol{g}(t)\cdot\boldsymbol{n} \right) dt.
\end{aligned}$$

Now assume that this condition holds. We again define a transformed pressure right hand side $\tilde{f}_p$ as

$$\begin{aligned}\tilde{f}_p &\in L^2(0,T;Q),\\ \tilde{f}_p(t) &= f_p(t) - \left(⨍_\Omega f_p(t)\right)\mathbb{1},\end{aligned}$$

and $\tilde{p}_0$ as the Q-projection of p_0. With these we solve the problem of finding $u_1 = (\boldsymbol{v}, p_1)$ with

$$\begin{aligned}\langle \boldsymbol{w}, \boldsymbol{v}'(t)\rangle_{\boldsymbol{V}\times\boldsymbol{V}'} + a(\boldsymbol{w},\boldsymbol{v}(t)) + b(p_1(t),\boldsymbol{w}) &= \langle \boldsymbol{w}, \boldsymbol{f}_v(t)\rangle_{\tilde{\boldsymbol{V}}\times\tilde{\boldsymbol{V}}'} && \text{for all } \boldsymbol{w}\in\boldsymbol{V},\\ (q, p_1'(t))_0 - b(q,\boldsymbol{v}(t)) &= (q,\tilde{f}_p(t))_0 && \text{for all } q\in Q,\\ & && \text{f. a. a. } t\in(0,T),\\ T(\boldsymbol{v}(t)) &= \boldsymbol{g}(t) && \text{f. a. a. } t\in(0,T),\\ u_1(0) &= u_1(T) && \text{in } H,\end{aligned}$$

which is possible due to Lemma 3.4.8, 2). We define the function p_2 as follows:

$$\begin{aligned}p_2 &\in H^1(0,T;\tilde{Q}),\\ p_2(t) &= \int_0^t \frac{1}{\lambda^n(\Omega)}\left(\int_\Omega f_p(\tau) - \int_\Gamma \boldsymbol{g}(\tau)\cdot\boldsymbol{n}\right)\mathbb{1}d\tau.\end{aligned}$$

As before we have

$$(c\mathbb{1}, p_2'(t))_0 = (c\mathbb{1}, f_p(t))_0 + b(c\mathbb{1},\boldsymbol{v}(t)),$$

for all $c\in\mathbb{R}$, as well as

$$0 = p_2(0) = p_2(T)$$

due to (3.49). We arrive at the estimate

$$\|p_2\|_{H^1(0,T;\tilde{Q})} \le C\left(\|f_p\|_{L^2(0,T;\tilde{Q})} + \|\boldsymbol{g}\|_{L^2(0,T;\boldsymbol{H}^{\frac{1}{2}}(\Gamma))}\right).$$

Now set $p := p_1 + p_2$. A similar calculation as in Theorem 3.4.13 confirms that the first two equations in ($\mathrm{P}_{per,gen}$) are satisfied. The periodicity is undamaged since

$$p(0) = p_1(0) + p_2(0) = p_1(T) + p_2(T) = p(T).$$

The a-priori estimate is easily verified by combining estimates for p_1 and p_2.

We still need to check the form of solutions. Assume $(\boldsymbol{v}, p)$ is any solution. As in Theorem 3.4.10 we see that $(\boldsymbol{v}, p + c\mathbb{1})$, $c\in\mathbb{R}$ is again a solution. Now assume $(\boldsymbol{v}, p)$ is the difference of two solutions. A similar argument as in the proof of Theorem 3.4.13 yields

$$(\mathbb{1}, p(t))_0 = (\mathbb{1}, p(0))_0 + \int_0^t (\mathbb{1}, p'(\tau))_0 d\tau = (\mathbb{1}, p(0))_0$$

for almost all $t\in(0,T)$, meaning that the pressure solution has constant mean in time. Setting $\tilde{p} := p(t) - \bar{p}$, $\bar{p} := (⨍_\Omega p)\mathbb{1}$ then yields a solution $(\boldsymbol{v}, \tilde{p})$ of the fully homogeneous periodic problem, and therefore $\tilde{p} = 0$. This proves that all pressure solutions differ by a constant. □

We finally turn to the last problem of generalized quasi-stationary solutions.

Problem 3.4.16 (Generalized quasi-stationary problem)
Given right hand sides $f_X \in \tilde{X}'$, $f_Y \in \tilde{Y}'$ and boundary values $g = (\boldsymbol{g}_c, \boldsymbol{g}_s) \in \boldsymbol{H}^{\frac{1}{2}}(\Gamma)$, find $(v,p) \in E_{qs}g + X \times \tilde{Y}$ so that

$$\begin{aligned} \mathfrak{a}(w,v) + \mathfrak{b}(p,w) &= \langle w, f_X \rangle_{X \times X'} \quad \text{for all } w \in X, \\ -\mathfrak{b}(q,v) + \mathfrak{c}(q,p) &= \langle q, f_Y \rangle_{\tilde{Y} \times \tilde{Y}'} \quad \text{for all } q \in \tilde{Y}. \end{aligned} \tag{$\mathrm{P}_{qs,gen}$}$$

It turns out that compatibility conditions are unnecessary for the quasi-stationary problem. This is intuitively clear since the compatibility condition for periodic problems is automatically fulfilled for right hand sides and boundary values with time harmonic behavior.

Theorem 3.4.17
Let $f_X \in \tilde{X}'$, $f_Y \in \tilde{Y}'$ and $g = (\boldsymbol{g}_c, \boldsymbol{g}_s) \in \boldsymbol{H}^{\frac{1}{2}}(\Gamma)$. There exists a unique solution $(v,p) \in E_{qs}g + X \times \tilde{Y}$ of ($\mathrm{P}_{qs,gen}$) satisfying the a-priori bound

$$\|v\|_X + \|p\|_Y \leq C(\|f_X\|_{\tilde{X}'} + \|f_Y\|_{\tilde{Y}'} + \|g\|_{\boldsymbol{H}^{\frac{1}{2}}(\Gamma)^2}).$$

Proof. Define a transformed pressure right hand side $\tilde{f}_Y$ as

$$\begin{aligned} &\tilde{f}_Y \in Y', \\ &\tilde{f}_{Y,c} := f_{Y,c} - \left(\fint_\Omega f_{Y,c}(t) \right) \mathbb{1}, \\ &\tilde{f}_{Y,s} := f_{Y,s} - \left(\fint_\Omega f_{Y,s}(t) \right) \mathbb{1}. \end{aligned}$$

Solve the problem of finding $(v, p_1) \in \mathcal{E}_{qs}g + X \times Y$ with

$$\begin{aligned} \mathfrak{a}(w,v) + \mathfrak{b}(p_1,w) &= \langle w, f_X \rangle_{X \times X'} \qquad \text{for all } w \in X, \\ -\mathfrak{b}(q,v) + \mathfrak{c}(q,p_1) &= \langle q, \tilde{f}_Y \rangle_{Y \times Y'} \qquad \text{for all } q \in Y, \end{aligned}$$

using Lemma 3.4.4, 2). Define the function $p_2 \in \tilde{Y}$ as follows:

$$\begin{aligned} &p_2 \in \tilde{Y}, \\ &p_{2,c} := \frac{1}{\omega \mu_p \lambda^n(\Omega)} \left(\int_\Omega f_{Y,s} - \int_\Gamma \boldsymbol{g}_s \cdot \boldsymbol{n} \right) \mathbb{1}, \\ &p_{2,s} := -\frac{1}{\omega \mu_p \lambda^n(\Omega)} \left(\int_\Omega f_{Y,c} - \int_\Gamma \boldsymbol{g}_c \cdot \boldsymbol{n} \right) \mathbb{1}. \end{aligned}$$

Define $p := p_1 + p_2 \in \tilde{Y}$. For all $q = \bar{q} + (q - \bar{q}) \in \tilde{Y}$, $\bar{q}_i := (\fint_\Omega q_i)\mathbb{1}$, $i \in \{c, s\}$

we verify that

$$\begin{aligned}-\mathfrak{b}(q,v)+\mathfrak{c}(q,p) =& -\mathfrak{b}(\bar{q},v)+\mathfrak{c}(\bar{q},p_2)\\ &\underbrace{-\mathfrak{b}(q-\bar{q},v)+\mathfrak{c}(q-\bar{q},p_1)}_{=(q-\bar{q},\tilde{f}_Y)_{Y\times Y'}=(q-\bar{q},f_Y)_{\tilde{Y}\times\tilde{Y}'}}+\underbrace{\mathfrak{c}(\bar{q},p_1)}_{=0}+\underbrace{\mathfrak{c}(q-\bar{q},p_2)}_{=0}\\ =& -\mathfrak{b}(\bar{q},v)+(q-\bar{q},f_Y)_{\tilde{Y}\times\tilde{Y}'}+\omega\mu_p\int_\Omega(p_{2,c}\bar{q}_s-p_{2,s}\bar{q}_c)\\ =& -\mathfrak{b}(\bar{q},v)+(q-\bar{q},f_Y)_{\tilde{Y}\times\tilde{Y}'}+(\bar{q},f_Y)_{\tilde{Y}\times\tilde{Y}'}+\mathfrak{b}(\bar{q},v)\\ =&(q,f_Y)_{\tilde{Y}\times\tilde{Y}'},\end{aligned}$$

which means that the second equation of ($P_{qs,gen}$) is fulfilled. The first equation is fulfilled since $w \in X$ as before.

It remains to check uniqueness of this solution. Once again we assume that $(v,p) \in \tilde{X}\times\tilde{Y}$ is the difference of two solutions. This implies that

$$\begin{aligned}\mathfrak{a}(w,v)+\mathfrak{b}(p,w)&=0 && \text{for all } w\in X,\\ -\mathfrak{b}(q,v)+\mathfrak{c}(q,p)&=0 && \text{for all } q\in\tilde{Y},\\ T\boldsymbol{v}_c=T\boldsymbol{v}_s&=0.\end{aligned}$$

The function $v=(\boldsymbol{v}_c,\boldsymbol{v}_s)$ is therefore in X. Choose $q=(\lambda_c\mathbb{1},\lambda_s\mathbb{1})$, $\lambda_c,\lambda_s\in\mathbb{R}$. The second equation yields

$$0=-\mathfrak{b}(q,v)+\mathfrak{c}(q,p)=\mathfrak{c}(q,p)=\omega\mu_p\int_\Omega(p_c\lambda_s-p_s\lambda_c),$$

or

$$\lambda_c\int_\Omega p_s=\lambda_s\int_\Omega p_c.$$

This implies that both integrals are zero since $\lambda_c,\lambda_s\in\mathbb{R}$ are arbitrary. Therefore $p\in Y$. As before we may use Theorem 3.3.3 to deduce $v=0$, $p=0$. The a-priori estimate follows as before. □

Chapter 4

Numerical discretization

In this chapter we will present a numerical discretization of the problems presented in Chapter 3. We will first introduce the finite element spaces used for spatial discretization. After presenting the discretization of the stationary problem 3.1.8 we will concentrate on the time dependent Problem 3.1.6, which we will discretize first in space and then in time (*Method of Lines*).

4.1 Finite elements

The aim of this section is the definition of suitable conforming finite element spaces $\boldsymbol{V}_h \subset \boldsymbol{V} = \boldsymbol{H}_0^1(\Omega)$ and $Q_h \subset Q = L_0^2(\Omega)$ for velocity and pressure, respectively. For simplicity we will not consider the more general setting of Section 3.4. The discretized spaces should yield optimal error estimates in terms of the mesh parameter h, as usual. As will become clear later, the spatial discretization must also be stable in the sense of fulfilling uniformly a discrete Babuška-Brezzi condition

$$\inf_{p_h \in Q_h \setminus \{0\}} \sup_{\boldsymbol{v}_h \in \boldsymbol{V}_h \setminus \{0\}} \frac{b(p_h, \boldsymbol{v}_h)}{\|p_h\|_0 \, \|\boldsymbol{v}_h\|_1} \geq \widetilde{c}_{b,h} \geq \widetilde{c}_b > 0. \tag{LBB$_h$}$$

The important point here is that the lower bound $\widetilde{c}_b$ is independent of the discretization parameter h.

The space Q_h being a subset of $L_0^2(\Omega)$ contains functions of mean zero. In practice we will not implement this space itself. Instead we will perform calculations in a more readily implemented space $\widetilde{Q}_h \subset L^2(\Omega)$ and enforce the condition of mean zero implicitly as described in Chapter 6.

4.1.1 Triangulations and finite element spaces

We will first define the concepts conforming triangulations and finite element spaces. In the following, we will assume that $\Omega \subset \mathbb{R}^d$ is a bounded domain with polygonal boundary. The definition and concepts are taken from [17, 9, 11, 64].

Definition 4.1.1 (Simplex)
Let $A := \{a_0, \ldots, a_s\} \subset \mathbb{R}^d$, $0 \leq s \leq d$. The s vectors $a_1 - a_0, \ldots, a_s - a_0$ are

assumed to be linear independent in $\mathbb{R}^d$. The set

$$S = \operatorname{conv} A = \left\{ \sum_{i=0}^{s} \lambda_i a_i \mid \lambda_i \in [0,1] \text{ and } \sum_{i=0}^{s} \lambda_i = 1 \right\},$$

is known as the *s-dimensional simplex* spanned by $a_0, \ldots, a_s$. 0-, 1-, 2- resp. 3-dimensional simplices are points, intervals, triangles, resp. tetrahedra. The coefficients λ_i describing a point $x \in S$ are unique and known as the *barycentric coordinates* of x in the simplex S.

If $B \subset A$ contains r elements, then

$$S' := \operatorname{conv} B$$

is an *r-dimensional subsimplex of S*.

For a simplex S we define the following characteristic quantities:

$$\begin{aligned} h(S) &:= \sup\{|x-y| \mid x, y \in S\}, \\ \rho(S) &:= \sup\{2R \mid B_R \subset S \text{ is a sphere of radius } R\}, \\ \sigma(S) &:= \frac{h(S)}{\rho(S)}. \end{aligned}$$

Definition 4.1.2
Let $\mathcal{T}$ be a finite set of d-simplices. Then $\mathcal{T}$ is a *conforming* triangulation of Ω iff the following conditions are fulfilled:

1) The domain Ω is the interior of the set $\bigcup_{S \in \mathcal{T}} S$.

2) The intersection $S_1 \cap S_2$ of any two elements $S_1, S_2 \in \mathcal{T}$ is either empty or a complete r-subsimplex of both S_1 and S_2, with $0 \le r \le d$.

A sequence $(\mathcal{T}_i)_{i \in \mathbb{N}}$ of conforming triangulations of Ω is *regular* iff the parameter $\sigma(S)$ remains bounded in the following sense:

$$\sup_{i \in \mathbb{N}} \max_{S \in \mathcal{T}_i} \sigma(S) < \infty.$$

Remark 4.1.3
The finite element algorithms in this work employ regular sequences of triangulations arising through iterated bisection of elements of a so-called macro triangulation $\mathcal{T}_0$ of Ω. The choice of bisection edge implemented in ALBERTA [64] guarantees the boundedness of $\sigma(S)$. This implies that simplices do not degenerate during successive refinement. As in the literature we will from now on use the maximal element diameter $h_i = \max_{S \in \mathcal{T}_i} h(S)$ as the index for a sequence of triangulations defined by successive refinement of a given macro triangulation $\mathcal{T}_0$.

Let $\mathcal{T}$ be a conforming triangulation of Ω. For any $S \in \mathcal{T}$ we will assume that $\mathbb{P}(S) \subset C^1(S)$ is a finite dimensional function space on S, typically containing polynomials up to a fixed order. An abstract finite element space X_h on the triangulation $\mathcal{T}$ is then defined as

$$X_h = X_h(\mathcal{T}, C^0) = \{\varphi_h \in C^0(\overline{\Omega}) \mid \varphi_h|_S \in \mathbb{P}(S) \text{ for all } S \in \mathcal{T}\}.$$

We require only global continuity which is sufficient to ensure that our finite element spaces are subspaces of $H^1(\Omega)$.

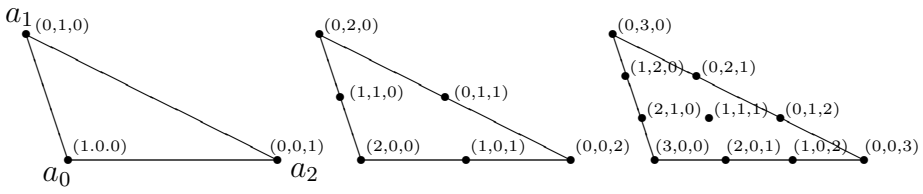

Figure 4.1: Lagrange meshes of first, second, and third order of a triangle spanned by a_0, a_1 and a_2, with multi-index $i = (i_0, i_1, i_2)$.

4.1.2 Lagrange and Taylor-Hood elements

Assume again that $\mathcal{T}$ is a conforming triangulation of Ω. We now specify $\mathbb{P}(S) := \mathbb{P}_k(S)$ as the space of polynomials up to order $k \geq 1$ on $S \in \mathcal{T}$. We define

$$\overline{S} := \left\{ \lambda = (\lambda_i)_{i=0}^d \in \mathbb{R}^{d+1} \mid \lambda_i \in [0,1], \quad \sum_{i=0}^d \lambda_i = 1 \right\}$$

as the so-called *reference simplex*. Every simplex $S \in \mathcal{T}$ is then the image $x^S(\overline{S})$ under an affine transformation x^S, this transformation being the conversion of barycentric coordinates to coordinates of $\mathbb{R}^d$,

$$\begin{aligned} x^S &: \overline{S} \to S \subset \mathbb{R}^d, \\ x^S(\lambda) &= a_0 + \sum_{i=1}^d \lambda_i (a_i - a_0) = \sum_{i=0}^d \lambda_i a_i, \end{aligned}$$

if $a_i \in \mathbb{R}^d$ are the vertices of S. Every function $\varphi : S \to \mathbb{R}$ may be transformed in a similar way to barycentric coordinates:

$$\begin{aligned} \overline{\varphi} &: \overline{S} \to \mathbb{R}, \\ \overline{\varphi}(\lambda) &:= \varphi \circ x^S(\lambda) = \varphi(x^S(\lambda)). \end{aligned}$$

The principle of element-wise evaluation of a FE-function through the evaluation of a reference function defined on $\overline{S}$ is important in the practical implementation.

Definition 4.1.4
Assume $S \in \mathcal{T}$ is spanned by $a_0, \ldots, a_n$, $k \in \mathbb{N}$. By

$$G_k(S) := \left\{ \sum_{l=0}^d \frac{i_l}{k} a_l \mid i \in \mathbb{N}_0^{d+1} \text{ with } |i| = k \right\} \subset S$$

we define the *Lagrange mesh of order k* on S. See Figure 4.1 for an illustration.

Lemma 4.1.5
Let $S \in \mathcal{T}$, $k \in \mathbb{N}$, and $p \in \mathbb{P}_k(S)$. Then p is uniquely identified by its values on the Lagrange mesh $G_k(S)$. We have the representation

$$p(x^S(\lambda)) = \overline{p}(\lambda) = \sum_{\substack{i \in \mathbb{N}_0^{d+1}, \\ |i| = k}} \overline{p}(\frac{i}{k}) \varphi_i(\lambda)$$

with $\frac{i}{k} := \left(\frac{i_l}{k}\right)_{l=0}^{d}$ *and*

$$\varphi_i \in \mathbb{P}_k(\overline{S}),$$
$$\varphi_i(\lambda) = \prod_{l=0}^{d} \prod_{j_l=0}^{i_l-1} \frac{\lambda_l - \frac{j_l}{k}}{\frac{i_l}{k} - \frac{j_l}{k}}.$$

We have $\dim \mathbb{P}_k(S) = \#G_k(S) = \binom{n+k}{k}$. *The set* $(\varphi_i)_{|i|=k}$ *has the following property:*

$$\varphi_i(\frac{j}{k}) = \delta_{ij} = \prod_{l=0}^{d} \delta_{i_l j_l} \qquad \text{for all } j \in \mathbb{N}_0^{d+1} \text{ with } |j| = k,$$

with the Kronecker symbol δ.

Proof. See e. g. [11]. □

Theorem and Definition 4.1.6 (Lagrange elements)
Let $k \in \mathbb{N}$ *and*

$$X_h^k = \{\varphi_h \in C^0(\overline{\Omega}) \mid \varphi_h|_S \in \mathbb{P}_k(S) \text{ for all } S \in \mathcal{T}\} \subset H^1(\Omega).$$

Define

$$G_k := \bigcup_{S \in \mathcal{T}} G_k(S) =: \{\overline{x}_\nu \in \overline{\Omega} \mid \nu = 1, \dots, N\}$$

as the Lagrange mesh of order k *for the triangulation* $\mathcal{T}$. *A function* $\varphi_h \in X_h^k$ *is uniquely defined by specifying the values in the nodes* $\overline{x}_\nu$. *The set of functions*

$$\varphi_\nu \in X_h^k \text{ with } \varphi_\nu(\overline{x}_\mu) := \delta_{\nu\mu} \text{ for all } \nu = 1, \dots, N,$$

is the nodal basis *of* X_h^k.

Proof. See e. g. [11]. □

We may now define the Taylor-Hood element, first proposed in [39], which we will use for the spatial discretization of the problems in Chapter 3.

Definition 4.1.7 (Taylor-Hood elements)
Let $k \in \mathbb{N}$. Define

$$\boldsymbol{V}_h^k = (X_h^{k+1})^d \cap \boldsymbol{V} \subset \boldsymbol{V},$$
$$Q_h^k = X_h^k \cap Q \subset Q,$$

as the *Taylor-Hood element space of order* k.

4.1.3 Properties of the Taylor-Hood element

From now on we will assume that $\Omega \subset \mathbb{R}^d$ with $d = 1, 2, 3$. This is not a restriction for practical problems, and it will simplify the definition of interpolation operators into finite element spaces. Due to the classical Sobolev embedding theorem we gain the continuous embedding

$$H^m(\Omega) \hookrightarrow C^0(\overline{\Omega})$$

if $m \geq 2$.

Let $\mathcal{T}_h$ be a conforming triangulation of Ω. For Lagrange finite elements

$$X_h^k = \{\varphi_h \in C^0(\overline{\Omega}) \mid \varphi_h|_S \in \mathbb{P}_k(S) \text{ for all } S \in \mathcal{T}\},$$

we may therefore define the standard *Lagrange interpolation operator* by evaluating functions at the Lagrange nodes:

$$\begin{aligned} &I_k : H^2(\Omega) \to X_h^k, \\ &(I_k f)(\overline{x}) := f(\overline{x}) \qquad \text{for all } \overline{x} \in G_k, \end{aligned}$$

The following interpolation estimate is well known:

Lemma 4.1.8
Let $\{\mathcal{T}_h\}_h$ be a regular family of conforming triangulations of $\Omega \subset \mathbb{R}^d$, $d \leq 3$. Let $f \in H^s(\Omega)$, $2 \leq s \leq k+1$. Then

$$|f - I_k f|_m \leq C h^{s-m} |f|_s , \tag{4.1}$$

for $m = 0, 1$, with C independent of f.

Proof. See e. g. [11, Remark 4.4.27]. □

We will also require more general interpolation operators which may be defined on spaces of rougher, not necessarily continuous functions. The basic ideas were presented in Clément, [18], with later improvements by Scott and Zhang, [66].

Lemma 4.1.9
Let $\{\mathcal{T}_h\}_h$ be a regular family of conforming triangulations of $\Omega \subset \mathbb{R}^d$. Let $f \in H^s(\Omega)$, $1 \leq s \leq k$, $k \in \mathbb{N}$. Then there exists a bounded, linear interpolation operator

$$J_k : H^1(\Omega) \to X_h^k$$

satisfying

$$\|f - J_k f\|_0 \leq C h^s |f|_s , \tag{4.2}$$

with C independent of f.

Proof. Follows from [11, Corollary 4.8.9]. □

The most significant property of the Taylor-Hood element is that it satisfies a discrete LBB condition as described above.

Theorem 4.1.10
Let $\{\mathcal{T}_h\}_h$ be a regular family of conforming triangulations of $\Omega \subset \mathbb{R}^d$, $d \leq 3$. The Taylor-Hood element spaces $\boldsymbol{V}_h^k \times Q_h^k$, $k \in \mathbb{N}$, satisfy the discrete LBB condition

$$\inf_{p_h \in Q_h^k \setminus \{0\}} \sup_{\boldsymbol{v}_h \in \boldsymbol{V}_h^k \setminus \{0\}} \frac{b(p_h, \boldsymbol{v}_h)}{\|p_h\|_0 \, \|\boldsymbol{v}_h\|_1} \geq \widetilde{c}_{b,hk} \geq \widetilde{c}_{b,k} > 0. \qquad (\mathrm{LBB}_h(\mathrm{TH}))$$

For $\boldsymbol{v} \in \boldsymbol{H}^{k+1}(\Omega) \cap \boldsymbol{V}$ and $p \in H^k(\Omega) \cap Q$ we have the following approximation properties:

$$\inf_{\boldsymbol{v}_h \in \boldsymbol{V}_h^k} \|\boldsymbol{v} - \boldsymbol{v}_h\|_1 \leq C h^s \, |\boldsymbol{v}|_{s+1} \,,$$
$$\inf_{p_h \in Q_h^k} \|p - p_h\|_0 \leq C h^s \, |p|_s \,,$$

with $0 \leq s \leq k$.

Proof. A proof of (LBB_h(TH)) may be found in [52].

Concerning the approximation properties we first note that the vector valued version $\boldsymbol{I}_k$ of the Lagrange interpolation operator retains homogenous Dirichlet boundary values:

$$\begin{aligned} \boldsymbol{I}_k : \boldsymbol{H}^2(\Omega) \cap \boldsymbol{V} &\to \boldsymbol{V}_h^k, \\ (\boldsymbol{I}_k \boldsymbol{v})(\overline{x}) &= \boldsymbol{v}(\overline{x}) \qquad \text{for all } \overline{x} \in G_k. \end{aligned}$$

We may therefore apply Lemma 4.1.8 to get

$$\inf_{\boldsymbol{v}_h \in \boldsymbol{V}_h^k} \|\boldsymbol{v} - \boldsymbol{v}_h\|_1 \leq \|\boldsymbol{v} - \boldsymbol{I}_k \boldsymbol{v}\|_1 \leq C h^s \, |\boldsymbol{v}|_{s+1} \,.$$

The pressure space estimate may be derived by defining the following improved interpolation operator retaining mean value zero:

$$\begin{aligned} \widetilde{J}_k : H^1(\Omega) \cap Q &\to Q_h^k, \\ \widetilde{J} p &= J_k p - \left(\fint_\Omega J_k p \right) \mathbb{1}, \end{aligned}$$

using the interpolation operator of Lemma 4.1.9. This yields

$$\begin{aligned} \inf_{p_h \in Q_h^k} \|p - p_h\|_0 &\leq \left\| p - \widetilde{J}_k p \right\|_0 \\ &= \left\| p - J_k p + \left(\fint_\Omega J_k p \right) \mathbb{1} \right\|_0 \\ &= \left\| p - J_k p + \left(\fint_\Omega (p - J_k p) \right) \mathbb{1} \right\|_0 \\ &\leq \|p - J_k p\|_0 + |\Omega|^{-\frac{1}{2}} \left| \int_\Omega (p - J_k p) \right| \\ &\leq 2 \, \|p - J_k p\|_0 \leq 2 C h^s \, |p|_s \,, \end{aligned}$$

using Lemma 4.1.9. □

4.2 Discretized problems on fixed domains

The standard convergence theory for the Stokes system is well known, see [29, 9, 17, 11, 72, 36, 32], to name just a few works. However, we will repeat the theory in a concise manner here since some details (e. g. the bilinear form a) of the posed problem differ from the classical treatments. Additionally, we will be able to make use of the presented theory when dealing with the less known quasi-stationary approach.

4.2.1 Stationary problem

Assume that $U_h = \boldsymbol{V}_h \times Q_h$ is a finite dimensional subspace of U fulfilling the discrete LBB-condition (LBB_h).

The abstract discretized version of Problem 3.1.8 is:

Problem 4.2.1 (Discrete stationary problem)
Let $f = (\boldsymbol{f}_v, f_p) \in U'$. Find $u_h = (\boldsymbol{v}_h, p_h) \in U_h$ so that

$$\begin{aligned} a(\boldsymbol{w}_h, \boldsymbol{v}_h) + b(p_h, \boldsymbol{w}_h) &= \langle \boldsymbol{w}_h, \boldsymbol{f}_v \rangle_{\boldsymbol{V} \times \boldsymbol{V}'} && \text{for all } \boldsymbol{w} \in \boldsymbol{V}_h, \\ -b(q_h, \boldsymbol{v}_h) &= (q_h, f_p)_0 && \text{for all } q_h \in Q_h. \end{aligned} \tag{$\mathrm{P}_{stat,h}$}$$

Lemma 4.2.2
Problem ($\mathrm{P}_{stat,h}$) has a unique solution $(\boldsymbol{v}_h, p_h) \in U_h$. The following a-priori estimate holds:

$$\|\boldsymbol{v}_h\|_1 + \|p_h\|_0 \leq C(\|\boldsymbol{f}_v\|_{-1} + \|f_p\|_0), \tag{4.3}$$

with a constant $C > 0$ independent of h.

Proof. We note that the bilinear form a automatically retains its coercivity when restricted to $\boldsymbol{V}_h$, while the LBB-condition for $\boldsymbol{V}_h \times Q_h$ had to be assumed. Existence, uniqueness, and the estimate of the solution then follow as in Lemma 3.2.1. The constant C is independent of h since we have a uniform lower bound $\widetilde{c}_b > 0$ in the LBB-condition (LBB_h). □

As an important tool for deriving error estimates we present a variant of the well-known Céa's Lemma for the stationary problem.

Lemma 4.2.3 (Quasi-optimality of solutions)
Assume $(\boldsymbol{v}_h, p_h) \in U_h$ and $(\boldsymbol{v}, p) \in U$ are the solutions of ($\mathrm{P}_{stat,h}$) and (P_{stat}) for the same right hand side $f = (\boldsymbol{f}_v, f_p) \in U'$. We then have the following quasi-optimality *property of the discrete solution:*

$$\|\boldsymbol{v}_h - \boldsymbol{v}\|_1 + \|p_h - p\|_0 \leq C \left(\inf_{\boldsymbol{\psi}_h \in \boldsymbol{V}_h} \|\boldsymbol{\psi}_h - \boldsymbol{v}\|_1 + \inf_{\varphi_h \in Q_h} \|\varphi_h - p\|_0 \right).$$

Proof. We may take the difference of the continuous and discrete equations to get

$$\begin{aligned} a(\boldsymbol{w}_h, \boldsymbol{v}_h - \boldsymbol{v}) + b(p_h - p, \boldsymbol{w}_h) &= 0, \\ -b(q_h, \boldsymbol{v}_h - \boldsymbol{v}) &= 0, \end{aligned}$$

for all $(\boldsymbol{w}_h, q_h) \in U_h$. This also implies

$$\begin{aligned} a(\boldsymbol{w}_h, \boldsymbol{v}_h - \boldsymbol{\psi}_h) + b(p_h - \varphi_h, \boldsymbol{w}_h) &= a(\boldsymbol{w}_h, \boldsymbol{v} - \boldsymbol{\psi}_h) + b(p - \varphi_h, \boldsymbol{w}_h), \\ -b(q_h, \boldsymbol{v}_h - \boldsymbol{\psi}_h) &= -b(q_h, \boldsymbol{v} - \boldsymbol{\psi}_h), \end{aligned}$$

for all $(\boldsymbol{w}_h, q_h)$, $(\boldsymbol{\psi}_h, \varphi_h) \in U_h$. We use the right hand side to define a functional $F = (\boldsymbol{F}_v, F_p) \in U'$ as follows:

$$\begin{aligned} \langle \boldsymbol{w}, \boldsymbol{F}_v \rangle_{\boldsymbol{V} \times \boldsymbol{V}'} &= a(\boldsymbol{w}, \boldsymbol{v} - \boldsymbol{\psi}_h) + b(p - \varphi_h, \boldsymbol{w}), \\ (q, F_p)_0 &= -b(q, \boldsymbol{v} - \boldsymbol{\psi}_h). \end{aligned}$$

With this definition we may use the a-priori estimate (4.3) to derive

$$\begin{aligned} \|\boldsymbol{v}_h - \boldsymbol{\psi}_h\|_1 + \|p_h - \varphi_h\|_0 &\leq C(\|\boldsymbol{F}_v\|_{-1} + \|F_p\|_0) \\ &\leq C\left(C_a \|\boldsymbol{v} - \boldsymbol{\psi}_h\|_1 + C_b(\|p - \varphi_h\|_0 + \|\boldsymbol{v} - \boldsymbol{\psi}_h\|_1)\right) \\ &\leq C\left(\|\boldsymbol{v} - \boldsymbol{\psi}_h\|_1 + \|p - \varphi_h\|_0\right). \end{aligned}$$

Finally we use the triangle inequality to get

$$\begin{aligned} \|\boldsymbol{v}_h - \boldsymbol{v}\|_1 + \|p_h - p\|_0 &\leq \|\boldsymbol{v}_h - \boldsymbol{\psi}_h\|_1 + \|\boldsymbol{\psi}_h - \boldsymbol{v}\|_1 + \|p_h - \varphi_h\|_0 + \|\varphi_h - p\|_0 \\ &\leq (C+1)\left(\|\boldsymbol{v} - \boldsymbol{\psi}_h\|_1 + \|p - \varphi_h\|_0\right). \end{aligned}$$

Since $\boldsymbol{\psi}_h$ and φ_h are arbitrary, we may take the inf on the right hand side. □

In the following we will use $U_h^k = \boldsymbol{V}_h^k \times Q_h^k$ as the Taylor-Hood finite element space defined above to define a convergent spatial discretization. Combining Theorem 4.1.10 and Lemma 4.2.3 we immediately have the following convergence theorem:

Theorem 4.2.4 (Convergence of stationary problem)
Let $\{\mathcal{T}_h\}_h$ be a regular family of conforming triangulations of $\Omega \subset \mathbb{R}^d$, $d \leq 3$. Let $U_h^k = \boldsymbol{V}_h^k \times Q_h^k$ be the Taylor-Hood element space of order $k \in \mathbb{N}$. Assume that the solution of (P_{stat}) fulfills the regularity property $(\boldsymbol{v}, p) \in \boldsymbol{H}^{k+1}(\Omega) \times H^k(\Omega)$.

We then have the error estimate

$$\|\boldsymbol{v}_h - \boldsymbol{v}\|_1 + \|p_h - p\|_0 \leq C h^s \left(|\boldsymbol{v}|_{s+1} + |p|_s\right), \tag{4.4}$$

with $0 \leq s \leq k$, where the constant C is independent of h.

Remark 4.2.5 (Regularity of (P_{stat}))
Unfortunately, we do not have satisfying regularity properties of the Stokes-like system (P_{stat}) on typical meshes used for finite element calculations.

Assume that the right hand sides satisfy $\boldsymbol{f}_v \in \boldsymbol{H}^m(\Omega)$, $f_p \in H^{m+1}(\Omega)$, $m \geq 0$. From [72, Proposition 2.3] we have

$$\partial\Omega \in C^{m+2}, \quad \nu_2 = 0, \quad d = 2, 3 \Longrightarrow (\boldsymbol{v}, p) \in \boldsymbol{H}^{m+2}(\Omega) \times H^{m+1}(\Omega).$$

Here, ν_2 is the coefficient of bulk viscosity, see (3.1) on page 19, and d is the dimension of the domain Ω. To gain optimal a-priori error estimates on a domain with smooth boundary we would have to use iso-parametric elements as described e. g. in [9]. Another regularity property applicable for non-smooth domains is specified in [42]:

$$\partial\Omega \in C^{0,1}, \quad \nu_2 = 0, \quad d = 2 \Longrightarrow (\boldsymbol{v}, p) \in \boldsymbol{H}^2(\Omega) \times H^1(\Omega).$$

4.2.2 Quasi-stationary approach

The quasi-stationary approach introduced in Chapter 3 was based on the assumption of time-harmonic acoustic solutions as a response to harmonic driving forces. Recalling the definition of the continuous spaces for the quasi-stationary approach in (3.27), page 39, we now assume that $X_h \subset X$ and $Y_h \subset Y$ are finite dimensional subspaces fulfilling the discrete LBB-condition

$$\inf_{p_h \in Y_h \setminus \{0\}} \sup_{u_h \in X_h \setminus \{0\}} \frac{\mathfrak{b}(p,u)}{\|p_h\|_Y \|u_h\|_X} \geq \widetilde{c}_{\mathfrak{b},h} \geq \widetilde{c}_{\mathfrak{b}} > 0. \tag{LBB$_{qs,h}$}$$

Problem 3.3.2 corresponds to:

Problem 4.2.6 (Discrete harmonic approach)
Given $f_X \in X'$, $f_Y \in Y'$ find $v_h = (\boldsymbol{v}_{h,c}, \boldsymbol{v}_{h,s}) \in X_h$ and $p_h = (p_{h,c}, p_{h,s}) \in Y_h$ so that

$$\begin{aligned} \mathfrak{a}(w_h, v_h) + \mathfrak{b}(p_h, w_h) &= \langle w_h, f_X \rangle_{X \times X'} \quad \text{for all } w_h \in X_h, \\ -\mathfrak{b}(q_h, v_h) + \mathfrak{c}(q_h, p_h) &= \langle q_h, f_Y \rangle_{Y \times Y'} \quad \text{for all } q_h \in Y_h. \end{aligned} \tag{P$_{qs,h}$}$$

The well-posedness of Problem 4.2.6 as stated in the next Lemma is obvious, using the same methods as before.

Lemma 4.2.7
Problem (P$_{qs,h}$) possesses a unique solution $(v_h, p_h) \in X_h \times Y_h$. The following a-priori estimate holds:

$$\|v_h\|_X + \|p_h\|_Y \leq C(\|f_X\|_{X'} + \|f_Y\|_{Y'}).$$

As finite element spaces X_h and Y_h we define

$$\begin{aligned} X_h^k &= \boldsymbol{V}_h^k \times \boldsymbol{V}_h^k \subset X, \\ Y_h^k &= Q_h^k \times Q_h^k \subset Y, \end{aligned} \tag{4.5}$$

for $k \in \mathbb{N}$. The finite element spaces thus simply consist of two copies of the Taylor-Hood element spaces defined above.

As in the proof of Lemma 3.3.1 we may quickly verify that the Taylor-Hood LBB condition (LBB$_h$(TH)) may be extended to an LBB-condition (LBB$_{qs,h}$) for the pair $X_h^k \times Y_h^k$. Making use of approximation properties of the finite element spaces $X_h^k \times Y_h^k$ we arrive at a convergence theorem as before.

Theorem 4.2.8 (Convergence of quasi-stationary problem)
Let $\{\mathcal{T}_h\}_h$ be a regular family of conforming triangulations of $\Omega \subset \mathbb{R}^d$, $d \leq 3$. Let $X_h^k \times Y_h^k \subset X \times Y$ be defined as above, $k \in \mathbb{N}$. Assume that the solution of (P$_{qs}$) fulfills the regularity property $(v,p) \in \boldsymbol{H}^{k+1}(\Omega)^2 \times H^k(\Omega)^2$.

We then have the error estimate

$$\|v_h - v\|_X + \|p_h - p\|_Y \leq C h^s \left(|v|_{s+1} + |p|_s \right), \tag{4.6}$$

with $0 \leq s \leq k$, where the constant C is independent of h.

4.2.3 Instationary problem

We now turn to the discretization of the instationary problem (P) on page 24. As before, we assume that $U_h = \boldsymbol{V}_h \times Q_h \subset U$ is a finite dimensional subspace fulfilling the LBB condition (LBB_h). If we replace U by the discrete space U_h in (P) we gain the semi-discretized problem

Problem 4.2.9 (Semi-discretized instationary problem)
Let $u_{h,0} = (\boldsymbol{v}_{h,0}, p_{h,0}) \in U_h$ and $f = (\boldsymbol{f}_v, f_p) \in L^2(0,T;U')$. Find $u_h = (\boldsymbol{v}_h, p_h) \in H^1(0,T;U_h)$ so that

$$\begin{aligned} \big(\psi_h, u_h'(t)\big)_H + s(\psi_h, u_h(t)) = \langle \psi_h, f(t)\rangle_{U\times U'} \quad &\text{for all } \psi_h \in U_h, \text{ a. e. in } (0,T), \\ u(0) = u_{h,0}. \end{aligned} \tag{P_h}$$

We observe that (P_h) is equivalent to an ODE initial-value problem in $\mathbb{R}^{n_h}$, where $n_h = \dim U_h$. Existence and uniqueness of solutions follow as in Lemma 3.2.7.

For a full discretization we choose a sequence of variable time steps $\tau_n > 0$, $n = 1, \dots, N$ and set

$$t_n := \sum_{m=1}^{n} \tau_m, \quad T = t_N, \quad \tau = \max_{m=1,\dots,N} \tau_m.$$

We are now looking for an approximation $u_h^n \in U_h$ of the semi-discrete solution $u_h(t_n) \in U_h$ at the discrete times t_n. As usual, this is achieved by replacing the time derivative $u_h'(t_n)$ with a difference quotient

$$\frac{du_h}{dt}(t_n) \approx \frac{u_h^n - u_h^{n-1}}{\tau_n}.$$

The time discretization schemes used in this work are the classical Backward Euler and Crank-Nicolson schemes (see [19]) which are of first resp. second order in time and possess good stability properties. Both schemes are special cases of the *Theta-scheme* which we now define.

Problem 4.2.10 (Theta-scheme for the instationary problem)
Choose $\theta \in [0,1]$. Let $u_{h,0} = (\boldsymbol{v}_{h,0}, p_{h,0}) \in U_h$ and $f = (\boldsymbol{f}_v, f_p) \in C([0,T], U')$. Find a sequence $(u_h^n)_n = ((\boldsymbol{v}_h^n, p_h^n))_n \subset U_h$ so that for all $n = 1, \dots, N$

$$\begin{aligned} \frac{1}{\tau_n}(\psi_h, u_h^n - u_h^{n-1})_H + s(\psi_h, u_h^{n-1+\theta}) = \langle \psi_h, f(t_{n-1+\theta})\rangle_{U\times U'} \quad &\text{for all } \psi_h \in U_h, \\ u_h^0 = u_{h,0}. \end{aligned} \tag{$\mathrm{P}_{h,\tau}$}$$

Here we have used the shortcuts

$$\begin{aligned} u_h^{n-1+\theta} &= u_h^{n-1} + \theta(u_h^n - u_h^{n-1}), \\ t_{n-1+\theta} &= t_{n-1} + \theta(t_n - t_{n-1}). \end{aligned}$$

Remark 4.2.11
For $\theta \in (0,1]$ the Theta-scheme is an implicit scheme since u_n must be found as the solution of a stationary Stokes-like system. However, even for $\theta = 0$ we still need an inversion of a mass matrix due to the scalar product $(\cdot,\cdot)_H$. Special values of θ yield well-known algorithms:

- $\theta = 0$: first order forward Euler scheme,
- $\theta = \frac{1}{2}$: second order Crank-Nicolson scheme,
- $\theta = 1$: first order backward (implicit) Euler scheme.

To derive error estimates for the solution of ($P_{h,\tau}$) we will assume from now on that the following hypothesis holds.

Assumption 4.2.12
Let $\Omega \subset \mathbb{R}^d$, $d = 1, 2, 3$. Assume that the discrete space $U_h \subset U$ is chosen so that

$$\inf_{u_h \in U_h} \|u_h - u\|_U \leq C h^k (|\boldsymbol{v}|_{k+1} + |p|_k),$$

for all $u = (\boldsymbol{v}, p) \in U \cap \left(\boldsymbol{H}^{k+1}(\Omega) \times H^k(\Omega)\right)$, with a fixed $k \in \mathbb{N}$ and C independent of h, $\boldsymbol{v}$, p.

Assumption 4.2.12 may be fulfilled by choosing the Taylor-Hood spaces defined above.

We now define define a projection operator which is an analog of the Ritz projection in the case of the heat equation.

Theorem and Definition 4.2.13 (Stokes projection)
There exists a continuous linear operator $\Pi_s : U \to U_h$ fulfilling

$$s(w_h, \Pi_s u) = s(w_h, u) \qquad \text{for all } w_h \in U_h, \tag{4.7}$$

for all $u \in U$. Furthermore, we have the estimate

$$\|u - \Pi_s u\|_U \leq C h^k (|\boldsymbol{v}|_2 + |p|_1), \tag{4.8}$$

for all $u = (\boldsymbol{v}, p) \in U \cap \left(\boldsymbol{H}^{k+1}(\Omega) \times H^k(\Omega)\right)$.

Proof. Let $u \in U$. We notice that the right hand side of (4.7) defines a functional $F \in U'$, $F_u = s(\cdot, u)$. Trivially, we have the property that u is the solution of

$$s(w, u) = \langle w, F_u \rangle_{U \times U'} \qquad \text{for all } w \in U.$$

We define $\Pi_s u = u_h$ as the solution of

$$s(w_h, u_h) = \langle w_h, F_u \rangle_{U \times U'} \qquad \text{for all } w_h \in U_h,$$

thus fulfilling (4.7). The continuity of the operator Π_s is guaranteed by the a-priori estimate for the stationary system (4.3).

Now assume that $u = (\boldsymbol{v}, p)$ is also regular, i. e. $u \in U \cap \left(\boldsymbol{H}^{k+1}(\Omega) \times H^k(\Omega)\right)$. Lemma 4.2.3 yields

$$\|u - \Pi_s u\|_U \leq C \inf_{w_h \in U_h} \|w_h - u\|_U ,$$

which may be improved using Assumption 4.2.12 to

$$\|u - \Pi_s u\|_U \leq Ch^k(|\boldsymbol{v}|_2 + |p|_1).$$

This proves (4.8). □

We will now prove error estimates in terms of h and τ for the backward Euler and Crank-Nicolson schemes. The following discrete analog of Gronwall's Lemma is standard and easily proved by induction. We present it here for the reader's convenience.

Lemma 4.2.14 (Discrete Gronwall inequality)
Let $\{z_n\}_{n\in\mathbb{N}}$ be a sequence of nonnegative real numbers satisfying

$$z_n \leq \alpha_n + \sum_{k=0}^{n-1} \beta_k z_k, \qquad n \geq 0,$$

where $\{\alpha_n\}_{n\in\mathbb{N}}$ is a nondecreasing sequence of nonnegative numbers and $\beta_k \geq 0$. Then

$$z_n \leq \alpha_n \exp\left(\sum_{k=0}^{n-1} \beta_k\right), \qquad n \geq 0.$$

Theorem 4.2.15 (Convergence of backward Euler)
Assume that the exact solution $u = (\boldsymbol{v}, p) \in W(0,T)$ of (P) satisfies

$$u \in H^2(0,T;H) \text{ and } u \in H^1(0,T;\boldsymbol{H}^2(\Omega) \times H^1(\Omega)).$$

Let u_h^n, $n = 1,\dots,N$ be the solution of Problem ($P_{h,\tau}$) using $\theta = 1$, that is backwards Euler scheme. Then

$$\max_{n=0,\dots,N} \|u_h^n - u^n\|_H \leq C\Big\{\|u_{h,0} - u_0\|_H + h\left(\|u_0\|_H + \|u'\|_{L^2(0,T;\boldsymbol{H}^2(\Omega)\times H^1(\Omega))}\right) + \tau\|u''\|_{L^2(0,T;H)}\Big\}. \quad (4.9)$$

Here we have set $u^n = u(t_n)$, $n = 0,\dots,N$ as well as $|(\boldsymbol{v},p)|^2 = |\boldsymbol{v}|_2^2 + |p|_1^2$.

Proof. Let $\psi_h \in U_h$, $n \in \mathbb{N}$. We will denote the H-scalar product and norm as simply $(\cdot,\cdot)$ resp. $\|\cdot\|$. The exact solution u corresponding to the data f, u_0 fulfills

$$(\psi_h, u'(t_n)) + s(\psi_h, u^n) = \langle \psi_h, f(t_n)\rangle_{U\times U'}.$$

Adding a difference quotient yields

$$\frac{1}{\tau_n}(\psi_j, u^n - u^{n-1}) + s(\psi_h, u^n) = \langle \psi_h, f(t_n)\rangle_{U\times U'} + (\psi_h, \frac{1}{\tau_n}(u^n - u^{n-1}) - u'(t_n)).$$

The discrete solution u_h calculated using backwards Euler satisfies

$$\frac{1}{\tau_n}(\psi_h, u_h^n - u_h^{n-1}) + s(\psi_h, u_h^n) = \langle \psi_h, f(t_n)\rangle_{U\times U'}.$$

Combining these gives us

$$\frac{1}{\tau_n}(\psi_h,(u_h^n-u^n)-(u_h^{n-1}-u^{n-1}))+s(\psi_h,u_h^n-u^n)=-(\psi_h,\frac{1}{\tau_n}(u^n-u^{n-1})-u'(t_n)).$$

We decompose the error according to

$$\begin{aligned} u_h^n-u^n &= E^n-e^n,\\ E^n &= u_h^n-\Pi_s u^n,\\ e^n &= u^n-\Pi_s u^n. \end{aligned}$$

The error term e^n is the "easy" part which may easily be treated using interpolation properties of Π_s. For the "difficult" part E^n we get

$$\begin{aligned}(\psi_h,E^n-E^{n-1})+\tau_n s(\psi_h,E^n) &= (\psi_h,e^n-e^{n-1})\\ &\quad+\tau_n\underbrace{s(\psi_h,e^n)}_{=0}-(\psi_h,u^n-u^{n-1}-\tau_n u'(t_n)).\end{aligned}$$

Now choose $\psi_h=E^n\in U^h$. This yields

$$\|E^n\|^2-(E^n,E^{n-1})+\tau s(E^n,E^n)=(E^n,e^n-e^{n-1})-(E^n,u^n-u^{n-1}-\tau_n u'(t_n)).$$

Using the identity

$$\left\|E^n-E^{n-1}\right\|^2=\|E^n\|^2-2(E^n,E^{n-1})+\left\|E^{n-1}\right\|^2$$

yields

$$(E^n,E^{n-1})=\frac{1}{2}(\|E^n\|^2+\left\|E^{n-1}\right\|^2)-\frac{1}{2}\left\|E^n-E^{n-1}\right\|^2$$

and thus

$$\begin{aligned}&\frac{1}{2}(\|E^n\|^2-\left\|E^{n-1}\right\|^2)+\frac{1}{2}\left\|E^n-E^{n-1}\right\|^2+\tau_n s(E^n,E^n)\\ &\qquad\le\|E^n\|\left(\left\|e^n-e^{n-1}\right\|+\left\|u^n-u^{n-1}-\tau_n u'(t_n)\right\|\right)\\ &\qquad=\frac{\tau_n}{4T}\|E^n\|^2+\frac{T}{\tau_n}\left(\left\|e^n-e^{n-1}\right\|+\left\|u^n-u^{n-1}-\tau_n u'(t_n)\right\|\right)^2.\end{aligned}$$

Summing this inequality for $n=1,\dots,k$ yields

$$\begin{aligned}\frac{1}{2}\left\|E^k\right\|^2 &\le \frac{1}{4T}\sum_{n=1}^{k}\tau_n\|E^n\|^2+\alpha_k\\ &\le \frac{1}{4}\left\|E^k\right\|^2+\frac{1}{4T}\sum_{n=1}^{k-1}\tau_n\|E_n\|^2+\alpha_k,\end{aligned}$$

where

$$\alpha_k=\frac{1}{2}\left\|E^0\right\|^2+T\sum_{n=1}^{k}\frac{1}{\tau_n}\left(\left\|e^n-e^{n-1}\right\|+\left\|u^n-u^{n-1}-\tau_n u'(t_n)\right\|\right)^2.$$

We may now apply the discrete Gronwall lemma 4.2.14 to get

$$\left\|E^k\right\|^2 \leq C(T)\Bigg(\left\|E^0\right\|^2 + \sum_{n=1}^{k} \frac{1}{\tau_n} \left(\left\|e^n - e^{n-1}\right\| + \left\|u^n - u^{n-1} - \tau_n u'(t_n)\right\|\right)^2\Bigg). \quad (4.10)$$

We will now estimate terms on the right hand side of (4.10). Since time derivatives commute with interpolation we have

$$\begin{aligned} e^n - e^{n-1} &= (u(t_n) - \Pi_s u(t_n)) - (u(t_{n-1}) - \Pi_s u(t_{n-1})) \\ &= \int_{t_{n-1}}^{t_n} \frac{d}{dt}\left(u(t) - \Pi_s u(t)\right) dt = \int_{t_{n-1}}^{t_n} u'(t) - \Pi_s u'(t) dt. \end{aligned}$$

Using (4.8) this yields

$$\left\|e^n - e^{n-1}\right\| \leq \int_{t_{n-1}}^{t_n} \left\|u'(t) - \Pi_s u'(t)\right\| dt \leq Ch \int_{t_{n-1}}^{t_n} \left\|u'(t)\right\| dt.$$

Using Hölder's inequality then leads to

$$\begin{aligned} \frac{1}{\tau_n}\left\|e^n - e^{n-1}\right\|^2 &\leq C\frac{h^2}{\tau_n}\left(\int_{t_{n-1}}^{t_n} \left\|u'(t)\right\| dt\right)^2 \\ &\leq Ch^2 \int_{t_{n-1}}^{t_n} \left\|u'(t)\right\|^2 dt. \end{aligned}$$

For the third term in (4.10) we may use a Taylor expansion to get

$$u(t_n) - u(t_{n-1}) - \tau_n u'(t_n) = -\int_{t_{n-1}}^{t_n} (t - t_{n-1}) u''(t) dt$$

and so

$$\left\|u^n - u^{n-1} - \tau_n u'(t_n)\right\| \leq \int_{t_{n-1}}^{t_n} (t - t_{n-1}) \left\|u''(t)\right\| dt \leq \tau_n \int_{t_{n-1}}^{t_n} \left\|u''(t)\right\| dt.$$

As before, this yields

$$\frac{1}{\tau_n}\left\|u^n - u^{n-1} - \tau_n u'(t_n)\right\|^2 \leq \frac{\tau_n^2}{\tau_n}\left(\int_{t_{n-1}}^{t_n} \left\|u''(t)\right\| dt\right)^2 \leq \tau_n^2 \int_{t_{n-1}}^{t_n} \left\|u''(t)\right\|^2 dt$$

The first term may be handled as follows:

$$\begin{aligned} \left\|E^0\right\| = \left\|u_{h,0} - \Pi_s u_0\right\| &\leq \left\|u_{h,0} - u_0\right\| + \left\|u_0 - \Pi_s u_0\right\| \\ &\leq \left\|u_{h,0} - u_0\right\| + Ch\left\|u_0\right\|, \end{aligned}$$

and therefore (4.10) finally leads to

$$\left\|E^k\right\|^2 \leq C\Big\{\|u_{h,0}-u_0\|^2 + h^2\left(\|u_0\|^2 + \int_0^T \|u'(t)\|^2\,dt\right) + \tau^2\int_0^T \|u''(t)\|^2\,dt\Big\}. \quad (4.11)$$

For the "easy" error e^k we derive

$$\begin{aligned}\left\|e^k\right\|^2 &= \|u(t_k)-\Pi_s u(t_k)\|^2\\ &\leq Ch^2\|u(t_k)\|^2\\ &= Ch^2\left\|u_0+\int_0^{t_k} u'(t)dt\right\|^2\\ &\leq Ch^2\left(2\|u_0\|^2 + 2T\int_0^T \|u'(t)\|^2\,dt\right).\end{aligned} \quad (4.12)$$

Using

$$\left\|u_h^k-u^k\right\|^2 \leq 2\left(\left\|E^k\right\|^2+\left\|e^k\right\|^2\right)$$

we finally combine (4.11) and (4.12) to yield the desired result (4.9). □

Remark 4.2.16 (Good starting values, optimal estimates)
If we choose $u_{h,0}$ well, e. g. $u_{h,0}=\Pi_s u_0$ so that

$$\|u_{h,0}-u_0\|_H \leq Ch\,\|u_0\|_H$$

we will get the overall estimate of the form

$$\max_{n=0,\dots,N}\|u_h^n-u^n\|_H \leq C(u)(h+\tau).$$

Note that this estimate is not optimal in the sense that we expect a higher order of spatial convergence $\mathcal{O}(h^2)$ for the velocity component $\boldsymbol{v}$ in the L^2-norm. Although a more careful and detailed treatment is expected to yield this better result, the prior simpler theorem was mainly intended to demonstrate the temporal order of convergence. The same holds true for the following theorem.

Theorem 4.2.17 (Convergence of Crank-Nicolson)
Assume that the exact solution $u=(\boldsymbol{v},p)\in W(0,T)$ of (P) satisfies

$$u\in H^3(0,T;H) \text{ and } u\in H^2(0,T;\boldsymbol{H}^2(\Omega)\times H^1(\Omega)).$$

Let u_h^n, $n=1,\dots,N$ be the solution of ($P_{h,\tau}$) using $\theta=\frac{1}{2}$, i. e. the Crank-Nicolson scheme. Then

$$\max_{n=0,\dots,N}\|u_h^n-u^n\|_H \leq C\Big\{\|u_{h,0}-u_0\|_H + h\left(\|u_0\|_H+\|u'\|_{L^2(0,T;\boldsymbol{H}^2(\Omega)\times H^1(\Omega))}\right) + \tau^2\left(\|Su''\|_{L^2(0,T;H)}+\|u'''\|_{L^2(0,T;H)}\right)\Big\}. \quad (4.13)$$

Here we have used the same notation as in Theorem 4.2.15 and the Stokes operator $S : U \to H$ as defined in (3.9) on page 23.

Proof. We will use the same methods as in the proof of Theorem 4.2.15. For $t_{n-\frac{1}{2}} = \frac{1}{2}(t_{n-1} + t_n)$ we have the Taylor expansions

$$u(t_n) = u(t_{n-\frac{1}{2}}) + \frac{\tau_n}{2}u'(t_{n-\frac{1}{2}}) + \frac{1}{2}\frac{\tau_n^2}{4}u''(t_{n-\frac{1}{2}}) + \frac{1}{2}\int_{t_{n-\frac{1}{2}}}^{t_n}(t-t_n)^2u'''(t)dt$$

as well as

$$u(t_{n-1}) = u(t_{n-\frac{1}{2}}) - \frac{\tau_n}{2}u'(t_{n-\frac{1}{2}}) + \frac{1}{2}\frac{\tau_n^2}{4}u''(t_{n-\frac{1}{2}}) + \frac{1}{2}\int_{t_{n-\frac{1}{2}}}^{t_{n-1}}(t-t_{n-1})^2u'''(t)dt.$$

Subtracting these yields

$$\begin{aligned} u^n - u^{n-1} &= \tau_n u'(t_{n-\frac{1}{2}}) + \underbrace{\frac{1}{2}\int_{t_{n-1}}^{t_{n-\frac{1}{2}}}(t-t_{n-1})^2u'''(t)dt + \frac{1}{2}\int_{t_{n-\frac{1}{2}}}^{t_n}(t-t_n)^2u'''(t)dt}_{=:-A^n} \\ &= \tau_n(f(t_{n-\frac{1}{2}}) - Su(t_{n-\frac{1}{2}})) - A^n. \end{aligned}$$

Let $\psi_h \in U_h$. Using the regularity of the solution u it follows that

$$\begin{aligned} &(\psi_h, u^n - u^{n-1}) + \frac{\tau_n}{2}s(\psi_h, u^n + u^{n-1}) \\ &\quad = \tau_n(\psi_h, \underbrace{\frac{1}{2}(Su^n + Su^{n-1}) - Su^{n-\frac{1}{2}}}_{=:-B^n}) + \tau_n\langle\psi_h, f(t_{n-\frac{1}{2}})\rangle_{U\times U'} - (\psi_h, A^n). \end{aligned}$$

The discrete solution gained using the Crank-Nicolson scheme satisfies

$$(\psi_h, u_h^n - u_h^{n-1}) + \frac{\tau_n}{2}s(\psi_h, u_h^n + u_h^{n-1}) = \tau_n\langle\psi_h, f(t_{n-\frac{1}{2}})\rangle_{U\times U'}.$$

This yields the error equation

$$\begin{aligned} (\psi_h, (u_h^n - u^n) - (u_h^{n-1} - u^{n-1})) + \frac{\tau_n}{2}s(\psi_h, (u_h^n - u^n) + (u_h^{n-1} - u^{n-1})) \\ = (\psi_h, A^n) + \tau_n(\psi_h, B^n). \end{aligned}$$

Again, we set $u_h^n - u^n = (u_h^n - \Pi_s u^n) - (u^n - \Pi_s u^n) = E^n - e^n$. We gain the following equation for E^n:

$$(\psi_h, E^n - E^{n-1}) + \frac{\tau_n}{2}s(\psi_h, E^n + E^{n-1}) = (\psi_h, e^n - e^{n-1}) + (\psi_h, A^n) + \tau_n(\psi_h, B^n).$$

Now choose $\psi_h = \frac{1}{2}(E^n + E^{n-1}) \in U_h$. As in the proof of Theorem 4.2.15 this leads to

$$\begin{aligned} \frac{1}{2}(\|E^n\|^2 - \left\|E^{n-1}\right\|^2) + \frac{\tau_n}{4}s(E^n + E^{n-1}, E^n + E^{n-1}) \le \frac{\tau_n}{4}(\|E^n\|^2 + \left\|E^{n-1}\right\|^2) \\ + \frac{C}{\tau_n}\left\|e^n - e^{n-1}\right\|^2 + \frac{C}{\tau_n}\|A^n\|^2 + C\tau_n\|B^n\|^2. \end{aligned}$$

Summing up this inequality and using the discrete Gronwall Lemma 4.2.14 as before yields the estimate

$$\|E^n\|^2 \leq C\left\{\|E^0\|^2 + \sum_{k=1}^{n}\left(\frac{1}{\tau_k}\left\|e^k - e^{k-1}\right\|^2 + \frac{1}{\tau_k}\left\|A^k\right\|^2 + \tau_k\left\|B^k\right\|^2\right)\right\}.$$

The first and second terms are treated as before. It remains to estimate the terms in A^n and B^n. For the third term we get

$$\frac{1}{\tau_n}\|A^n\|^2 \leq \frac{1}{\tau_n}\tau_n^4\left(\int_{t_n-1}^{t_n}\left\|u'''(dt)\right\|dt\right)^2 \leq \tau^4\int_{t_{n-1}}^{t_n}\left\|u'''(t)\right\|^2 dt.$$

For the fourth term we make use of the Taylor expansions

$$Su^n = Su(t_n) = Su(t_{n-\frac{1}{2}}) + \frac{\tau_n}{2}Su'(t_{n-\frac{1}{2}}) + \frac{1}{2}\int_{t_{n-\frac{1}{2}}}^{t_n}(t_n - t)Su''(t)dt,$$

$$Su^{n-1} = Su(t_{n-1}) = Su(t_{n-\frac{1}{2}}) - \frac{\tau_n}{2}Su'(t_{n-\frac{1}{2}}) + \frac{1}{2}\int_{t_{n-\frac{1}{2}}}^{t_{n-1}}(t_{n-1} - t)Su''(t)dt,$$

hence

$$\begin{aligned}\tau_n\|B^n\|^2 &= \tau_n\left\|\frac{1}{2}(Su^n + Su^{n-1}) - Su^{n-\frac{1}{2}}\right\|^2 \\ &\leq \frac{\tau_n}{4}\tau_n^2\left(\int_{t_{n-1}}^{t_n}\left\|Su''(t)\right\|dt\right)^2 \leq \frac{\tau^4}{4}\int_{t_{n-1}}^{t_n}\left\|Su''(t)\right\|^2 dt.\end{aligned}$$

The remainder of the proof is similar to the backward Euler case. □

4.2.4 Periodic problem

We have already covered the discretization of periodic problems for which the quasi-stationary approach is valid, i. e. with problem data having harmonic time dependence. The question of how to discretize the general periodic problem 3.2.4, though, has not been treated yet.

If the problem data is regular enough then the solution of the initial value problem will converge towards the unique periodic equilibrium state, see Theorem 3.2.10. This immediately suggests a straightforward method for finding discrete periodic solutions with period $T > 0$.

We use a discrete time step τ with $T = m\tau$, $m \in \mathbb{N}$. Starting from an arbitrary starting value $u_{h,0}$ we may use the Theta-Scheme 4.2.10 to calculate a sufficient number of time step solutions u_h^n until a specified condition for periodicity of u_h^n is reached. In practice we use the following condition based on the pressure p_h:

$$\left\|\frac{1}{m}\sum_{i=n-m}^{n} e_i\right\|_0 / \|p_h^n\|_0 \leq \varepsilon, \tag{4.14}$$

where $e_i := p_h^i - p_h^{i-m}$ and $\varepsilon > 0$.

We have the following theoretical convergence result.

Lemma 4.2.18
Let $0 < T < \infty$ and $f = (\boldsymbol{f}_v, f_p)$ be a T-periodic function in H, $f|_{(0,T)} \in L^2(0,T;H)$. Set $u_0 = 0$. Assume that the solution u of the initial value problem

$$\begin{aligned} \langle w, u'(t)\rangle_{U\times U'} + s(w,u(t)) &= \langle w, f(t)\rangle_{U\times U'} \quad \text{for all } w \in U, \text{ a. e. in } \mathbb{R}, \\ u(0) &= u_0 = 0, \end{aligned}$$

for f and u_0 meets the regularity criteria of Theorem 3.2.10. Let u_h^n be a corresponding discrete solution of the initial value problem as given by Problem 4.2.10.

Define $u_{per}(t) \in H$ as the solution of the periodic problem

$$\begin{aligned} \langle w, u'_{per}(t)\rangle_{U\times U'} + s(w,u_{per}(t)) &= (w, f(t))_H \quad \text{for all } w \in U, \text{ f. a. a. } t \in \mathbb{R}, \\ u_{per}(t) &= u_{per}(t+T) \quad \text{in } H, \text{ f. a. a. } t \in \mathbb{R}. \end{aligned}$$

For any $\varepsilon > 0$ there exists a sufficiently large time $\tilde{t} > 0$ and sufficiently fine discretization parameters $h > 0$, $\tau > 0$ so that

$$\max_{\substack{i\in\mathbb{N} \\ t_i\in[\tilde{t},\tilde{t}+T]}} \left\|u_h^i - u_{per}(t_i)\right\|_H \leq \varepsilon.$$

Proof. Let $\varepsilon > 0$. Choose $\tilde{t} > 0$ according to Theorem 3.2.10 so that

$$\|u(t) - u_{per}(t)\|_H \leq \frac{C}{\sqrt{t}} \leq \frac{\varepsilon}{2}$$

for all $t \geq \tilde{t}$. Now choose a sufficiently fine discretization $h > 0$, $\tau > 0$ so that for certain $r, s \in \mathbb{N}$, $r, s \geq 1$

$$\max_{\substack{i\in\mathbb{N} \\ t_i\in[\tilde{t},\tilde{t}+T]}} \left\|u_h^i - u(t_i)\right\|_H \leq C(h^r + \tau^s) \leq \frac{\varepsilon}{2}.$$

This may be reached e. g. using the the Crank-Nicolson time discretization together with Taylor-Hood elements. Note that the constant will generally depend on $\tilde{t}$. Combining both inequalities yields

$$\left\|u_h^i - u_{per}(t_i)\right\|_H \leq \left\|u_h^i - u(t_i)\right\|_H + \|u(t_i) - u_{per}(t_i)\|_H \leq \varepsilon$$

for all $i \in \mathbb{N}$ with $t_i \in [\tilde{t}, \tilde{t}+T]$. □

The prior result is naturally not very satisfying for practical purposes. There are other methods for determining approximate solutions to time-periodic differential equations, for example shooting methods. Very promising recent techniques may be found under the keywords *waveform relaxation* or *dynamic iteration*. For these the reader is referred to [75] and references therein. The investigation of waveform relaxation techniques for the periodic systems is future work.

Chapter 5

Free boundary problems

5.1 Free capillary boundaries

This chapter will treat the discretization of free capillary problems associated with (3.1) on page 19. Most of the available literature for free capillary boundary problems concentrates on the incompressible (nonlinear) Navier-Stokes system, see [3] and references therein. It is interesting to note that the nonlinear convection term, together with the assumption of incompressibility may actually serve to prove stability of numerical schemes, see [3, page 6]. Analytical results of existence and uniqueness, even for the more well known case of incompressible Navier-Stokes, are applicable only to special domains, small times, or rely on function spaces with high regularity properties unsuitable for a FEM discretization, see [69, 65].

5.1.1 Free boundaries and acoustic streaming

We will treat the case of Dirichlet and free capillary boundary conditions specified on subsets Γ_d, resp. Γ_f of $\partial\Omega$, $\Gamma_d \cup \Gamma_f = \partial\Omega$. We will assume that Γ_d is a topologically closed surface, implying that the contact line between free surface and walls remains fixed. We note that this hypothesis is not always valid in physical situations. However, moving contact lines cause problems in mathematical formulations due to the incompatibility of boundary conditions, see the first section of [69]. See Figure 5.1 for an illustration.

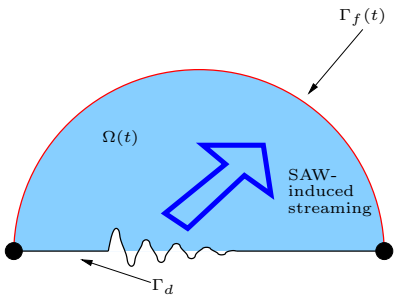

Figure 5.1: Domain $\Omega(t)$ with free capillary boundary and Dirichlet boundary.

This yields the following system:

$$\mu_v \frac{\partial \boldsymbol{v}}{\partial t} - \nabla \cdot \Sigma = \boldsymbol{f}_v \qquad \text{in } \Omega(t), t > 0, \tag{5.1a}$$

$$\mu_p \frac{\partial p}{\partial t} + \nabla \cdot \boldsymbol{v} = f_p \qquad \text{in } \Omega(t),\ t > 0, \tag{5.1b}$$

$$\boldsymbol{v} = \boldsymbol{g} \qquad \text{on } \Gamma_d, \tag{5.1c}$$

$$\Sigma \boldsymbol{n} = \sigma(d-1)\boldsymbol{\kappa} \qquad \text{on } \Gamma_f(t),\ t > 0, \tag{5.1d}$$

$$\boldsymbol{v} \cdot \boldsymbol{n} = V \qquad \text{on } \Gamma_f(t),\ t > 0, \tag{5.1e}$$

$$\Omega(0) = \Omega_0, \tag{5.1f}$$

$$\boldsymbol{v}(t = 0, \boldsymbol{x}) = \boldsymbol{v}_0 \qquad \text{in } \Omega_0, \tag{5.1g}$$

$$p(t = 0, \boldsymbol{x}) = p_0 \qquad \text{in } \Omega_0. \tag{5.1h}$$

with

$$\Sigma_{ij} = -p\delta_{ij} + \nu_1 \left(\frac{\partial v_i}{\partial x_j} + \frac{\partial v_j}{\partial x_i} \right) + (\nu_2 - \nu_1)(\nabla \cdot \boldsymbol{v})\delta_{ij} \qquad \text{the stress tensor,}$$

V the normal velocity of $\Gamma_f(t)$,

$\boldsymbol{\kappa}$ the vector of mean curvature,

$\sigma > 0$ the coefficient of surface tension.

We are interested in a sharp interface approach where the domain essentially follows the motion of the fluid. This seems most promising because of its simplicity, at the price of not being able to deal with domain topology changes, for example due to the formation of cusps. Examples of more general methods are Volume-of-Fluid [37] or the more recent Level Set methods [51, 71, 68, 70, 67]. In the standard physical situations considered we do not expect topology changes.

5.1.2 Variational formulation including curvature

To incorporate free capillary boundaries in the finite element framework, we will need a variational formulation of the curvature term, [21, 22].

We assume $\Gamma \subset \mathbb{R}^d$ to be a subset of an orientable $(d-1)$-dimensional smooth manifold M, and $\boldsymbol{\chi} : U \to \Gamma$, U open subset of $\mathbb{R}^{d-1}$ as a local parameterization of Γ. We define $g_{ij} = \partial_i \boldsymbol{\chi} \cdot \partial_j \boldsymbol{\chi}$ as the metric tensor of Γ and $g^{ij} = (g^{-1})_{ij}$ as its inverse.

For functions $f : \Gamma \to \mathbb{R}$, $\boldsymbol{f} : \Gamma \to \mathbb{R}^d$ we introduce the following differential operators on Γ:

$$(\nabla_\Gamma f) \circ \boldsymbol{\chi} := \sum_{i,j=1}^{d-1} g^{ij} \partial_i (f \circ \boldsymbol{\chi}) \partial_j \boldsymbol{\chi},$$

as the tangential derivative of f,

$$(\nabla_\Gamma \cdot \boldsymbol{f}) \circ \boldsymbol{\chi} := \sum_{i,j=1}^{d-1} g^{ij} \partial_i (\boldsymbol{f} \circ \boldsymbol{\chi}) \cdot \partial_j \boldsymbol{\chi}.$$

as the tangential divergence of $\boldsymbol{f}$, and

$$(\Delta_\Gamma f)\circ\boldsymbol{\chi} := (\nabla_\Gamma\cdot\nabla_\Gamma f)\circ\boldsymbol{\chi} = \sum_{i,j=1}^{d-1}\frac{1}{\sqrt{\det g}}\partial_i\left(\sqrt{\det g}\,g^{ij}\partial_j(f\circ\boldsymbol{\chi})\right)$$

as the Laplace-Beltrami operator of f, see for instance [2, 14]. We have the following identity:

$$\Delta_\Gamma \mathrm{id}_\Gamma = \boldsymbol{\kappa},$$

where $\boldsymbol{\kappa}$ is the mean curvature vector on Γ. Let $\boldsymbol{\psi}$ be a smooth vector valued function defined on Γ, with $\boldsymbol{\psi}=0$ on the relative boundary relbd(Γ) in M. Using partial integration on Γ we get

$$\begin{aligned}\int_\Gamma \boldsymbol{\kappa}\cdot\boldsymbol{\psi}\,d\mathcal{H}^{d-1} &= \int_\Gamma(\Delta_\Gamma\,\mathrm{id}_\Gamma)\cdot\boldsymbol{\psi}\,d\mathcal{H}^{d-1}\\ &= -\int_\Gamma \nabla_\Gamma\,\mathrm{id}_\Gamma : \nabla_\Gamma\boldsymbol{\psi}\,d\mathcal{H}^{d-1} = -\int_\Gamma \nabla_\Gamma\cdot\boldsymbol{\psi}\,d\mathcal{H}^{d-1}. \quad (5.2)\end{aligned}$$

There is no boundary term in the partial integration because $\boldsymbol{\psi}=0$ on relbd(Γ). We now return to the system (5.1). If we test (5.1a) with a smooth function $\boldsymbol{\psi}$ defined on $\bar{\Omega}(t)$ and fulfilling $\boldsymbol{\psi}=0$ on Γ_d, we get

$$\begin{aligned}\mu_v\int_\Omega\boldsymbol{\psi}\cdot\frac{\partial\boldsymbol{v}}{\partial t} - \int_\Omega\boldsymbol{\psi}\cdot\boldsymbol{f}_v &= \int_\Omega\boldsymbol{\psi}\cdot(\nabla\cdot\Sigma),\\ &= \int_\Omega\nabla\cdot(\Sigma\boldsymbol{\psi}) - \int_\Omega\Sigma:\nabla\boldsymbol{\psi},\\ &= \int_{\partial\Omega}(\Sigma\boldsymbol{\psi})\cdot\boldsymbol{n}\,d\mathcal{H}^{d-1} - \int_\Omega\Sigma:\nabla\boldsymbol{\psi}.\end{aligned}$$

Thanks to (5.2) and the boundary condition (5.1d) the boundary integral is equal to

$$\int_{\partial\Omega}(\Sigma\boldsymbol{\psi})\cdot\boldsymbol{n}\,d\mathcal{H}^{d-1} = \int_{\partial\Omega}(\Sigma\boldsymbol{n})\cdot\boldsymbol{\psi}\,d\mathcal{H}^{d-1} = -\sigma(d-1)\int_{\Gamma_f}\nabla_\Gamma\cdot\boldsymbol{\psi}\,d\mathcal{H}^{d-1}.$$

The second integral evaluates to

$$\begin{aligned}-\int_\Omega\Sigma:\nabla\boldsymbol{\psi} &= \int_\Omega p(\nabla\cdot\boldsymbol{\psi}) - \frac{\nu_1}{2}\int_\Omega D(\boldsymbol{v}):D(\boldsymbol{\psi})\\ &\quad -(\nu_2-\nu_1)\int_\Omega(\nabla\cdot\boldsymbol{v})(\nabla\cdot\boldsymbol{\psi}),\end{aligned}$$

with the *deformation tensor* $D(\boldsymbol{v}) := \nabla\boldsymbol{v}+\nabla\boldsymbol{v}^T$. Combining the last equations finally yields

$$\begin{aligned}\mu_v\int_\Omega\boldsymbol{\psi}\cdot\frac{\partial\boldsymbol{v}}{\partial t} + \frac{\nu_1}{2}\int_\Omega D(\boldsymbol{v}):D(\boldsymbol{\psi}) + (\nu_2-\nu_1)\int_\Omega(\nabla\cdot\boldsymbol{v})(\nabla\cdot\boldsymbol{\psi})\\ -\int_\Omega p(\nabla\cdot\boldsymbol{\psi}) = \int_\Omega\boldsymbol{\psi}\cdot\boldsymbol{f}_v - \sigma(d-1)\int_{\Gamma_f}\nabla_\Gamma\cdot\boldsymbol{\psi}\,d\mathcal{H}^{d-1}. \quad (5.3)\end{aligned}$$

This will be the starting point of the discrete formulation of the free boundary problem in the following section.

5.2 Discretization of free boundary problem

We will first introduce the concept of moving finite elements. The basic idea is to use a special finite element space defined on a reference triangulation which will contain the coordinate function defining the mesh nodes at any time step. We will use a time marching procedure as before to calculate the evolution of the velocity and pressure fields. The velocity at the free capillary boundary will be used to update the mesh position for the next time step.

5.2.1 Concepts of moving finite elements

For the beginning we consider the extension of the evolution problem (P), page 24, to a time dependent, but given domain $\Omega(t)$. Let $\hat{\Omega} \subset \mathbb{R}^d$ be a bounded reference domain. We define a time dependent continuous transformation to map $\hat{\Omega}$ to the current domain $\Omega(t)$:

$$\begin{aligned} \boldsymbol{\Phi} : [0,T] \times \hat{\Omega} &\to \mathbb{R}^d, \\ \boldsymbol{\Phi}(t, \hat{\Omega}) &= \Omega(t), \\ G &= \{(t, \boldsymbol{x}) \in [0,T] \times \mathbb{R}^d \mid \boldsymbol{x} \in \Omega(t)\}. \end{aligned}$$

We define a reverse transformation $\boldsymbol{\Psi}$ as follows:

$$\begin{aligned} \boldsymbol{\Psi} &: G \to \hat{\Omega}, \\ \boldsymbol{\Psi}(t, \boldsymbol{\Phi}(t, \hat{\boldsymbol{x}})) &= \hat{\boldsymbol{x}}. \end{aligned}$$

We will assume that the following natural requirements for a proper space-time domain G are fulfilled:

Assumption 5.2.1 (Admissible transformation)
Let $t \in [0,T]$. Then

- $\boldsymbol{\Phi}(t, \cdot) : \hat{\Omega} \to \Omega(t)$ is injective, and
- $\inf_{\hat{x} \in \hat{\Omega}} \det D_{\hat{x}} \boldsymbol{\Phi}(t, \hat{x}) > 0$.

Here $D_{\hat{x}} \boldsymbol{\Phi}(t, \hat{x})$ stands for the Jacobian of $\boldsymbol{\Phi}$ with respect to the space variable.

We refer to Figure 5.2 for an illustration of a time dependent domain in one space dimension. For a given function $\varphi : G \to \mathbb{R}$ we may therefore define a related reference function as

$$\begin{aligned} \hat{\varphi} : [0,T] \times \hat{\Omega} &\to \mathbb{R}, \\ \hat{\varphi}(t, \hat{x}) &= \varphi(t, \boldsymbol{\Phi}(t, \hat{x})). \end{aligned}$$

Let $\boldsymbol{\Phi}$ and $\varphi : G \to \mathbb{R}$ be sufficiently smooth to apply the chain rule of differentiation. We have:

$$\begin{aligned} D_t \hat{\varphi}(t, \hat{x}) &= D_t \varphi(t, \boldsymbol{\Phi}(t, \hat{x})) + D_x \varphi(t, \boldsymbol{\Phi}(t, \hat{x})) D_t \boldsymbol{\Phi}(t, \hat{x}) \\ &= D_t \varphi(t, x) + D_x \varphi(t, x) D_t \boldsymbol{\Phi}(t, \hat{x}), \end{aligned} \tag{5.4}$$

where $x = \boldsymbol{\Phi}(t, \hat{x})$.

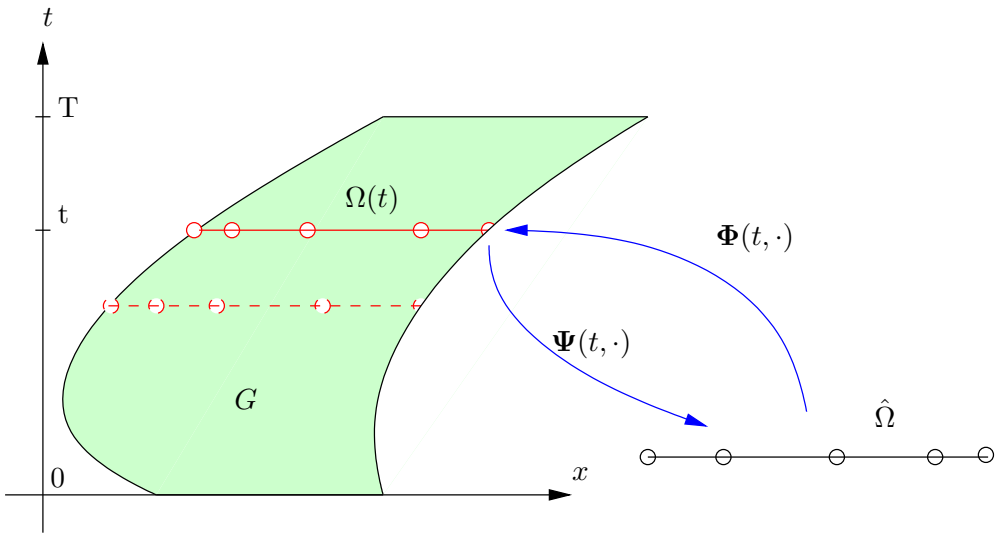

Figure 5.2: Time dependent 1D-domain with transformations.

Now we will perform a discretization in space as well as in time, as in Subsection 4.2.3. Assume that we have a finite dimensional reference subspace $\hat{U}_h \subset \hat{U}$ defined on $\hat{\Omega} = \Omega_0$. Furthermore, we assume that a sequence of discrete time steps $0 = t_0 < t_1 < \cdots < t_N = T$ are given with corresponding mesh transformations $\mathbf{\Phi}_h^n : \hat{\Omega} \to \Omega_n$, $\mathbf{\Psi}_h^n : \Omega_n \to \hat{\Omega}$.

We now seek the discrete solution

$$u_h^n \in U_{h,n} = \{\hat{\varphi}_h \circ \mathbf{\Psi}_h^n \mid \hat{\varphi}_h \in \hat{U}_h\},$$

for $n = 1, \ldots, N$. When formulating a full discretization analogous to ($P_{h,\tau}$) on page 66 we have the problem that a straight-forward replacement of a time derivative by a difference quotient is no longer possible since the domains and finite element spaces of u_h^n, u_h^{n-1} differ. However, we may use the formula (5.4) to motivate the choice of time discretization. Let $(t_{n-1}, x) \in G$, $\hat{x} = \mathbf{\Psi}(t, x)$. Then

$$\begin{aligned} D_t u(t_{n-1}, x) &= D_t \hat{u}(t_{n-1}, \hat{x}) - D_x u(t_{n-1}, x) D_t \mathbf{\Phi}(t_{n-1}, \hat{x}) \\ &\approx \frac{\hat{u}_h^n(\mathbf{\Psi}_h^{n-1} x) - \hat{u}_h^{n-1}(\mathbf{\Psi}_h^{n-1} x)}{\tau_n} \\ &\quad - D_x u_h^{n-1}(x) \left(\frac{\mathbf{\Phi}_h^n(\mathbf{\Psi}_h^{n-1} x) - \mathbf{\Phi}_h^{n-1}(\mathbf{\Psi}_h^{n-1} x)}{\tau_n} \right) \\ &= \frac{1}{\tau_n} \left(\tilde{u}_h^n(x) - u_h^{n-1}(x) \right) - \frac{1}{\tau_n} \left(D_x u_h^{n-1}(x) (\mathbf{\Phi}_h^n(\mathbf{\Psi}_h^{n-1} x) - x) \right), \end{aligned} \tag{5.5}$$

with $\tilde{u}_h^n = u_h^n \circ \mathbf{\Phi}_h^n \circ \mathbf{\Psi}_h^{n-1}$.

Remark 5.2.2 (Higher order term in (5.5))
In the practical algorithm described in the next section the transformation $\mathbf{\Phi}_n$ will naturally not be given a-priori, but must instead be calculated at each time

step. The second term on the right hand side of (5.5) is thus implicit, since $\mathbf{\Phi}_n$ is unknown. Because we wish to decouple the update of the mesh from the calculation of flow terms (cf. Algorithm 5.2.4) this term is troublesome.

The condition (5.1e) will fix the normal velocity V of the free capillary boundary, therefore it makes sense to require that the mesh change at time step $n-1$

$$\Delta_h^{n-1} := \mathbf{\Phi}_h^n \circ \mathbf{\Psi}_h^{n-1} - \mathrm{id}_{\Omega_{n-1}},$$

is of the order

$$\left\|\Delta_h^{n-1} x\right\| = \left\|\mathbf{\Phi}_h^n(\mathbf{\Psi}_h^{n-1}(x)) - x\right\| \approx \left\|x + \boldsymbol{v}_h^{n-1}(x)\tau_n - x\right\| = \tau_n \left\|\boldsymbol{v}_h^{n-1}(x)\right\|,$$

for all $x \in \Omega_{n-1}$.

If we are solving a free boundary problem for the acoustic streaming terms $\boldsymbol{v}^{(2)}$, $p^{(2)}$ in (2.6) on page 14, then the second term in (5.5) will be of order $\mathcal{O}(\epsilon^4)$. It is therefore justified to neglect that term in the algorithm below.

5.2.2 Algorithm

We will now define an algorithm to discretize the free boundary problem (5.1). We assume that a reference domain $\hat{\Omega}$ with a conforming triangulation $\hat{\mathcal{T}}$ is given. We define $\hat{\Gamma}_f \subset \partial\hat{\Omega}$ as the part of the boundary where free capillary boundary conditions are prescribed, and $\hat{\Gamma}_d \subset \partial\hat{\Omega}$ as the part with Dirichlet boundary conditions. We choose $\hat{\Gamma}_d$ to be a relatively closed surface in $\partial\hat{\Omega}$ and require $\partial\hat{\Omega} = \hat{\Gamma}_f \cup \hat{\Gamma}_d$, $\hat{\Gamma}_f \cap \hat{\Gamma}_d = \emptyset$.

We assume that $\hat{\mathcal{T}}$ is chosen in such a way that the boundary faces of the simplices $\hat{S} \in \hat{\mathcal{T}}$ induce a conforming triangulation $\hat{\mathcal{R}}$ of dimension $d-1$ of $\hat{\Gamma}_f$. We split the simplices of $\hat{\mathcal{T}}$ into two sets

$$\hat{\mathcal{T}}_i := \{S \in \hat{\mathcal{T}} \mid S \cap \hat{\Gamma}_f = \emptyset\},$$
$$\hat{\mathcal{T}}_f := \mathcal{T} \setminus \hat{\mathcal{T}}_i,$$

We thus have the property

$$\hat{\mathcal{R}} = \{\hat{T} \mid \hat{T} \text{ is } d-1 \text{ dim. simplex, } \hat{T} = \hat{S} \cap \partial\hat{\Omega},\ \hat{S} \in \mathcal{T}_f\}.$$

We define the finite element spaces for the discrete velocity, pressure, and mesh position in the interior and at the free boundary as follows:

$$\hat{\boldsymbol{V}}_h = \{\boldsymbol{w}_h \in C^0(\overline{\hat{\Omega}})^d \mid \boldsymbol{w}_h|_S \in \mathbb{P}_2(S)^d \text{ for all } S \in \hat{\mathcal{T}}, \boldsymbol{w}_h|_{\Gamma_d} = 0\},$$
$$\hat{Q}_h = \{q_h \in C^0(\overline{\hat{\Omega}}) \mid q_h|_S \in \mathbb{P}_1(S) \text{ for all } S \in \hat{\mathcal{T}}\},$$
$$\hat{M}_h = \{\mathbf{\Phi}_h \in C^0(\overline{\hat{\Omega}})^d \mid \mathbf{\Phi}_h|_S \in \mathbb{P}_1(S)^d \text{ for } S \in \hat{\mathcal{T}}_i \text{ and } \mathbf{\Phi}_h|_S \in \mathbb{P}_2(S)^d \text{ for } S \in \hat{\mathcal{T}}_f\},$$
$$\hat{R}_h = \{\boldsymbol{x}_h \in C^0(\overline{\hat{\Gamma}}_f)^d \mid \boldsymbol{x}_h|_T \in \mathbb{P}_2(T)^d \text{ for } T \in \hat{\mathcal{R}}\}.$$

In other words we use the Taylor-Hood element of order 1 for velocity and pressure, piecewise linears for the interior simplices, and piecewise quadratics for the boundary simplices. The choice of piecewise quadratics implies the use of curved simplices at the free boundary which is desirable for precise modeling of discrete curvature, cf. [3].

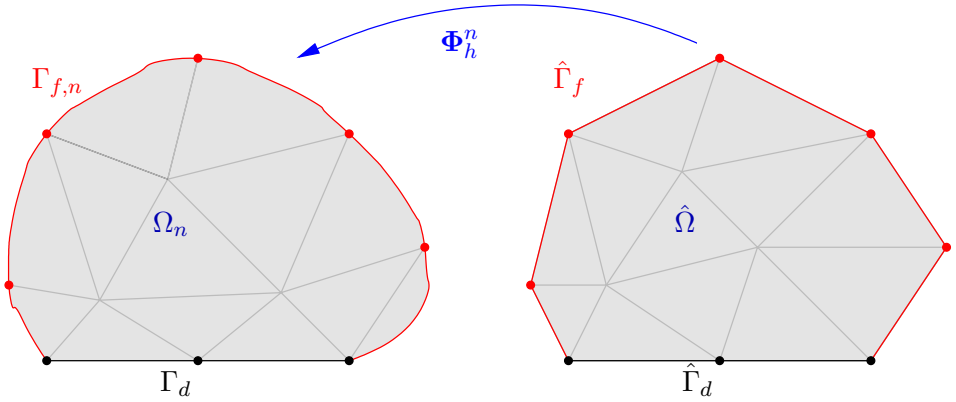

Figure 5.3: On the left: discrete transformed 2D mesh Ω_n with corresponding triangulations $\mathcal{T}^n$ and $\mathcal{R}^n$.

Remark 5.2.3 (Mean of pressure)
By our choice of $\hat{Q}_h$ we have given up the requirement $\fint_{\hat{\Omega}} p_h = 0$ for the discrete pressure p_h, confer Definition 4.1.7. It makes no sense to require this of $\hat{Q}_h$ or $Q_{h,n}$, since there are indeed situations where the mean pressure will vary with time, see the numerical experiments.

Given a transformation $\boldsymbol{\Phi}_h^n \in \hat{M}_h$ at time step n, we define the transformed mesh and spaces as follows:

$$
\begin{aligned}
\Omega_n &:= \boldsymbol{\Phi}_h^n(\hat{\Omega}),\\
\Gamma_d &:= \boldsymbol{\Phi}_h^0(\hat{\Gamma}_d),\ \text{(stays fixed)}\\
\Gamma_{f,n} &:= \boldsymbol{\Phi}_h^n(\hat{\Gamma}_f),\\
\mathcal{T}^n &:= \{\boldsymbol{\Phi}_h^n(S) \mid S \in \hat{\mathcal{T}}\},\\
\mathcal{T}_i^n &:= \{\boldsymbol{\Phi}_h^n(S) \mid S \in \hat{\mathcal{T}}_i\},\\
\mathcal{T}_f^n &:= \{\boldsymbol{\Phi}_h^n(S) \mid S \in \hat{\mathcal{T}}_f\},\\
\mathcal{R}^n &:= \{\boldsymbol{\Phi}_h^n(T) \mid T \in \hat{\mathcal{R}}\},\\
\boldsymbol{\Psi}_h^n &:= (\boldsymbol{\Phi}_h^n)^{-1} : \Omega_n \to \hat{\Omega},\\
\boldsymbol{V}_{h,n} &:= \{\hat{\boldsymbol{w}}_h \circ \boldsymbol{\Psi}_h^n \mid \hat{\boldsymbol{w}}_h \in \hat{\boldsymbol{V}}_h\},\\
Q_{h,n} &:= \{\hat{q}_h \circ \boldsymbol{\Psi}_h^n \mid \hat{q}_h \in \hat{Q}_h\},\\
M_{h,n} &:= \{\hat{\boldsymbol{x}}_h \circ \boldsymbol{\Psi}_h^n \mid \hat{\boldsymbol{x}}_h \in \hat{M}_h\},\\
R_{h,n} &:= \{\hat{\boldsymbol{x}}_h \circ \boldsymbol{\Psi}_h^n \mid \hat{\boldsymbol{x}}_h \in \hat{R}_h\}.
\end{aligned}
\tag{5.6}
$$

Figure 5.3 demonstrates how a time dependent 2D mesh is mapped from the reference mesh.

Since the domain will change with time, we define time dependent bilinear

forms on the domain $\Omega_n = \mathbf{\Phi}_h^n(\hat{\Omega})$ for a variational formulation.

$$
\begin{aligned}
&a_n : \boldsymbol{V}_{h,n} \times \boldsymbol{V}_{h,n} \to \mathbb{R},\\
&a_n(\boldsymbol{v}_h, \boldsymbol{w}_h) = \frac{\nu_1}{2} \int_{\Omega_n} D(\boldsymbol{v}_h) : D(\boldsymbol{w}_h) + (\nu_2 - \nu_1) \int_{\Omega_n} (\nabla \cdot \boldsymbol{v}_h)(\nabla \cdot \boldsymbol{w}_h),\\
&b_n : Q_{h,n} \times \boldsymbol{V}_{h,n} \to \mathbb{R},\\
&b_n(q_h, \boldsymbol{v}_h) = -\int_{\Omega_n} q_h \nabla \cdot \boldsymbol{v}_h,\\
&d_n : R_{h,n} \times R_{h,n} \to \mathbb{R},\\
&d_n(\boldsymbol{v}_h, \boldsymbol{w}_h) = \tau_n \sigma (d-1) \int_{\Gamma_{f,n}} \nabla_{\Gamma_{f,n}} \boldsymbol{v}_h \cdot \nabla_{\Gamma_{f,n}} \boldsymbol{w}_h \, \mathcal{H}^{d-1}.
\end{aligned}
\tag{5.7}
$$

Two more tools are needed to define the discretized free boundary algorithm: A discrete outer unit normal vector $\boldsymbol{n}_h^n \in R_{h,n}$ to the mesh boundary $\Gamma_{f,n}$, and a suitable extension operator $E_h : \hat{R}_h \times \hat{M}_h \to \hat{M}_h$.

The function $\boldsymbol{n}_h^n \in R_{h,n}$ is defined by setting the values in the nodes of the quadratic Lagrange mesh G_2 of $\Gamma_{f,n}$. If $T \in \mathcal{R}_n$ is a $d-1$ dimensional simplex we set

$$
\begin{aligned}
\widetilde{\boldsymbol{n}}_T &:= \boldsymbol{n}_T \mathcal{H}^{d-1}(T),\\
P(x) &:= \{T' \in \mathcal{R}_n \mid x \in T'\}.
\end{aligned}
$$

Here $\boldsymbol{n}_T$ is the (well-defined) outer unit normal vector on T. Now define $\boldsymbol{n}_h^n \in R_{h,n}$ as

$$
\boldsymbol{n}_h^n(\overline{x}) := \begin{cases} \frac{\sum_{T \in P(\overline{x})} \widetilde{\boldsymbol{n}}_T}{\left|\sum_{T \in P(\overline{x})} \widetilde{\boldsymbol{n}}_T\right|} & \text{if } \overline{x} \in \Gamma_{f,n} \\ 0 & \text{otherwise} \end{cases}
$$

for all nodes $\overline{x}$ of G_2. This means that the (well-defined) normal on faces is averaged to define values on corners or edges.

The extension operator E_h is used to define the interior nodes of Ω_n, based on the position of $\Gamma_{f,n}$ and the old mesh Ω_{n-1}:

$$
\mathbf{\Phi}_h^n = E_h(\mathbf{\Phi}_h^n|_{\hat{\Gamma}_f}, \mathbf{\Phi}_h^{n-1}).
$$

This is necessary, since the boundary condition (5.1e) only prescribes the motion of the free boundary. The interior nodes should be selected in such a manner as to guarantee a good quality of the mesh triangulation $\mathcal{T}^n$.

Algorithm 5.2.4 (Free boundary discretization)
Let $\mathbf{\Phi}_h^0 \in \hat{M}_h$ and $\boldsymbol{v}_h^0 \in \boldsymbol{V}_{h,0}$, $p_h^0 \in Q_{h,0}$, as well as $\boldsymbol{f}_v^n$, f_p^n as locally integrable functions on $\mathbb{R}^d$, $n \in \mathbb{N}$, and $\boldsymbol{g}_h$ as Dirichlet boundary conditions for the velocity. Loop over $n = 1, 2, \ldots$:

1. Solve for $(\tilde{\boldsymbol{v}}_h^n, \tilde{p}_h^n) \in (\boldsymbol{g}_h + \boldsymbol{V}_{h,n-1}) \times Q_{h,n-1}$:

$$\begin{aligned}\frac{1}{\tau_n}\int_{\Omega_{n-1}} \boldsymbol{\psi}_h \cdot \tilde{\boldsymbol{v}}_h^n + a_{n-1}(\boldsymbol{\psi}_h, \tilde{\boldsymbol{v}}_h^n) + d_{n-1}(\boldsymbol{\psi}_h, \tilde{\boldsymbol{v}}_h^n) + b_{n-1}(\tilde{p}_h^n, \boldsymbol{\psi}_h) \\ = \frac{1}{\tau_n}\int_{\Omega_{n-1}} \boldsymbol{\psi}_h \cdot \boldsymbol{v}_h^{n-1} + \int_{\Omega_{n-1}} \boldsymbol{\psi}_h \cdot \boldsymbol{f}_v^{n-1} \\ - \sigma(d-1)\int_{\Gamma_{f,n-1}} \nabla_{\Gamma_{f,n-1}} \cdot \boldsymbol{\psi}_h \, d\mathcal{H}^{d-1}, \quad (5.8)\end{aligned}$$

for all $\boldsymbol{\psi}_h \in \boldsymbol{V}_{h,n-1}$, and

$$\begin{aligned}\frac{1}{\tau_n}\int_{\Omega_{n-1}} \varphi_h \cdot \tilde{p}_h^n - b_{n-1}(\varphi_h, \tilde{\boldsymbol{v}}_h) \\ = \frac{1}{\tau_n}\int_{\Omega_{n-1}} \varphi_h \cdot p_h^{n-1} + \int_{\Omega_{n-1}} \varphi_h f_p^{n-1} \quad (5.9)\end{aligned}$$

for all $\varphi_h \in Q_{h,n-1}$.

2. Update the position of the free boundary as follows: Define

$$\begin{aligned}\boldsymbol{\Delta}_h^{n-1} &:= \tau_n(\tilde{\boldsymbol{v}}_h^n|_{\Gamma_{f,n}} \cdot \boldsymbol{n}_h^{n-1})\boldsymbol{n}_h^{n-1} \in R_{h,n-1}, \\ \boldsymbol{\Phi}_h^n|_{\hat{\Gamma}_f} &:= \left(\mathrm{id}_{\Gamma_{f,n-1}} + \boldsymbol{\Delta}_h^n\right) \circ \boldsymbol{\Phi}_h^{n-1}|_{\hat{\Gamma}_f}.\end{aligned}$$

3. Now update the position of the entire mesh:

$$\boldsymbol{\Phi}_h^n := E_h(\boldsymbol{\Phi}_h^n|_{\hat{\Gamma}_f}, \boldsymbol{\Phi}_h^{n-1}),$$

with a suitable extension operator E_h. If $\boldsymbol{\Phi}_h^n$ is not an admissible mesh transformation according to Assumption 5.2.1, then STOP.

4. Finally, set

$$\begin{aligned}\Omega_n &:= \boldsymbol{\Phi}_h^n(\hat{\Omega}), \\ \Gamma_{f,n} &:= \boldsymbol{\Phi}_h^n(\hat{\Gamma}_f), \\ \mathcal{T}^n &:= \{\boldsymbol{\Phi}_h^n(S) \mid S \in \hat{\mathcal{T}}\}, \\ \mathcal{R}^n &:= \{\boldsymbol{\Phi}_h^n(T) \mid T \in \hat{\mathcal{R}}\}, \\ \boldsymbol{\Psi}_h^n &:= (\boldsymbol{\Phi}_h^n)^{-1}, \\ \boldsymbol{v}_h^n &:= \tilde{\boldsymbol{v}}_h^n \circ \boldsymbol{\Phi}_h^{n-1} \circ \boldsymbol{\Psi}_h^n, \\ p_h^n &:= \tilde{p}_h^n \circ \boldsymbol{\Phi}_h^{n-1} \circ \boldsymbol{\Psi}_h^n.\end{aligned}$$

Remark 5.2.5
Several remarks about the free boundary algorithm are in order.

- The algorithm employs a decoupling of the bulk equations and the geometry updates, which would otherwise be coupled in a nonlinear way.

- The discretization has the following property:

$$\begin{aligned} -d_{n-1}(\boldsymbol{\psi}_h, \tilde{\boldsymbol{v}}_h^n) - \sigma(d-1) \int_{\Gamma_{f,n-1}} \nabla_{\Gamma_{f,n-1}} \cdot \boldsymbol{\psi}_h \, d\mathcal{H}^{d-1} \\ = -\sigma(d-1) \int_{\Gamma_{f,n-1}} \nabla_{\Gamma_{f,n-1}} \boldsymbol{\psi}_h \cdot \nabla_{\Gamma_{f,n-1}} (\mathrm{id}_{\Gamma_{f,n-1}} + \tau_n \tilde{\boldsymbol{v}}_h^n) \, d\mathcal{H}^{d-1}, \\ \approx \sigma(d-1) \int_{\Gamma_{f,n}} \boldsymbol{\kappa} \, d\mathcal{H}^{d-1}, \end{aligned} \tag{5.10}$$

  cf. (5.3). The capillary boundary condition is thus treated in a semi-implicit manner, since information about the new boundary position $\Gamma_{f,n}$ enters the definition of the curvature term. Furthermore, note that the term d_n adds additional coercivity on the left hand side.

  The idea for this discretization of curvature was taken from [3] where it is crucial for proving stability of a Discontinuous Galerkin scheme for the free boundary incompressible Navier-Stokes equations.

- We have defined the update of the free boundary as

$$\boldsymbol{\Phi}_h^n|_{\hat{\Gamma}_f} := \left(\mathrm{id}_{\Gamma_{f,n-1}} + \tau_n (\tilde{\boldsymbol{v}}_h^n|_{\Gamma_{f,n}} \cdot \boldsymbol{n}_h^{n-1}) \boldsymbol{n}_h^{n-1}\right) \circ \boldsymbol{\Phi}_h^{n-1}|_{\hat{\Gamma}_f}.$$

  A simpler formula, motivated by (5.10), is

$$\boldsymbol{\Phi}_h^n|_{\hat{\Gamma}_f} := \left(\mathrm{id}_{\Gamma_{f,n-1}} + \tau_n \tilde{\boldsymbol{v}}_h^n|_{\Gamma_{f,n}}\right) \circ \boldsymbol{\Phi}_h^{n-1}|_{\hat{\Gamma}_f}. \tag{5.11}$$

  This method is actually used during the mesh update algorithm 5.2.6 below.

  However, in the case of large variations of the tangential velocity at the boundary (5.11) may lead to a quick distortion of the mesh, making the definition of a suitable mesh extension E_h even more difficult. Moving the free boundary only in normal direction is justified since the set $\Gamma_{f,n}$ remains essentially the same – only the nodes defining the triangulation $\mathcal{R}_n$ are placed differently.

We conclude the discussion of the algorithm by presenting two implemented algorithms to define the mesh extension $E_h^n : \hat{R}_h \times \hat{M}_h \to \hat{M}_h$.

Algorithm 5.2.6 (Mesh update algorithm 1)
Given old mesh positions $\boldsymbol{\Phi}_h^{n-1} \in \hat{R}_h$ and the velocity field $\tilde{\boldsymbol{v}}_h^n \in \boldsymbol{V}_{h,n-1}$ of Step 1 in Algorithm 5.2.4 define $\boldsymbol{\Phi}_h^n = E(\boldsymbol{\Phi}_h^n|_{\hat{\Gamma}_f}, \boldsymbol{\Phi}_h^{n-1})$ as follows:

$$\begin{aligned} \boldsymbol{\Phi}_h^n|_{\hat{\Omega} \cup \hat{\Gamma}_f} &:= \left(\mathrm{id}_{\Omega_{n-1}} + \tau_n \tilde{\boldsymbol{v}}_h^n\right) \circ \boldsymbol{\Phi}_h^{n-1}|_{\hat{\Omega} \cup \hat{\Gamma}_f}, \\ \boldsymbol{\Phi}_h^n|_{\hat{\Gamma}_d} &:= \boldsymbol{\Phi}_h^0|_{\hat{\Gamma}_d}. \end{aligned}$$

In other words, all interior nodes as well as the nodes on the free boundary are moved with the velocity field $\tilde{\boldsymbol{v}}_h^n$.

Remark 5.2.7
This is actually a Lagrangian formulation of the flow – each mesh node can be considered to be a particle advected with the fluid. If we set the parameter μ_p as well as the mass source f_p of (3.1), page 19, to zero for our calculation, corresponding to incompressible flow without pressure time derivatives, then this method yields a consistent discretization of the standard incompressible *nonlinear* Navier-Stokes equations. We will demonstrate this surprising fact heuristically.

Let $\hat{\boldsymbol{x}} \in \hat{\Omega} \cup \hat{\Gamma}_f$ be one of the movable Lagrange grid nodes and $\boldsymbol{x}^n = \boldsymbol{\Phi}_h^n(\hat{\boldsymbol{x}})$ the position of the node at time step n, $n \in \mathbb{N}_0$. With E_h calculated using Algorithm 5.2.6 the time discretization yields

$$\begin{aligned}
\boldsymbol{v}_h^n(\boldsymbol{x}^n) &= (\boldsymbol{v}_h^n \circ \boldsymbol{\Phi}_h^n \circ \boldsymbol{\Psi}_h^{n-1})(\boldsymbol{x}^{n-1}) \\
&= (\boldsymbol{v}_h^n \circ (\mathrm{id}_{\Omega_{n-1}} + \tau_n \tilde{\boldsymbol{v}}_h^n) \circ \boldsymbol{\Phi}_h^{n-1} \circ \boldsymbol{\Psi}_h^{n-1})(\boldsymbol{x}^{n-1}) \\
&= (\boldsymbol{v}_h^n \circ (\mathrm{id}_{\Omega_{n-1}} + \tau_n \tilde{\boldsymbol{v}}_h^n))(\boldsymbol{x}^{n-1}) \\
&= \boldsymbol{v}_h^n(\boldsymbol{x}^{n-1} + \tau_n \tilde{\boldsymbol{v}}_h^n(\boldsymbol{x}^{n-1})),
\end{aligned}$$

hence

$$\begin{aligned}
\frac{1}{\tau_n}(\tilde{\boldsymbol{v}}_h^n(\boldsymbol{x}^{n-1}) - \boldsymbol{v}_h^{n-1}(\boldsymbol{x}^{n-1})) &= \frac{1}{\tau_n}(\boldsymbol{v}_h^n(\boldsymbol{x}^{n-1} + \tau_n \tilde{\boldsymbol{v}}_h^n(\boldsymbol{x}^{n-1})) - \boldsymbol{v}_h^{n-1}(\boldsymbol{x}^{n-1}) \\
&\approx \frac{d}{dt}\boldsymbol{v}_L(t_{n-1}, \boldsymbol{x}^0).
\end{aligned}$$

Here we have defined $\boldsymbol{v}_L(t, \boldsymbol{x}^0) := \boldsymbol{v}(t, \boldsymbol{\chi}(t; \boldsymbol{x}^0))$, with a particle trajectory $\boldsymbol{\chi}$ as solution of the ODE

$$\begin{aligned}
\boldsymbol{\chi}(0; \boldsymbol{x}^0) &= \boldsymbol{x}^0, \\
\frac{d}{dt}\boldsymbol{\chi}(t; \boldsymbol{x}^0) &= \boldsymbol{v}(t, \boldsymbol{\chi}(t; \boldsymbol{x}^0)),
\end{aligned}$$

for the given velocity field $\boldsymbol{v}$. The derivative of the Lagrangian velocity field $\boldsymbol{v}_L$ is

$$\begin{aligned}
\frac{d}{dt}\boldsymbol{v}_L(t_{n-1}, \boldsymbol{x}^0) &= \frac{\partial \boldsymbol{v}}{\partial t}(t_{n-1}, \boldsymbol{\chi}(t_{n-1}; \boldsymbol{x}^0)) + (\nabla \boldsymbol{v}(t_{n-1}, \boldsymbol{\chi}(t_{n-1}; \boldsymbol{x}^0)))\frac{d\boldsymbol{\chi}}{dt}(t_{n-1}; \boldsymbol{x}^0) \\
&= \frac{\partial \boldsymbol{v}}{\partial t}(t_{n-1}, \boldsymbol{\chi}(t_{n-1}; \boldsymbol{x}^0)) \\
&\quad + (\nabla \boldsymbol{v}(t_{n-1}, \boldsymbol{\chi}(t_{n-1}; \boldsymbol{x}^0)))\boldsymbol{v}(t_{n-1}, \boldsymbol{\chi}(t_{n-1}; \boldsymbol{x}^0)) \\
&\approx \frac{\partial \boldsymbol{v}}{\partial t}(t_{n-1}, \boldsymbol{x}^{n-1}) + (\nabla \boldsymbol{v}(t_{n-1}, \boldsymbol{x}^{n-1}))\boldsymbol{v}(t_{n-1}, \boldsymbol{x}^{n-1}).
\end{aligned}$$

In other words

$$\frac{1}{\tau_n}(\tilde{\boldsymbol{v}}_h^n(\boldsymbol{x}^{n-1}) - \boldsymbol{v}_h^{n-1}(\boldsymbol{x}^{n-1})) \approx \frac{\partial \boldsymbol{v}}{\partial t}(t_{n-1}, \boldsymbol{x}^{n-1}) + (\nabla \boldsymbol{v}(t_{n-1}, \boldsymbol{x}^{n-1}))\boldsymbol{v}(t_{n-1}, \boldsymbol{x}^{n-1}),$$

which shows that the solution $(\tilde{\boldsymbol{v}}_h, p_h)$ (5.8) and (5.9) approximates the nonlinear incompressible Navier-Stokes equations

$$\begin{aligned}
\frac{\partial \boldsymbol{v}}{\partial t} + (\nabla \boldsymbol{v})\boldsymbol{v} &= \nabla \cdot \Sigma(\boldsymbol{v}, p) + \boldsymbol{f}_v, \\
\nabla \cdot \boldsymbol{v} &= 0,
\end{aligned}$$

with the stress tensor Σ.

Algorithm 5.2.8 (Mesh update algorithm 2)
Given are old mesh positions $\mathbf{\Phi}_h^{n-1} \in \hat{R}_h$ as well as the new positions of the free boundary $\mathbf{\Phi}_h^n|_{\hat{\Gamma}_f}$. Determine $\mathbf{\Xi}_h \in M_{h,n-1}$ (see (5.6)) as the solution of the elliptic system

$$\begin{aligned} \int_{\Omega_{n-1}} \nabla \boldsymbol{\psi}_h : \nabla \mathbf{\Xi}_h = 0 \qquad & \text{for all } \boldsymbol{\psi}_h \in M_{h,n-1}, \\ \mathbf{\Xi}_h = \mathbf{\Phi}_h^n|_{\hat{\Gamma}_f} \circ \mathbf{\Psi}_h^{n-1} \qquad & \text{on } \Gamma_{f,n-1}, \\ \mathbf{\Xi}_h = \mathrm{id}_{\Gamma_d} \qquad & \text{on } \Gamma_d. \end{aligned}$$

Now set $\mathbf{\Phi}_h^n = E(\mathbf{\Phi}_h^n|_{\hat{\Gamma}_f}, \mathbf{\Phi}_h^{n-1})$ as

$$\mathbf{\Phi}_h^n := \mathbf{\Xi}_h \circ \mathbf{\Phi}_h^{n-1}.$$

This idea of using the Laplace operator to smooth the mesh nodes was taken from [3]. Although simple and efficient to implement this method has certain drawbacks, e. g. it can not deal with non-convex domains without modifications. Nevertheless, this algorithm was sufficient for our purposes. We refer to [59] for more sophisticated ideas on mesh smoothing.

Chapter 6

Details of the implementation

In the preceding three chapters we have covered the mathematical theory and numerical analysis of Problem 3.1.6 on fixed domains as well as the possibilities of extending this problem to capillary free boundaries. Some important details concerning the choice of algorithms to solve saddle point systems and, at the lowest level, the resulting sparse linear systems will be treated in this chapter.

Later on we will return to the central problem of this thesis, the numerical simulation of SAW-induced fluid streaming. We will present the big picture – an overview of how all methods and algorithms introduced in detail in prior chapters will be combined. The chapter is rounded off with a compact description of the software implementation.

6.1 Efficient solution of linear systems

The basic principle of many numerical computations is to reduce a given abstract problem to a system of linear equations in $\mathbb{R}^n$, $n \in \mathbb{N}$,

$$\mathrm{A}\mathrm{x} = \mathrm{b}, \tag{6.1}$$

with a system matrix $\mathrm{A} \in \mathbb{R}^{n\times n}$, a vector of unknowns $\mathrm{x} \in \mathbb{R}^n$ and a given right hand side $\mathrm{b} \in \mathbb{R}^n$. The solution of these linear systems is often the most expensive part of a solver in terms of CPU time. It is therefore worthwhile to invest effort in optimizing this step.

The spatial discretization of a system of partial differential equations by means of the Finite Element Method typically leads to large but sparsely populated system matrices. Classical direct solvers such as Gauß's method scale poorly with problem size and are not suited for the solution of these systems. Although special direct solvers for sparse systems have been developed the preferred alternative is to use modern iterative solvers such as CG or GMRES. We will introduce these solvers later in this section.

6.1.1 Sample derivation of a linear system

As an example we will present the assembly of the linear system resulting from the finite element discretization of a variational problem with a symmetric

and coercive bilinear form a. In this subsection we assume a vector valued Lagrange finite element space $\tilde{\boldsymbol{V}}_h \subset \boldsymbol{H}^1(\Omega)$ as introduced in Subsection 4.1.2. Set $\boldsymbol{V}_h := \tilde{\boldsymbol{V}}_h \cap \boldsymbol{H}^1_0(\Omega)$, $\boldsymbol{f}_v \in \boldsymbol{V}_h'$, and $\boldsymbol{g}_h \in \tilde{\boldsymbol{V}}_h$ as Dirichlet boundary values.

Our example problem is: Find $\boldsymbol{v}_h \in \tilde{\boldsymbol{V}}_h$ satisfying

$$\begin{aligned} a(\boldsymbol{w}_h, \boldsymbol{v}_h) &= \langle \boldsymbol{w}_h, \boldsymbol{f}_v \rangle_{\boldsymbol{V}_h \times \boldsymbol{V}_h'} && \text{for all } \boldsymbol{w}_h \in \boldsymbol{V}_h, \\ \boldsymbol{w}_h &= \boldsymbol{g}_h && \text{on } \partial\Omega. \end{aligned} \tag{6.2}$$

This system is not just a model problem, but arises as a subproblem, for example during the solution of saddle point systems in Section 6.2. We will now construct a basis of the space $\tilde{\boldsymbol{V}}_h$.

$$(\boldsymbol{\psi}_i)_{i=1}^{n_v} \subset \tilde{\boldsymbol{V}}_h.$$

To define the exact form of the basis functions we will first consider the scalar valued Lagrange finite element space $\tilde{X}_h \subset H^1(\Omega)$ containing the components $v_{h,i}$, $\boldsymbol{v}_h = (v_{h,1}, \ldots, v_{h,d})$. We will denote by $(\varphi_j)_{j=1}^{n}$ the nodal basis of $\tilde{X}_h$ defined in Definition 4.1.6. Without restriction we will demand that the functions $(\varphi_j)_{j=1}^{\mathring{n}}$ assume their maximal value 1 on interior nodes of Ω, whereas $(\varphi_j)_{j=\mathring{n}+1}^{n}$ do this on nodes belonging the the boundary of Ω.

Since $\tilde{\boldsymbol{V}}_h$ is equal to the Cartesian product $\prod_{i=1}^{d} \tilde{X}_h$ we may choose the following vector valued basis functions on $\tilde{\boldsymbol{V}}_h$:

$$\begin{aligned} \boldsymbol{\psi}_i &= (\psi_{i,1} \ldots, \psi_{i,d}), \\ \psi_{dl+j,k} &:= \delta_{jk} \varphi_{l+1}, \end{aligned}$$

where d is the space dimension, $l \in \{0, \ldots, n-1\}$, $j, k \in \{1, \ldots, d\}$. This implies that $(\boldsymbol{\psi}_1, \ldots, \boldsymbol{\psi}_{d\mathring{n}})$ forms a basis of $\boldsymbol{V}_h$. The functions $\boldsymbol{v}_h, \boldsymbol{g}_h \in \tilde{\boldsymbol{V}}_h$ permit unique decompositions of the form

$$\begin{aligned} \boldsymbol{v}_h &= \sum_{i=1}^{n_v} \mathrm{v}_i \boldsymbol{\psi}_i, \text{ with } \mathrm{v}_i \in \mathbb{R}, \\ \boldsymbol{g}_h &= \sum_{i=1}^{n_v} \mathrm{g}_i \boldsymbol{\psi}_i, \text{ with } \mathrm{g}_i \in \mathbb{R}. \end{aligned}$$

We may now define a system matrix $\mathrm{A} \in \mathbb{R}^{n_v \times n_v}$,

$$\mathrm{A} := \begin{bmatrix} a(\boldsymbol{\psi}_1, \boldsymbol{\psi}_1) & \ldots & a(\boldsymbol{\psi}_1, \boldsymbol{\psi}_{d\mathring{n}}) & a(\boldsymbol{\psi}_1, \boldsymbol{\psi}_{d\mathring{n}+1}) & & \ldots & a(\boldsymbol{\psi}_1, \boldsymbol{\psi}_{n_v}) \\ \vdots & \ddots & \vdots & \vdots & & \ddots & \vdots \\ a(\boldsymbol{\psi}_{d\mathring{n}}, \boldsymbol{\psi}_1) & \ldots & a(\boldsymbol{\psi}_{d\mathring{n}}, \boldsymbol{\psi}_{d\mathring{n}}) & a(\boldsymbol{\psi}_{d\mathring{n}}, \boldsymbol{\psi}_{d\mathring{n}+1}) & & \ldots & a(\boldsymbol{\psi}_{d\mathring{n}}, \boldsymbol{\psi}_{n_v}) \\ 0 & \ldots & 0 & 1 & 0 & \ldots & 0 \\ 0 & \ldots & 0 & 0 & 1 & \ldots & 0 \\ \vdots & \ddots & 0 & 0 & 0 & \ddots & \vdots \\ 0 & \ldots & 0 & 0 & 0 & \ldots & 1 \end{bmatrix}, \tag{6.3}$$

as well as a right hand side $\mathrm{b} \in \mathbb{R}^{n_v}$

$$\mathrm{b} := \begin{bmatrix} \langle \boldsymbol{\psi}_1, \boldsymbol{f}_v \rangle_{\boldsymbol{V}_h \times \boldsymbol{V}_h'} \\ \vdots \\ \langle \boldsymbol{\psi}_{d\mathring{n}}, \boldsymbol{f}_v \rangle_{\boldsymbol{V}_h \times \boldsymbol{V}_h'} \\ g_{d\mathring{n}+1} \\ \vdots \\ g_{n_v} \end{bmatrix},$$

The system (6.2) may be equivalently formulated as:
Find $\boldsymbol{v}_h = \sum_{i=1}^{n_v} \mathrm{v}_i \boldsymbol{\psi}_i \in \tilde{\boldsymbol{V}}_h$ satisfying

$$\sum_{j=1}^{n_v} a(\boldsymbol{\psi}_i, \boldsymbol{\psi}_j)\mathrm{v}_j = \langle \boldsymbol{\psi}_i, \boldsymbol{f}_v \rangle_{\boldsymbol{V}_h \times \boldsymbol{V}_h'} \qquad \text{for } i = 1, \ldots, d\mathring{n}$$

$$\mathrm{v}_i = \mathrm{g}_i \qquad \text{for } i = d\mathring{n} + 1, \ldots, n_v.$$

In matrix notation this is simply

$$\mathrm{Av} = \mathrm{b}. \tag{6.4}$$

6.1.2 Krylov space methods

In this subsection we will introduce a class of iterative solvers known as projection methods. Krylov space methods are special projection methods, among which are the well-known conjugate gradient (CG) and generalized minimum residual (GMRES) solvers. These last two solvers are used in the implementation and therefore treated with some detail. For the background we refer to the book of Saad, [60].

We consider the linear system (6.1). Note that we will use indices to denote iterates instead of components in this subsection. The meaning should be clear from the context.

Algorithm 6.1.1 (Projection method)
Let $\mathrm{x}_0 \in \mathbb{R}^n$ be an arbitrary starting value and $K_m, R_m \subset \mathbb{R}^n$ given subspaces of dimension m. For $m \in \mathbb{N}$ calculate approximate solutions of (6.1) of the form

$$\mathrm{x}_m \in \mathrm{x}_0 + K_m$$

with the constraint

$$\mathrm{r}_m \perp R_m, \tag{6.5}$$

where $\perp$ stands for orthogonality with respect to the standard Euclidean scalar product $(\cdot, \cdot)_2$ in $\mathbb{R}^n$ and $\mathrm{r}_m := \mathrm{b} - \mathrm{Ax}_m$ is the m-th residual vector.

After at most $m = n$ steps we have

$$(\mathrm{r}_n, \mathbb{R}^n)_2 = 0 \Longleftrightarrow \mathrm{r}_n = 0 \Longleftrightarrow \mathrm{Ax}_n = \mathrm{b}, \tag{6.6}$$

and the algorithm will stop with the exact solution. Projection methods as defined above may therefore be interpreted as direct methods.

Definition 6.1.2
For the choice $K_m = R_m$ Algorithm 6.1.1 is known as an *orthogonal projection method* and the constraint (6.5) is known as the *Galerkin conditions*. In the case $K_m \neq R_m$ we have an *oblique projection method* with (6.5) known as the *Petrov-Galerkin conditions*.

A *Krylov space method* is characterized by the choice

$$K_m := K_m(\mathrm{A}, \mathrm{r}_0) := \operatorname{span}\{\mathrm{r}_0, \mathrm{A}\mathrm{r}_0, \ldots, \mathrm{A}^{m-1}\mathrm{r}_0\}.$$

6.1.2.1 The CG method

The method of conjugate gradients was introduced by Hestenes and Stiefel [35]. It is a Krylov subspace method suited for symmetric and positive definite matrices. We will therefore assume that A is symmetric and positive definite (SPD) when using the CG method.

Algorithm 6.1.3 (CG method)
The CG method is defined by

1. Choose $\mathrm{x}_0 \in \mathbb{R}^n$ and a tolerance $\varepsilon > 0$, set $\mathrm{p}_0 := \mathrm{r}_0 = \mathrm{b} - \mathrm{A}\mathrm{x}_0$, and $\alpha_0 := |\mathrm{r}_0|_2^2$.
2. For $m = 0, \ldots, N-1$
   (a) If $\alpha_m < \varepsilon$, then x_m is the solution, STOP. Otherwise calculate
   (b) $\mathrm{v}_m := \mathrm{A}\mathrm{p}_m$, $\lambda_m := \frac{\alpha_m}{(\mathrm{v}_m, \mathrm{p}_m)_2}$
   (c) $\mathrm{x}_{m+1} := \mathrm{x}_m + \lambda_m \mathrm{p}_m$
   (d) $\mathrm{r}_{m+1} := \mathrm{r}_m - \lambda_m \mathrm{v}_m$
   (e) $\alpha_{m+1} := |\mathrm{r}_{m+1}|_2^2$
   (f) $\mathrm{p}_{m+1} := \mathrm{r}_{m+1} + \frac{\alpha_{m+1}}{\alpha_m}\mathrm{p}_m$

Remark 6.1.4
The iterates of the CG method fulfill

$$\begin{aligned} K_m &= \operatorname{span}\{\mathrm{p}_0, \ldots, \mathrm{p}_{m-1}\} = \operatorname{span}\{\mathrm{r}_0, \ldots, \mathrm{A}^{m-1}\mathrm{r}_0\}, \\ \mathrm{x}_m &\in \mathrm{x}_0 + K_m, \\ \mathrm{r}_m &\perp K_m, \end{aligned}$$

for $m \in \mathbb{N}_0$ which means that CG is an orthogonal Krylov space method.

The following bound on the convergence rate of the CG iteration is classical.

Lemma 6.1.5 (Convergence of CG)
Let A *be SPD. Let* $|\cdot|_A$ *be the norm induced by the scalar product* $(\cdot,\cdot)_\mathrm{A} := (\mathrm{A}\cdot,\cdot)_2$. *The errors* $\mathrm{e}_m := \mathrm{x}_m - \mathrm{x}$ *of the CG iterates satisfy*

$$|\mathrm{e}_m|_\mathrm{A} \leq 2\left(\frac{\sqrt{\kappa}-1}{\sqrt{\kappa}+1}\right)^m |\mathrm{e}_0|_\mathrm{A}\,,$$

where $\kappa := \operatorname{cond}_2(\mathrm{A})$ *is the condition number of* A.

Proof. See [33, Theorem 9.4.12] □

6.1.2.2 The GMRES method

The Generalized Minimal Residual Method was presented by Saad and Schultz [61]. It is applicable for arbitrary regular matrices. One may view GMRES as a method to efficiently calculate solutions of the following minimization problem:

Problem 6.1.6 (Minimization problem associated with (6.1))
Define

$$\begin{aligned} F &: \mathbb{R}^n \to \mathbb{R} \\ F(\mathrm{x}) &= |\mathrm{b} - \mathrm{A}\mathrm{x}|_2^2 . \end{aligned} \tag{6.7}$$

Find $\mathrm{x}^* \in \mathbb{R}^n$ *with*

$$\mathrm{x}^* = \arg\min_{\mathrm{x}\in\mathbb{R}^n} F(\mathrm{x}). \tag{6.8}$$

The solution of (6.8) is obviously $\mathrm{x} = \mathrm{A}^{-1}b$.

As the following lemma shows this minimization problem is related to an oblique projection method.

Lemma 6.1.7
Define $F : \mathbb{R}^n \to \mathbb{R}$ *as in* (6.7) *and let* K_m, $m = 1, \ldots, n$ *be a sequence of* m*-dimensional subspaces of* $\mathbb{R}^n$. *Let* $\mathrm{x}_0 \in \mathbb{R}^n$ *be an arbitrary starting vector. Then*

$$\mathrm{x}_m = \arg\min_{\mathrm{y}\in\mathrm{x}_0+K_m} F(\mathrm{y})$$

holds iff

$$(\mathrm{r}_m, L_m)_2 = 0, \qquad \text{where } L_m := \mathrm{A}K_m.$$

Proof. See [48, Lemma 4.75]. □

The idea of GMRES is to iteratively define a set of orthonormal basis vectors $(\mathrm{v}_1, \ldots, \mathrm{v}_m)$ spanning the m-th Krylov space K_m. This reduces the minimization problem 6.1.6 to a simpler form. There are several different approaches to construct this basis, for example Arnoldi's method, Gram-Schmidt orthogonalization, or the Householder method. The software implementation of this work presented below uses a modified Householder method, see [76].

If this method were used all the way to $m = n$ then we would certainly reach the exact solution, as shown by (6.6). However, this would necessitate a prohibitively large amount of memory, of the order $n \times n$ numbers to store all basis vectors v_i. The GMRES method is therefore usually employed as a "restarted" version. For this the dimension m of the Krylov spaces K_m is kept bounded to some $k \leq n$ while searching for an approximate solution $\mathrm{x}_k \in \mathrm{x}_0 + K_k$. At this point the method is restarted using this x_k as a new starting value. This method is guaranteed to yield a monotone decline of the residual norm $|\mathrm{r}_m| = |\mathrm{b} - \mathrm{A}\mathrm{x}_m|$ but not necessarily convergence, see [48].

Algorithm 6.1.8 (Restarted GMRES method)
Given are $\varepsilon > 0$ as a tolerance for the residual and $k \in \mathbb{N}$ as the maximal dimension of the Krylov spaces. Let $\mathrm{I}_n \in \mathbb{R}^{n\times n}$ be the unit matrix and $\{\mathrm{e}_1, \ldots, \mathrm{e}_n\}$ the canonical basis vectors of $\mathbb{R}^n$.

1. (a) Set $r := b - Ax_0$. If $|r|_2 < \varepsilon$, STOP.
   (b) Calculate a Householder transformation $P_1 := I_n - 2u_1 u_1^\top$, such that $P_1 r = \pm |r| e_1$. The sign is chosen to avoid cancellation of digits.
   (c) Set
$$\begin{aligned} w &:= P_1 r \\ U_1 &:= [u_1] \in \mathbb{R}^{n\times 1}, \text{ and} \\ L_1 &:= [1] \in \mathbb{R}^{1\times 1}. \end{aligned}$$

2. For $m = 1, \ldots, k$
   (a) Calculate
$$r := \big(I_n - 2U_m L_m^{-1} U_m^\top\big) A \big(I_n - 2U_m L_m^{-\top} U_m^\top\big) e_m.$$
   (b) If the component $(r)_i = 0$ for $i = m+2, \ldots, n$, set $P_{m+1} = I_n$, otherwise determine Householder transformation $P_{m+1} = I_n - 2u_{m+1}u_{m+1}^\top$, such that $(P_{m+1}r)_i = 0$ for $i = m+2, \ldots, n$. Set $r := P_{m+1}r$.
   (c) If $m > 1$, set $r := G_{m-1} \cdots G_1 r$.
   (d) If $(r)_{m+1} \neq 0$, determine a Givens rotation G_m, such that $(G_m r)_{m+1} = 0$ and set $r := G_m r$, $w := G_m w$.
   (e) Set
$$R_m := \begin{cases} [r] & \text{for } m = 1 \\ [R_{m-1}, r] & \text{for } m > 1. \end{cases}$$
   (f) If $|(w)_{m+1}| < \varepsilon$, goto 3.
   (g) Set $U_{m+1} := [U_m, u_{m+1}]$ and calculate
$$L_{m+1} := \begin{bmatrix} L_m & 0 \\ 2u_{m+1}^\top U_m & 1 \end{bmatrix}$$

3. (a) Determine $y_m \in \mathbb{R}^m$ as the solution of the triangular system with upper triangular matrix $\widetilde{R}_m$, stored in the first m lines of R_m, and the right hand side $\widetilde{w} := (w)_{i=1}^m$.
   (b) Set $x_0 := x_0 + (I_n - 2U_m L_m^{-\top} U_m^\top)[e_1 \cdots e_m] y_m$.
   (c) If $|(w)_{m+1}| < \varepsilon$ then STOP, else goto 1.

6.1.2.3 Krylov space methods on subspaces

We return to our sample linear system (6.4) arising from the discrete variational problem (6.2). Although the bilinear form a was assumed to be symmetric and coercive the matrix A is neither symmetric nor positive definite, as is clearly visible in the definition (6.3). This is due to the chosen method of incorporating the inhomogeneous Dirichlet boundary values in the linear system. Nevertheless, we may use the CG method to solve this system. The theoretical background for this is presented below.

Lemma 6.1.9 (CG on subspaces)
Let $U \subset \mathbb{R}^n$ be an l-dimensional subspace and $\mathrm{A} \in \mathbb{R}^{n\times n}$ a matrix such that the corresponding linear operator on U,

$$\begin{aligned} \alpha : U &\to U, \\ \alpha(\mathrm{u}) &:= \mathrm{Au}, \end{aligned} \tag{6.9}$$

is symmetric and positive definite, meaning

$$(\alpha(\mathrm{u}), \mathrm{v})_2 = (\mathrm{u}, \alpha(\mathrm{v}))_2 \text{ and } (\alpha(\mathrm{u}), \mathrm{u})_2 \geq c_\alpha > 0 \text{ for all } \mathrm{u}, \mathrm{v} \in U.$$

Let $\mathrm{z} \in \mathbb{R}^n$ be arbitrary with $\mathrm{Az} = \mathrm{z}$. Assume a right hand side $\mathrm{b} \in \mathrm{z} + U$ and a starting value $\mathrm{x}_0 \in \mathrm{z} + U$ are given. The CG method will then converge against the unique solution $\mathrm{x} \in \mathrm{z} + U$ of $\mathrm{Ax} = \mathrm{b}$.

Proof. We first need to verify that there exists a unique solution of $\mathrm{Ax} = \mathrm{b}$. Since we are dealing with a finite dimensional space it is sufficient to verify uniqueness. This holds because for $\mathrm{x} \in \mathrm{z} + U$

$$\mathrm{Ax} = \mathrm{b} \iff \mathrm{A}(\mathrm{x} - \mathrm{z}) = \mathrm{b} - \mathrm{z} \iff \alpha(\mathrm{x} - \mathrm{z}) = \mathrm{b} - \mathrm{z} \in U.$$

The last equation is uniquely solvable for $\tilde{\mathrm{x}} := \mathrm{x} - \mathrm{z}$ since α is positive definite and therefore invertible.

Let $I : U \to \mathbb{R}^l$ be an arbitrary linear isomorphism. By

$$(I(\mathrm{u}), I(\mathrm{v}))_I := (\mathrm{u}, \mathrm{v})_2, \qquad \mathrm{u}, \mathrm{v} \in U,$$

we define a suitable scalar product on $\mathbb{R}^l$. We may now transform the terms appearing in the CG algorithm 6.1.3:

$$\begin{aligned} \bar{\mathrm{A}} \in \mathbb{R}^{l\times l} &\text{ with } \bar{\mathrm{A}} I(\mathrm{u}) := I(\mathrm{Au}), \\ &\implies (\bar{\mathrm{A}} I(\mathrm{u}), I(\mathrm{v}))_I = (\mathrm{Au}, \mathrm{v})_2, \\ \bar{\mathrm{x}}_0 &:= I(\mathrm{x}_0 - \mathrm{z}), \\ \bar{\mathrm{b}} &:= I(\mathrm{b} - \mathrm{z}), \\ \bar{\mathrm{p}}_0 = \bar{\mathrm{r}}_0 &:= I(\mathrm{b} - \mathrm{Ax}_0) = I((\mathrm{b} - \mathrm{z}) - T(\mathrm{x}_0 - \mathrm{z})) = \bar{\mathrm{b}} - \bar{\mathrm{A}}\bar{\mathrm{x}}_0, \\ \bar{\mathrm{v}}_m &:= I(\mathrm{Ap}_m) = \bar{\mathrm{A}}\bar{\mathrm{p}}_m, \\ \bar{\alpha}_m &:= \|\mathrm{r}_m\|_2^2 = \|\bar{\mathrm{r}}_m\|_I, \\ &\text{etc.} \end{aligned}$$

It is clear that $\bar{\mathrm{A}}$ is an SPD matrix on $\mathbb{R}^l$ and that the CG method on $\mathbb{R}^l$ is completely transported into $\mathbb{R}^l$. The CG method on $\mathbb{R}^l$ converges towards a $\bar{\mathrm{x}} \in \mathbb{R}^L$ with

$$\bar{\mathrm{A}}\bar{\mathrm{x}} = \bar{\mathrm{b}} \implies \mathrm{A}I^{-1}(\bar{\mathrm{x}}) = \mathrm{b} - \mathrm{z}.$$

Setting $\mathrm{x} := \mathrm{z} + I^{-1}(\bar{\mathrm{x}}) \in \mathrm{z} + U$ we finally gain $\mathrm{Ax} = \mathrm{b}$. □

An obvious application to (6.4) is

$$\begin{aligned} \mathrm{z} &:= \mathrm{g}, \\ U &:= \{\mathrm{u} \in \mathbb{R}^{n_v} \mid \sum_{i=1}^{n_v} \mathrm{u}_i \boldsymbol{\psi}_i \in \boldsymbol{V}_h\}. \end{aligned}$$

This applicability of the CG method to subspaces is also useful when solving elliptic systems in pressure space that require $p_h \in Q_h \subset L^2_0(\Omega)$. As mentioned before, we do not explicitly implement a conforming finite element space Q_h with functions of mean zero. Lemma 6.1.9 states that is is sufficient to work with a more readily available space $\tilde{Q}_h \subset L^2(\Omega)$ as long as starting value and right hand sides are coefficient vectors belonging to functions in Q_h.

A similar property, not proven here, holds for the GMRES method.

Lemma 6.1.10 (GMRES on subspaces)
Assume $\mathrm{A} \in \mathbb{R}^{n \times n}$ *is regular. Let* $\mathrm{z} \in \mathbb{R}^n$ *with* $\mathrm{Az} = \mathrm{z}$ *and* U *be an* l*-dimensional subspace of* $\mathbb{R}^l$*. If* α *defined as in* (6.9) *is invertible, then GMRES will converge for the system* $\mathrm{Ax} = \mathrm{b}$*, provided that the starting value* x_0 *and right hand side* b *are both contained in* $\mathrm{z} + U$*.*

6.1.3 Preconditioning

The convergence properties of iterative solvers are determined by the condition of the system matrix, see Lemma 6.1.5 for the case of the CG solver. One is therefore interested in improving the condition of system matrices, which is known as *preconditioning*.

For a given system

$$\mathrm{Ax} = \mathrm{b} \tag{6.10}$$

in $\mathbb{R}^n$ we choose two regular linear operators P_l and P_r, which may or may not be given explicitly in the form of matrices. The system (6.10) is equivalent to the preconditioned system

$$[P_l \mathrm{A} P_r][P_r^{-1}\mathrm{x}] = [P_l \mathrm{b}].$$

The operators P_l, P_r are known as left and right preconditioners, respectively. To choose suitable preconditioners we must balance between the competing goals of small condition of the transformed operator $P_l \mathrm{A} P_r$ and low CPU/memory cost of applying the operators in each iteration.

Preconditioning in this work is used in two instances.

- For elliptic systems in velocity space $\boldsymbol{V}_h$ of the form (6.2): Here we use
  1. the classical hierarchical basis method described by [80]
  2. the Bramble-Pasciak-Xu method as in [10]. Under certain circumstances this method provides optimal preconditioning in the sense that the condition number of the transformed system is bounded by a constant independent of the discretization parameter h.

These two methods are already provided by the underlying software package ALBERTA. Both methods are multilevel preconditioners in that they make use of the hierarchical structure of triangulations described in Remark 4.1.3. We use the preconditioned variant PCG of the CG iteration for these systems.

- For the discretization of non-symmetric systems of the form

$$\begin{bmatrix} \widetilde{\mathrm{A}} & \omega\mu_v \mathrm{M}_V & \mathrm{B} & 0 \\ -\omega\mu_v \mathrm{M}_V & \widetilde{\mathrm{A}} & 0 & \mathrm{B} \\ \mathrm{B}^* & 0 & 0 & -\omega\mu_p \mathrm{M}_P \\ 0 & \mathrm{B}^* & \omega\mu_p \mathrm{M}_P & 0 \end{bmatrix} \begin{bmatrix} \mathrm{v}_c \\ \mathrm{v}_s \\ \mathrm{p}_c \\ \mathrm{p}_s \end{bmatrix} = \begin{bmatrix} \mathrm{F}_{vc} \\ \mathrm{F}_{vs} \\ -\mathrm{F}_{pc} \\ -\mathrm{F}_{ps} \end{bmatrix}. \tag{6.11}$$

where $\omega, \mu_v, \mu_p > 0$, $\widetilde{\mathrm{A}}$ is an SPD stiffness matrix in velocity space, B has full column rank, and M_V and M_P are SPD mass matrices in velocity and pressure space respectively. Systems of this form arise during the discretization of the quasi-stationary problem 4.2.6. For these we have implemented an incomplete lower/upper decomposition with thresholding and pivoting (ILUTP) as preconditioner, see [60, Algorithm 10.6]. The ILUTP preconditioner is used as a right preconditioner for the GMRES iteration.

6.2 Saddle point solvers

A very important and recurring task is the solution of systems of equations resulting from saddle point problems. The systems we are specifically interested in are the following:

1. Stationary problems on fixed grids, Problem 4.2.1.
2. Solution of a single time step using the Theta Scheme, Problem 4.2.10.
3. Solution of a single time step for the free boundary problem, Algorithm 5.2.4, Step 1.

All of these problems fit into a common framework which we will lay out now. Let $\boldsymbol{V}_h \subset \boldsymbol{V} = \boldsymbol{H}_0^1(\Omega)$ and $Q_h \subset Q = L_0^2(\Omega)$ be finite dimensional subspaces. On $\boldsymbol{V}$ we are given a symmetric $\boldsymbol{V}$-elliptic bilinear form a with

$$\begin{aligned} a &: \boldsymbol{V} \times \boldsymbol{V} \to \mathbb{R}, \\ |a(\boldsymbol{v}, \boldsymbol{w})| &\leq C_a \|\boldsymbol{v}\|_1 \|\boldsymbol{w}\|_1, \\ a(\boldsymbol{v}, \boldsymbol{v}) &\geq c_a \|\boldsymbol{v}\|_1^2, \end{aligned}$$

for all $\boldsymbol{v}, \boldsymbol{w} \in \boldsymbol{V}$, with constants $c_a, C_a > 0$. We have a continuous form b

$$\begin{aligned} b &: Q \times \boldsymbol{V} \to \mathbb{R}, \\ |b(p, \boldsymbol{v})| &\leq C_b \|p\|_0 \|v\|_1, \end{aligned}$$

for all $p \in Q$, $\boldsymbol{v} \in \boldsymbol{V}$ and constant $C_b > 0$. We assume that inf-sup conditions hold for the pairs $\boldsymbol{V} \times Q$ and $\boldsymbol{V}_h \times Q_h$:

$$\inf_{p \in Q \setminus \{0\}} \sup_{\boldsymbol{v} \in \boldsymbol{V} \setminus \{0\}} \frac{b(p, \boldsymbol{v})}{\|p\|_0 \, \|\boldsymbol{v}\|_1} \geq c_b > 0,$$

$$\inf_{p_h \in Q_h \setminus \{0\}} \sup_{\boldsymbol{v}_h \in \boldsymbol{V}_h \setminus \{0\}} \frac{b(p_h, \boldsymbol{v}_h)}{\|p_h\|_0 \, \|\boldsymbol{v}_h\|_1} \geq c_{b,h} > 0.$$

Finally, we have a third symmetric and weakly coercive form c on Q with

$$\begin{aligned} c &: Q \times Q \to \mathbb{R}, \\ |c(p, q)| &\leq C_c \, \|p\|_0 \, \|q\|_0 \,, \\ c(p, p) &\geq 0, \end{aligned}$$

for all $p \in Q$, with $C_c > 0$. Note the c can be the zero form.

Problem 6.2.1 (Discrete saddle point system)
Let $f = (\boldsymbol{f}_v, f_p) \in \boldsymbol{V}' \times Q'$. Find $u_h = (\boldsymbol{v}_h, p_h) \in \boldsymbol{V}_h \times Q_h$ so that

$$\begin{aligned} a(\boldsymbol{w}_h, \boldsymbol{v}_h) + b(p_h, \boldsymbol{w}_h) &= \langle \boldsymbol{w}_h, \boldsymbol{f}_v \rangle_{\boldsymbol{V} \times \boldsymbol{V}'} \quad \text{for all } \boldsymbol{w}_h \in \boldsymbol{V}_h, \\ -b(q_h, \boldsymbol{v}_h) + c(q_h, p_h) &= (q_h, f_p)_0 \qquad \text{for all } q_h \in Q_h. \end{aligned} \tag{SP$_h$}$$

For a comprehensive overview of the numerical methods available for solving saddle point systems we refer the reader to [5]. As a short aside we will proceed to justify the labeling of Problem 6.2.1 as a "saddle point problem". In the case of the symmetric elliptic model problem of finding $\boldsymbol{v}_h \in \boldsymbol{V}_h$ with

$$a(\boldsymbol{w}_h, \boldsymbol{v}_h) = \langle \boldsymbol{w}_h, \boldsymbol{f}_v \rangle_{\boldsymbol{V} \times \boldsymbol{V}'} \qquad \text{for all } \boldsymbol{w}_h \in \boldsymbol{V}_h,$$

we may characterize $\boldsymbol{v}_h$ as the unique minimum of the energy functional

$$I_a(\boldsymbol{w}_h) := \frac{1}{2} a(\boldsymbol{w}_h, \boldsymbol{w}_h) - \langle \boldsymbol{w}_h, \boldsymbol{f}_v \rangle_{\boldsymbol{V} \times \boldsymbol{V}'} \qquad \text{for all } \boldsymbol{w}_h \in \boldsymbol{V}_h, \tag{6.12}$$

on $\boldsymbol{V}_h$, see [32, Theorem 6.5.12]. For Problem 6.2.1 with the form $c = 0$ the corresponding functional I_s is defined as

$$\begin{aligned} I_s(\boldsymbol{w}_h, q_h) := \frac{1}{2} a(\boldsymbol{w}_h, \boldsymbol{w}_h) + b(q_h, \boldsymbol{w}_h) \\ - \langle \boldsymbol{w}_h, \boldsymbol{f}_v \rangle_{\boldsymbol{V} \times \boldsymbol{V}'} - (q_h, f_p)_0 \qquad \text{for all } \boldsymbol{w}_h \in \boldsymbol{V}_h, \; q_h \in Q_h. \end{aligned}$$

A solution $(\boldsymbol{v}_h, p_h) \in \boldsymbol{V}_h \times Q_h$ of (SP$_h$) will not minimize the functional I_s, in fact I_s is not even bounded from below. However, $(\boldsymbol{v}_h, p_h)$ may be interpreted as a *saddle point* of I_s:

Lemma 6.2.2
Assume $f = (\boldsymbol{f}_v, f_p) \in \boldsymbol{V}' \times Q'$ and $c = 0$. The function $(\boldsymbol{v}_h, p_h) \in \boldsymbol{V}_h \times Q_h$ is a solution of (SP$_h$) iff

$$I_s(\boldsymbol{v}_h, q_h) \leq I_s(\boldsymbol{v}_h, p_h) \leq I_s(\boldsymbol{w}_h, p_h) \qquad \text{for all } \boldsymbol{w} \in \boldsymbol{V}_h, q_h \in Q_h$$

holds. This is also equivalent to the minimax problem

$$I_s(\boldsymbol{v}_h, p_h) = \min_{\boldsymbol{w}_h \in \boldsymbol{V}_h} I_s(\boldsymbol{w}_h, p_h) = \max_{q_h \in Q_h} \min_{\boldsymbol{w}_h \in \boldsymbol{V}_h} I_s(\boldsymbol{w}_h, q_h).$$

Proof. See [32, Theorem 12.2.4]. □

Let us define operators corresponding to the bilinear forms as before:

$$\begin{aligned}
&A_h \in L(\boldsymbol{V}_h, \boldsymbol{V}_h'), && \langle A_h \boldsymbol{v}_h, \boldsymbol{w}_h \rangle_{\boldsymbol{V}_h' \times \boldsymbol{V}_h} = a(\boldsymbol{v}_h, \boldsymbol{w}_h),\\
&B_h \in L(Q_h, \boldsymbol{V}_h'), && \langle B_h p_h, \boldsymbol{v}_h \rangle_{\boldsymbol{V}_h' \times \boldsymbol{V}_h} = b(p_h, \boldsymbol{v}_h),\\
&B_h^* \in L(\boldsymbol{V}_h, Q_h), && (B_h^* \boldsymbol{v}_h, p_h)_0 = b(p_h, \boldsymbol{v}_h),\\
&C_h \in L(Q_h, Q_h), && (C_h p_h, q_h)_0 = c(p_h, q_h),\\
&K_h \in L(Q_h, Q_h), && K_h = B_h^* A_h^{-1} B_h + C_h.
\end{aligned}$$

The elliptic operator A_h is continuously invertible with $\left\|A_h^{-1}\right\| \leq 1/c_a$ due to the well-known Lax-Milgram Theorem, therefore K_h is well-defined. In addition we may define

$$\begin{aligned}
\boldsymbol{f}_{v,h} &\text{ as the restriction to } \boldsymbol{V}_h \text{ of } \boldsymbol{f}_v,\\
f_{p,h} &\text{ as the } Q_h\text{-projection of } f_p.
\end{aligned}$$

With these we reformulate (SP_h) as

Find $\boldsymbol{v}_h \in \boldsymbol{V}_h$, $q_h \in Q_h$ with

$$\begin{aligned}
A_h \boldsymbol{v}_h + B_h p_h &= \boldsymbol{f}_{v,h},\\
-B_h^* \boldsymbol{v}_h + C_h p_h &= f_{p,h}.
\end{aligned}$$

Using the Schur complement operator $K_h = B_h^* A_h^{-1} B_h + C_h$ this yields

$$K_h p_h = B_h^* A_h^{-1} \boldsymbol{f}_v + f_p, \tag{6.13a}$$

$$\boldsymbol{v}_h = A_h^{-1} \boldsymbol{f}_v - A_h^{-1} B p_h. \tag{6.13b}$$

We know that the operator $K_h \in L(Q_h, Q_h)$ has good properties.

Lemma 6.2.3
The operator $K_h \in L(Q_h, Q_h)$ is self-adjoint. Furthermore, we have the following spectral bounds:

$$0 < \frac{c_a c_{b,h}^2}{C_a^2} =: c_K < \frac{(K_h q_h, q_h)_0}{\|q_h\|_0^2} < C_K := \frac{C_b^2}{c_a} + C_c < \infty, \tag{6.14}$$

for all $q_h \in Q_h$.

Proof. We have

$$K_h^* = (B_h^* A_h^{-1} B_h + C_h)^* = B_h^* (A_h^{-1})^* B_h + C_h^* = B_h^* A_h^{-1} B_h + C_h,$$

therefore K_h is self-adjoint. The decomposition of $\boldsymbol{V}$ and $\boldsymbol{V}'$ explained at the beginning of Section 3.2.4 can be carried out in an analogous fashion for the discrete spaces $\boldsymbol{V}_h$ and $\boldsymbol{V}_h'$. Adapting the arguments of Lemma 3.2.9 we have that B_h maps Q_h onto a subspace $\boldsymbol{V}_{h,\perp}'$ of $\boldsymbol{V}_h'$ with a continuous inverse B_h^{-1}, $\left\|B_h^{-1}\right\| \leq 1/c_{b,h}$.

Let $q_h \in Q_h$. The upper bound in (6.14) is clear. For the lower bound we calculate

$$\begin{aligned}\|q_h\|_0^2 &\leq \frac{1}{c_{b,h}^2}\|B_h q_h\|_{-1}^2 = \frac{1}{c_{b,h}^2}\left\|A_h(A_h^{-1}B_h q_h)\right\|_{-1}^2 \\ &\leq \frac{C_a^2}{c_{b,h}^2}\left\|A_h^{-1}B_h q_h\right\|_1^2 \leq \frac{C_a^2}{c_a c_{b,h}^2}\langle A_h(A_h^{-1}B_h q_h), A_h^{-1}B_h q_h\rangle_{\boldsymbol{V}_h'\times\boldsymbol{V}_h} \\ &= \frac{C_a^2}{c_a c_{b,h}^2}(q_h, B_h^* A_h^{-1}B_h q_h)_0 \leq \frac{C_a^2}{c_a c_{b,h}^2}(q_h, K_h q_h)_0.\end{aligned}$$

□

We note that for a stable discretization fulfilling (LBB_h) on page 57, Lemma 3.2.9 provides bounds on the spectrum of K_h which are independent of h. This suggests the use of a conjugate gradient method in the finite dimensional Hilbert space Q_h, see [34, 54, 79]. For such a method we have the following classical bound on the convergence rate of the iterates $q_h^{(n)} \in Q_h$:

$$\left\|q_h^{(n)}\right\|_{K_h} \leq 2\left(\frac{\sqrt{C_K/c_K}-1}{\sqrt{C_K/c_k}+1}\right)^n \left\|q_h^{(0)}\right\|_{K_h},$$

where

$$\|\cdot\|_{K_h} := (\cdot, K_h\cdot)_0^{\frac{1}{2}},$$

see [79, Theorem 1.2.2]. We will now present a variant of the CG method for solving the saddle point system (SP_h) which will calculate the velocity $\boldsymbol{v}$ according to (6.13b) as an integral part of the algorithm. The basis for this algorithm was the saddle point solver for the Stokes equations presented in [13].

Algorithm 6.2.4 (Saddle point CG method)
Choose a starting value $p_0 \in Q_h$, tolerance $\varepsilon > 0$, and a maximal number of iterations $M \in \mathbb{N}$. Calculate an approximation $p \in Q_h$ as follows.

1. (a) Solve for $\boldsymbol{v}_0 \in \boldsymbol{V}_h$: $A_h\boldsymbol{v}_0 = \boldsymbol{f}_v - B_h p_0$.
   (b) Set $r_0 := -B_h^*\boldsymbol{v}_0 + C_h p_0 + f_p$.
   (c) Set $d_0 := r_0$ and $\delta_0 := \|r_0\|_0^2$.
2. For $m = 0, \ldots, M$ do:
   (a) If $\delta_m < \varepsilon$ set $(\boldsymbol{v}, p) := (\boldsymbol{v}_m, p_m)$, STOP.
   (b) Solve for $\chi_m \in \boldsymbol{V}_h$: $A_h\chi_m = B_h d_m$.
   (c) Set
   $$\rho_m := \frac{\delta_m}{(d_m, B_h^*\chi_m + C_h d_m)_0}.$$
   (d) Updates:
   $$\begin{aligned}p_{m+1} &:= p_m - \rho_m d_m, \\ \boldsymbol{v}_{m+1} &:= \boldsymbol{v}_m + \rho_m\chi_m \\ &\quad \left(= \boldsymbol{f}_v - B_h p_{m+1}\right).\end{aligned}$$

(e) New residual: $r_{m+1} := -B_h^* \boldsymbol{v}_{m+1} + C_h p_{m+1} + f_p$.
(f) Set $\delta_{m+1} := \|r_{m+1}\|_0^2$.
(g) New search direction: $d_{m+1} := r_{m+1} + \frac{\delta_{m+1}}{\delta_m} d_m$.

The Schur complement systems typically arising in this work are not too badly conditioned; we therefore did not implement preconditioning of the CG iteration above.

Remark 6.2.5
The steps 1(a) and 2(b) above involve the solution of an elliptic system in the velocity space $\boldsymbol{V}_h$, done in practice using a preconditioned CG subiteration in $\mathbb{R}^{n_v}$ with n_v as the dimension of $\boldsymbol{V}_h$. These are the most costly parts of the algorithm.

In steps 1(b) and 2(e) we have applications of B_h^* and C_h on the right hand sides. In practice this means that we will solve a system with a mass matrix in pressure space. This is also done with a CG subiteration.

6.3 Overview of algorithms

The main goal of this thesis – the simulation of acoustic streaming induced by SAWs – was realized by a two-stage model already introduced in Chapter 2. We now present the detailed algorithms to calculate solutions. We differentiate between the fixed mesh case and the case of free capillary boundaries.

6.3.1 Fixed meshes

For the simulation of acoustic streaming we need to specify the following physical and numerical parameters. We have supplied typical values as a reference, see Table 6.1.

Algorithm 6.3.1 (Acoustic streaming, fixed domain)
Given is a computational domain $\Omega \subset \mathbb{R}^d$, parameters as in Table 6.1, and a periodic function $\boldsymbol{u}$ as the SAW displacement on Γ_d.

1. Solve the acoustics subproblem (2.10) on page 17 for $(\boldsymbol{v}^{(1)}, p^{(1)})$:

$$\begin{aligned}
\frac{VT}{L}\frac{\partial \boldsymbol{v}^{(1)}}{\partial t} - \frac{VT^2}{L^3}\left(\widetilde{\nu}_1 \Delta \boldsymbol{v}^{(1)} + \widetilde{\nu}_2 \nabla(\nabla \cdot \boldsymbol{v}^{(1)})\right) + \nabla p^{(1)} &= 0 && \text{in } \Omega,\ t > 0,\\
\frac{L^3}{c_0^2 VT^3}\frac{\partial p^{(1)}}{\partial t} + \nabla \cdot \boldsymbol{v}^{(1)} &= 0 && \text{in } \Omega,\ t > 0\\
\frac{VT}{L}\boldsymbol{v}^{(1)} &= \frac{\partial \boldsymbol{u}}{\partial t} && \text{on } \Gamma_d,\ t > 0\\
\boldsymbol{v}^{(1)} \cdot \boldsymbol{n} &= 0 && \text{on } \Gamma_s, t > 0\\
\Sigma^{(1)} \boldsymbol{n} &= 0 && \text{on } \Gamma_n,\ t > 0\\
\boldsymbol{v}^{(1)} = 0, \quad p^{(1)} &= 0 && \text{for } t = 0,
\end{aligned}$$

in a weak formulation. We are interested in the periodic equilibrium state corresponding to the periodic forcing terms. We use one of the following algorithms:

Parameter	Value and units	Description
Constants for dimensionless formulation and scaling		
V	$1.0 \cdot 10^{-1}$ m/s	Velocity scale
L	$1.0 \cdot 10^{-7}$ m	Length scale
T	$1.0 \cdot 10^{-8}$ m	Time scale
Physical parameters		
f	$1.0 \cdot 10^{8}$ Hz	Frequency of the SAW device
$c_{0,l}$	$1.484 \cdot 10^{3}$ m/s	Small signal sound speed in water
$c_{0,s}$	$3.8 \cdot 10^{3}$ m/s	Small signal sound speed in solid
ρ_0	$1.0 \cdot 10^{3}$ kg/m^3	Density of liquid
ν_1	$1.002 \cdot 10^{-6}$ m^2/s	Kinematic viscosity of water
ν_2	$1.002 \cdot 10^{-6}$ m^2/s	Kinematic bulk viscosity of water
Numerical discretization parameters		
h	2^{-6}	Maximal finite element diameter
$\tau^{(1)}$	$1 \cdot 10^{-1}$	Time step size for the acoustic (microscale) subproblem
$\tau^{(2)}$	$1 \cdot 10^{3}$	Time step size for the acoustic streaming (macroscale) subproblem

Table 6.1: Parameters for a typical SAW simulation

(a) Theta-scheme time discretization according to Problem 4.2.10 with fixed time step size $\tau^{(1)} > 0$ together with Taylor-Hood finite elements with mesh parameter h. We use either $\theta = \frac{1}{2}$ or $\theta = 1$, corresponding to backwards Euler or Crank-Nicolson. We perform either a fixed number of time steps or iterate until the periodicity condition (4.14), page 73, is fulfilled at a time t_{end}.

(b) Quasi-stationary approach (no time discretization!) according to Problem 4.2.6. The solution $((\boldsymbol{v}_c, \boldsymbol{v}_s), (p_c, p_s))$ can be transformed into a time dependent solution of the original problem using (3.25), page 38.

2. Calculate right hand terms and boundary conditions for (2.11) on page 18 according to:

$$
\begin{aligned}
(\boldsymbol{\psi}, \boldsymbol{f}_v^{(2)})_0 &:= \left(\boldsymbol{\psi}, -\frac{V^2T^2}{L^2} \fint_t (\nabla \cdot \boldsymbol{v}^{(1)})\boldsymbol{v}^{(1)} + (\nabla \boldsymbol{v}^{(1)})\boldsymbol{v}^{(1)}\right)_0, \\
(\varphi, f_p^{(2)})_0 &:= \left(\varphi, -\frac{L^2}{T^2 c_0^2} \fint_t \nabla \cdot (p^{(1)}\boldsymbol{v}^{(1)})\right)_0, \\
(\boldsymbol{\chi}, \boldsymbol{g}^{(2)})_{\Gamma_d,0} &:= \left(\boldsymbol{\chi}, -(\nabla \boldsymbol{v}^{(1)})\boldsymbol{u}\right)_{\Gamma_d,0},
\end{aligned}
\tag{6.15}
$$

for all $\boldsymbol{\psi} \in \boldsymbol{V}_h$, $\varphi \in Q_h$, $\boldsymbol{\chi}$ in the trace of $\boldsymbol{V}_h$ to Γ_d. The symbol $\fint_t$ denotes taking the temporal average over one period of the solution $(\boldsymbol{v}^{(1)}, p^{(1)})$ of Step 1.

(a) When using a time discretization in Step 1 above use a numerical quadrature to calculate the time averages in (6.15).

(b) When using the quasi-stationary approach in Step 1 it is possible to calculate the time average directly from the c- and s-terms as follows:

$$\begin{aligned}(\boldsymbol{\psi}, \boldsymbol{f}_v^{(2)})_0 &:= \Big(\boldsymbol{\psi}, -\frac{V^2T^2}{2L^2}\big((\nabla\cdot\boldsymbol{v}_c)\boldsymbol{v}_c + (\nabla\cdot\boldsymbol{v}_s)\boldsymbol{v}_s \\ &\qquad + (\nabla\boldsymbol{v}_c)\boldsymbol{v}_c + (\nabla\boldsymbol{v}_s)\boldsymbol{v}_s\big)\Big)_0, \\ (\varphi, f_p^{(2)})_0 &:= \left(\varphi, -\frac{L^2}{2T^2c_0^2}\left(\nabla\cdot(p_c^{(1)}\boldsymbol{v}_c^{(1)}) + \nabla\cdot(p_s^{(1)}\boldsymbol{v}_s^{(1)})\right)\right)_0, \\ (\boldsymbol{\chi}, \boldsymbol{g}^{(2)})_{\Gamma_d,0} &:= \left(\boldsymbol{\chi}, -\frac{1}{2}\left((\nabla\boldsymbol{v}_c^{(1)})\boldsymbol{u}_c + (\nabla\boldsymbol{v}_s^{(1)})\boldsymbol{u}_s\right)\right)_{\Gamma_d,0},\end{aligned} \tag{6.16}$$

In both cases we may have to adjust the problem data to fulfill compatibility conditions (see Theorem 3.4.10) to guarantee good numerical behavior for the next step. The reason for this difficulty is that we are not using a subspace of $L_0^2(\Omega)$ as pressure space, see also the remarks at the end of 6.1.2.3 above.

3. Solve the acoustic streaming subproblem (2.11), page 18, for $(\boldsymbol{v}^{(2)}, p^{(2)})$:

$$\begin{aligned} -\widetilde{\nu}_1\frac{VT^2}{L^3}\Delta\boldsymbol{v}^{(2)} - \widetilde{\nu}_2\frac{VT^2}{L^3}\nabla(\nabla\cdot\boldsymbol{v}^{(2)}) + \nabla p^{(2)} &= \boldsymbol{f}_v^{(2)} && \text{in } \Omega, \\ \nabla\cdot\boldsymbol{v}^{(2)} &= f_p^{(2)} && \text{in } \Omega, \\ \boldsymbol{v}^{(2)} &= \boldsymbol{g}^{(2)} && \text{on } \Gamma_d, \\ \boldsymbol{v}^{(2)}\cdot\boldsymbol{n} &= 0 && \text{on } \Gamma_s, \\ \Sigma^{(2)}\boldsymbol{n} &= 0 && \text{on } \Gamma_n. \end{aligned} \tag{6.17}$$

Here we have the following alternatives:

(a) We solve the stationary problem (6.17).

(b) We solve an instationary variant of (6.17) by means of the Theta scheme with fixed time step size $\tau^{(2)}$. This is primarily of interest when determining the relaxation time of the acoustic streaming flow.

6.3.2 Free capillary boundaries

For the simulation of acoustic streaming with free capillary boundaries we will need the same parameters as before, and additionally a coefficient σ of surface tension. A typical value would be $\sigma = 7.3\cdot 10^{-2}$ N/m.

The basis of this algorithm was already presented as Algorithm 5.2.4. It remains to specify the right hand sides $\boldsymbol{f}_v^n$, f_p^n for each time step. These are now determined by solving the acoustics subproblem as above.

Algorithm 6.3.2 (Acoustic streaming, free boundaries)
Given is a starting domain $\Omega_0 \subset \mathbb{R}^d$, parameters as before, and a periodic function $\boldsymbol{u}$ as the SAW displacement on Γ_d. Loop over $n = 0, 1, 2, \ldots$:

1. Solve the acoustics subproblem (2.10) on page 17 for $(\boldsymbol{v}^{(1)}, p^{(1)})$ on the domain Ω_n up to the periodic equilibrium state. This is done as above in Algorithm 6.3.1, with either a time discretization or the quasi-stationary approach. In the former case iterate until periodicity is reached.

2. Calculate right hand terms $\boldsymbol{f}_v^{(2),n}$, $f_p^{(2),n}$ and boundary conditions for the acoustic streaming solution at time step t_n using $\boldsymbol{v}^{(1)}$ and $p^{(1)}$ as above.

3. Perform Step 1 of Algorithm 5.2.4 to determine the acoustic streaming solution $(\boldsymbol{v}^{(2),n}, p^{(2),n})$ at time step t_n with $\tau_n := \tau^{(2)}$. We may specify more general boundary conditions (slip boundary conditions on Γ_s and free flow boundary conditions on Γ_n).

4. Update the position of the mesh to determine Ω_{n+1}, as described in Steps 2 and 3 of Algorithm 5.2.4. We have the alternatives 5.2.6 and 5.2.8 as mesh smoothing methods.

Remark 6.3.3
Recalculating the acoustics solution $(\boldsymbol{v}^{(1)}, p^{(1)})$ in each time step t_n of the main iteration is extremely costly. In practice we have relaxed this requirement by continuing to use $\boldsymbol{f}_v^{(2),n}$, $f_p^{(2),n}$ for several time steps before recomputing. Numerical experiments show that the additional error involved does not have a significant effect on the equilibrium state of the solution $(\Omega_n, \boldsymbol{v}^{(2),n}, p^{(2),n})$ reached for large n.

6.4 Software

The software implementation is based on the finite element library ALBERTA developed by Schmidt and Siebert. ALBERTA is a very general toolbox for the implementation of (adaptive) finite element methods in space dimensions $d = 1, 2, 3$. It is based on hierarchical simplicial grids and employs refinement by bisection. ALBERTA is easily extendible for special purposes. It offers

- Tools for triangulations in any dimension, e. g. quadrature formulae for element-wise integration
- Lagrange elements up to order 4 as well as discontinuous piecewise polynomial elements of orders 0, 1, 2
- Comfortable routines for assembling system matrices and right hand sides
- General algorithms for instationary or stationary problems with adaptive local refinement and coarsening
- Integrated iterative solvers for the resulting linear systems

- Support for multigrid solvers

ALBERTA has been under ongoing development since 1995 with a printed manual available as of 2005, see [63]. The current stable version of ALBERTA is available for download at http://www.alberta-fem.de. For this work we extended ALBERTA to include new features listed below.

- Grids of different dimension in one simulation. A so-called master/slave-mechanism makes it possible to automatically define triangulations of submanifolds such as boundaries of original meshes. These slave meshes are automatically refined and coarsened with a master mesh.
- Trace operations for slave meshes
- New visualization interfaces
- Mesh projection mechanism. This is useful to automatically determine triangulations of geometric objects such as the unit sphere S^2.

For the visualization of results we used GMV (General Mesh Viewer) developed at the Los Alamos National Laboratory, http://laws.lanl.gov/XCM/gmv.

Calculations were done on AMD Opteron^{TM} 64 bit 2.6GHz dual-head processors with 8GB memory.

Chapter 7

Numerical Results

The final chapter of this thesis is devoted to the presentation of numerical experiments. The experiments are divided into test problems which serve to verify the correctness of the implementation, and problems with realistic physical parameters. We also present the results of physical experiments intended to validate the numerical model.

7.1 Test problems

7.1.1 Fixed domains

7.1.1.1 Experimental order of convergence

We will first study the model problem on a fixed domain

$$\begin{aligned} \mu_v \frac{\partial \boldsymbol{v}}{\partial t} - \nu_1 \Delta \boldsymbol{v} - \nu_2 \nabla(\nabla \cdot \boldsymbol{v}) + \nabla p &= \boldsymbol{f}_v && \text{in } \Omega, \\ \mu_p \frac{\partial p}{\partial t} + \nabla \cdot \boldsymbol{v} &= f_p && \text{in } \Omega, \\ \boldsymbol{v} &= \boldsymbol{g} && \text{on } \partial\Omega, \\ \boldsymbol{v} &= \boldsymbol{v}_0 && \text{for } t = 0, \\ p &= p_0 && \text{for } t = 0. \end{aligned} \tag{7.1}$$

which was analyzed in Chapter 3.

We test the discretization using finite elements and the Theta-Scheme as described in Problem 4.2.10. As usual we measure the effect of the the maximal element diameter h and maximal time step τ on the discretization error. The error will naturally depend on the used norms.

For the spatial discretization we will use Taylor-Hood elements

$$\begin{aligned} \tilde{\boldsymbol{V}}_h^k &= (X_h^{k+1})^d \subset \tilde{\boldsymbol{V}} := \boldsymbol{H}^1(\Omega), \\ \tilde{Q}_h^k &= X_h^k \subset \tilde{Q} := L^2(\Omega), \end{aligned}$$

of order $k \in \{1, 2, 3, 4\}$, confer also 4.1.6. The triangulations are created by successive global bisectional refinement of a macro triangulation. The time discretization is done by either the backward Euler or Crank-Nicolson scheme.

We will use fixed time steps $\tau_n = \tau$, $N = T/\tau$. The typical result predicted by Theorems 4.2.15 and 4.2.17 is of the form

$$\max_{n=0,\dots,N} \|u_h^n - u(n\tau)\|_H \leq C_1 h^r + C_2 \tau^s, \qquad r, s \in \mathbb{N} \tag{7.2}$$

Here we have $u(n\tau) \in H$ as the exact solution of (7.1) and $u_h^n \in \tilde{\boldsymbol{V}}_h^k \times \tilde{Q}_h^k$ as the discrete solution at time step $n \in \{0, \dots, N\}$. The constants C_1, C_2 are independent of h and τ, but will generally depend on the exact solution u or its derivatives. We will construct smooth problems thus avoiding the caveats of insufficient regularity. The maximal values r, s for which such an estimate holds are known as the *spatial* resp. *temporal order of convergence*.

It is our aim to determine experimental bounds on the order of convergence. We define

$$\begin{aligned} \boldsymbol{v}_{h,\tau} &= (\boldsymbol{v}_h^n)_{n=0}^N, \\ p_{h,\tau} &= (p_h^n)_{n=0}^N, \\ u_{h,\tau} &= (u_h^n)_{n=0}^N, \end{aligned}$$

as the sequences of calculated solutions $u_h^n = (\boldsymbol{v}_h^n, p_h^n)$.

We will measure maximal time errors as in (7.2) or temporal L^2-norms in time, approximated by the Trapezoidal Rule

$$\left(\int_0^T f(t)^2 dt\right)^{\frac{1}{2}} \approx \left(\frac{\tau}{2}\left(f(0)^2 + \sum_{n=1}^{N-1} 2f(n\tau)^2 + f(N\tau)^2\right)\right)^{\frac{1}{2}}, \tag{7.3}$$

with a given function $f : [0, T] \to \mathbb{R}$. We use the suggestive notations

$$\|\cdot\|_{L^\infty(Z)} \text{ and } \|\cdot\|_{L^2(Z)},$$

for the discrete L^∞- and L^2-norms in time combined with the Z-norm in space. For velocity error in space we are interested in the possibilities of using the $\boldsymbol{H}^1(\Omega)$-seminorm $|\cdot|_1$, denoted by $Z = H^1$, as well as the $\boldsymbol{L}^2(\Omega)$-norm $\|\cdot\|_0$, denoted by $Z = L^2$. For pressure, we will restrict ourselves to $Z = L^2$.

We will now proceed to motivate the concept of experimental order of convergence. By choosing a very fine time discretization $0 < \tau_0 \ll 1$ the measured error in a given norm is expected to be

$$\begin{aligned} \|u - u_{h,\tau_0}\| &\leq C_1 h^r + C_2 \tau_0^s \\ &\approx C_1 h^r, \end{aligned} \tag{7.4}$$

in other words, the spatial error will be dominant. By running simulations on a sequence of increasingly fine meshes with parameters h_j, $j = 1, 2, \dots$ we may thus eliminate the constant C_1 for $j > 1$:

$$\frac{\|u - u_{h_{j-1},\tau_0}\|}{\|u - u_{h_j,\tau_0}\|} \approx \left(\frac{h_{j-1}}{h_j}\right)^r.$$

Thus

$$r \approx \ln\left(\frac{\left\|u - u_{h_{j-1},\tau_0}\right\|}{\left\|u - u_{h_j,\tau_0}\right\|}\right) \Bigg/ \ln\left(\frac{h_{j-1}}{h_j}\right),$$

assuming the denominators are nonzero.

Hence, we define

Definition 7.1.1 (Experimental order of convergence)
Let $(\boldsymbol{v}, p)$ be the exact solution of (7.1) and $(\boldsymbol{v}_{h,\tau}, p_{h,\tau})$ the discrete solution calculated on a triangulation $\mathcal{T}_h$ with maximal element diameter h and time step size τ.

1) For a sequence of triangulations $\mathcal{T}_{h_j}$ with $j = 1, 2, \ldots$ and fixed time step τ_0 we define

$$\begin{aligned}
\mathrm{EOC}^j_{\|\cdot\|}(h, \boldsymbol{v}) &:= \ln\left(\frac{\left\|\boldsymbol{v} - \boldsymbol{v}_{h_{j-1},\tau}\right\|}{\left\|\boldsymbol{v} - \boldsymbol{v}_{h_j,\tau}\right\|}\right) \Bigg/ \ln\left(\frac{h_{j-1}}{h_j}\right), \\
\mathrm{EOC}^j_{\|\cdot\|}(h, p) &:= \ln\left(\frac{\left\|p - p_{h_{j-1},\tau}\right\|}{\left\|p - p_{h_j,\tau}\right\|}\right) \Bigg/ \ln\left(\frac{h_{j-1}}{h_j}\right),
\end{aligned} \tag{7.5}$$

as the *experimental spatial order of convergence* for $\boldsymbol{v}$ and p.

2) For a sequence of time steps τ_j with $j = 1, 2, \ldots$ and fixed mesh parameter h_0 let

$$\begin{aligned}
\mathrm{EOC}^j_{\|\cdot\|}(\tau, \boldsymbol{v}) &:= \ln\left(\frac{\left\|\boldsymbol{v} - \boldsymbol{v}_{h_0,\tau_{j-1}}\right\|}{\left\|\boldsymbol{v} - \boldsymbol{v}_{h_0,\tau_j}\right\|}\right) \Bigg/ \ln\left(\frac{\tau_{j-1}}{\tau_j}\right), \\
\mathrm{EOC}^j_{\|\cdot\|}(\tau, p) &:= \ln\left(\frac{\left\|p - p_{h_0,\tau_{j-1}}\right\|}{\left\|p - p_{h_0,\tau_j}\right\|}\right) \Bigg/ \ln\left(\frac{\tau_{j-1}}{\tau_j}\right),
\end{aligned} \tag{7.6}$$

be the *experimental temporal order of convergence* of $\boldsymbol{v}$ and p.

3) For a sequence of mesh parameters h_j, $j = 1, 2, \ldots$ as well as coupled time step sizes $\tau_j = Ch_j^k$ with fixed C, k, define

$$\begin{aligned}
\mathrm{EOC}^j_{\|\cdot\|}(\boldsymbol{v}) &:= \ln\left(\frac{\left\|\boldsymbol{v} - \boldsymbol{v}_{h_{j-1},\tau_{j-1}}\right\|}{\left\|\boldsymbol{v} - \boldsymbol{v}_{h_j,\tau_j}\right\|}\right) \Bigg/ \ln\left(\frac{h_{j-1}}{h_j}\right), \\
\mathrm{EOC}^j_{\|\cdot\|}(p) &:= \ln\left(\frac{\left\|p - p_{h_{j-1},\tau_{j-1}}\right\|}{\left\|p - p_{h_j,\tau_j}\right\|}\right) \Bigg/ \ln\left(\frac{h_{j-1}}{h_j}\right),
\end{aligned}$$

as the *general experimental order of convergence* for $\boldsymbol{v}$ and p.

7.1.1.2 Validity of time and space discretization

7.1.1.2.1 2D test problem

We use the following data:

- Domain $\Omega = [0, 1]^2$ with macro triangulation as in Figure 7.1.

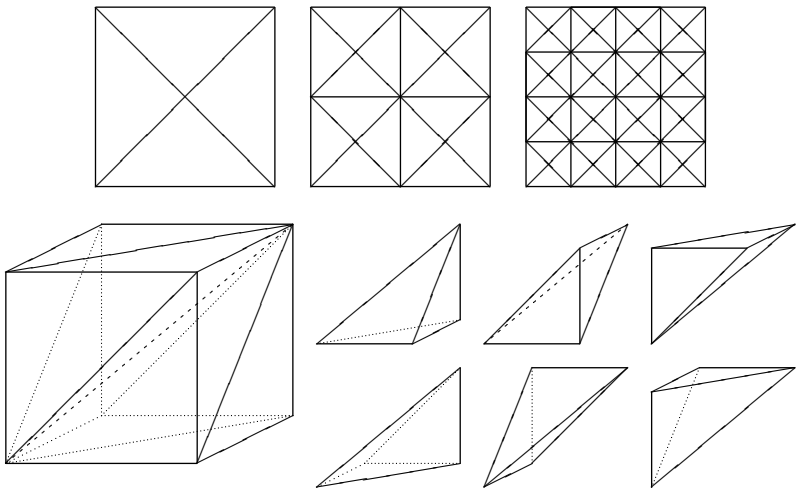

Figure 7.1: Top left: macro triangulation in 2D, Top middle, right: first and second refinement levels defined by double bisection of all triangles.
Bottom left: macro triangulation in 3D, the longest diagonal is the refinement edge. Bottom right: detail of the six macro tetrahedra.

- Time interval $[0, T]$, $T = 1$.
- Parameters: $\mu_v = \mu_p = 1$, $\nu_1 = \nu_2 = 1$.
- Velocity and pressure functions:

$$\begin{aligned} v_1(t, \boldsymbol{x}) &= \sin(2\pi t)\sin(3\pi x_1)\cos(5\pi x_2), \\ v_2(t, \boldsymbol{x}) &= \sin(2\pi t)\cos(2\pi x_1)\sin(7\pi x_2), \\ p(t, \boldsymbol{x}) &= \sin(2\pi t)\left(\exp(x_1 + x_2) - \sqrt{e-1}\right), \end{aligned}$$

  which satisfies $p(t) \in L_0^2(\Omega)$ for all $t \in \mathbb{R}$.

The right hand side $(\boldsymbol{f}_v, f_p)$, Dirichlet boundary values $\boldsymbol{g}$, and starting values $(\boldsymbol{v}_0, p_0)$ are chosen to match this solution, as described above.

7.1.1.2.2 3D test problem

The data used is

- Domain $\Omega = [0, 1]^3$ with macro triangulation as in Figure 7.1.
- Time interval $[0, T]$, $T = 1$.
- Parameters: $\mu_v = \mu_p = 1$, $\nu_1 = \nu_2 = 1$.
- Velocity and pressure functions:

$$\begin{aligned} v_1(t, \boldsymbol{x}) &= \sin(c_0 t)\cos(c_0 x_1)\sin(c_0 x_2)\sin(c_0 x_3), \\ v_2(t, \boldsymbol{x}) &= \sin(c_0 t)\sin(c_0 x_1)\cos(c_0 x_2)\sin(c_0 x_3), \\ v_3(t, \boldsymbol{x}) &= -3\sin(c_0 t)\sin(c_0 x_1)\sin(c_0 x_2)\cos(c_0 x_3), \\ p(t, \boldsymbol{x}) &= \cos(c_0 t)\exp(-x_1^2 - x_2^2 - x_3^2), \end{aligned}$$

7.1.1.2.3 Temporal convergence results of the 2D test problem

Implicit Euler, L^∞-norm in time

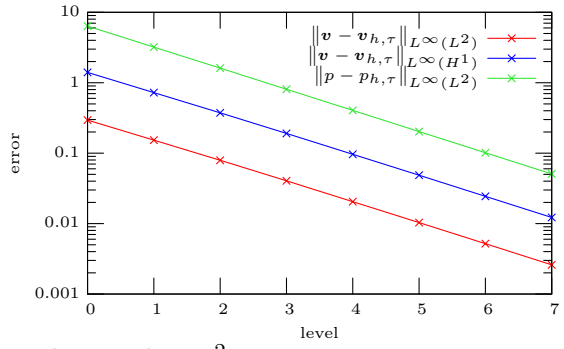

τ	$\boldsymbol{v}, L^2$	$\boldsymbol{v}, H^1$	p, L^2
2^{-1}	—	—	—
2^{-2}	0.95	0.95	0.99
2^{-3}	0.95	0.95	0.99
2^{-4}	0.97	0.97	1.00
2^{-5}	0.98	0.98	1.00
2^{-6}	0.99	0.99	1.00
2^{-7}	0.99	0.99	1.00
2^{-8}	1.00	1.00	1.00

Implicit Euler, L^2-norm in time

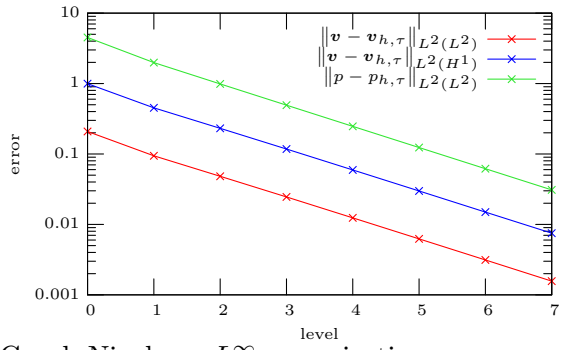

τ	$\boldsymbol{v}, L^2$	$\boldsymbol{v}, H^1$	p, L^2
2^{-1}	—	—	—
2^{-2}	1.15	1.14	1.18
2^{-3}	0.97	0.97	1.01
2^{-4}	0.97	0.98	1.00
2^{-5}	0.99	0.99	1.00
2^{-6}	0.99	0.99	1.00
2^{-7}	1.00	1.00	1.00
2^{-8}	1.00	1.00	1.00

Crank-Nicolson, L^∞-norm in time

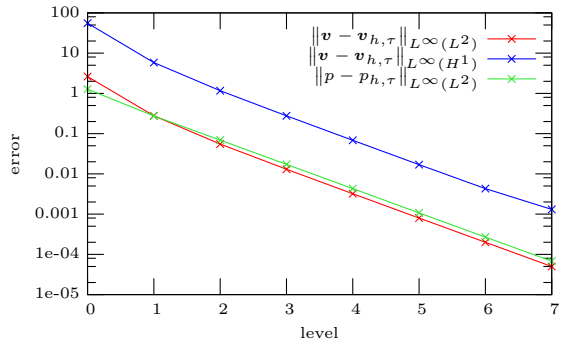

τ	$\boldsymbol{v}, L^2$	$\boldsymbol{v}, H^1$	p, L^2
2^{-1}	—	—	—
2^{-2}	3.24	3.25	2.21
2^{-3}	2.34	2.32	1.99
2^{-4}	2.08	2.08	2.01
2^{-5}	2.02	2.02	2.00
2^{-6}	2.01	2.00	2.00
2^{-7}	2.00	1.98	2.00
2^{-8}	2.00	1.72	1.99

Crank-Nicolson, L^2-norm in time

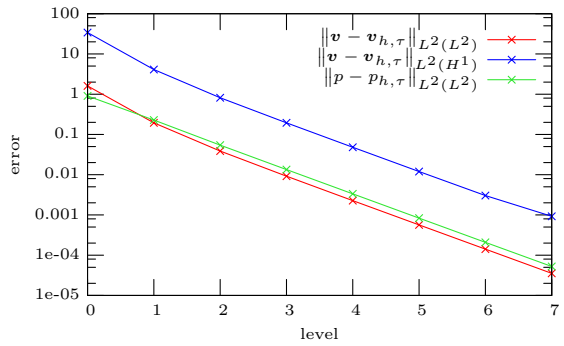

τ	$\boldsymbol{v}, L^2$	$\boldsymbol{v}, H^1$	p, L^2
2^{-1}	—	—	—
2^{-2}	3.05	3.05	1.99
2^{-3}	2.33	2.33	2.07
2^{-4}	2.07	2.07	2.02
2^{-5}	2.02	2.02	2.00
2^{-6}	2.00	2.00	2.00
2^{-7}	2.00	1.98	2.00
2^{-8}	2.00	1.71	1.99

Table 7.1: Left column: errors for $\boldsymbol{v}_{h,\tau}$ and $p_{h,\tau}$. Right column: values of $\mathrm{EOC}^j_{\|\cdot\|}(\tau)$ for $h_0 = 2^{-5}$ using Taylor-Hood order 2.

7.1.1.2.4 Spatial convergence results of the 2D test problem

Taylor-Hood order 1 in space

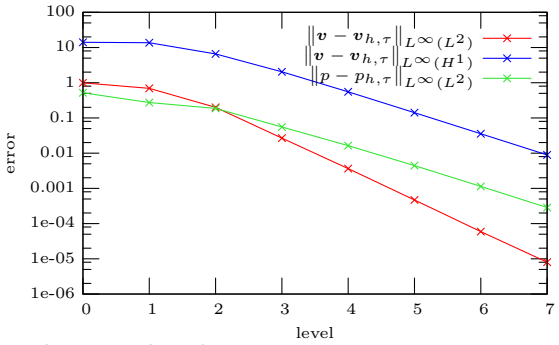

h	$\boldsymbol{v}, L^2$	$\boldsymbol{v}, H^1$	p, L^2
1	—	—	—
2^{-1}	0.52	0.04	0.92
2^{-2}	1.79	1.06	0.55
2^{-3}	2.90	1.69	1.75
2^{-4}	2.88	1.89	1.76
2^{-5}	2.96	1.97	1.88
2^{-6}	2.99	1.99	1.97
2^{-7}	2.88	2.00	1.99

Taylor-Hood order 2 in space

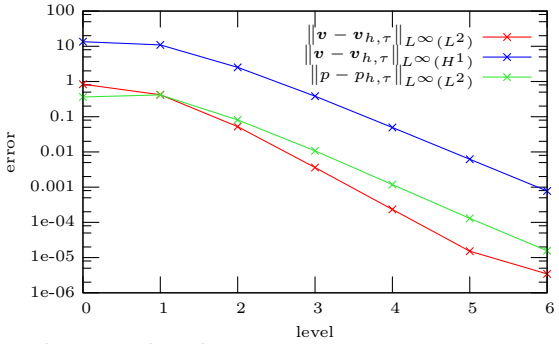

h	$\boldsymbol{v}, L^2$	$\boldsymbol{v}, H^1$	p, L^2
1	—	—	—
2^{-1}	0.99	0.30	−0.19
2^{-2}	3.01	2.12	2.36
2^{-3}	3.85	2.72	2.92
2^{-4}	3.95	2.96	3.19
2^{-5}	3.95	2.99	3.18
2^{-6}	2.14	2.99	3.05

Taylor-Hood order 3 in space

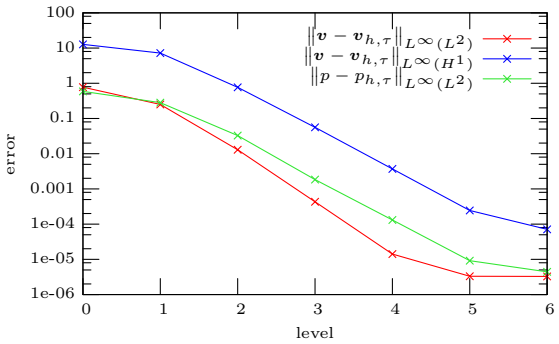

h	$\boldsymbol{v}, L^2$	$\boldsymbol{v}, H^1$	p, L^2
1	—	—	—
2^{-1}	1.63	0.82	1.06
2^{-2}	4.27	3.23	3.11
2^{-3}	4.91	3.77	4.15
2^{-4}	4.93	3.92	3.81
2^{-5}	2.09	3.92	3.84
2^{-6}	0.01	1.78	1.05

Table 7.2: Left column: error for $\boldsymbol{v}_{h,\tau}$ and $p_{h,\tau}$. Right column: values of $\mathrm{EOC}^j_{\|\cdot\|}(h)$ for $\tau_0 = 10^{-3}$ using the Crank-Nicolson scheme.

The results in Table 7.1 demonstrate the correctness of the time discretization. The order of the implicit Euler method is 1 while the Crank-Nicolson scheme is of order 2. The linear solvers and the saddle point solver were run with a tolerance of 10^{-10}.

The decline of EOC(h)-rates for higher order Taylor-Hood in Table 7.2 is due to the fact that the EOC(h) calculation relies on a sufficiently small contribution of temporal error terms to the total error, confer (7.4). For very fine space discretizations the total error will no longer be dominated by space error contributions causing the stagnation effect. The numerical behavior is therefore correct. Similar effects are visible in the subsequent two tables.

7.1.1.2.5 Temporal convergence results of the 3D test problem

Implicit Euler, L^∞-norm in time

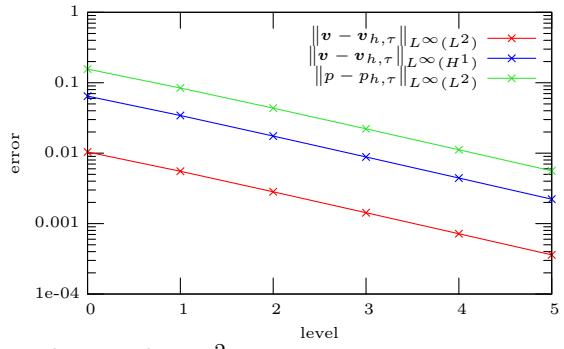

τ	$\boldsymbol{v}, L^2$	$\boldsymbol{v}, H^1$	p, L^2
2^{-1}	—	—	—
2^{-2}	0.91	0.91	0.89
2^{-3}	0.97	0.97	0.95
2^{-4}	0.99	0.99	0.98
2^{-5}	0.99	0.99	0.99
2^{-6}	1.00	1.00	0.99

Implicit Euler, L^2-norm in time

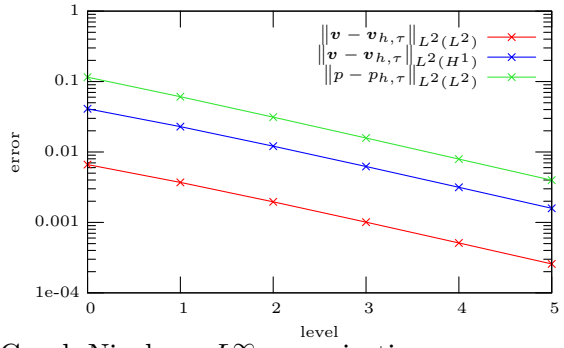

τ	$\boldsymbol{v}, L^2$	$\boldsymbol{v}, H^1$	p, L^2
2^{-1}	—	—	—
2^{-2}	0.84	0.84	0.92
2^{-3}	0.92	0.92	0.97
2^{-4}	0.96	0.96	0.98
2^{-5}	0.98	0.98	0.99
2^{-6}	0.99	0.99	1.00

Crank-Nicolson, L^∞-norm in time

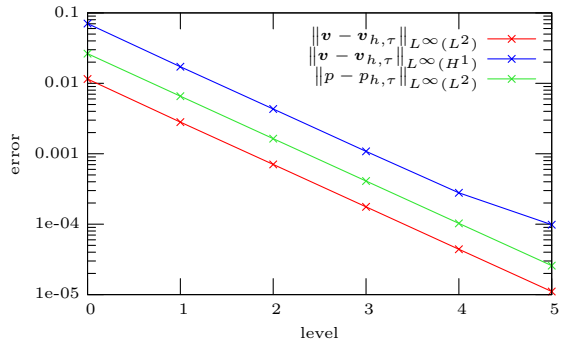

τ	$\boldsymbol{v}, L^2$	$\boldsymbol{v}, H^1$	p, L^2
2^{-1}	—	—	—
2^{-2}	2.04	2.04	2.01
2^{-3}	1.99	1.99	2.00
2^{-4}	2.00	2.00	2.00
2^{-5}	2.00	1.96	2.00
2^{-6}	1.99	1.51	1.99

Crank-Nicolson, L^2-norm in time

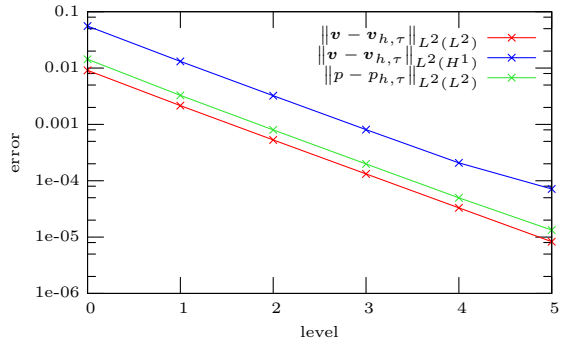

τ	$\boldsymbol{v}, L^2$	$\boldsymbol{v}, H^1$	p, L^2
2^{-1}	—	—	—
2^{-2}	2.08	2.08	2.13
2^{-3}	2.02	2.02	2.04
2^{-4}	2.00	2.00	2.01
2^{-5}	2.00	1.96	2.00
2^{-6}	1.99	1.54	1.90

Table 7.3: Left column: errors for $\boldsymbol{v}_{h,\tau}$ and $p_{h,\tau}$. Right column: values of $\mathrm{EOC}^j_{\|\cdot\|}(\tau)$ for $h_0 = 2^{-4}$ using Taylor-Hood order 2.

7.1.1.2.6 Spatial convergence results of the 3D test problem

Taylor-Hood order 1 in space

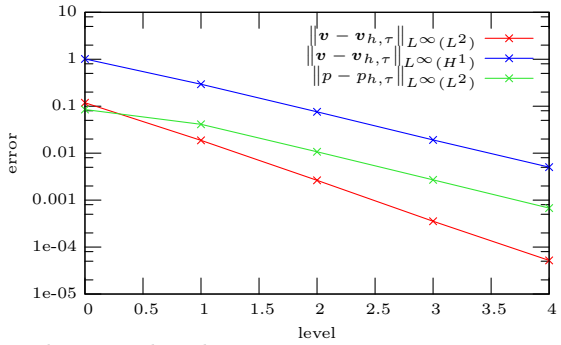

h	$\boldsymbol{v}, L^2$	$\boldsymbol{v}, H^1$	p, L^2
1	—	—	—
2^{-1}	2.66	1.79	1.05
2^{-2}	2.83	1.95	1.95
2^{-3}	2.89	1.99	1.98
2^{-4}	2.77	1.93	2.00

Taylor-Hood order 2 in space

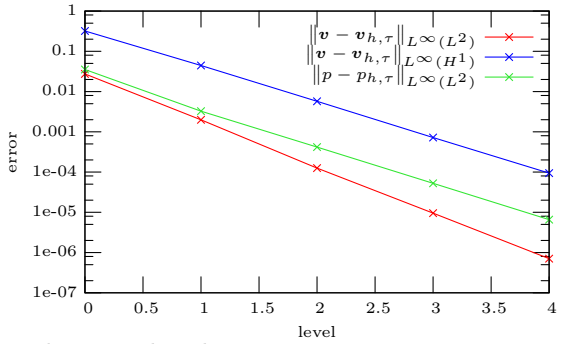

h	$\boldsymbol{v}, L^2$	$\boldsymbol{v}, H^1$	p, L^2
1	—	—	—
2^{-1}	3.78	2.85	3.44
2^{-2}	3.99	2.96	2.97
2^{-3}	3.72	2.99	2.99
2^{-4}	3.76	2.94	3.00

Taylor-Hood order 3 in space

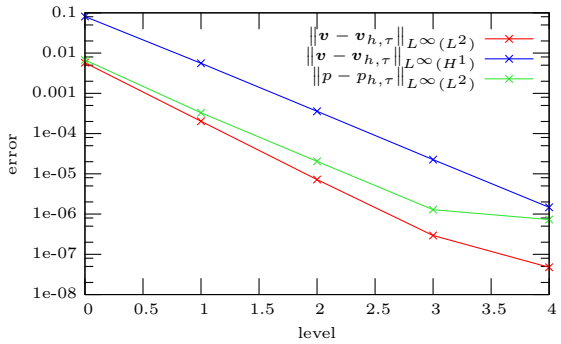

h	$\boldsymbol{v}, L^2$	$\boldsymbol{v}, H^1$	p, L^2
1	—	—	—
2^{-1}	4.83	3.86	4.36
2^{-2}	4.81	3.96	4.01
2^{-3}	4.62	3.99	3.99
2^{-4}	2.62	3.94	0.82

Table 7.4: Left column: error for $\boldsymbol{v}_{h,\tau}$ and $p_{h,\tau}$. Right column: values of $\mathrm{EOC}^j_{\|\cdot\|}(h)$ for $\tau_0 = 10^{-3}$ using the Crank-Nicolson scheme.

The convergence tests of Table 7.3 show that time discretization works correctly in three dimensions as well. The CPU time to run the largest 3D-tests was approximately one day.

7.1.1.3 Validity of the quasi-stationary approach

Now we will turn to the implementation of the quasi-stationary approach for the evolution problem with the model equations

$$\begin{aligned}
\omega\mu_v\widehat{\boldsymbol{v}}_s - \nu_1\Delta\widehat{\boldsymbol{v}}_c - \nu_2\nabla(\nabla\cdot\widehat{\boldsymbol{v}}_c) + \nabla\widehat{p}_c &= \widehat{\boldsymbol{f}}_{vc},\\
-\omega\mu_v\widehat{\boldsymbol{v}}_c - \nu_1\Delta\widehat{\boldsymbol{v}}_s - \nu_2\nabla(\nabla\cdot\widehat{\boldsymbol{v}}_s) + \nabla\widehat{p}_s &= \widehat{\boldsymbol{f}}_{vp},\\
\omega\mu_p\widehat{p}_s + \nabla\cdot\widehat{\boldsymbol{v}}_c &= \widehat{f}_{pc},\\
-\omega\mu_p\widehat{p}_c + \nabla\cdot\widehat{\boldsymbol{v}}_s &= \widehat{f}_{ps} \quad \text{in } \Omega,\\
\widehat{\boldsymbol{v}}_c &= \widehat{\boldsymbol{g}}_c,\\
\widehat{\boldsymbol{v}}_s &= \widehat{\boldsymbol{g}}_s \quad \text{on } \partial\Omega.
\end{aligned} \tag{7.7}$$

studied in Section 3.3. This problem only involves a spatial discretization with twice as many unknowns as before. We use the double Taylor-Hood element $\tilde{X}_h^k \times \tilde{Y}_h^k$ of order k, the tilde denoting the generalized spaces as in Section 3.4. By virtue of Theorem 4.2.8 we expect convergence rates

$$\|v_h - v\|_X + \|p_h - p\|_Y \le Ch^r,$$

where $v = (\widehat{\boldsymbol{v}}_c, \widehat{\boldsymbol{v}}_s) \in \tilde{X} = \boldsymbol{H}^1(\Omega)^2$, $p = (\widehat{p}_c, \widehat{p}_s) \in \tilde{Y} = L^2(\Omega)^2$ are the exact solutions of (7.7) and $(v_h, p_h) \in \tilde{X}_h^k \times \tilde{Y}_h^k$ are the discrete solutions given by Problem 4.2.6.

Analogously to Definition 7.1.1 we define suitable EOC terms as

$$\begin{aligned}
\mathrm{EOC}^j_{\|\cdot\|}(h, \boldsymbol{v}) &:= \ln\left(\frac{\|\boldsymbol{v} - \boldsymbol{v}_{h_{j-1}}\|}{\|\boldsymbol{v} - \boldsymbol{v}_{h_j}\|}\right) \Bigg/ \ln\left(\frac{h_{j-1}}{h_j}\right),\\
\mathrm{EOC}^j_{\|\cdot\|}(h, p) &:= \ln\left(\frac{\|p - p_{h_{j-1}}\|}{\|p - p_{h_j}\|}\right) \Bigg/ \ln\left(\frac{h_{j-1}}{h_j}\right),
\end{aligned}$$

where $\boldsymbol{v}$ may be either $\widehat{\boldsymbol{v}}_c$ or $\widehat{\boldsymbol{v}}_s$, similarly for p. We will only consider a 2D problem for brevity here.

7.1.1.3.1 2D quasi-stationary test problem

The data for the quasi-stationary test problem in 2D:

- Domain $\Omega = [0,1]^2$ with macro triangulation as in Figure 7.1.
- Parameters: $\mu_v = \mu_p = 1$, $\nu_1 = \nu_2 = 1$, $\omega = 2\pi$.
- Velocity and pressure functions:

$$\begin{aligned}
\widehat{v}_{c,1}(\boldsymbol{x}) &= \exp(-x_1)\sin(x_1),\\
\widehat{v}_{c,2}(\boldsymbol{x}) &= \sin(x_1)\cos(x_2),\\
\widehat{p}_c(\boldsymbol{x}) &= \exp(-x_1)\sin(x_1),\\
\widehat{v}_{s,1}(\boldsymbol{x}) &= -\exp(-x_1)\cos(x_1),\\
\widehat{v}_{s,2}(\boldsymbol{x}) &= 2\cos(x_1)\sin(x_2),\\
\widehat{p}_s(\boldsymbol{x}) &= -\exp(-x_1)\cos(x_1).
\end{aligned}$$

The right hand side (f_X, f_Y) and Dirichlet boundary values g are again chosen to match this solution.

7.1.1.3.2 Convergence results 2D quasi-stationary test problem

Taylor-Hood order 1

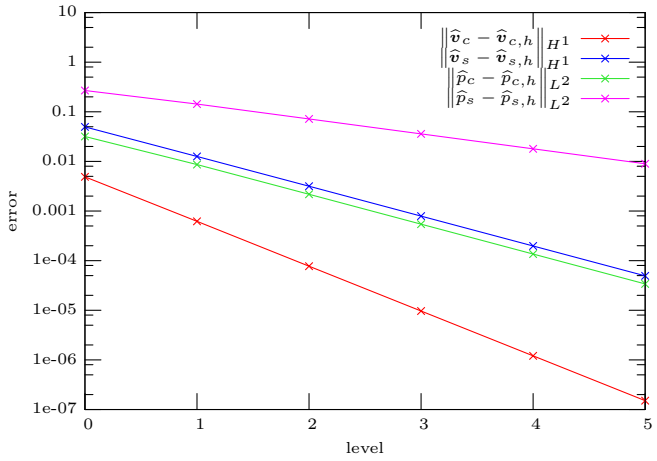

h	$\widehat{\boldsymbol{v}}_c, H^1$	$\widehat{\boldsymbol{v}}_s, H^1$
1	—	—
2^{-1}	1.98	1.94
2^{-2}	2.00	1.98
2^{-3}	2.00	2.00
2^{-4}	2.00	2.00
2^{-5}	2.00	2.00
h	$\widehat{p}_c, L^2$	$\widehat{p}_s, L^2$
1	—	—
2^{-1}	1.88	2.06
2^{-2}	1.99	2.00
2^{-3}	2.00	2.00
2^{-4}	2.00	2.00
2^{-5}	2.00	2.00

Taylor-Hood order 2

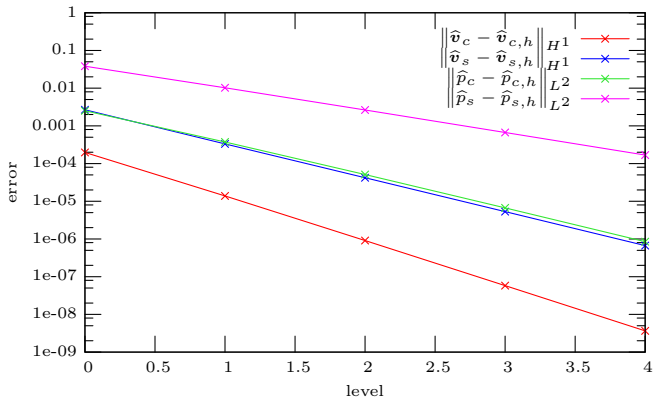

h	$\widehat{\boldsymbol{v}}_c, H^1$	$\widehat{\boldsymbol{v}}_s, H^1$
1	—	—
2^{-1}	3.01	2.96
2^{-2}	2.98	3.00
2^{-3}	2.99	3.01
2^{-4}	2.99	3.00
h	$\widehat{p}_c, L^2$	$\widehat{p}_s, L^2$
1	—	—
2^{-1}	2.75	2.37
2^{-2}	2.87	2.76
2^{-3}	2.94	2.87
2^{-4}	2.97	2.93

Taylor-Hood order 3

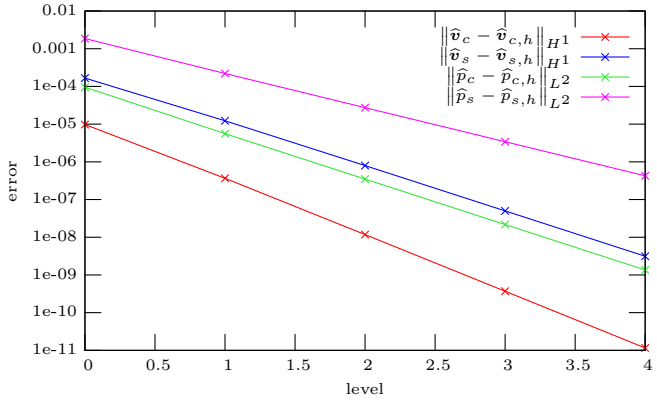

h	$\widehat{\boldsymbol{v}}_c, H^1$	$\widehat{\boldsymbol{v}}_s, H^1$
1	—	—
2^{-1}	3.76	4.01
2^{-2}	3.95	4.01
2^{-3}	3.99	4.01
2^{-4}	4.00	4.00
h	$\widehat{p}_c, L^2$	$\widehat{p}_s, L^2$
1	—	—
2^{-1}	4.09	3.87
2^{-2}	4.01	3.98
2^{-3}	4.00	4.00
2^{-4}	4.00	4.00

Table 7.5: Left column: error for $\widehat{\boldsymbol{v}}_{c,h}$, $\widehat{\boldsymbol{v}}_{s,h}$, $\widehat{p}_{c,h}$, and $\widehat{p}_{s,h}$. Right column: values of $\mathrm{EOC}^j_{\|\cdot\|}(h)$.

The results shown in Table 7.5 show the expected decline of errors.

7.1.1.4 Acoustic streaming right hand sides

When carrying out complete SAW-fluid interaction simulations we have the subproblem of transforming the acoustic subproblem solution $(\boldsymbol{v}^{(1)}, p^{(1)})$ into the correct right hand sides of the acoustic streaming subproblem, see Algorithm 6.3.1, Step 2. Since this process implies numerical averaging over time as well as forming nonlinear terms involving finite element functions additional discretization errors will occur at this stage. We are again interested in verifying the correctness of the implementation.

Recalling (6.16) on page 101 the time averaging at least may be done exactly when using the quasi-stationary approach for calculating the acoustics subproblem solution.

Let $\widehat{\boldsymbol{v}}_c$, $\widehat{\boldsymbol{v}}_s$, $\widehat{p}_c$, $\widehat{p}_s$ be the sufficiently smooth exact solution of the acoustics subproblem given by the quasi-stationary approach. The exact right hand sides and Dirichlet boundary values are given by

$$\begin{aligned}
\boldsymbol{f}_v &= -\frac{\beta_v}{2}\left((\nabla\cdot\widehat{\boldsymbol{v}}_c)\widehat{\boldsymbol{v}}_c + (\nabla\widehat{\boldsymbol{v}}_c)\widehat{\boldsymbol{v}}_c + (\nabla\cdot\widehat{\boldsymbol{v}}_s)\widehat{\boldsymbol{v}}_s + (\nabla\widehat{\boldsymbol{v}}_s)\widehat{\boldsymbol{v}}_s\right),\\
f_p &= -\frac{\beta_p}{2}\left(\nabla\cdot(\widehat{p}_c\widehat{\boldsymbol{v}}_c) + \nabla\cdot(\widehat{p}_s\widehat{\boldsymbol{v}}_s)\right),\\
\boldsymbol{g} &= -\frac{1}{2\omega}\left(-(\nabla\widehat{\boldsymbol{v}}_c)\widehat{\boldsymbol{v}}_s + (\nabla\widehat{\boldsymbol{v}}_s)\widehat{\boldsymbol{v}}_c\right),
\end{aligned}$$

with parameters $\beta_v, \beta_p > 0$ introduced by the scaling. The discrete terms corresponding to $\boldsymbol{f}_v$ and f_p available in practice are

$$\begin{aligned}
\mathrm{F}_{v,h} &= ((\boldsymbol{f}_{v,h}, \boldsymbol{\psi}_i)_0)_{i=1}^{\mathring{n}_v} \in \mathbb{R}^{\mathring{n}_v},\\
\mathrm{F}_{p,h} &= ((f_{p,h}, \varphi_i)_0)_{i=1}^{n_p} \in \mathbb{R}^{n_p},
\end{aligned}$$

where $\boldsymbol{\psi}_i$ and φ_i are the Lagrange basis functions of the finite element spaces $\boldsymbol{V}_h$ and $\tilde{Q}_h$ respectively. These are the right hand side vectors for the linear systems arising from (6.17) on page 101.

Accordingly, we calculate

$$\begin{aligned}
\mathrm{F}_v &= ((\boldsymbol{f}_v, \boldsymbol{\psi}_i)_0)_{i=1}^{\mathring{n}_v},\\
\mathrm{F}_p &= ((f_p, \varphi_i)_0)_{i=1}^{n_p},
\end{aligned}$$

based on the exact solutions and high degree quadrature formulae. We use the l^∞-error norms in R^n

$$\left|\mathrm{F}_v - \mathrm{F}_{v,h}\right|_\infty, \quad \left|\mathrm{F}_p - \mathrm{F}_{p,h}\right|_\infty,$$

as well as the $\boldsymbol{L}^2(\Gamma)$-norm on the boundary

$$\|\boldsymbol{g} - \boldsymbol{g}_h\|_{L^2} := \|\boldsymbol{g} - \boldsymbol{g}_h\|_{\boldsymbol{L}^2(\Gamma)},$$

to test the correctness of the approximation. For the numerical test we again use Test Problem 7.1.1.3.1 at different levels of refinement and with Taylor-Hood elements of orders $1, 2, 3$.

7.1.1.4.1 Errors in the right hand sides

Taylor-Hood order 1

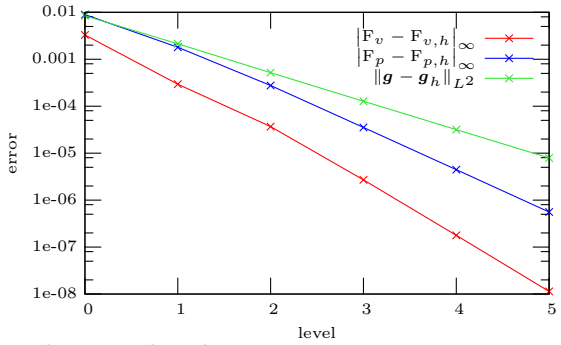

h	F_v, l^∞	F_p, l^∞	$\boldsymbol{g}, L^2$
1	—	—	—
2^{-1}	3.49	2.31	1.98
2^{-2}	3.00	2.71	2.04
2^{-3}	3.76	2.97	2.02
2^{-4}	3.93	2.98	2.01
2^{-5}	3.97	3.00	2.00

Taylor-Hood order 2

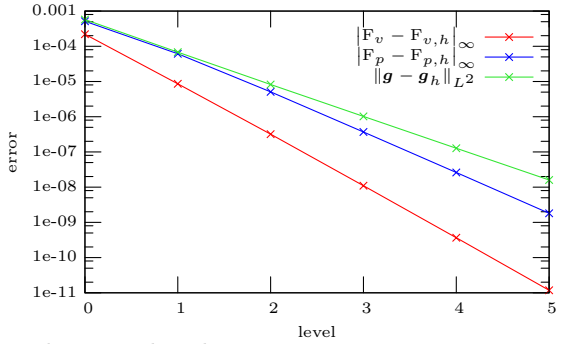

h	F_v, l^∞	F_p, l^∞	$\boldsymbol{g}, L^2$
1	—	—	—
2^{-1}	4.68	3.07	3.08
2^{-2}	4.75	3.59	3.05
2^{-3}	4.86	3.79	3.01
2^{-4}	4.91	3.82	3.00
2^{-5}	4.96	3.85	3.00

Taylor-Hood order 3

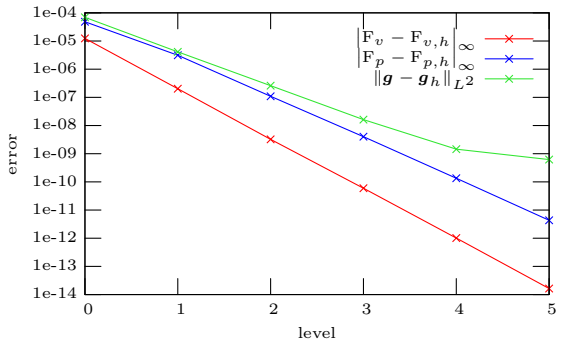

h	F_v, l^∞	F_p, l^∞	$\boldsymbol{g}, L^2$
1	—	—	—
2^{-1}	5.94	3.95	4.07
2^{-2}	5.97	4.84	3.99
2^{-3}	5.76	4.76	4.00
2^{-4}	5.88	4.90	3.48
2^{-5}	5.95	4.96	1.23

Table 7.6: Left column: differences $|\mathrm{F}_v - \mathrm{F}_{v,h}|_\infty$,$|\mathrm{F}_p - \mathrm{F}_{p,h}|_\infty$, $\|\boldsymbol{g} - \boldsymbol{g}_h\|_{L^2}$. Right column: corresponding EOCs.

The results shown in Table 7.6 demonstrate a correct implementation of the discrete right hand sides for the acoustic streaming problem.

7.1.2 Free boundaries

In this subsection we will present two test situations for the free boundary problem

$$\begin{aligned}
\mu_v \frac{\partial \boldsymbol{v}}{\partial t} - \nabla \cdot \Sigma &= \boldsymbol{f}_v && \text{in } \Omega(t), && \text{(7.8a)}\\
\mu_p \frac{\partial p}{\partial t} + \nabla \cdot \boldsymbol{v} &= f_p && \text{in } \Omega(t), && \text{(7.8b)}\\
\boldsymbol{v} &= \boldsymbol{g} && \text{on } \Gamma_d, &&\\
\Sigma \boldsymbol{n} &= \sigma(d-1)\boldsymbol{\kappa} && \text{on } \Gamma_f(t), && \text{(7.8c)}\\
\boldsymbol{v} \cdot \boldsymbol{n} &= V && \text{on } \Gamma_f(t), &&\\
\Omega(0) &= \Omega_0, &&&&\\
\boldsymbol{v}(t=0,\boldsymbol{x}) = \boldsymbol{v}_0, \quad p(t=0,\boldsymbol{x}) &= p_0 && \text{in } \Omega_0. &&
\end{aligned}$$

with

$$\Sigma_{ij} = -p\delta_{ij} + \nu_1 \left(\frac{\partial v_i}{\partial x_j} + \frac{\partial v_j}{\partial x_i} \right) + (\nu_2 - \nu_1)(\nabla \cdot \boldsymbol{v})\delta_{ij} \qquad \text{as the stress tensor,}$$

V as the normal velocity of $\Gamma_f(t)$,

$\boldsymbol{\kappa}$ as the vector of mean curvature,

$\sigma > 0$ as a coefficient of surface tension.

treated in Chapter 5. Performing convergence tests as above is difficult due to the complex nonlinear nature of the problem which makes it hard to find exact solutions and corresponding data. We will perform several simple experiments:

- A circular 2D drop of compressible fluid falling under the influence of an external force such as gravity: This setup will demonstrate the correctness of the mesh update algorithm.

- A circular 2D drop of compressible fluid performing volume oscillations: The equilibrium state will show whether the capillary force terms are implemented correctly. Furthermore, this test may provide some evidence that the introduction of compressibility in the Navier-Stokes system does not destroy the stability of the free boundary algorithm.

- Elliptical/Ellipsoidal incompressible 2D/3D drops oscillating solely through the action of capillary forces. This setup was also studied in [3]. The results of this work and [3] coincide, providing further confirmation of the correct implementation.

7.1.2.1 Falling droplet

7.1.2.1.1 Data of the falling droplet problem

The reference domain $\hat{\Omega}$ is the diamond-shaped set

$$\operatorname{conv}\{(-1,0),(0,-1),(1,0),(0,1)\} \subset \mathbb{R}^2.$$

The reference free capillary boundary $\hat{\Gamma}_f$ is the entire boundary $\partial\hat{\Omega}$. The initial domain Ω_0 is defined as follows: The reference domain is refined several times. After each refinement step, the new mesh nodes lying on the boundary are projected to the boundary of the unit circle using

$$\begin{aligned} \phi : \mathbb{R}^2 \setminus \{0\} &\to S^1, \\ \phi(\boldsymbol{x}) &= \frac{\boldsymbol{x}}{|\boldsymbol{x}|}, \end{aligned} \tag{7.9}$$

see Figure 7.2. The resulting triangulation represents Ω_0 and approximates the unit circle. The further data:

- $\boldsymbol{f}_v(t,\boldsymbol{x}) = (0,-1)$ ("gravity pulling downwards"), $f_p = 0$.
- $\mu_v = 1$, $\mu_p = 1$.
- $\boldsymbol{v}_0 = p_0 = 0$, time interval $[0,1]$.
- $\sigma = 1$, $\nu_1 = \nu_2 = 0.1$.
- Mesh update algorithm 5.2.6 is used (simple transport of all mesh points using the current velocity).

The exact solution is obviously

$$\begin{aligned} \boldsymbol{v}(t,\boldsymbol{x}) &= (0,-t), \\ p(t,\boldsymbol{x}) &= 1, \\ \Omega(t) &= \{\boldsymbol{x} \in \mathbb{R}^2 \mid \left|\boldsymbol{x} - \left(0, -\frac{1}{2}t^2\right)\right| \leq 1\}, \end{aligned}$$

meaning that velocity and pressure will actually lie in the finite element spaces. We therefore expect extremely high accuracy. For the results we measure the error norms $\|\cdot\|_{L^2(Z)}$, $\|\cdot\|_{L^\infty(Z)}$ as in the beginning of the section – however, we replace the fixed domain Ω by the current domain Ω_n for space integrals.

Since the discretization is first order in τ, we couple τ and h according to $\tau = h^{k+1}$ with k as the order of the Taylor-Hood element space to define the refinement levels. We also provide data on the relative mesh volume change $\rho_V = \lambda^2(\Omega_N)/\lambda^2(\Omega_0)$ between beginning and end of the simulation.

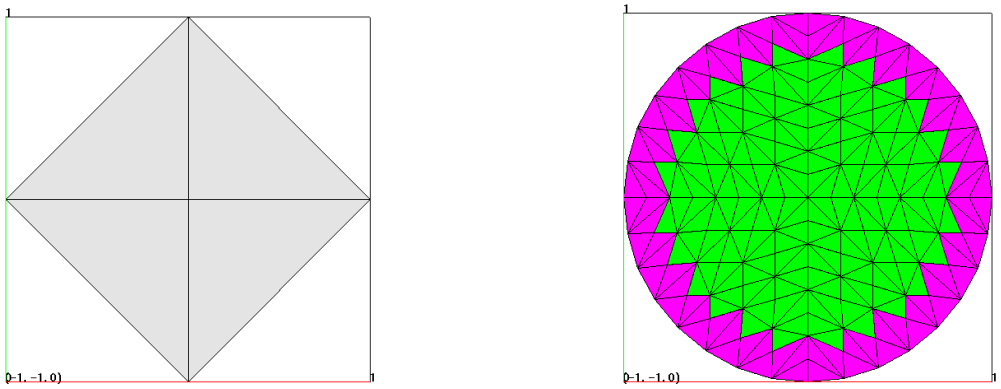

Figure 7.2: Left: Reference domain $\hat{\Omega}$. Right: Domain Ω_0 using six bisection refinement steps. Triangulation of $\mathcal{T}_i^0$ is shown in green, $\mathcal{T}_f^0$ is drawn in purple (see (5.6) on page 81)

7.1.2.1.2 Results of the falling droplet problem

Taylor-Hood order 1 in space, L^2-norm in time

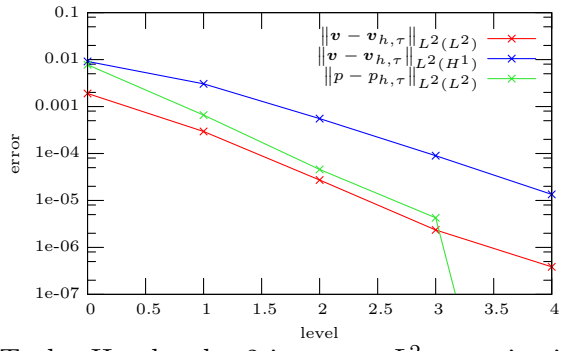

$h/\sqrt{2}$	ρ_V
1	$9.940901 \cdot 10^{-1}$
2^{-1}	$9.996112 \cdot 10^{-1}$
2^{-2}	$9.999753 \cdot 10^{-1}$
2^{-3}	$9.999983 \cdot 10^{-1}$
2^{-4}	$9.999996 \cdot 10^{-1}$

Taylor-Hood order 2 in space, L^2-norm in time

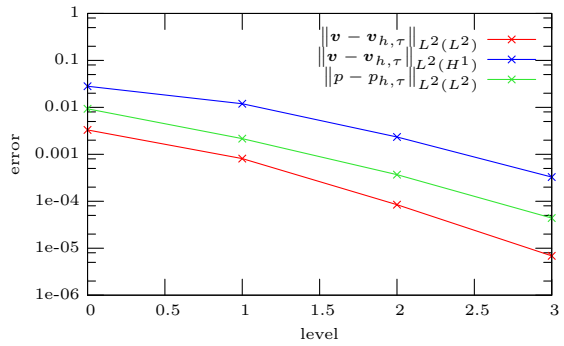

$h/\sqrt{2}$	ρ_V
1	$9.940901 \cdot 10^{-1}$
2^{-1}	$9.994681 \cdot 10^{-1}$
2^{-2}	$9.999630 \cdot 10^{-1}$
2^{-3}	$9.999976 \cdot 10^{-1}$

Table 7.7: Left: Errors $\|\boldsymbol{v} - \boldsymbol{v}_{h,\tau}\|$ and $\|p - p_{h,\tau}\|$ with $\tau = h^{k+1}$, Right: Values of the relative mesh volume ρ_V. Note that EOC tests are not useful since the true solution lies in the finite element space.

7.1.2.2 Contracting and expanding droplet

For the contracting and expanding droplet experiment we start with the same starting mesh Ω_0 as in the prior experiment. However, we now prescribe a

starting pressure p_0 which is not in equilibrium with capillary forces. If the starting pressure is too low, then the capillary forces will start to compress the droplet radially, otherwise expansion will occur.

Oscillations between contraction and expansion may occur due to the interaction between capillary forces and the equation of mass conservation (7.8b). This may easily be explained heuristically in the case of the radially symmetric 2D droplet.

Choosing $\sigma = 1$, the capillary stress $\boldsymbol{F}_c$ at any point $\boldsymbol{x}$ and time t on the boundary is exactly equal to the curvature

$$\boldsymbol{F}_c(t, \boldsymbol{x}) = \Sigma(t, \boldsymbol{x})\boldsymbol{n}(t, \boldsymbol{x}) = \sigma(d-1)\boldsymbol{\kappa}(t, \boldsymbol{x}) = -\frac{1}{r}\boldsymbol{n}(t, \boldsymbol{x}),$$

using the boundary condition (7.8c). If the pressure stress $\boldsymbol{F}_p = p\boldsymbol{n}$ at the boundary is less than $\boldsymbol{F}_c$ in magnitude, a radial inward flow will result. Due to symmetry the domain $\Omega(t)$ will remain a circle of radius $r(t)$. We may assume that the pressure is more or less constant in the domain and solely dependent on the radius $r(t)$. The pressure buildup in the domain may then be estimated using (7.8b) as follows:

$$\begin{aligned}
\frac{dp}{dr}(r(t))\frac{dr}{dt}(t) = \frac{dp}{dt}(t) &= \frac{1}{\pi r(t)^2}\int_{\Omega(t)} \frac{dp}{dt}(t)\, d\boldsymbol{x} \\
&= -\frac{1}{\pi r(t)^2}\int_{\Omega(t)} \nabla \cdot \boldsymbol{v}(t, \boldsymbol{x})\, d\boldsymbol{x} \\
&= -\frac{1}{\pi r(t)^2}\int_{\Gamma_f(t)} \boldsymbol{v}(t, \boldsymbol{x}) \cdot \boldsymbol{n}(t, \boldsymbol{x})\, d\mathcal{H}^{d-1}(\boldsymbol{x}) \\
&= -\frac{1}{\pi r(t)^2}\int_{\Gamma_f(t)} \frac{dr}{dt}(t)\, d\mathcal{H}^{d-1}(\boldsymbol{x}), \\
&= -\frac{2}{r(t)}\frac{dr}{dt}(t).
\end{aligned} \tag{7.10}$$

This implies the simple ODE for pressure

$$\frac{dp}{dr} = -\frac{2}{r} \Longrightarrow p(r) = p_0 - 2\ln(r). \tag{7.11}$$

As the plots of Figure 7.3 show, the pressure approximated by (7.11) may rise faster than capillary stress. If we neglect viscous stresses, this implies that the total stress $\boldsymbol{F} = \boldsymbol{F}_c + \boldsymbol{F}_p$ at the boundary may change direction and point outwards at some point. The result is an oscillating behavior of the radius r with time for certain values of p_0. Viscous damping (and damping effects of the time discretization) will attenuate the oscillation. The equilibrium radius is expected to be p_0 if the implementation is correct.

7.1.2.2.1 Data of the contracting/expanding droplet

Several experiments to measure the time evolution of the radius, measured as $r(t) := \sqrt{\lambda^2(\Omega(t))/\pi}$ were performed. We used the data

- $\Omega_0 \subset \mathbb{R}^2$ as an approximation to the unit circle as above.

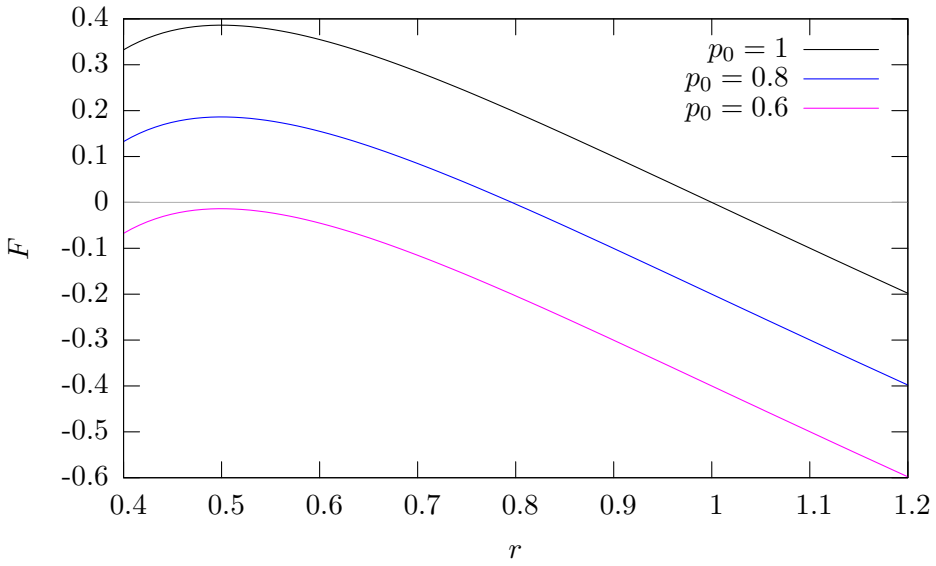

Figure 7.3: Total stress in normal direction $F = \boldsymbol{F} \cdot \boldsymbol{n} = p_0 - 1/r - 2\ln(r)$ for several values of p_0

- $\boldsymbol{f}_v(t, \boldsymbol{x}) = (0, 0)$, $f_p = 0$.
- $\mu_v = 1$, $\mu_p = 1$.
- $\boldsymbol{v}_0 = 0$, time interval $[0, 10]$.
- Refinement level: $h = 2^{-3}$, $\tau = 0.01$.
- $\sigma = 1$, $\nu_1 = \nu_2 = \nu$.
- Mesh update algorithm 2 is used (Laplace smoothing to define interior nodes)

Figure 7.4 features a plot of the droplet radius over time for different values of starting pressure and viscosity. Interestingly, Figure 7.4 shows one run in magenta with $p_0 = 0.6$ which led to a collapsing droplet, meaning that the droplet radius went to zero (at which point the simulation naturally crashed). The corresponding magenta line in Figure 7.3 already suggests this result since F does not change sign.

7.1.2.3 Comparison with another work

As a final testing case for the free boundary algorithm we set up a test using the same data as specified in [3, Section 4.1]. We define starting domains which approximate ellipses in 2D and ellipsoids in 3D with main axes along the coordinate axes. This is done by altering the definition of (7.9) to project points in $\mathbb{R}^d$ to the boundary of an ellipse/ellipsoid. The fluid is made incompressible by setting $\mu_p = 0$. Since the the mean curvature of $\Gamma_f = \partial\Omega$ is larger at the tips corresponding to smaller radii and vice versa we expect oscillatory motion with axial/planar symmetry, this time with conserved domain volume.

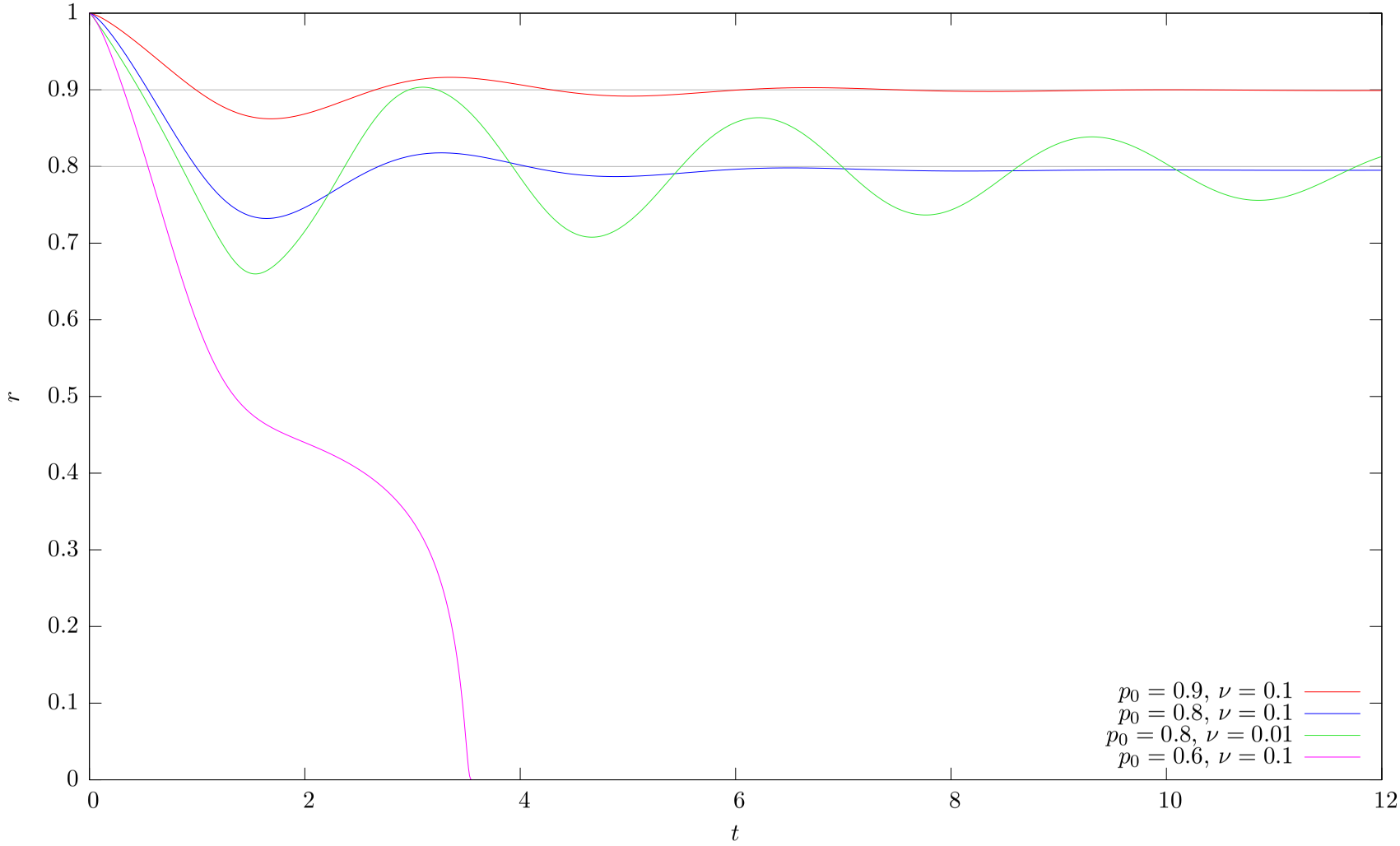

Figure 7.4: Different cases of starting pressure p_0 and viscosity ν. Observe that the final run with $p_0 = 0.6$ led to a collapsing droplet.

7.1.2.3.1 Data of the ellipse/ellipsoid simulation

In the simulation we measured the motion of the tips with time. The data used is

- All cases:
  - $\boldsymbol{f}_v = 0$, $f_p = 0$, $\mu_v = 1$, $\mu_p = 0$, $\boldsymbol{v}_0 = 0$, $p_0 = 0$, time interval $[0, 7]$, $\sigma = 1$.
  - Mesh update algorithm 2 is used (Laplace smoothing to define interior nodes)
- 2D case:
  - $\Omega_0 \subset \mathbb{R}^2$ as an ellipse with principal radii $r_1 = 1$, $r_2 = 1.2$.
  - Refinement level: $h = 2^{-5}$, $\tau = 0.0025$.
  - Viscosity coefficients: $\nu_1 = 1/300$, $\nu_2 = 0$.
- First 3D case:
  - $\Omega_0 \subset \mathbb{R}^3$ as an ellipsoid. Principal radii were $r_i = 1, 1, 1.2$
  - Refinement level: $h = 2^{-3}$, $\tau = 0.008$.
  - Viscosity coefficients: $\nu_1 = 1/300$, $\nu_2 = 0$.
- Second 3D case:
  - $\Omega_0 \subset \mathbb{R}^3$ as an ellipsoid. Principal radii were $r_i = 0.9, 1.0, 1.2$.
  - Refinement level: $h = 2^{-3}$, $\tau = 0.005$.
  - Viscosity coefficients: $\nu_1 = 1/200$, $\nu_2 = 0$.

Figure 7.5 shows a plot of the trajectories of the 2D droplet tips over time. Figures 7.6 and 7.7 show corresponding plots for the two 3D cases. Figure 7.8 features a series of six 2D droplet shapes.

The results coincide very well with those of [3].

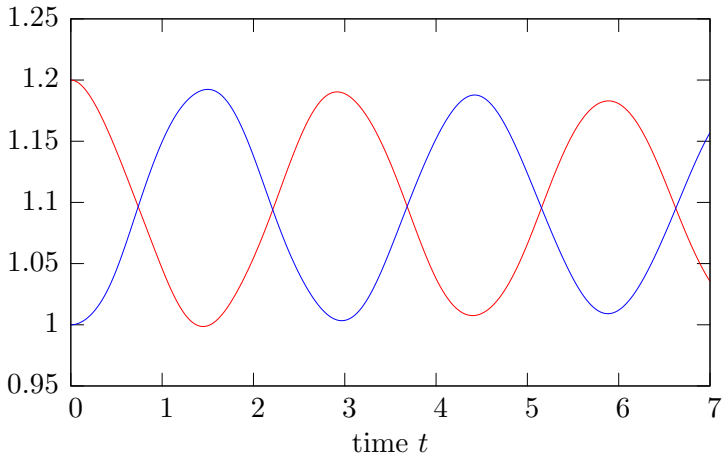

Figure 7.5: Trajectories of the 2D droplet tips.

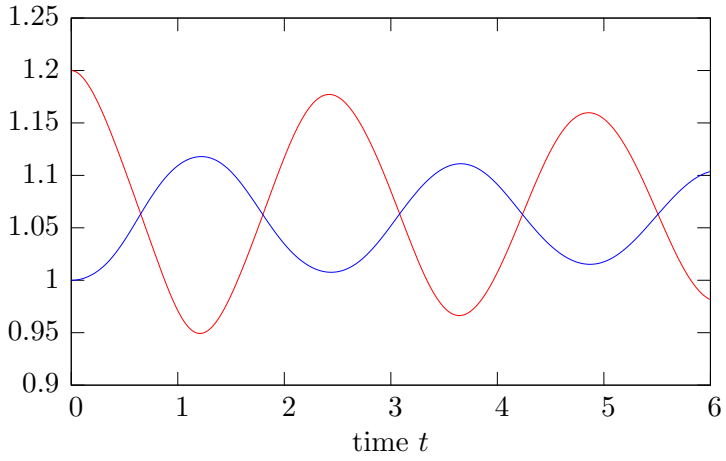

Figure 7.6: Trajectories of the 3D droplet tips, first case.

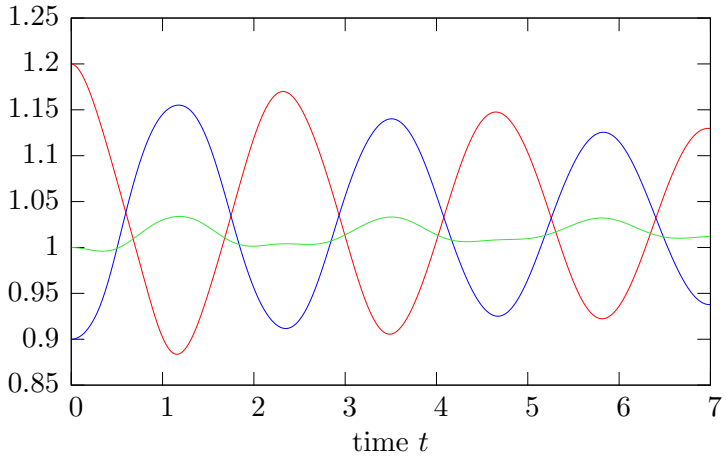

Figure 7.7: Trajectories of the 3D droplet tips, second case.

7.2 Realistic problems

The goal of this section is to present simulation results of SAW-induced streaming with realistic physical parameters. The computational effort for solving fixed domain problems is still acceptable for our 3D setup – the simulation of streaming effects including free capillary boundaries, however, is only possible in a simple 2D configuration using the current implementation. The reason for this is that the change of the domain in each time step necessitates the recalculation of the acoustic field solution, confer Remark 6.3.3.

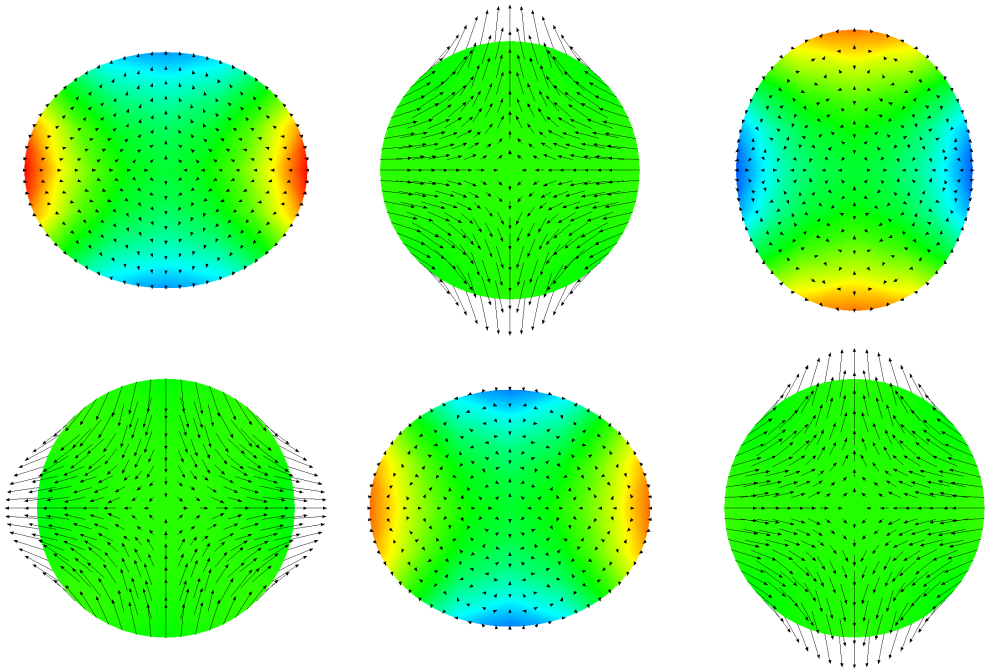

Figure 7.8: Solution of the 2D droplet at the times $t_1 = 0.025$, $t_2 = 0.725$, $t_3 = 1.475$, $t_4 = 2.2$, $t_5 = 2.95$, $t_6 = 3.675$. The color indicates pressure and the arrows velocity.

7.2.1 Fixed domains

7.2.1.1 2D simulation

We refer to (2.1) on page 10 for the notation. The 2D simulation setting is a fluid-filled square cavity $\Omega = [0, 1\text{ mm}]^2$ with SAW displacements $\boldsymbol{u}$ prescribed on the bottom edge. The velocity $\boldsymbol{v}$ is set to zero on the other three edges. The SAW propagates from left to right with exponential attenuation. The exact shape assumed in this work is based on wavelengths, wave velocities, amplitudes, and damping parameters of a typical lithium niobate crystal as described in [31].

This setup approximates the case of a vertically oriented thin slice of water trapped in a container and touching the SAW-traversed solid surface at the bottom. The fluid is assumed to be initially at rest, i. e. $\boldsymbol{v}_0 = 0$, $p_0 = 0$.

7.2.1.1.1 Data of the 2D SAW device simulation

The function $\boldsymbol{u}$ to describe the SAW displacement at the lower edge is defined in dimensionless form as

$$\begin{aligned} u_1(t, \boldsymbol{x}) &= 0.6\epsilon \exp(-\widehat{C}_d x_1) \sin(2\pi(-\widehat{k}x_1 + \widehat{f}t)), \\ u_2(t, \boldsymbol{x}) &= -\epsilon \exp(-\widehat{C}_d x_1) \cos(2\pi(-\widehat{k}x_1 + \widehat{f}t)), \end{aligned} \tag{7.12}$$

for $\boldsymbol{x} \in \partial\Omega$, $x_2 = 0$ with parameters $\epsilon = u_0/L$, $\widehat{C}_d = C_d L$, $\widehat{k} = L/\lambda$, $\widehat{f} = fT$. Note that the discretization parameter ϵ is 0.1, confer (2.3), page 12. Additional

Parameter	Value and units	Description
V	$1.0 \cdot 10^{-1}$ m/s	Dimensionless velocity scale
L	$1.0 \cdot 10^{-7}$ m	Dimensionless length scale
T	$1.0 \cdot 10^{-8}$ s	Dimensionless time scale
f	$1.0 \cdot 10^{8}$ Hz	Frequency of the SAW device
$c_{0,l}$	$1.484 \cdot 10^{3}$ m/s	Small signal sound speed in water
$c_{0,s}$	$3.8 \cdot 10^{3}$ m/s	Small signal sound speed in solid
ρ_0	$1.0 \cdot 10^{3}$ kg/m^3	Density of liquid
u_0	$1.0 \cdot 10^{-9}$ m	Maximal SAW displacement
C_d	$8.06 \cdot 10^{3}$ 1/m	Damping parameter of the LSAW
ν_1	$1.002 \cdot 10^{-6}$ m^2/s	Kinematic viscosity of water
ν_2	$1.002 \cdot 10^{-6}$ m^2/s	Kinematic bulk viscosity of water

Table 7.8: Numerical and physical parameters for the 2D SAW simulation.

damping terms, not mentioned here, serve to avoid sharp jumps of the function $\boldsymbol{u}$ at $\boldsymbol{x} = 0$ and $t = 0$. The other parameters used in the simulation are given in Table 7.8.

As described in Chapter 2 and Algorithm 6.3.1 the acoustic streaming field $(\boldsymbol{v}^{(2)}, p^{(2)})$ is calculated via a two-stage algorithm using the intermediate acoustics field solution $(\boldsymbol{v}^{(1)}, p^{(1)})$. We use the Crank-Nicolson variant of the time discretization procedure 6.3.1, Step 1a, to solve the acoustics field $(\boldsymbol{v}^{(1)}, p^{(1)})$. The tolerance *tol* for characterizing the oscillating equilibrium state is set to 0.01. To get the acoustic streaming field we utilize the stationary algorithm in 6.3.1, Step 3a.

7.2.1.1.2 Results of the 2D SAW device simulation

The CPU time necessary for the full calculation was approximately two hours.

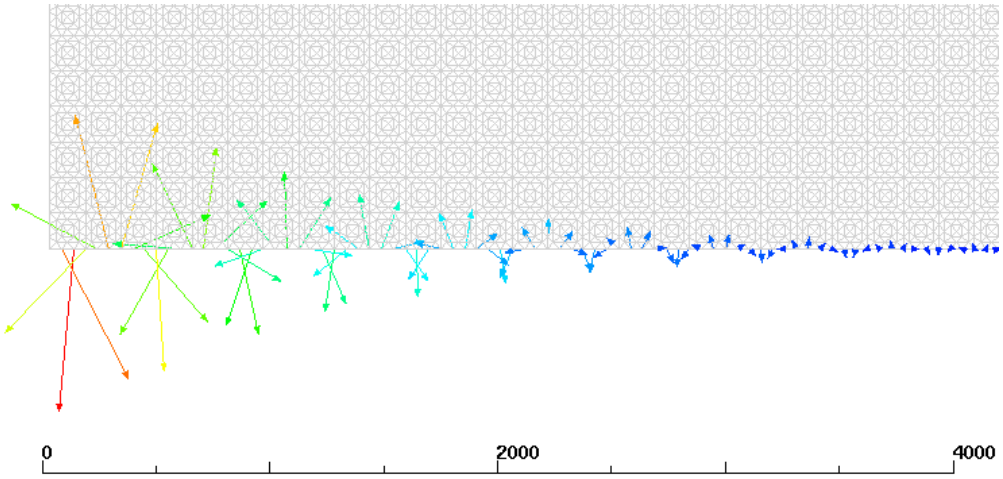

Figure 7.9: Detail of computational mesh and SAW displacement field in the bottom left corner of the domain with computational length scale (1 unit $\equiv$ $10^{-1}\mu$m)

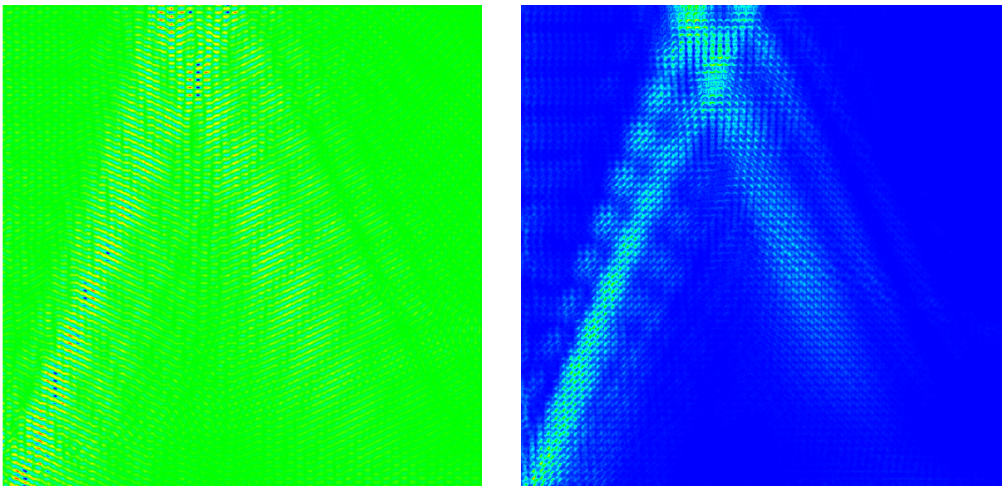

Figure 7.10: Left: Acoustics subproblem solution: pressure field $p^{(1)}$ at time $t = 142 \equiv 1.42\mu$s. Right: Plot of effective force $\boldsymbol{f}_v$ for the acoustic streaming solution. Clearly visible is the reflection of the pressure wave at the top boundary of the domain as well as the typical Rayleigh angle corresponding to the ratio of sound speeds in liquid and substrate.

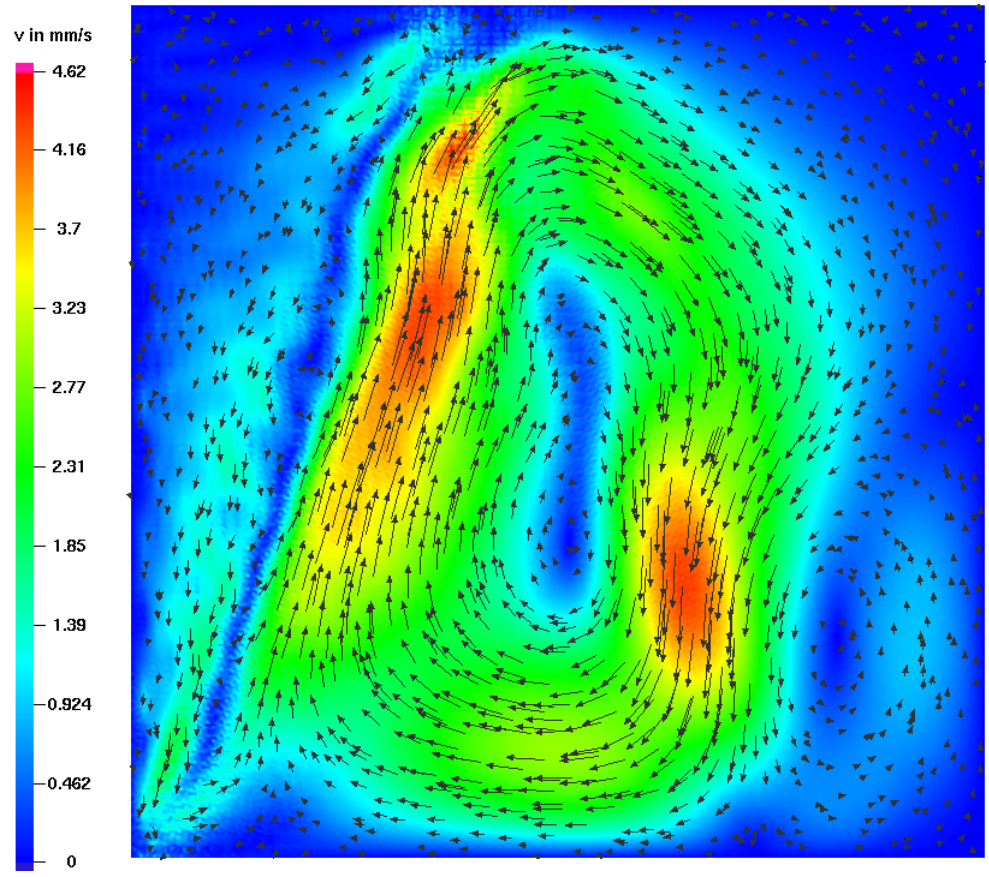

Figure 7.11: Acoustic streaming solution: velocity field $\boldsymbol{v}^{(2)}$ in mm/s.

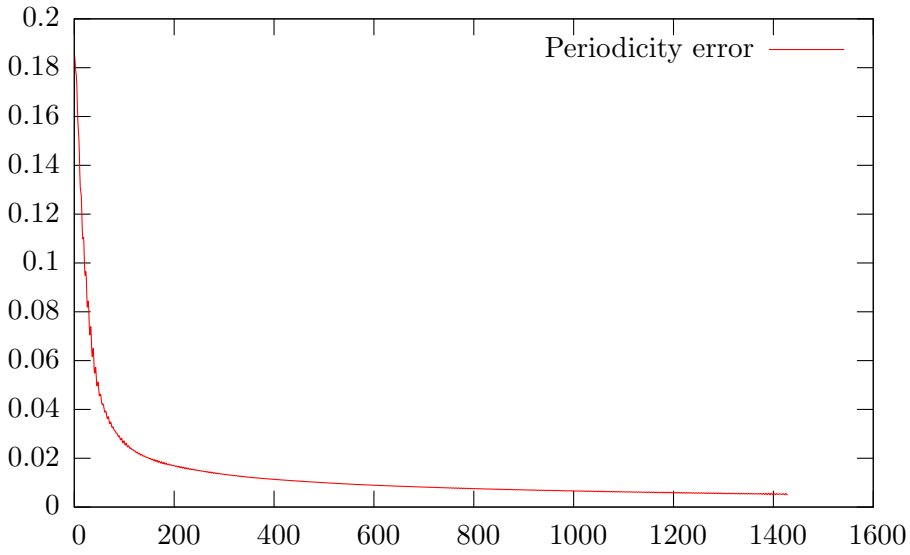

Figure 7.12: Convergence to periodicity. The red line shows the value of the left hand side of (4.14) on page 73 at each time step.

7.2.1.2 3D simulation

The parameters used for the 3D simulation are similar to the 2D case. The domain will again be a fluid-filled rectangular cavity. We set $\Omega = [0, 250\ \mu\text{m}]^2 \times [-50\ \mu\text{m}, 50\ \mu\text{m}]$, see Figure 7.13. The SAW traverses the bottom face, on the other walls we again prescribe zero Dirichlet boundary conditions for fluid velocity.

7.2.1.2.1 Data of the 3D SAW device simulation

The parameters are set to the same values as before. The function $\boldsymbol{u}$ is defined in dimensionless form as

$$\begin{aligned} u_1(t, \boldsymbol{x}) &= 0.6\epsilon \exp(-\widehat{C}_d x_1) \sin(2\pi(-\widehat{k}x_1 + \widehat{f}t))d(x_3), \\ u_2(t, \boldsymbol{x}) &= -\epsilon \exp(-\widehat{C}_d x_1) \cos(2\pi(-\widehat{k}x_1 + \widehat{f}t))d(x_3), \\ u_3(t, \boldsymbol{x}) &= 0. \end{aligned} \tag{7.13}$$

The terms have the same meaning as in (7.12) above. What is new is the term $d(x_3)$, defined as

$$d(x_3) = 4 \cdot 10^{-6}(x_3 - 500)(x_3 + 500).$$

Observing that the domain depth 100 μm corresponds to the dimensionless depth of 1000 units, we have thus extended the SAW shape of the 2D simulation to a parabolic profile over the bottom face.

7.2.1.2.2 Results of the 3D SAW device simulation

The CPU time necessary for the full calculation was approximately six days. The acoustic streaming velocity values $\boldsymbol{v}^{(2)}$ are shown in Figure 7.14.

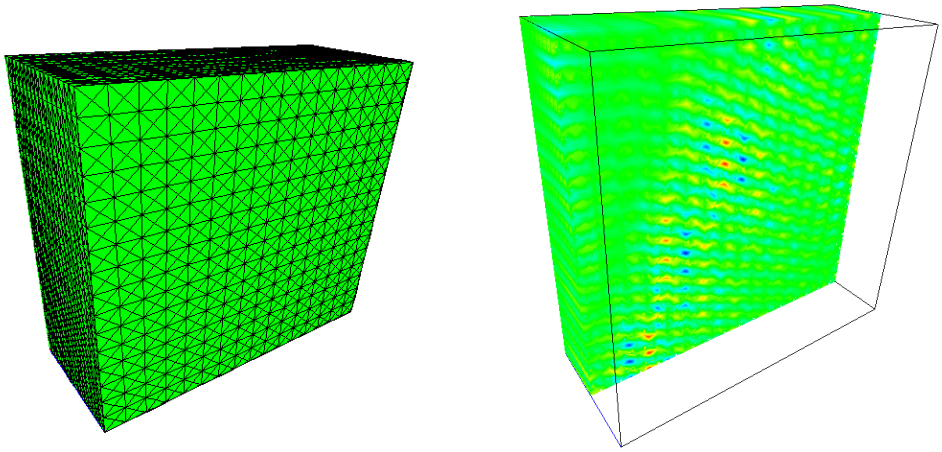

Figure 7.13: Left: domain for the 3D simulation runs. Right: acoustics subproblem solution: slab $x_3 \geq 0$ of the pressure field $p^{(1)}$ at time $t = 200 \equiv 2\ \mu$s

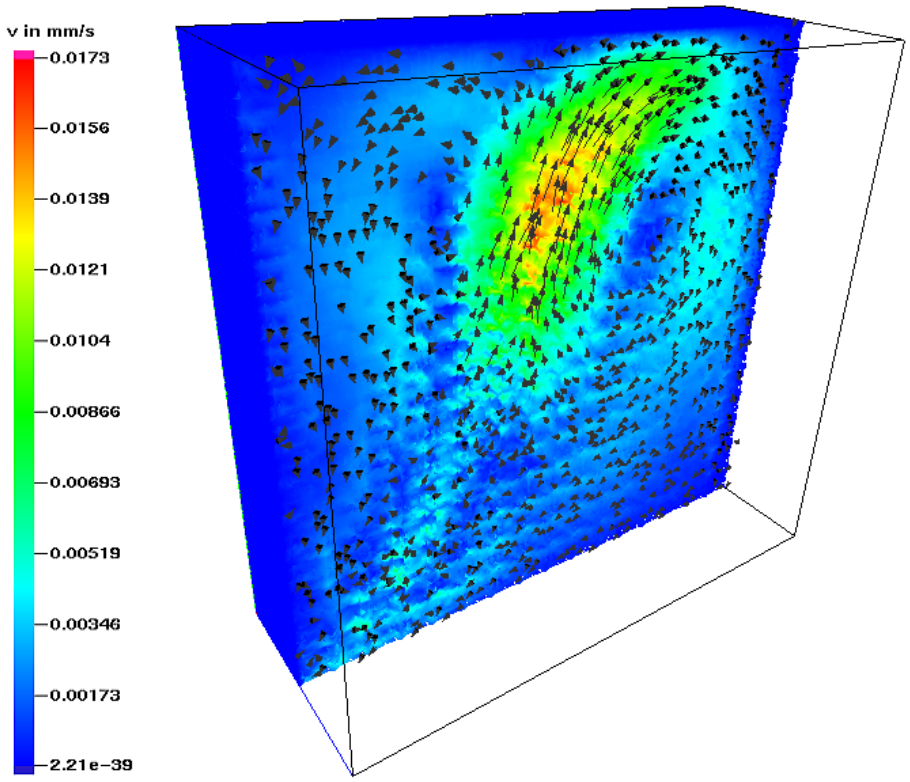

Figure 7.14: Acoustic streaming solution: slab $x_3 \geq 0$ of the velocity field $\boldsymbol{v}^{(2)}$.

We additionally took a vertical cross section of the 3D mesh to define a 2D mesh, together with values of the SAW displacement field $\boldsymbol{u}$ along the cross section. This permits a comparison of a 3D solution with a corresponding 2D solution. Figure 7.15 shows that the result is qualitatively close to the 3D field.

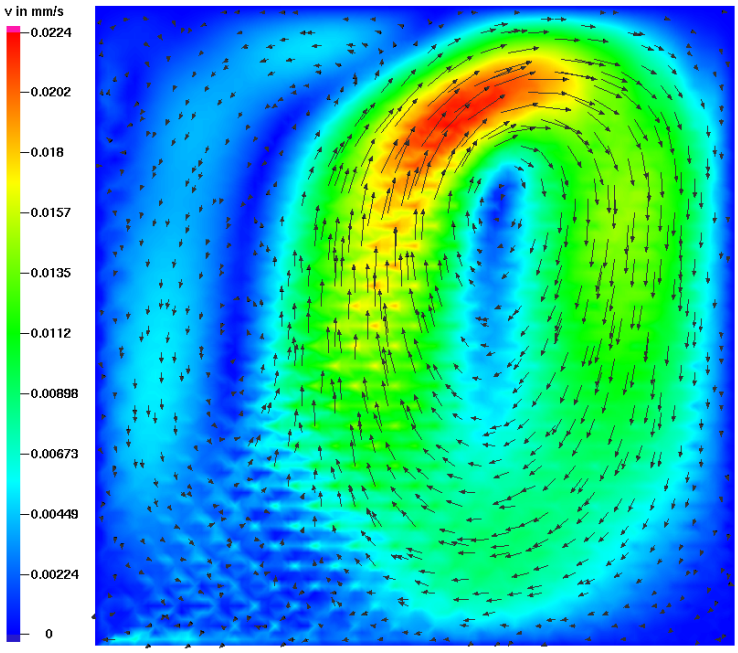

Figure 7.15: Comparison with the corresponding 2D simulation: acoustic streaming velocity field $\boldsymbol{v}^{(2)}$.

7.2.2 Free boundaries

As described above, we will restrict ourselves to performing a 2D simulation. We will describe the deformation of an originally semicircular drop of water of radius $2500 \equiv 0.25$ mm posed above a SAW wave of the same shape as in the fixed domain 2D simulations. The maximal SAW amplitude was $\boldsymbol{u}_0 = 100$ nm, a much higher value compared to the fixed domain simulations. The coefficient of surface tension assumed in the simulations is $\sigma = 7.3 \cdot 10^{-2}$ N/m corresponding to a water/vacuum interface.

We used Algorithm 6.3.2 to perform the calculation. The acoustics subproblem in Step 1 was solved using the Crank-Nicolson scheme using 200 microscopic time steps of length $\tau^{(1)} = 0.1 \equiv 1.0 \cdot 1$ ns. The acoustic streaming solution in Step 3 was done using a macroscopic time steps of length $\tau^{(2)} = 1000 \equiv 10$ μs. The recalculation of the acoustic field $\boldsymbol{v}^{(1)}$, $p^{(1)}$ as explained in Remark 6.3.3 was performed at every tenth macroscopic time step.

One important change was done in the calculations. The mass generation rate $f_p^{(2),n}$ and outflow $\boldsymbol{g}^{(2),n} \cdot \boldsymbol{n}$ used in Step 3 of Algorithm 6.3.2 will in general not be balanced as described in Subsection 3.4.2. This implies a change in the pressure mean over time. In the presence of free capillary boundaries a change in the overall pressure leads to a change in volume — this is undesirable and non-physical behavior. We therefore restored the balance between outflow and mass generation in the numerical calculations by multiplying $\boldsymbol{g}^{(2),n}$ with a correction factor. Numerical experiments performed without this correction indeed displayed a continuously decreasing volume of the droplets.

7.2.2.0.3 Results of the free boundary SAW simulation

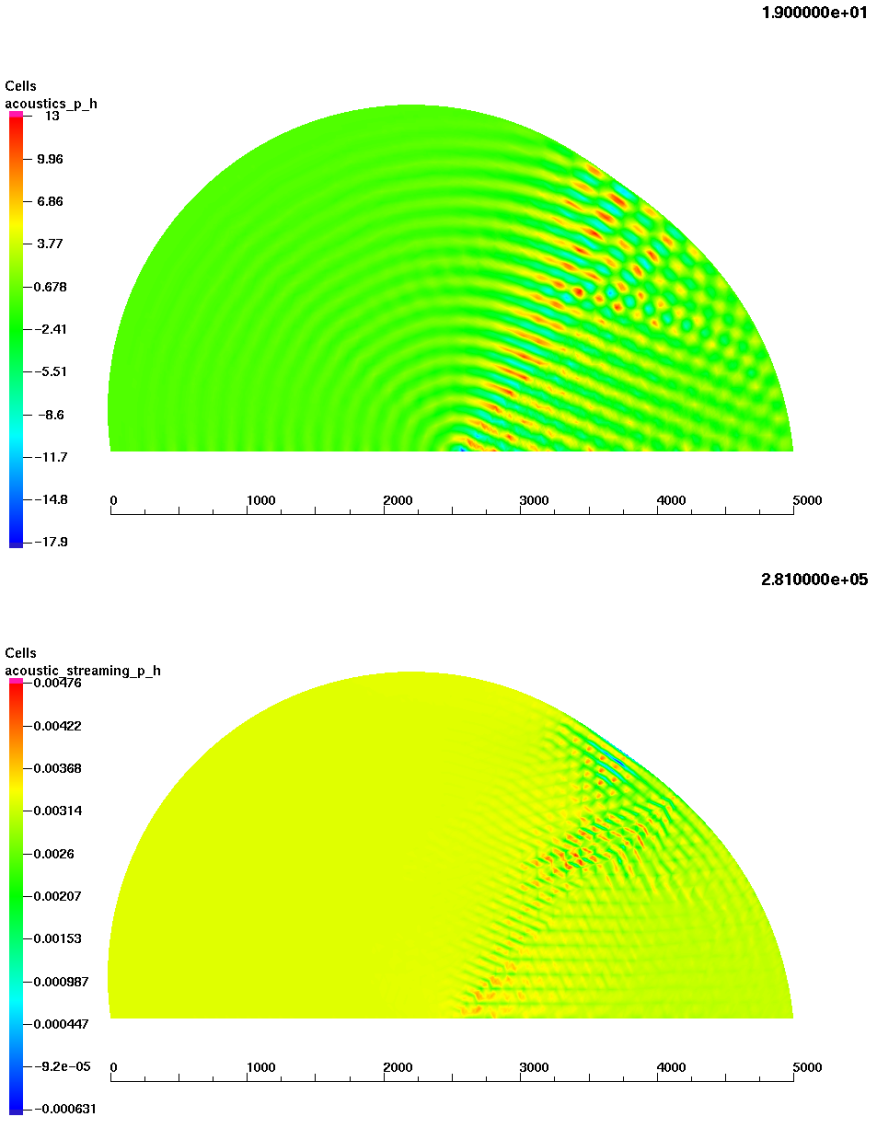

Figure 7.16: Top: Acoustic pressure field $p^{(1)}$ at microscopic time $t^{(1)} = 19$ and macroscopic time $t^{(2)} = 2.81 \cdot 10^5$. Bottom: Acoustic streaming pressure field $p^{(2)}$ at macroscopic time $t^{(2)} = 2.81 \cdot 10^5$.

The maximal CPU time for the calculation of 10 time steps (including one recalculation of the acoustic field) was approximately five hours. The observed behavior of the drop is characterized by initial damped oscillations. A deformed equilibrium position is assumed after a short period of time.

Figure 7.16 shows the acoustic and acoustic streaming pressure fields $p^{(1)}$ resp. $p^{(2)}$ in the droplet at different times. The figures on pages 132 and 133 show a macroscopic time series of the droplet shape together with values of the acoustic streaming velocity.

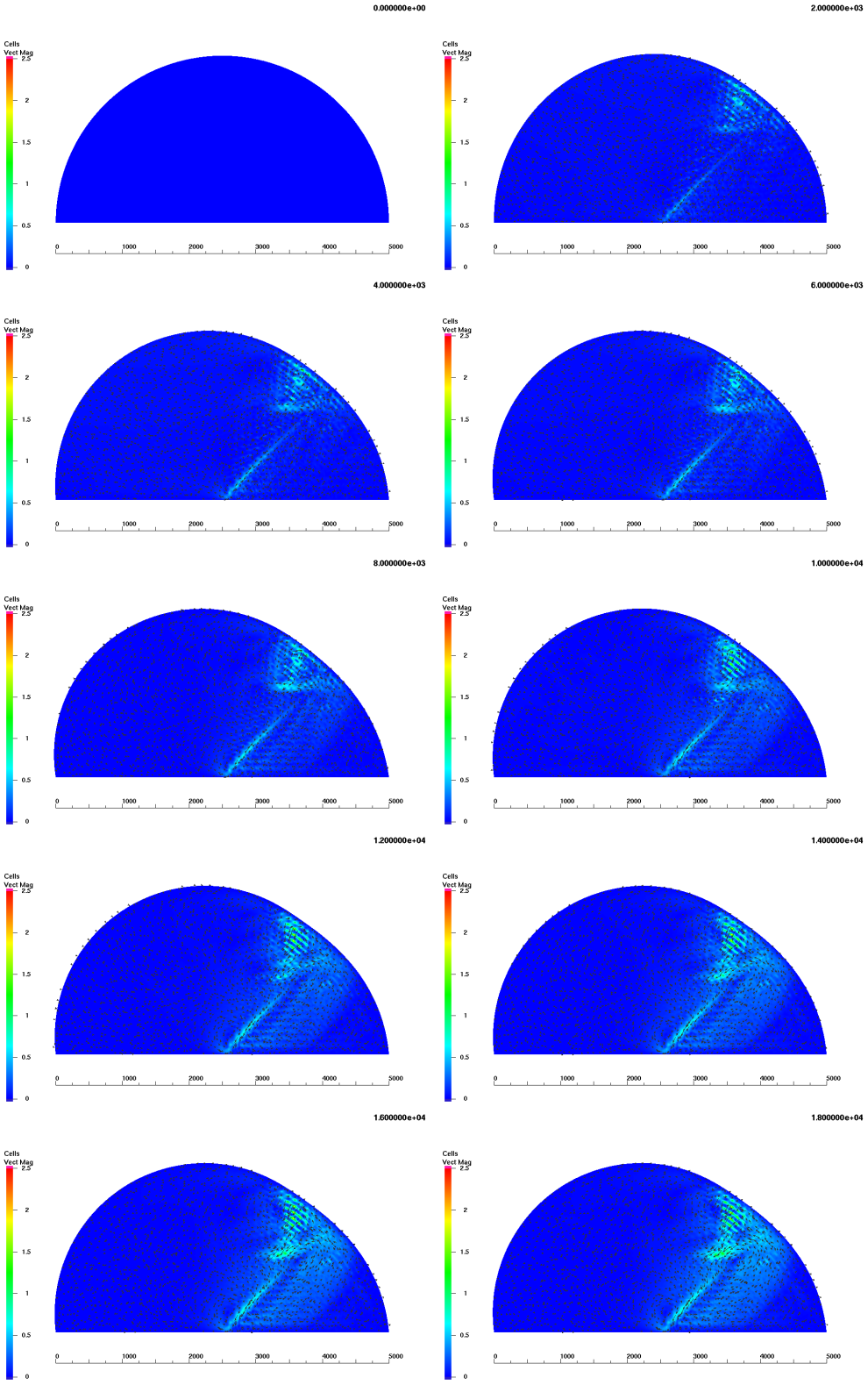
0.000000e+00
2.000000e+03
4.000000e+03
6.000000e+03
8.000000e+03
1.000000e+04
1.200000e+04
1.400000e+04
1.600000e+04
1.800000e+04
Cells
Vect Mag
2.5
2
1.5
1
0.5
0
0
1000
2000
3000
4000
5000

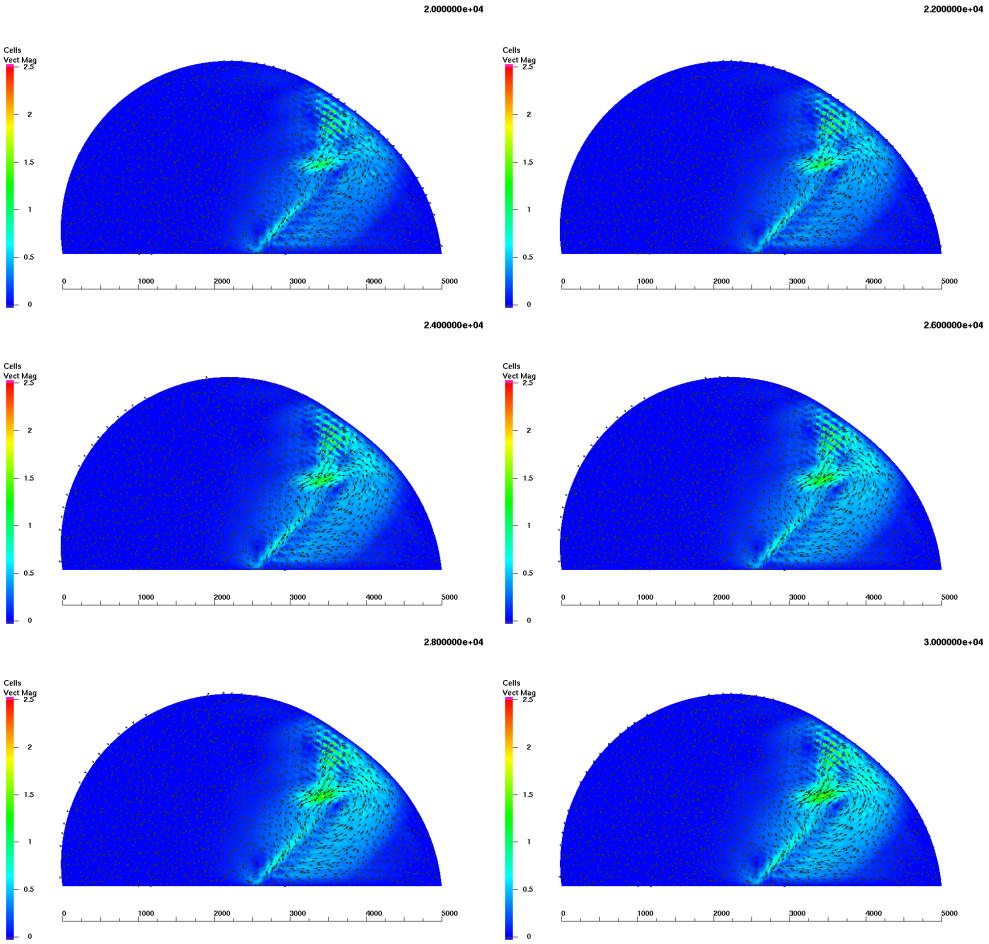

Figure 7.17: Sixteen panels: Acoustic streaming velocity field shown at various (numerical) times.

7.3 Physical experiments

The first two sections of this chapter dealt with numerical experiments. We now present a series of preliminary physical experiments performed in cooperation with the Chair of Experimental Physics I at the University of Augsburg. The experiments were performed by the author together with Dipl.-Math. Thomas Frommelt under the supervision of Prof. Dr. A. Wixforth. The statistical evaluation of results is due to Thomas Frommelt.

The aims in performing these experiments were

- to demonstrate the quadratic dependence of the streaming velocity $\boldsymbol{v}$ on the maximal SAW amplitude $\boldsymbol{u}_0$. A quadratic dependence is predicted by our model since the acoustic terms $p^{(1)}$, $\boldsymbol{v}^{(1)}$ depend linearly on $\boldsymbol{u}_0$, confer (2.4) on page 13. The acoustic streaming velocity $\boldsymbol{v}$ in turn depends quadratically on $p^{(1)}$ and $\boldsymbol{v}^{(1)}$, see (2.6), page 14.

- to demonstrate that the numerically calculated acoustic streaming veloc-

ity $\boldsymbol{v} := \boldsymbol{v}^{(2)}$ is of the correct order of magnitude. Due to still unknown parameters, among these the exact geometric shape and amplitude of the SAWs, we can not yet expect more precision, see below.

7.3.1 Experimental layout

We now describe the experimental layout. We use a typical SAW chip incorporating an IDT (Interdigital Transducer) embedded on a standard $LiNbO_3$ YXl 128° substrate. We refer to [28, 40] for an explanation of the crystal cut nomenclature. The resonance frequency of the chip lies at 114 MHz. On top of the chip were placed two vertical glass slides 250 μm apart with a water film trapped between them, see Figure 7.18. The idea is to construct a quasi two dimensional fluid environment similar to the numerical experiments explained above.

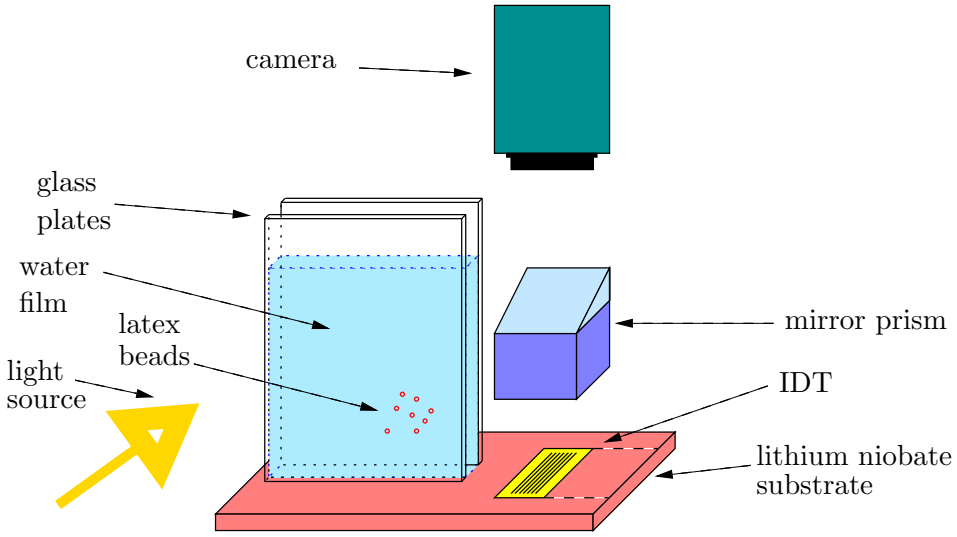

Figure 7.18: Layout of the SAW measurements

The SAW induced by the IDT couples with the water to produce acoustic streaming. The square of the amplitude of the SAW wave is proportional to the electric signal power P if linear behavior of the electronic components is assumed – a reasonable assumption at low P. The signal power P is varied using an oscilloscope to produce different streaming patterns. Sufficiently low P also guarantees a stationary laminar streaming pattern, hence the dependence of $\boldsymbol{v}$ on the time t may be neglected. Latex beads of diameter 20 μm serve to visualize the streaming motion. The setup is completed by a light source, a mirror in the background, and a standard camera to record the motion of the latex beads with time. Figure 7.19 shows a sample recorded movie.

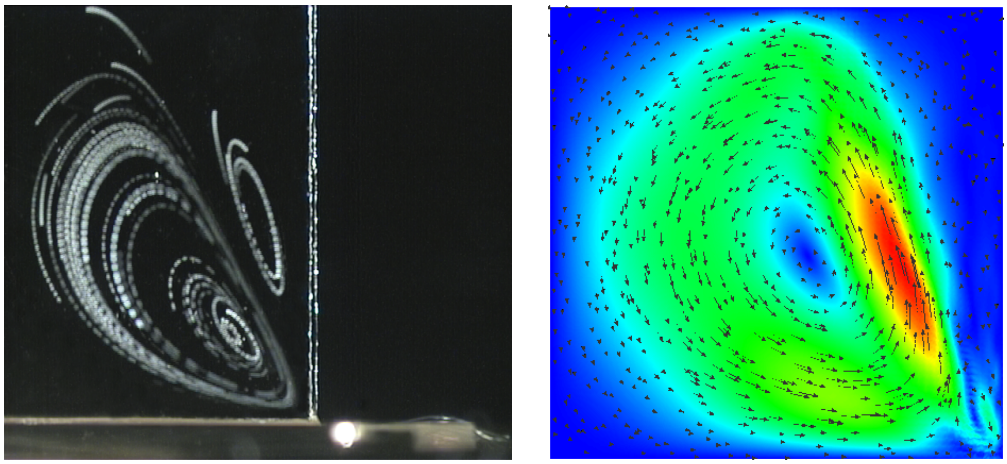

Figure 7.19: Left: The superposition of several movie frames gives an impression of the streaming motion. The visible fluid region is approximately 3.4 mm in width and 3.3 mm in height, the IDT and wiring is visible at the bottom. Right: A simulation run showing similar qualitative behavior.

7.3.2 Particle tracking

We used the particle tracking functionality of the dedicated software package OpenBox 1.74, [62]. After some image processing including decompression, conversion to grayscale, and subtraction of static background noise we used the integrated particle tracking algorithms to follow individual beads. The output for each tracking particle is a list of X-Y positions $\boldsymbol{x}_n$ indexed by the movie frame n. At 25 frames per second each movie frame corresponds to a time step $\tau = 0.04$ sec.

From these trajectory lists we derived velocity data. The straightforward definition

$$\tilde{\boldsymbol{v}}_n := \frac{\boldsymbol{x}_{n+1} - \boldsymbol{x}_n}{\tau}$$

is not always well suited due to the errors introduced by the tracking algorithm and finite camera resolution. Instead, we use a variably defined difference quotient.

To calculate the particle velocity $\boldsymbol{v}_n$ at time step n we searched the preceding positions $\boldsymbol{x}_{n-1}$, $\boldsymbol{x}_{n-2}$, ..., until a position difference of $|\boldsymbol{x}_n - \boldsymbol{x}_i| > 6$ image pixels was reached. The same was done in forward direction to find the first $\boldsymbol{x}_j$ with $|\boldsymbol{x}_j - \boldsymbol{x}_n| > 6$ pixels. The length of 6 image pixels corresponds to 34 μm or about 1.5 times the bead diameter. The velocity $\boldsymbol{v}_n$ is then defined as the difference quotient

$$\boldsymbol{v}_n := \frac{\boldsymbol{x}_j - \boldsymbol{x}_i}{(j-i)\tau}.$$

Choosing the time difference adaptively as described implies more smoothing in regions with small velocity and less smoothing in regions with large velocity, see Figure 7.20.

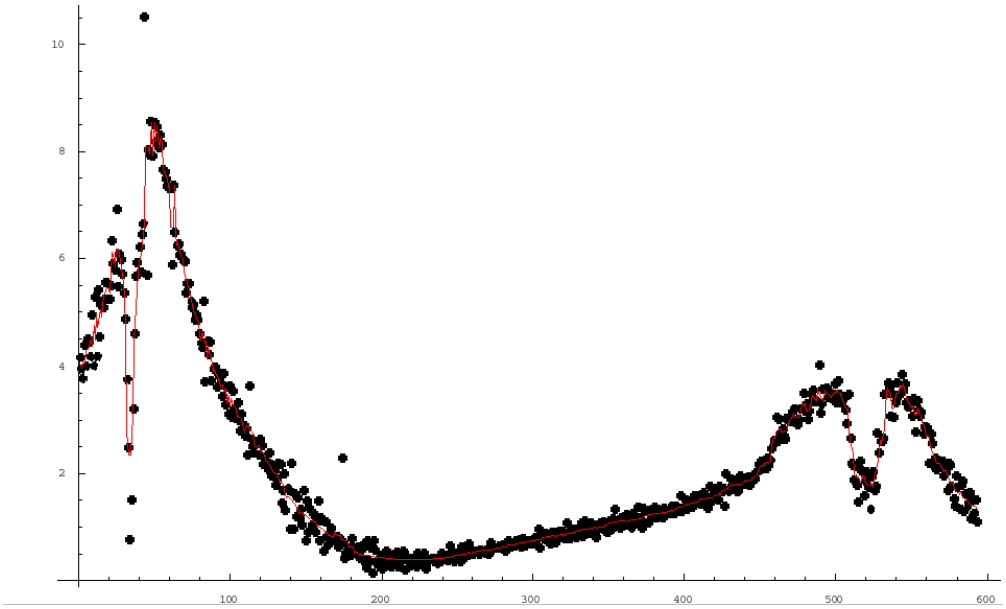

Figure 7.20: Time history of the velocity of a single particle. The dots represent values of $\tilde{\boldsymbol{v}}$ while the red curve demonstrates the smoothing effect introduced by using $\boldsymbol{v}$.

Measuring fluid streaming velocities by tracking small beads naturally introduces further errors due to the finite mass and size of the beads. The latex beads should ideally have sufficiently small size to guarantee minimal effects on the fluid streaming and sufficiently large size to guarantee visibility in the movie images.

7.3.3 Streaming velocity versus SAW amplitude

As mentioned above, the numerical model implies quadratic dependence of the acoustic streaming velocity $\boldsymbol{v}$ on the maximal SAW amplitude $\boldsymbol{u}_0$.

In the experiment the SAW amplitude in turn is proportional to the square of the radio frequency signal power P used to drive the chip, if P is not too large. We therefore expect the experiments to show a *linear* dependence $|\boldsymbol{v}| \sim P$.

This behavior was confirmed, within certain limits, in [31]. To measure the effect of the input power P on the streaming velocity $\boldsymbol{v}$ we compared different tracking experiments performed using the same geometric setup but varying signal power P_i, $i = 1, \ldots, n$. A direct comparison of velocities $\boldsymbol{v}(P_i, \boldsymbol{x})$ at a given position $\boldsymbol{x}$ is difficult since only a small set of particle trajectories is available which do not necessarily coincide in space.

To overcome this problem we divided the observation area into "boxes" B^i_j, $j = 1, \ldots, M$, of size 6×6 pixels. For each experiment i we collected and averaged all velocity information belonging to a given box. This process yields a subset of boxes $B^i_{j_k}$, $k = 1, \ldots, N^i$, containing useful velocity information. For two given experiments i_1 and i_2 we may use the intersection of the sets of useful boxes to compare velocity information, see Figure 7.21.

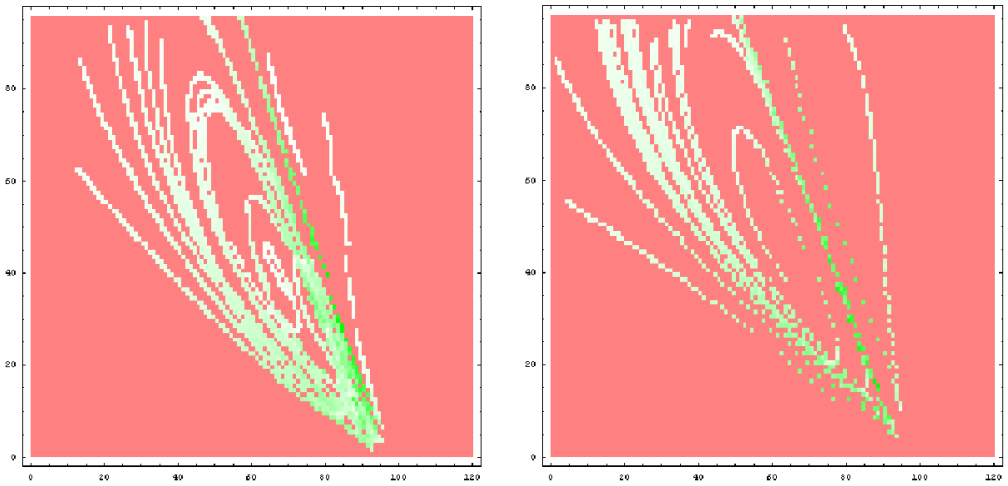

Figure 7.21: Boxed velocity information for two separate experiments where only the power P was varied. The green shades represent relative values of $\boldsymbol{v}$ in either experiment, boxes with no velocity information are rendered in red. A comparison is possible in those boxes shared among both experiments.

Since we are only interested in relative velocities we select one experiment containing as many usable boxes as possible as the reference case 0 corresponding to a power P_0. We then compared the velocity magnitudes $v := |\boldsymbol{v}|$ of a series of seven other experiments against this reference experiment. This yields a set of several hundred relative velocity measurements for each of the seven test cases. Note that this procedure only makes sense if the the velocity fields $\boldsymbol{v}(P_i, \cdot)$ at different powers P_i, $i = 1, \ldots, 7$ are more or less proportional to $\boldsymbol{v}(P_0, \cdot)$. Ideally we would require

$$\boldsymbol{v}(P_i, \boldsymbol{x}) = c_i \boldsymbol{v}(P_0, \boldsymbol{x}) \qquad \text{for all } \boldsymbol{x},$$

with a constant c_i independent of $\boldsymbol{x}$, $i = 1, \ldots, 7$.

For a given experiment $i \in \{1, \ldots, 7\}$ corresponding to power P_i we denote the set of relative velocity magnitudes as

$$Q_i := \{w_0, \ldots, w_{K_i}\}.$$

We treat these as approximate measurements of the ideal relative velocity given by

$$\overline{w}_i := \frac{P_i}{P_0}.$$

In the following we are concerned with how well the measured values in Q_i correspond to $\overline{w}_i$. We define a histogram function Ψ_i as follows:

$$\Psi_i(w) := \#\{j \in \{0, \ldots, K_i\} \mid |w_j - w| \leq \xi_i\},$$

with $\#$ as the set cardinality and $w \in [0, \max_{j=1,\ldots,K_i} w_j]$. Here ξ_i denotes the so called *category width*, chosen as $\overline{w}_i/8$ in practice. The histogram function Ψ_i is thus an extension of the concept of a histogram in that it counts the number of values in a bin of width $2\xi_i$ centered around a given value w.

7.3.4 Results

The resulting distributions are presented in Figure 7.22. The results confirm the first hypothesis stated above that the streaming velocity $\boldsymbol{v}$ is proportional to P. Concerning the second hypothesis, we arrived at the following conclusions.

In principle, it is possible to compare the streaming velocity values of the particle tracking experiments to the resulting field $\boldsymbol{v} = \boldsymbol{v}^{(2)}$ of the numerical simulations. Several difficulties must be overcome, however, before simulations can be expected to yield truly realistic results.

- The numerical simulations accept a given SAW displacement field $\boldsymbol{u}$ at the solid/liquid interface to calculate streaming velocity values. In contrast to this, the experimental variable is the electric input power. A precise formula relating input power and SAW amplitude must still be determined, either theoretically or experimentally.

- A second problem concerns the precise shape of the surface acoustic wave, including possible errors involved when reducing the problem to two dimensions. The simulation tool developed by A. Gantner, [28], could be used to calculate precise SAW shapes, alternatively, direct experimental measurements could also be conceived to solve this problem.

- A third problem is the neglected backward coupling of the water on the surface of the SAW chip. The numerical simulations performed here used heuristical parameters in the definition of $\boldsymbol{u}$ to treat the damping influence of water on the SAW, confer (7.12). One possibility to solve this problem is to develop a fully coupled solver incorporating elastic/electromagnetic effects in the solid substrate and fluid streaming effects in the water layer.

Due to these problems, we can only expect numerical streaming velocity values to be of the right order of magnitude. This means that values of $\boldsymbol{v}$ should be in the range 1–10 mm/s. This is indeed the case. Table 7.9 gives a statistical overview of streaming velocities measured at different input powers P_i. These results are of the same order of magnitude as the velocities of comparable numerical simulations, cf. Figure 7.11.

Exp.	P/P_0	v_{min} in mm/s	v_{max} in mm/s	v_{mean} in mm/s
1	0.50	$1.69 \cdot 10^{-5}$	2.31	$2.63 \cdot 10^{-1}$
2	0.63	$4.98 \cdot 10^{-5}$	1.89	$2.920 \cdot 10^{-1}$
3	0.79	$6.95 \cdot 10^{-5}$	2.78	$2.927 \cdot 10^{-1}$
4	1.26	$5.47 \cdot 10^{-5}$	3.87	$4.50 \cdot 10^{-1}$
5	1.58	$2.55 \cdot 10^{-5}$	6.02	$7.31 \cdot 10^{-1}$
6	2.00	$1.32 \cdot 10^{-5}$	6.71	$9.09 \cdot 10^{-1}$
7	2.51	$1.26 \cdot 10^{-5}$	7.45	1.10

Table 7.9: Statistical information about measured velocities along the particle trajectories. The values for different experiments are not directly comparable due to differing velocity measurement locations along trajectories.

$K_1 = 387$, $\overline{w}_1 = 0.5$

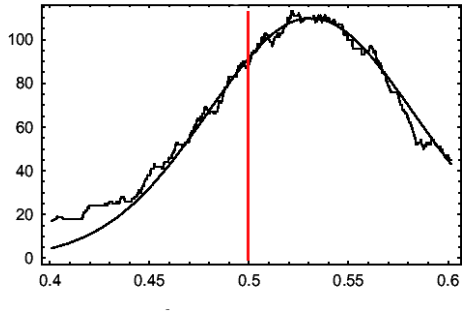

$K_2 = 187$, $\overline{w}_2 = 0.63$

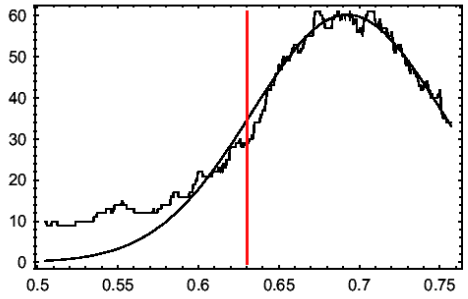

$K_3 = 296$, $\overline{w}_3 = 0.79$

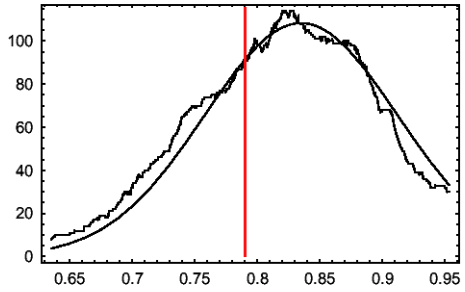

$K_4 = 314$, $\overline{w}_4 = 1.26$

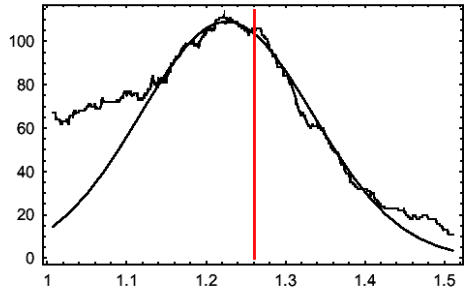

$K_5 = 128$, $\overline{w}_5 = 1.58$

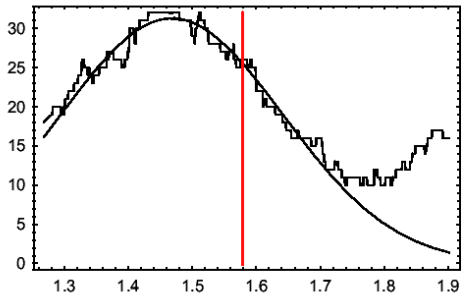

$K_6 = 292$, $\overline{w}_6 = 2.00$

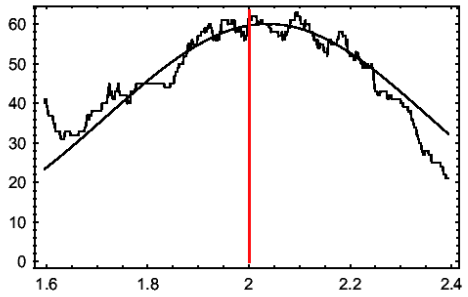

$K_7 = 262$, $\overline{w}_7 = 2.51$

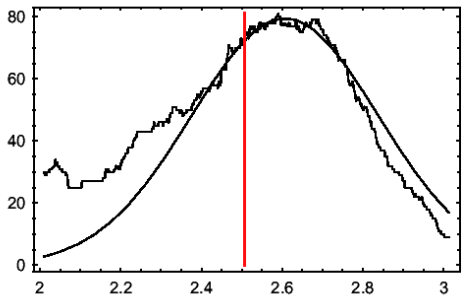

Figure 7.22: Histogram functions Ψ_i of experiments $i = 1, \ldots, 7$ together with the ideal value $\overline{w}_i$ marked as a red line. Additionally, a Gauss curve fitted to Ψ_i is shown as a smooth curve.

7.4 Conclusions and outlook

We have presented a numerical model for the calculation of acoustic streaming patterns generated by high frequency surface acoustic waves. The model equations were of linear parabolic structure, thus opening the way to theoretical analysis using well-known methods. With the software implementation it is possible to solve problems on fixed domains in two or three space dimensions.

We have also considered an algorithm to solve the acoustic streaming problem in the presence of free capillary boundaries. However, due to the amount of computational work necessary to implement the presented algorithm we are only able to solve two dimensional problems here.

The numerical tests confirm the correctness of the code. The comparison of simulation runs using realistic parameters and a series of simple preliminary physical experiments also showed promising coincidence of results.

Future work might concentrate on the following points:

- Improvement of the algorithm or new faster algorithms to calculate acoustic solutions $\boldsymbol{v}^{(1)}$, $p^{(1)}$. This is mainly of interest in the case of free capillary boundary problems where the acoustic field should ideally be recalculated on every change of the domain geometry, see Remark 6.3.3.
- More validation of the model using physical experiments.
- Research on the possibilities of treating fully coupled problems involving the piezoelectric substrate and fluid layers. The resulting problems would incorporate elastic, fluidic, and electro-magnetic effects.
- Optimization problems in the design of SAW biochips.

Appendix A

Bibliography

[1] H. W. Alt. *Lineare Funktionalanalysis*. Springer Verlag, 1999.

[2] H. W. Alt. Analysis III, 2004. Lecture notes at the University of Bonn.

[3] E. Bänsch. Numerical methods for the instationary Navier–Stokes equations with a free capillary surface. Habilitation thesis, University of Freiburg, 1998.

[4] G. Barles and P. E. Souganidis. Space-time periodic solutions and long-time behavior of solutions to quasi-linear parabolic equations. *SIAM Journal on Mathematical Analysis*, 32(6), 2001.

[5] M. Benzi, G. H. Golub, and J. Liesen. Numerical solution of saddle point problems. *Acta Numerica*, pages 1–137, 2005.

[6] M. Benzi and V. Simoncini. On the eigenvalues of a class of saddle point matrices. Technical report, Dipartimento di Matematica, Università di Bologna, 2005.

[7] N. D. Botkin and V. L. Turova. Mathematical models of a biosensor. Preprint 31, caesar-smm, Center of Advanced European Studies and Research, 2002.

[8] C. E. Bradley. Acoustic streaming field structure: The influence of the radiator. *J. Acoust. Soc. Am.*, 100(3):1399–1408, 1996.

[9] D. Braess. *Finite Elemente*. Springer Verlag, 1992.

[10] J. H. Bramble, J. E. Pasciak, and J. Xu. Parallel multilevel preconditioners. *Math. Comp.*, 55:1–22, 1990.

[11] S. C. Brenner and L. R. Scott. *The Mathematical Theory of Finite Element Methods*. Springer Verlag, 1994.

[12] F. Brezzi and M. Fortin. *Mixed and Hybrid Finite Element Methods*. Springer Verlag, 1991.

[13] M. O. Bristeau, R. Glowinski, and J. Periaux. Numerical methods for the Navier–Stokes equations. Applications to the simulation of compressible and incompressible viscous flows. *Comp. Phys. Rep.*, 6:73–187, 1987.

[14] M. P. Do Carmo. *Differentialgeometrie von Kurven und Flächen*. Vieweg Verlag, 1998.

[15] J. Nečas. Equations aux dérivées partielles. Presses de l'Université de Montréal, Quebec, 1965.

[16] K. Chakrabarty and J. Zeng. Design automation for microfluidics-based biochips. *ACM Journal on Emerging Technologies in Computing Systems*, 1:186–223, 2005.

[17] P. G. Ciarlet. *The Finite Element Method for Elliptic Problems*. North-Holland Publishing Company, 1978.

[18] Ph. Clément. Approximation by finite element functions using local regularization. *Revue Franc. Automat. Inform. Rech. Operat.*, 9(R-2):77–84, 1975.

[19] J. Crank and P. Nicolson. A practical method for the numerical evaluation of solutions of partial differential equations of the heat-conduction type. *Proc. Camb. Phil. Soc.*, 43:50–67, 1947.

[20] B. Desjardins and C.-K. Lin. A survey of the compressible Navier–Stokes equations. *Taiwanese Journal of Mathematics*, 3(2):123–137, 1999.

[21] G. Dziuk. Finite elements for the Beltrami operator on arbitrary surfaces. In S. Hildebrandt and R. Leis, editors, *Partial Differential Equations and Calculus of Variations*, pages 142–155. Springer Verlag, 1988.

[22] G. Dziuk. An algorithm for evolutionary surfaces. *Numerische Mathematik*, 58:603–611, 1991.

[23] Weinan E and B. Engquist. The heterogeneous multiscale methods. *Communications in Mathematical Sciences*, 1(1):87–132, 2003.

[24] Weinan E and B. Engquist. The heterogenous multi-scale method, 2006.

[25] C. Eckart. Vortices and streams caused by sound waves. *Phys. Rev.*, 73(1):68–76, 1947.

[26] L. C. Evans. *Partial Differential Equations*. American Mathematical Society, 1998.

[27] M. Farkas. *Periodic Motions*. Springer Verlag, 1994.

[28] A. Gantner. *Mathematical Modeling and Numerical Simulation of Piezoelectrical Agitated Surface Acoustic Waves*. PhD thesis, University of Augsburg, 2005.

[29] V. Girault and P.-A. Raviart. *Finite Element Approximation of the Navier–Stokes Equations*. Springer Verlag, 1979.

[30] P. Grisvard. *Elliptic Problems in Nonsmooth Domains*. Pitman Advanced Publishing Program, 1985.

[31] Z. Guttenberg, A. Rathgeber, S. Keller, et al. Flow profiling of a surface acoustic wave nanopump, 2004.

[32] W. Hackbusch. *Elliptic Differential Equations*. Springer Series in Computational Mechanics, 1992.

[33] W. Hackbusch. *Iterative Solution of Large Sparse Systems of Equations*. Springer Verlag, 1994.

[34] R. M. Hayes. Iterative methods of solving linear problems in Hilbert space. *Nat. Bur. Standards Appl. Math. Ser.*, 39:71–104, 1954.

[35] M. Hestenes and E. Stiefel. Method of conjugate gradients for solving linear systems. *J. Res. Nat. Bur. Standards Sect. B*, 49:409–436, 1952.

[36] J. G. Heywood and R. Rannacher. Finite element approximation of the nonstationary Navier–Stokes problem. I. Regularity of solutions and second-order error estimates for spatial discretization. *SIAM J. Numer. Anal.*, 19(2):275–311, 1982.

[37] C. W. Hirt and B. D. Nichols. Volume of fluid (VOF) method for the dynamics of free boundaries. *J. Comp. Phys.*, 39:201–225, 1981.

[38] J. Hoffelner, H. Landes, and R. Lerch. Calculation of acoustic streaming velocity and radiation force based on finite element simulation of nonlinear wave propagation. In *2000 IEEE Ultrasonics Symposium*, pages 585–588. IEEE, 2000.

[39] P. Hood and C. Taylor. A numerical solution of the Navier–Stokes equations using the finite element technique. *Comput. Fluids*, 1:73–100, 1973.

[40] IEEE standard on piezoelectricity. IEEE Transactions on Sonics and Ultrasonics, 3rd edition, 1978.

[41] G. Karniadakis, A. Beskok, and N. Aluru. *Microflows and Nanoflows. Fundamentals and Simulation*. Springer Verlag, 2005.

[42] R. Bruce Kellog and J. E. Osborn. A regulary result for the Stokes problem in a convex polygon. *J. Funct. Anal.*, 21:397–431, 1976.

[43] R. Bruce Kellogg and Biyue Liu. A finite element method for the compressible Stokes equations. *SIAM Journal on Numerical Analysis*, 33(2):780–788, 1996.

[44] L. D. Landau and E. M. Lifschitz. *Lehrbuch der Theoretischen Physik VI: Hydrodynamik*. Akademie Verlag, 1991.

[45] H. Leiva. Stability of a periodic solution for a system of parabolic equations. *Journal of Applicable Analysis*, 60(3):277–300, 1996.

[46] J. Lighthill. Acoustic streaming. Academic Press Inc. (London), 1978.

[47] J. L. Lions and E. Magenes. *Non-homogeneous Boundary Value Problems and Applications*. Springer Verlag, 1972.

[48] A. Meister. *Numerik Linearer Gleichungssysteme*. Vieweg Verlag, 1999.

[49] W. L. Nyborg. Acoustic streaming. *Phys. Acoust. Princ. Meth.*, II(13), 1965.

[50] W. L. Nyborg. Acoustic streaming. In M. F. Hamilton and D. T. Blackstock, editors, *Nonlinear Acoustics*, pages 207–231. Academic Press, 1998.

[51] S. Osher and J.A. Sethian. Fronts propagating with curvature-dependent speed: Algorithms based on Hamilton-Jacobi-formulations. *J. Comp. Phys.*, 79(1):12–49, 1988.

[52] F. Otto. Die Babuška-Brezzi Bedingung für das Taylor-Hood-Element. Diploma thesis, University of Bonn, 1990.

[53] Jr. P. Ciarlet, J. Huang, and J. Zou. Some observations on generalized saddle point problems. *SIAM J. on Matrix Anal. and Appl.*, 25(1):224–236, 2003.

[54] W. V. Petryshyn. Direct and iterative methods for the solution of linear operator equations in Hilbert space. *Trans. Amer. Math. Soc.*, 105:136–175, 1962.

[55] Lord Rayleigh. On the circulation of air observed in Kundt's tubes, and on some allied acoustical problems. *Philosophical Transactions of the Royal Society of London*, 175:1–21, 1884.

[56] N. Riley. Oscillating viscous flows. *Mathematika*, 12:161–175, 1965.

[57] N. Riley. Acoustic streaming. *Theoretical and Computational Fluid Dynamics*, 10:349–356, 1998.

[58] L. D. Rozenberg, editor. *Ultrasonic Technology*, chapter High-Intensity Ultrasonic Fields. Plenum Press, New York-London, 1971.

[59] M. Rumpf. A variational approach to optimal meshes. *Numer. Math.*, 72:523–540, 1996.

[60] Y. Saad. *Iterative Methods for Sparse Linear Systems*. SIAM, 2003.

[61] Y. Saad and M. Schultz. GMRES: A generalized minimal residual algorithm for solving nonsymmetric linear systems. *SIAM J. Sci. Stat. Comput.*, 7:856–869, 1986.

[62] J. Schilling, E. Sackmann, and A. R. Bausch. Digital image processing for biophysical applications. *Rev. Scient. Instr.*, 75(9):2822–2827, 2004.

[63] A. Schmidt and K. G. Siebert. *Design of Adaptive Finite Element Software: The Finite Element Toolbox ALBERTA*. Springer Verlag, 2005.

[64] Alfred Schmidt and Kunibert G. Siebert. ALBERT: An adaptive hierarchical finite element toolbox. Preprint Nr. 06/2000 - 31.03.2000, 2000.

[65] B. Schweizer. Free boundary fluid systems in a semigroup approach and oscillatory behavior. *SIAM Journal on Mathematical Analysis*, 28(5):1135–1157, 1997.

[66] L. R. Scott and S. Zhang. Finite element interpolation of nonsmooth functions satisfying boundary conditions. *Mathematics of Computation*, 54(190):483–493, 1990.

[67] J. A. Sethian. *Level Set Methods and Fast Marching Methods*. Cambridge Monographs on Applied and Computational Mathematics, 1999.

[68] P. Smereka. Level set methods for two-fluid flows. Lecture notes from a short course given at INRIA, 1996.

[69] V. A. Solonnikov. On some free boundary problems for the Navier–Stokes equations with moving contact points and lines. *Mathematische Annalen, Springer Verlag*, 302:743–772, 1995.

[70] M. Sussman, E. Fatemi, P. Smereka, and S. Osher. An improved level set method for incompressible two-phase flows. *Computers and Fluids*, 27(5/6), 1997.

[71] M. Sussman, P. Smereka, and S. J. Osher. A level set approach for computing solutions to incompressible two-phase flow. *J. Comp. Phys.*, 114:146–159, 1994.

[72] R. Temam. *Navier–Stokes Equations*. North-Holland Publishing Company, 1984.

[73] T. Uchida, T. Suzuki, and S. Shiokawa. Investigation of acoustic streaming excited by surface acoustic waves. In *1995 IEEE Ultrasonics Symposium*, pages 1081–1084. IEEE, 1995.

[74] A. Valli. Navier–Stokes equations for compressible fluids: Global estimates and periodic solutions. *Proc. Symp. Pure Math.*, 45:467–476, 1986.

[75] S. Vandewalle and R. Piessens. On dynamic iteration methods for solving time-periodic differential equations. *SIAM J. Numer. Anal.*, 30:286–303, 1993.

[76] Homer F. Walker. Implementation of the GMRES method using Householder transformations. *SIAM J. Sci. Stat. Comput.*, 9(1):152–163, 1988.

[77] A. Wixforth, C. Strobl, Ch. Gauer, et al. Acoustic manipulation of small droplets. *Anal. Bioanal. Chem*, 379:982–991, 2004.

[78] J. Wloka. *Partielle Differentialgleichungen*. B. G. Teubner, Stuttgart, 1982.

[79] J. Xu. The conjugate gradient method for linear and nonlinear operator equations. *SIAM Review*, 34:581–613, 1992.

[80] H. Yserentant. On the multi-level splitting of of finite element spaces. *Numer. Math.*, 49:379–412, 1986.

Appendix B

Reference of notation and symbols

$\mathbb{N}$	set of nonzero natural numbers
$\mathbb{N}_0$	natural numbers with zero: $\mathbb{N} \cup \{0\}$
$\mathbb{R}$	set of real numbers
$\mathbb{C}$	set of complex numbers
i	imaginary unit, $\sqrt{-1}$, if not an index
$\Re z$, $\Re \mathrm{z}$	real part,
$\Im z$, $\Im \mathrm{z}$	imaginary part, and
$\bar{z}$, $\bar{\mathrm{z}}$	complex conjugate of a complex number $z \in \mathbb{C}$ or vector $\mathrm{z} \in \mathbb{C}^n$
$A \oplus B$	direct sum of vector spaces A and B
$\overline{A}$	topological closure of a set $A \subset \mathbb{R}^d$
∂A	boundary set of a set $A \subset \mathbb{R}^d$
$\operatorname{conv} A$	convex hull of a set $A \subset \mathbb{R}^d$
$\operatorname{relbd}(A)$	relative boundary of $A \subset M$ in M, where M is a submanifold of $\mathbb{R}^d$
$\lambda^d(A)$	Lebesgue measure of a set $A \subset \mathbb{R}^d$
$\operatorname{ess\,sup} f$	essential supremum of a function f
$\operatorname{supp} f$	support of a function f
$A \subset\subset B$	set A is compactly contained in B
$\mathrm{A}^\top$	transpose of a matrix $\mathrm{A} \in \mathbb{R}^{n \times m}$
$\mathrm{A} : \mathrm{B}$	for matrices $\mathrm{A}, \mathrm{B} \in \mathbb{R}^{n \times m}$ the scalar product $\mathrm{A} : \mathrm{B} := \sum_{i,j} \mathrm{A}_{ij} \mathrm{B}_{ij}$
SPD	symmetric and positive definite
(v, w)	scalar product of v and w
$v \perp w$	orthogonality of v and w with respect to a given scalar product
$L(E, F)$	space of bounded linear mappings between two normed spaces E and F
E'	dual space of a Banach space E, defined as the space of bounded linear functionals on E

$B^* : F' \to E'$	dual operator of a bounded linear operator $B : E \to F$ between Banach spaces
$\langle g, f \rangle_{E \times E'}$	duality pairing of $f \in E'$ with $g \in E$, defined as $f(g)$
$\lvert \mathrm{x} \rvert_p$	l^p-norm of $\mathrm{x} \in \mathbb{R}^n$, defined as $\lvert \mathrm{x} \rvert_p = (\sum_{i=1}^n \lvert \mathrm{x}_i \rvert^p)^{1/p}$
$\lvert \mathrm{x} \rvert$	Euclidean l^2-norm of $\mathrm{x} \in \mathbb{R}^n$
S^{d-1}	boundary of the unit sphere in R^d; $S^{d-1} := \{\mathrm{x} \in \mathbb{R}^d \mid \lvert \mathrm{x} \rvert_2 = 1\}$
$L^p(\Omega)$	Lebesgue space of p-integrable functions on Ω
$L^p_0(\Omega)$	p-integrable functions with mean zero over Ω
$H^m(\Omega)$	Sobolev space of scalar functions with weak derivatives up to order m in $L^2(\Omega)$
$\boldsymbol{H}^m(\Omega)$	Sobolev space of vector valued functions; $\boldsymbol{H}^m(\Omega) := \boldsymbol{H}^m(\Omega, \mathbb{R}^d)$
$\boldsymbol{H}^m_0(\Omega)$	subpace of $\boldsymbol{H}^m_0(\Omega)$ with functions of zero trace
$\lVert u \rVert_m$	norm of the Sobolev space $H^m(\Omega)$ or $\boldsymbol{H}^m(\Omega)$
f. a. a.	"for almost all", short notation for "for all elements except those contained in a set of (Lebesgue) measure zero"
a. e.	"almost everywhere", meaning that a property is fulfilled f. a. a. elements
$⨍_\Omega p$	mean of a function p over Ω, defined as $\frac{1}{\lambda^d(\Omega)} \int_\Omega p$
Σ	Newtonian stress tensor $\boldsymbol{\Sigma} = \boldsymbol{\Sigma}(\boldsymbol{v}, p)$
EOC	experimental order of convergence